Development and application of a modelling approach for distributed karst aquifer characterization and groundwater residence time derivation

Dissertation

zur Erlangung des mathematisch-naturwissenschaftlichen Doktorgrades
"Doctor rerum naturalium"
der Georg-August-Universität Göttingen

im Promotionsprogramm Geowissenschaften
der Georg-August University School of Science (GAUSS)

vorgelegt von

Sandra Oehlmann

aus Hannover

Göttingen 2015

Betreuungsausschuss:

Prof. Dr. Martin Sauter,
Abteilung Angewandte Geologie, Georg-August-Universität Göttingen
Dr. Tobias Geyer,
Ref. 94 – Landeshydrogeologie und -geothermie, Abt. 9 – Landesamt für Geologie, Rohstoffe und Bergbau, Regierungspräsidium Freiburg

Mitglieder der Prüfungskommission:

Referent: Prof. Dr. Martin Sauter,
Abteilung Angewandte Geologie, Georg-August-Universität Göttingen
Korreferent: Prof. Dr. Rudolf Liedl,
Institut für Grundwasserwirtschaft, Technische Universität Dresden

weitere Mitglieder der Prüfungskommission:

Dr. Tobias Geyer,
Ref. 94 – Landeshydrogeologie und -geothermie, Abt. 9 – Landesamt für Geologie, Rohstoffe und Bergbau, Regierungspräsidium Freiburg
PD Dr. Tobias Licha,
Abteilung Angewandte Geologie, Georg-August-Universität Göttingen
Prof. Dr. Thomas Ptak,
Abteilung Angewandte Geologie, Georg-August-Universität Göttingen
Prof. Dr. Ekkehard Holzbecher,
Applied Geology, German University of Technology in Oman

Tag der mündlichen Prüfung: 9. September 2015

Abstract

Spring protection in karst aquifers is particularly challenging since their high complexity thwarts their characterization by traditional field investigated methods. Especially the properties of the highly conductive conduit system are often poorly known. Therefore, most studies in karst aquifers are limited to spring responses and do not give any information on spatial distributions. Spatial information is required for the implementation of spring protection methods, however. Above all, the delineation of spring catchment areas and the distributions of groundwater residence times are essential for defining protection areas and estimating the effects of contamination events.

The aim of this thesis is developing a modelling approach for the spatially distributed characterization of karst aquifers and the simulation of their groundwater residence time distributions. The main objectives during model development are determining the necessary model complexity, the kind and amount of required field data and the new information on aquifer structure and hydraulic parameters provided by the model, i.e. the contribution of the model to aquifer characterization. The simulations are divided into three modelling steps each of which focusing on a concrete simulation aim. The first aim is the delineation of spring catchment areas, the second the simulation of the velocity distribution within the conduit system and the third the spatial residence time distribution within the aquifer. The simulations are applied to the area of the Gallusquelle spring, a well-investigated field site in south-western Germany, where the results can be checked with field data. The models increase step-by-step in their complexity and parameter requirements so that the required minimum complexity for each simulation aim can be deduced.

For spring catchment delineation, the average annual spring discharge of the Gallusquelle and the hydraulic head distribution derived from 20 observation wells are successfully employed for calibration. The spring discharge of five other springs within the model area is used for checking the plausibility of the results. Regarding the modelling approach, a hybrid model is recommended explicitly representing the karst conduits. The approximate location of the conduits is required as input data, while the large-scale lateral changes in conduit cross-section can be deduced from the model.

The flow velocities in the conduit system are calibrated adding the breakthrough curves of two artificial tracer tests as objective functions. This greatly reduces the ambiguity of the model, so that not only the lateral change in conduit cross-section but also the total conduit volume can be deduced. Further, the roughness of the conduit system can be estimated with this approach. The

simulation shows that the conduit roughness varies systematically throughout the conduit system of the Gallusquelle, which is necessary to take into account for reproducing the velocity distribution.

For simulating the residence time distribution, a new modelling approach is developed combining a hybrid and a double-continuum approach. This new approach is successfully applied for two process studies. It is able to simulate the groundwater ages, life expectancies and residence times in the conduit network, the fissured system and the porous matrix of karst aquifers. The approach is applied for the Gallusquelle area and shows reasonable results. However, a lack of spatially distributed field data for calibration prohibits the verification of the residence time simulation at this stage. For this, groundwater age measurements at the surrounding springs would be required. However, sensitivity studies show that groundwater residence times have the potential to assist with the derivation of aquifer thicknesses, if such measurements are available.

Zusammenfassung

Grundwasserschutz in Karstgrundwasserleitern ist eine besondere Herausforderung, da diese aufgrund ihrer hohen Komplexität nicht mit Hilfe traditioneller Feldmethoden charakterisiert werden können. Vor allem über die Eigenschaften des hochdurchlässigen Karströhrensystems liegen oft nur wenige Informationen vor. Deshalb fokussieren die meisten Grundwasserstudien in Karstgebieten ausschließlich die Karstquellen und ihr Verhalten und liefern keine räumlich verteilten Informationen. Räumliche Informationen sind jedoch vor allem für die Implementierung von Quellschutzmaßnahmen von großer Bedeutung. Insbesondere die Abgrenzung von Quelleinzugsgebieten und die Verteilung der Grundwasserverweilzeiten sind essentiell für die Definition von Quellschutzzonen und die Einschätzung der Folgen von Kontaminationsereignissen.

Ziel dieser Arbeit ist die Entwicklung eines Modellansatzes für die distributive Karstgrundwasserleiter-Charakterisierung und die Simulation ihrer Verweilzeitenverteilung. Während der Modellentwicklung werden drei Hauptziele verfolgt: die Ermittlung der erforderlichen Modellkomplexität, die Ermittlung der Art und Menge der benötigten Geländedaten und die Ermittlung der neuen Informationen, die hinsichtlich der Struktur und hydraulischen Parametern des Grundwasserleiters aus dem Modell gezogen werden können, also des Beitrags des Modells zur Grundwasserleitercharakterisierung. Die Simulationen sind in drei Modellierungsschritte eingeteilt, die jeweils ein unterschiedliches konkretes Simulationsziel fokussieren. Das erste Ziel ist die Abgrenzung der Quelleinzugsgebiete, das zweite die Simulation der Geschwindigkeitsverteilung im Röhrensystem und das dritte die räumliche Verweilzeitenverteilung innerhalb des gesamten Grundwasserleiters. Die Modelle werden auf das Gebiet der Gallusquelle, einer gut erforschten Karstquelle in Südwest-Deutschland, angewendet, sodass die Simulationsergebnisse mit Geländedaten überprüft werden können. Die Komplexität und die Parameteranforderungen der Modelle werden schrittweise mit jedem Simulationsschritt erhöht, wodurch die minimal nötige Komplexität für jedes Simulationsziel abgeleitet werden kann.

Für die erfolgreiche Abgrenzung der Quelleinzugsgebiete werden die mittlere jährliche Schüttung der Gallusquelle und die Standrohrspiegelhöhenverteilung aus 20 Beobachtungsbrunnen für die Kalibration verwendet. Die Quellschüttungen von fünf weiteren Quellen innerhalb des Modellgebiets dienen zur Prüfung der Plausibilität der Modellergebnisse. Als Modellansatz wird ein Hybridansatz genutzt, der die Karströhren explizit repräsentiert. Eine Abschätzung der Position der Karströhren wird als Eingangsdaten benötigt. Das Modell selbst liefert Informationen über die großskalige laterale Änderung der Röhrengeometrie.

Die Kalibration der Strömungsgeschwindigkeiten innerhalb des Röhrensystems erfordert die Durchbruchskurven zweier künstlicher Markierungsversuche als zusätzliche Zielfunktionen. Dies verringert die Mehrdeutigkeit des Modells signifikant, sodass nicht nur laterale Änderungen der Röhrenquerschnittsfläche sondern auch das Gesamtvolumen des Röhrennetzwerks bestimmt werden können. Des weiteren dient dieser Ansatz zur Abschätzung der Rauigkeit des Röhrensystems. Die Simulationen zeigen, dass die Rauigkeit innerhalb des Röhrensystems der Gallusquelle systematisch variiert, was beachtet werden muss um die Geschwindigkeitsverteilung zu reproduzieren.

Für die Simulation der Verweilzeitenverteilung wird ein neuer Modellansatz entwickelt, der einen Hybrid- und einen Doppelkontinuumansatz kombiniert, und erfolgreich auf zwei Prozessstudien angewendet. Dieser ist in der Lage die Grundwasseralter, Verweilzeiten und *Life Expectancies* im Röhrensystem, im Kluftsystem und in der porösen Matrix von Karstgrundwasserleitern zu simulieren. Bei der Anwendung auf das Gebiet der Gallusquelle zeigt der Ansatz sinnvolle Ergebnisse. Ein Mangel an räumlich verteilten Geländedaten für die Kalibration verhindert, dass die Ergebnisse gegenwärtig verifiziert werden können. Hierfür wären zusätzliche Messungen des Grundwasseralters an den umliegenden Karstquellen notwendig. Sensitivitätsstudien zeigen jedoch, dass die Grundwasserverweilzeiten das Potenzial haben zur Charakterisierung der Grundwasserleiter-Mächtigkeiten beizutragen, falls Messungen an mehreren Quellen vorliegen.

Danksagung

An erster Stelle möchte ich meinen beiden Betreuern Dr. Tobias Geyer und Prof. Martin Sauter danken, die mir die Möglichkeit gaben an diesem spannenden Thema zu arbeiten. Durch die große Erfahrung der beiden auf dem Gebiet der Karsthydrogeologie waren die Diskussionen mit ihnen stets eine große Hilfe. Vor allem in der Anfangsphase half Dr. Geyer mir Ansatzpunkte zu finden, auf denen ich meine Arbeit aufbauen konnte.

Natürlich möchte ich auch allen weiteren Mitgliedern meiner Prüfungskommission herzlich dafür danken, dass sie sich ohne zu zögern bereit erklärt haben, diese Aufgabe zu übernehmen. Vor allem meinem Korreferenten Prof. Rudolf Liedl gilt mein Dank für das gründliche Korrekturlesen der Arbeit. Durch seinen Beitrag konnte noch einiges an kleineren Fehlern oder Ungereimtheiten rechtzeitig vor der Veröffentlichung beseitigt werden. Hervorheben möchte ich zudem PD Dr. Tobias Licha, der nicht nur in meiner Prüfungskommission mitwirkte, sondern auch als Koordinator des Projektes AGRO fungierte, in dessen Rahmen ich diese Arbeit anfertigte. Für das Korrekturlesen etwaiger Zwischenberichte und natürlich den Beitrag als Koautor bei meinen ersten beiden Veröffentlichungen möchte ich mich herzlich bedanken. In diesem Zusammenhang möchte ich auch dem Bundesministerium für Bildung und Forschung (BMBF) danken, welches das Projekt finanziert und somit die Arbeiten erst ermöglicht hat.

Mein Dank gilt ebenso meinem Koautor Prof. Steffen Birk, der einiges zum Gelingen meines ersten Papers und damit zu einem erfolgreichen Start in die kumulative Dissertation beigetragen hat. Und natürlich allen Kollegen der Abteilung Angewandte Geologie, insbesondere meinen (zeitweisen) Bürokollegen Shadha Musallam, Markus Giese, Rasi Prasetio, Teuku Firman und Elena Shigorina, die dafür gesorgt haben, dass es im Büro nie langweilig wurde. Besonderen Dank auch an Beka Peters-Kewitz, die mir bei so manchen organisatorischen Problemen zur Seite stand.

Zu guter Letzt möchte ich natürlich auch meiner Familie und meinen Freunden danken, die mich während der gesamten Zeit immer unterstützt und mir dadurch auch durch die arbeitsreichsten Phasen hindurchgeholfen haben.

Table of Contents

List of Figures

List of Tables

Chapter 1

1 Introduction

1.1 Motivation

Karst aquifers are important sources of drinking water for over 20% of the world's population (Ford and Williams, 2007). Compared to other aquifer types, they have a high amount of large springs, i.e. with discharges of over 100 L s^{-1}, which make them especially suited for water abstraction (Worthington, 2009). However, the highly conductive pathways that channel water to these springs also serve as fast transport paths for contaminants. The hydraulic conductivity of the surrounding aquifer material is usually several magnitudes lower leading to a large difference in flow velocities (Atkinson, 1977) and a highly heterogeneous distribution of groundwater residence times within the aquifer (Cornaton, 2004). Therefore, the water quality of karst springs is threatened by long lasting contamination as well as sharp contamination peaks (Hillebrand et al., 2014). Due to these reasons, assessing the residence time distribution within karst aquifers is highly important and at the same time especially challenging.

The first step towards such an assessment is aquifer characterization. The properties of the fast and slow flow systems must be known for estimating the flow behaviour and velocities. However, established hydraulic field investigation methods such as slug tests or borehole pumping tests do not have a large enough scale of investigation to encompass the different flow compartments of the aquifer (Sauter, 1991). Tapping the highly conductive conduit system by drilling is highly unlikely since it often constitutes less than 1% of the total aquifer volume (Worthington, 2009). Therefore, hydraulic borehole tests usually only give information on the lowly conductive parts of the system. Long-term pumping tests within the conduit system are very rare, but can give information on the karst conduits and the surrounding matrix, if the drawdown is high enough (Maréchal et al., 2008). Spring responses, i.e. spring discharge and physico-chemical spring water parameters, are global response functions and give integral information about the whole aquifer system. However, in both cases distinguishing between the influence of the conduit system and the surrounding fissured matrix is not always straightforward (e.g. Birk et al., 2005; Király, 2002). Furthermore, the use of global response functions only allows for the calibration of effective global parameters and gives no information about their spatial distribution. Spatial information is essential for local spring protection methods, e.g. delineating protection zones.

Therefore, a differentiated aquifer characterization approach for an integral interpretation of different investigation techniques is necessary for characterizing the whole aquifer (Geyer et al., 2013). Physically based numerical models have the potential to include a wide number of field investigations and be therefore a tool for aquifer characterization. Since they are based on the physical processes in the catchment area, they can potentially also be used for prognostic simulations even outside of the observed variation ranges (Kovács and Sauter, 2007; Rehrl and Birk, 2010). For assessing the spatial distribution of aquifer parameters and simulation objectives, e.g. groundwater residence times, distributed numerical models are needed. They are rarely applied for natural karst systems due to lack of input information. If they are, the simulated aquifers are usually strongly simplified and only calibrated for a single objective (e.g. Birk et al., 2005; Doummar et al., 2012). Furthermore, distributed models often get numerically complex, if karst features need to explicitly be taken into account or several objectives need to be calibrated for. Therefore, the available time and computer capacity often limit the amount of model runs that can reasonably be performed. Due to these difficulties, the most powerful tool for spatially distributed karst aquifer characterization and assessment of pollution risks has not been used to its full potential so far.

This thesis addresses the complex subject of simulating groundwater residence time distributions in natural karst aquifers in several steps. A well-investigated field site is chosen and a distributed groundwater flow and solute transport model is developed. In each modelling step, further simulation objectives are added and the complexity of the model is increased to meet the necessary requirements until a reasonable estimate of the residence time distribution can be made. *Two main objectives are pursued during modelling. Firstly, the necessary field data and model complexity are to be derived since these are the most important aspects for applying the developed approach to other areas. Secondly, it is investigated whether distributed numerical models can be employed for aquifer characterization, i.e. if unknown aquifer parameters and their lateral distributions can be derived directly from the model. In this chapter, a short overview of the specifics of karst aquifers, the different modelling approaches and the chosen field site is provided, as well as a short description of the thesis structure and different modelling steps.*

1.2 Karst aquifers

1.2.1 Conceptual model

Figure 1.1 shows a conceptual overview of a karst system. Karst aquifers develop in moderately soluble carbonate or evaporate rocks due to chemical dissolution processes (Worthington et al., 2000). The dissolution process widens already existing discontinuities such as small fissures, fractures

or joints along bedding planes generating highly conductive karst conduits or caves (Dreybrodt and Gabrovšek, 2003). These highly conductive structures are often described as the tertiary porosity of the aquifer and are a unique feature of karst systems (Worthington et al., 2000). The other two porosities are also found in other aquifer types. The primary porosity consists of the pore spaces generated during rock formation, while the secondary porosity is generated by fissures and fractures that develop due to mechanical or thermal stresses (Worthington et al., 2000). Therefore, groundwater flow and transport in karst occur in three different compartments of the aquifer.

The hydraulic parameters of these three compartments strongly differ from one another. The porous matrix usually displays the highest porosity but only low permeabilities, since the primary pores are often small and only poorly interconnected. The karst conduits provide most of the flow due to their high permeability but often constitute of the smallest part of the total aquifer porosity (Worthington et al., 2000). The fissured system takes an intermediate role in both porosity and permeability. For groundwater flow simulations, the porous matrix and the fissured system are often viewed as a representative elementary volume (REV) and lumped into a single continuum termed *fissured matrix* (e.g. Teutsch and Sauter, 1991; Liedl et al., 2003; Reimann et al., 2011) (Figure 1.1). This conceptual view essentially reduces the aquifer to a double-permeability system with respect to flow. The described heterogeneities have several important consequences for groundwater flow:

1. In addition to **diffuse seepage** from the fissured matrix system, the focusing of flow in karst conduits leads to a **focused discharge** to a limited number of springs. The number and size of these springs are determined by the configuration of the karst conduit network, i.e. size, number and interconnection of conduits (Worthington and Ford, 2009).
2. While groundwater flow in the matrix is generally considered negligible, it provides a high percentage of **groundwater storage** in many karst aquifers (e.g. Worthington et al., 2000). This has a high importance for groundwater residence times and transport behaviour. Groundwater ages in the matrix and the conduits can differ by several decades (e.g. Geyer, 2008).
3. The duality of aquifer permeability is accompanied by a **duality of recharge**. Direct recharge reaches the conduits within a few minutes or hours via vertical shafts and is directly transported to the karst springs. Diffuse recharge slowly percolates into the fissured system, where it can take years for it to reach an outlet (Király, 1998).

The influence of subsurface karstification can in many regions be observed on the ground surface by specific landscape features such as dry valleys, sinkholes or sinking streams (Figure 1.1). There is a comparatively low amount of surface streams in karstic areas, especially for mature karst systems. Beneath the soil zone, many unconfined karst aquifers exhibit a karstified zone called epikarst, where

the rock is dissolved due to the arrival of recharge water with a high undersaturation with respect to Ca^{2+}. The epikarst is usually followed by an unsaturated zone that can have a high thickness of over 100 m (e.g. Doummar et al., 2012).

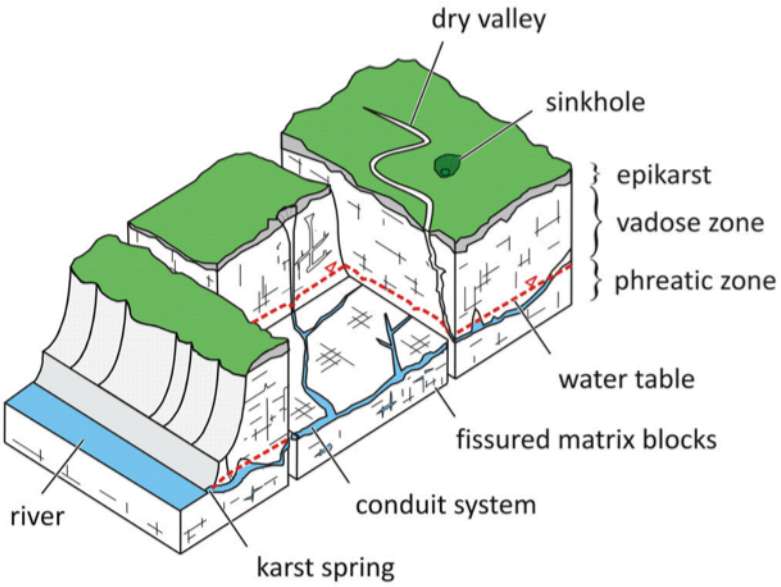

Figure 1.1. Conceptual model of a karst aquifer (Geyer, 2008).

1.2.2 Characteristics and evolution of highly conductive karst features

The development of karst aquifers can proceed in a wide range of time-scales and result in a wide range of karst conduit geometries. The term karst *conduit* is usually used for describing karst features in the range of several centimetres, while smaller features are termed fissures or channels. If the conduits get large enough for people to enter, they are generally called caves (Maurice et al., 2006; Worthington and Ford, 2009). Large cave systems are sometimes accessible for direct investigations and geometric measurements, so that their locations and geometries are well known (e.g. Jeannin, 2001; Worthington, 2009). However, in most karst aquifers, localizing the major channels, conduits or caves and deriving their hydraulic and geometric parameters is a large challenge. If karstic landscape features are present, they are signs of intense karstification and can be used for estimating the locations of major karst features (Mohrlok and Sauter, 1997; Mohrlok, 2014). A dense network of observation wells can also be used for deriving the locations of karst conduits or caves from troughs in the hydraulic head distribution (Worthington, 2009; Joodi et al., 2010).

However, these approaches only serve for locating the dominant conduits but do not give any information about their geometries. Integral information on the conduit volume and average conduit cross-section can be gained by interpretation of artificial tracer tests (e.g. Birk et al., 2005; Geyer et al., 2008). However, due to an unknown contribution of water from the fissured matrix these analyses only provide the maximum volume (Birk et al., 2005). Luhmann et al. (2012) showed that the combined use of reactive and non-reactive tracers can be used to derive more detailed information about flow path geometry, i.e. circular or rectangular shape, when injected synchronously into the same sinkhole. However, flow path information is still integral with this approach, i.e. only average size and shape of the conduit can be derived with no information about the lateral changes in conduit geometry.

One way to learn more about the geometry of karst conduits is employing karst genesis simulations. These simulations focus on understanding the processes and different influences on karst development for being able to predict conduit positions and geometries. There are several parameters and boundary conditions that were recognized as key influences for karst genesis processes:

1. Initial **fracture spacing and apertures** have a high influence on the location of the preferential development of flow paths. A dense network of small fractures favours the development of caves at the water table, while widely spaced large fractures can lead to the development of deep phreatic loops, where the solution processes follows the dominant fractures (Ford and Ewers, 1978; Kaufmann, 2002; Ford, 2003). If a preferential path is already provided by a set of larger fractures the dissolution predominantly follows this path, even if other influences, e.g. water chemistry, do not necessarily favour it (Hückinghaus, 1998).
2. The **water chemistry**, especially the acidity and the Ca^{2+} saturation, are important for the rate of calcite dissolution. The dissolution capability of the recharged water is mainly provided by dissolved CO_2 from the atmosphere and the soil zone, but other acids can contribute if present (Bauer et al., 2003; Ford, 2003). The saturation with respect to Ca^{2+} in the different compartments, i.e. conduits and fissured matrix, and their exchange controls the location of preferential enlargement and the development rate to a large degree (e.g. Hückinghaus, 1998; Bauer et al., 2003; Liedl et al., 2003). If the chemical composition of mixing waters is different, mixing corrosion can enhance the dissolution significantly (e.g. Dreybrodt and Gabrovšek, 2003; Gabrovšek and Dreybrodt, 2010).
3. The **mode of recharge**, i.e. predominantly diffuse through the fissured matrix or localized by sinkholes or sinking streams, has a strong influence on the lateral widening of the conduits

and the choice of preferential flow paths (Hückinghaus, 1998; Liedl et al., 2003). Hückinghaus (1998) found that localized recharge favours the development of the down-gradient conduits for its fast flow through the vadose zone implies a comparatively low Ca^{2+} saturation. A good connection to other conduit branches or the fissured matrix carrying highly saturated water diminishes the effect (Hückinghaus, 1998; Bauer et al., 2003). Therefore, the rate of **water exchange** between fissured and conduit system is an important parameter. Liedl et al. (2003) showed a practically linear lateral increase of conduit diameter towards the spring that develops more gradually without direct recharge and stepwise for a distributed direct recharge component.

4. The **amount of recharge** and **elevations of discharge points** determine the hydraulic gradient of the system and therefore the position of the water table. In many karst genesis scenarios, the water table quickly drops to the elevation of the outlet when karstification increases the hydraulic conductivity of the aquifer. A high constant recharge or a constant head boundary condition can uphold a relatively high hydraulic gradient for extended periods of time and lead to the formation of steeply dipping conduits (Kaufmann, 2002). High recharge rates can also favour the evolution of maze-like cave systems (Kaufmann and Braun, 1999).

These investigations show that the development of karst aquifers is complex and depends on changing boundary conditions, making the prediction of karst conduit locations and geometries difficult. Therefore, simulations of karst genesis are often only applied to theoretical studies, instead of trying to approximate the conduit networks of actual field sites. However, combined with field observations, knowledge of karst genetic processes can help to estimate the plausibility of different conceptual scenarios.

1.2.3 Numerical modelling approaches

There are several publications giving overviews about the different modelling approaches applicable to karst aquifers (e.g. Teutsch and Sauter, 1991; Hartmann et al., 2014). Karst aquifers are mostly simulated with so-called lumped-parameter models. Those models view the aquifer as a whole and derive integral properties by use of integral input and output functions and integral aquifer parameters (e.g. Hartmann et al., 2013; Schmidt et al., 2014). The main advantage of these models is the relatively low demand on input data, which is usually rare in karst aquifers. The measurement of integral response functions can be conducted at the springs and is therefore relatively easy to derive in the field. Furthermore, lumped-parameter models require relatively little computer capacity and are therefore suited for automatic multi-parameter calibrations and the simulation of several

objective functions. Therefore, if physico-chemical spring water parameters such as temperature, electrical conductivity or environmental tracers are measured, they can easily be integrated into the models (e.g. Hartmann et al., 2013). However, these models are limited to effective aquifer parameters and cannot give any information on spatial distributions.

For spatially distributed information on aquifer characteristics and simulation objectives, e.g. groundwater residence times, distributed modelling approaches have to be applied. The basic approaches after Teutsch and Sauter (1991) are summarized in Figure 1.2. **Single continuum** models have the highest field applicability. They treat the whole aquifer system as a continuum with respect to flow and transport. If information on the location of the highly conductive conduit system is available, it can be integrated by assigning different hydraulic properties, e.g. a higher hydraulic conductivity, to one or more rows of grid cells (e.g. Reimann et al., 2011). However, the geometry of the conduit system depends on the grid size, possibly leading to excessive meshing requirements. If the conduit size is not representative of the real system, point-to-point connections might be possible to simulate, but flow velocities cannot be reproduced (e.g. Worthington, 2009). Furthermore, it is not possible to apply different flow equations for the lowly and highly conductive parts of the system, which necessitates alternative approaches for simulating turbulent flow in the conduit system (e.g. Reimann et al., 2012; Mayaud et al., 2014).

Double continuum approaches focus on the dual-permeability behaviour of karst aquifers and have become relatively popular for karst aquifer simulations in the past decades (e.g. Sauter, 1992; Maréchal et al., 2008; Kordilla et al., 2012). They represent the karst aquifer by two overlapping continua, one representing the fissured matrix and the other representing the conduit system. Those two continua are interconnected by a linear exchange term (Barenblatt et al., 1960). With this approach, the duality of flow can be simulated without the need of defining the conduit positions, limiting the amount of necessary input data. The information about spatial distributions and conduit parameters that can be derived from these models is limited, however, since they do not represent the conduit locations and geometries.

This is different for **discrete fracture/conduit** models. Those represent the discrete structures with one- or two-dimensional elements. They have a very high potential of representing the heterogeneities of the aquifer because, contrary to continuum models, two points lying directly next to each other can have completely different properties. The discrete fracture sets for discrete fracture models are usually generated with stochastic approaches (e.g. Dershovitz et al., 1991). This introduces a certain degree of spatial uncertainty (Kovács and Sauter, 2007). The matrix blocks between the discrete elements are treated as impermeable. Therefore, a realistic model requires the representation of all fractures allowing groundwater flow as discrete elements. This is one of the

major drawbacks of the approach, since computer capacity severely limits the amount of fractures that can be simulated, leading often to the neglect of minor fissures that contribute to groundwater flow (Kovács and Sauter, 2007).

Hybrid models combine the continuum and the discrete approach. They represent the karst conduit system by discrete one-dimensional elements while the fissured matrix is simulated with a continuum approach. This allows for the direct consideration of karst conduit parameters, geometries and flow laws without the need to explicitly take each fracture in the aquifer into consideration. On the scheme of balance between model complexity and the ability to represent karst aquifer heterogeneity developed by Teutsch and Sauter (1991), hybrid models take an intermediate position (Figure 1.2). Their ability to represent the processes inside the conduit system and the conduit geometry and at the same time take into account water and solute exchange with the fissured matrix makes hybrid models the standard approach for karst genesis scenario simulations (e.g. Liedl et al., 2003). They are rarely applied to natural systems, however, since the required amount of input data is relatively high and especially data on the conduit geometry and positions is usually scarce or not available (Reimann et al., 2011).

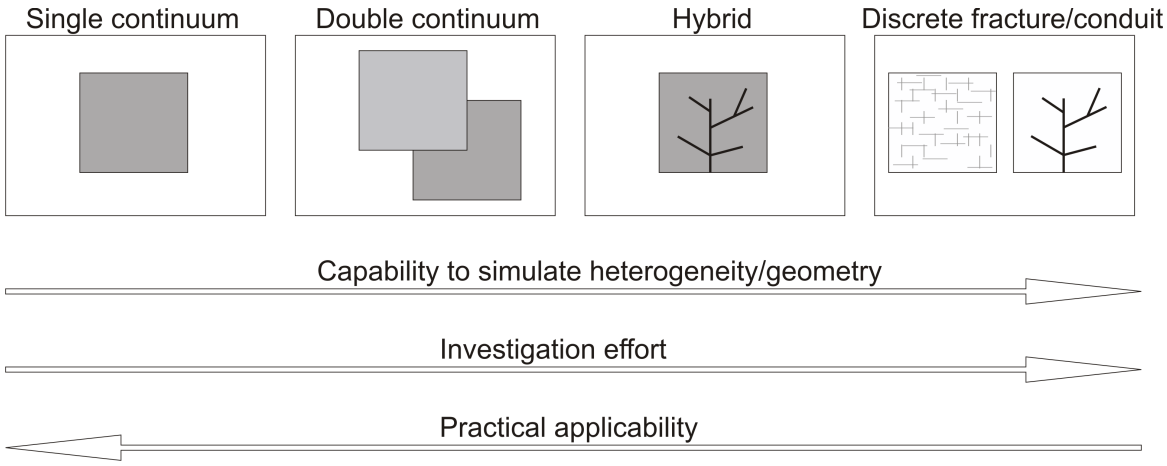

Figure 1.2 Distributive numerical modeling approaches for karst aquifers (modified after Teutsch and Sauter, 1991).

1.3 Field site and data availability

The field site was chosen with regard to available input data. The Gallusquelle area on the Swabian Alb in south-western Germany (Figure 1.3) was already the subject of numerous field investigations and numerical models (e.g. Sauter, 1992; Doummar et al., 2012; Mohrlok, 2014). The Gallusquelle spring, a perennial karst spring with an average annual discharge of 0.5 $m^3 s^{-1}$, is the main point

outlet of the 150 km^2 large model area. The assumed catchment of the Gallusquelle (Figure 1.3) encompasses an area of ca. 45 km^2 and was derived by Villinger (1977) and Sauter (1992) based on the water balance, hydraulic head data and tracer tests. The spring discharge of the Gallusquelle is documented on a daily basis since 1955 by the *Landesanstalt für Umwelt, Messungen und Naturschutz Baden-Württemberg* (LUBW). The spring discharge varied between less than 0.1 $m^3 s^{-1}$ and ca. 2.6 $m^3 s^{-1}$ in this time period. In the vicinity of the Gallusquelle, several minor springs and spring groups exist. Figure 1.3 shows the ones for which data on flow paths or average annual spring discharge is available.

The annual precipitation in the model area varies between 600 and 1 200 mm yr^{-1}. Sauter (1992) calculated the groundwater recharge for the time period from 1965 to 1990 and Geyer (2008) extended the calculations for the years 1955 to 2005. Both derived an average recharge of ca. 1 mm d^{-1}. The authors also approximated the percentage of direct recharge, which lay for all calculations between 5% and 10%. The hydraulic head distribution in the model area is monitored by 20 observation wells (Figure 1.3).

The stratigraphy of the Gallusquelle aquifer is described in detail by Golwer (1978) and Gwinner (1993). Except for quaternary sediments which fill the valleys and are only of minor importance for the groundwater flow, the area consists of Upper Jurassic limestone, the whole sequence dipping to the south-east with approximately 1.2°. Massive limestones of the Kimmeridgium 2 and 3 compose the main part of the aquifer. The less soluble marly limestones of the Kimmeridgium 1 act as an aquitard in the eastern part of the area. In the central area, where they lie closer to the ground surface, they are also karstified and contribute to the aquifer (Villinger, 1977; Sauter 1992). In the west of the area, the karst aquifer cuts into the layered limestone of the underlying Oxfordian 2 (Villinger, 1977; Sauter, 1992).

The stratigraphic sequence is displaced by two major fault zones (Figure 1.3). The Hohenzollerngraben lies in the central part of the model area striking northwest-southeast. The Lauchertgraben strikes north-south and lies in the west of the area. Both graben structures have maximal displacements of up to 100 m (Golwer, 1978; Gwinner, 1993). There is no information about the hydraulic properties of the Lauchertgraben fault zones. The Hohenzollerngraben was crossed by tunnelling work for a regional water pipeline and the northern boundary fault was found to be highly conductive by the high amount of water entering the tunnel (Gwinner, 1993).

The locations of the highly conductive conduit system of the Gallusquelle were derived by Mohrlok and Sauter (1997) and adapted by Doummar et al. (2012) based on surface lineaments, dry valleys, sinkholes and the qualitative evaluation of tracer tests (Figure 1.3). A total of 40 tracer tests is

documented in the model area, 35 of which were observed at one or more outlets, 19 of those were registered at the Gallusquelle (Merkel, 1991; Sauter, 1992; Birk et al., 2005; Geyer et al., 2007; Reiber et al., 2010; Hillebrand et al., 2012, 2015). Different conservative and reactive substances were used to gain information on flow velocities, dispersion coefficients and degradation rates. Sauter (1992) concluded from an analysis of conduit flow velocity and spring discharge for several recharge events and tracer tests, that the karst conduits are fully phreatic. Geyer et al. (2008) estimated the maximum volume of the conduit system feeding the Gallusquelle with an artificial tracer test to be in the range of 200 000 m^3. Birk et al. (2005) assessed the volume for the last segment of the conduit system, i.e. the last 3 km, with another tracer test and different calculation methods. The authors derived a volume of 42 000 m^3 to 70 000 m^3 depending on the applied method. In addition to the artificial tracer tests, Geyer (2008) analysed different environmental tracers and estimated the average groundwater age at the Gallusquelle to be in the range of 3 to 4 years.

The hydraulic conductivity and the effective porosity of the aquifer were estimated by Sauter (1992) with different investigation methods. The author derived a hydraulic conductivity of 1×10^{-6} m s^{-1} to 2×10^{-5} m s^{-1} on the local scale, i.e. with borehole tests, and 2×10^{-5} m s^{-1} to 1×10^{-4} m s^{-1} on the regional scale. The effective porosity for the fissured matrix was estimated to be 1–2 %.

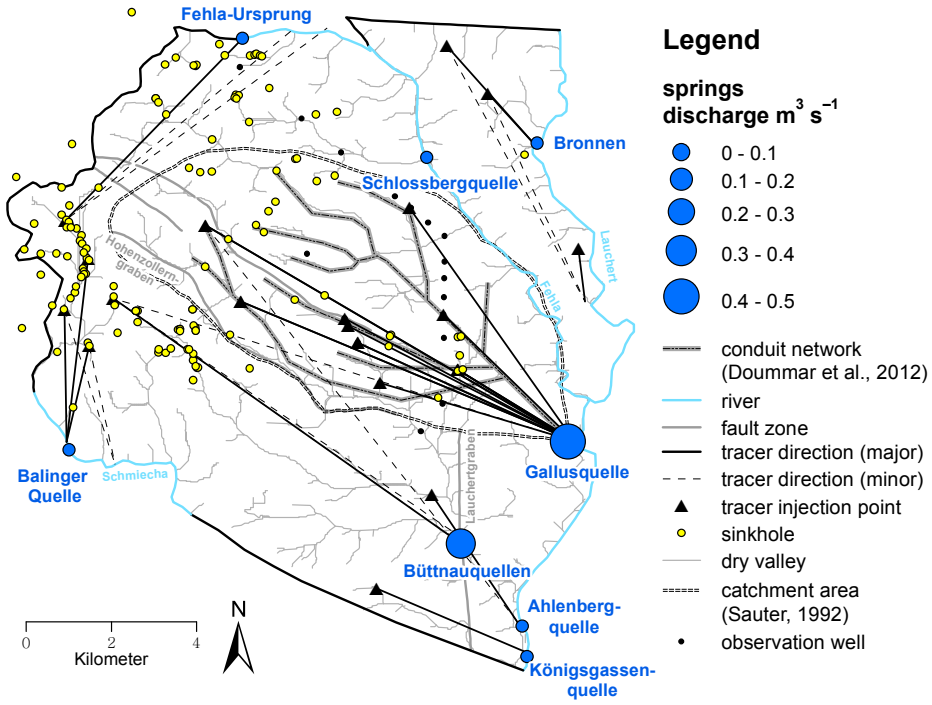

Figure 1.3. Top view of the model area. The karst conduit network of Doummar et al. 2012 is based on the prior work of Mohrlok and Sauter (1997).

1.4 Format of the thesis

This thesis aims at developing a modelling approach for the distributed simulation of aquifer parameters and residence times and applying it directly for the chosen field site. The model development and application is structured in several chapters focusing on different objective functions. The model complexity gradually increases for the different modelling steps clearly outlining which degree of complexity is necessary for which simulation objectives. The value for aquifer characterization is discussed for each sub-model.

In *Chapter 2* different distributed modelling approaches are tested for simulating the catchment areas of the main springs in the model area. A focus is set on the representation of aquifer heterogeneities and their influence on the flow system and spring discharge. The objective functions for model calibration are the average hydraulic head distribution derived from 20 observation wells and the average spring discharge of five springs.

In *Chapter 3* the groundwater flow simulation is coupled to a transport interface. Two artificial tracer tests are employed for calibrating the flow velocity distribution inside the conduit system and as a consequence, approximating the conduit system geometry and total conduit volume.

Chapter 4 presents a new approach for simulating the groundwater residence time distribution in all three porosities of a karst aquifer. The approach is applied to two simplified karst aquifer scenarios for analysing parameter sensitivity. The sensitivity analysis provides data on the most important field measurements for residence time simulations and on the possibility of such simulations for assisting aquifer characterization. A comparison of the transit time distribution curve at the spring with the ones derived by traditional lumped-parameter models is provided to check the effect of considering all three porosities explicitly.

In *Chapter 5* the approach developed in Chapter 4 is applied to the Gallusquelle aquifer model developed in Chapters 2 and 3. A groundwater residence time model is presented for the whole aquifer system and uncertainties and possibilities for aquifer characterization are discussed.

The thesis is finalized by *Chapter 6* summarizing the general conclusions and giving an outlook for future perspectives and research possibilities.

Due to the cumulative nature of the thesis, references are given at the end of each chapter. Due to formal consistency reasons and a few formal corrections, the chapters can deviate slightly from the original publications.

References

Barenblatt, G. I., Zheltov, I. P., and Kochina, I. N., 1960. Basic concepts in the theory of seepage of homogeneous liquids in fissured rocks (strata). Journal of Applied Mathematics and Mechanics 24 (5), 1286–1303.

Bauer, S., Liedl, R., and Sauter, M.. 2003. Modeling of karst aquifer genesis: Influence of exchange flow. Water Resources Research 39 (10), 1285, doi:10.1029/2003WR002218.

Birk, S., Geyer, T., Liedl, R., and Sauter, M., 2005. Process-based interpretation of tracer tests in carbonate aquifers. Ground Water 43 (3), 381–388.

Cornaton, F., 2004. Deterministic models of groundwater age, life expectancy and transit time distributions in advective-dispersive systems. Ph.D. thesis, University of Neuchâtal.

Doummar, J., Sauter, M., and Geyer, T., 2012. Simulation of flow processes in a large scale karst system with an integrated catchment model (Mike She) – Identification of relevant parameters influencing spring discharge. Journal of Hydrology 426–427, 112–123, doi:10.1016/j.jhydrol.2012.01.021.

Dreybrodt, W. and Gabrovšek, F., 2003. Basic processes and mechanisms governing the evolution of karst. Speleogenesis and Evolution of Karst Aquifers 1, 1–26.

Ford, D. C., 2003. Perspectives in karst hydrogeology and cavern genesis. Speleogenesis and Evolution of Karst Aquifers 1 (1), 1–12.

Ford, D. C. and Ewers, R. O., 1978. The development of limestone cave systems in the dimensions of length and depth. International Journal of Speleology 10, 213–244.

Ford, D.C. and Williams, P.W., 2007. Karst geomorphology and hydrology. Wiley, West Sussex, 562 pp.

Gabrovšek, F. and Dreybrodt, W., 2010. Karstification in unconfined limestone aquifers by mixing phreatic water with surface water from a local input: A model. Journal of Hydrology 386, 130–141.

Geyer, T., 2008. Process-based characterisation of flow and transport in karst aquifers at catchment scale. Ph.D. thesis, University of Göttingen.

Geyer, T., Birk, S., Liedl, R., and Sauter, M., 2008. Quantification of temporal distribution of recharge in karst systems from spring hydrographs. Journal of Hydrology 348, 452–463.

Geyer, T., Birk, S., Reimann, T., Dörfliger, N., and Sauter, M., 2013. Differentiated characterization of karst aquifers: some contributions. Carbonates and Evaporites 28, 41–46, doi:10.1007/s13146-013-0150-9.

Golwer, A., 1978. Erläuterungen zu Blatt 7821 Veringenstadt, Geologische Karte 1 : 25 000 von Baden-Württemberg. Geologisches Landesamt Baden-Württemberg, Stuttgart, 151 pp..

Gwinner, M. P., 1993. Erläuterungen zu Blatt 7721 Gammertingen, Geologische Karte 1 : 25 000 von Baden-Württemberg. Geologisches Landesamt Baden-Württemberg, Freiburg/Stuttgart, 78 pp.

Hartmann, A., Weiler, M., Wagener, T., Lange, J., Kralik, M., Humer, F., Mizyed, N., Rimmer, A., Barberá, J. A., Andreo, B., Butscher, C., and Huggenberger, P., 2013. Process-based karst modelling to relate hydrodynamics and hydrochemical characteristics to system properties. Hydrology and Earth System Sciences 17, 3305–3321, doi: 10.5194/hess-17-3305-2013.

Hartmann, A., Goldscheider, N., Wagener, T., Lange, J., and Weiler, M., 2014. Karst water resources in a changing world: Review of hydrological modeling approaches. Reviews of Geyophysics 52, doi: 10.1002/2013RG000443.

Hillebrand, O., Nödler, K., Geyer, T., and Licha, T., 2014: Investigating the dynamics of two herbicides at a karst spring in Germany: Consequences for sustainable raw water management. Science of the Total Environment 482–483, 193–200.

Hückinghaus, D., 1998. Simulation der Aquifergenese und des Wärmetransports in Karstaquiferen. Tübinger Geowissenschaftliche Arbeiten C42, Tübingen.

Jeannin, P. Y., 2001. Modeling flow in phreatic and epiphreatic karst conduits in the Hölloch cave (Muotatal, Switzerland). Water Resources Research 37 (2), 191–200.

Joodi, A. S., Sizaret, S., Binet, S., Bruand, A., Alberic, P., and Lepiller, M., 2010. Development of a Darcy-Brinkman model to simulate water flow and tracer transport in a heterogeneous karstic aquifer (Val d'Orléans, France). Hydrogeology Journal 18, 295–309, doi:10.1007/s10040-009.0536-x.

Kaufmann, G., 2002. Karst aquifer evolution in a changing water table environment. Water Resources Research 38 (6), 1090, doi:10.1029/2001WR000256.

Kaufmann, G. and Braun, J., 1999. Karst aquifer evolution in fractured rocks. Water Resources. Research 35 (11), 3223–3238.

Király, L., 1998. Modelling karst aquifers by the combined discrete channel and continuum approach. Bulletin d'Hydrogéologie 16, 77–98, Centre d'Hydrogéologie, Université Neuchâtel.

Király, L, 2002. Karstification and groundwater flow. Evolution of karst: from prekarst to cessation, 155–190, Ljubljana-Postojna.

Kovács, A. and Sauter, M., 2007. Modelling karst hydrodynamics. In: Methods in karst hydrogeology, International contributions to hydrogeology 26, editors: Goldscheider, N. and Drew, D., 201–222, Taylor and Fracis, London.

Liedl, R., Sauter, M., Hückinghaus, D., Clemens, T., and Teutsch, G., 2003. Simulation of the development of karst aquifers using a coupled continuum pipe flow model. Water Resources Research 39 (3), 1057, doi:10.1029/2001WR001206.

Luhmann, A. J., Covington, M. D., Alexander, S. C., Chai, S. Y., Schwartz, B. F., Groten, J. T., and Alexander, E. C., 2012. Comparing conservative and nonconservative tracers in karst and using them to estimate flow path geometry. Journal of Hydrology 448–449, 201–211, doi:10.1016/j.jhydrol.2012.04.044.

Maréchal, J. C., Ladouche, B., Dörfliger, N., and Lachassagne, P., 2008. Interpretation of pumping tests in a mixed flow karst system, Water Resources Research 44, W05401, doi:10.1029/2007WR006288.

Maurice, L. D., Atkinson, T. C., Barker, J. A., Bloomfield, J. P., Farrant, A. R., and Williams, A. T., 2006. Karstic behaviour of groundwater in English Chalk. Journal of Hydrology 330, 63–70.

Mayaud, C., Walker, P., Hergarten, S., and Birk, S., 2014. Nonlinear Flow Process: A New Package to Compute Nonlinear Flow in MODFLOW. Ground Water 1–6, doi:10.1111/gwat.12243.

Mohrlok, U., 2014. Numerische Modellierung der Grundwasserströmung im Einzugsgebiet der Gallusquelle unter Festlegung eines Drainagesystems. Grundwasser 19, 73–85, doi:10.1007/s00767-013-0249-x.

Mohrlok, U. and Sauter, M., 1997. Modelling groundwater flow in a karst terraine using discrete and double-continuum approaches: importance of spatial and temporal distribution of recharge. In: Proceedings of the 12th International Congress of Speology, 2/6th Conference on

Limestone Hydrology and Fissured Media, La Chaux-de-Fonds, Switzerland, 10–17 August 1997, 167–170.

Perrin, J., Pochon, A., Jeannin, P.-Y., and Zwahlen, F., 2004. Vulnerability assessment in karstic areas: validation by field experiments. Environmental Geology 46 (2), 237–245.

Rehrl, C. and Birk, S., 2010. Hydrogeological characterisation and modelling of spring catchments in a changing environment. Austrian Journal of Earth Sciences 103 (2), 106–117, Vienna.

Reiber, H., Klein, F., Selg, M., and Heidland, S., 2010. Hydrogeologische Erkundung Baden-Württemberg – Mittlere Alb 4 – Markierungsversuche, Abwassereinleitungen. Landesamt für Umwelt, Messungen und Naturschutz Baden-Württemberg, Tübingen, 71 pp.

Reimann, T., Rehrl, C., Shoemaker, W. B., Geyer, T., and Birk, S., 2011. The significance of turbulent flow representation in single-continuum models. Water Resources Research 47, W09503, doi:10.1029/2010WR010133.

Reimann, T., Birk, S., Rehrl, C., and Showmaker W. B., 2012. Modifications to the Conduit Flow Process Mode 2 for MODFLOW-2005. Ground Water 50 (1), 144–148.

Sauter, M., 1991. Assessment of hydraulic conductivity in a karst aquifer at local and at regional scale. 3rd conference on Hydrogeology, Ecology, Monitoring and Management of Ground Water in Karst Terranes, U.S. Environ. Prot. Agency, Nashville, USA.

Sauter, M., 1992. Quantification and forecasting of regional groundwater flow and transport in a karst aquifer (Gallusqulle, Malm, SW Germany). Tübinger Geowissenschaftliche Arbeiten C13, Tübingen.

Schmidt, S., Geyer, T., Guttman, J., Marei, A., Ries, F. and Sauter, M., 2014. Characterisation and modelling of conduit restricted karst aquifers – Example of the Auja spring, Jordan Valley. Journal of Hydrology 511, 750–763, doi:10.1016/j.jhydrol.2014.02.019.

Teutsch, G. and Sauter, M.,1991. Groundwater modeling in karst terranes: scale effects, data aquisition and field validatio. In: Proceedings of the 3rd Conference on Hydrogeology, Ecology, Monitoring and Management of Ground Water in Karst Terranes, 4–6 December 1991, Nashville, USA, 17–34.

Villinger, E., 1977. Über die Potentialverteilung und Strömungssysteme im Karstwasser der Schwäbischen Alb (Oberer Jura, SW-Deutschland). Geologisches Jahrbuch C18, Hannover.

Worthington, S. R. H., Ford, D. C., and Beddows, P. A., 2000. Porosity and Permeability Enhancement in Unconfined Carbonate Aquifers as a Result of Solution. In: Speleogenesis — Evolution of Karst Aquifers, edited by Klimchouk et al., 463–472, Natl. Geol. Soc., Huntsville, Alabama.

Worthington, S. R. H., 2009. Diagnostic hydrogeologic characteristics of a karst aquifer (Kentucky, USA). Hydrogeology Journal 17, 1665–1678, doi: 10.007/s10040-009-0489-0.

Worthington, S. R. H. and Ford, D. C., 2009. Self-Organized Permeability in Carbonate Aquifers. Ground Water 47 (3), 326–336.

Chapter 2

2 Influence of aquifer heterogeneity on karst hydraulics and catchment delineation employing distributive modeling approaches

Sandra Oehlmann[a], Tobias Geyer[a], Tobias Licha[a], Steffen Birk[b]

Citation:

Oehlmann, S., Geyer, T., Licha, T., and Birk, S., 2013. Influence of aquifer heterogeneity on karst hydraulics and catchment delineation employing distributive modeling approaches. Hydrology and Earth System Sciences 17, 4729–4742, doi:10.5194/hess-17-4729-2013.

[a]Geoscience Center, University of Göttingen, Göttingen, Germany

[b]Institute for Earth Sciences, University of Graz, Austria

Abstract

Due to their heterogeneous nature, karst aquifers pose a major challenge for hydrogeological investigations. Important procedures like the delineation of catchment areas for springs are hindered by the unknown locations and hydraulic properties of highly conductive karstic zones.

In this work numerical modeling was employed as a tool in delineating catchment areas of several springs within a karst area in southwestern Germany. For this purpose, different distributive modeling approaches were implemented in the finite element simulation software Comsol Multiphysics®. The investigation focuses on the question to which degree the effect of karstification has to be taken into account for accurately simulating the hydraulic head distribution and the observed spring discharges.

The results reveal that the representation of heterogeneities has a large influence on the delineation of the catchment areas. Not only the location of highly conductive elements but also their geometries play a major role for the resulting hydraulic head distribution and thus for catchment area delineation. The size distribution of the karst conduits derived from the numerical models agrees with knowledge from karst genesis. It was thus shown that numerical modeling is a useful tool for catchment delineation in karst aquifers based on results from different field observations.

2.1 Introduction

Karst aquifers are strongly heterogeneous systems due to a local development of large-scale discontinuities such as conduit systems. This heterogeneity also causes a large anisotropy in the hydraulic parameter field. Conceptually, karst aquifers can be described as dual-flow systems consisting of a fissured matrix with a relatively low hydraulic conductivity and highly conductive karst conduits (Liedl et al., 2003). A characteristic attribute of many karst aquifers is their high discharge focused to large springs. This makes them especially interesting as drinking water resources. However, the delineation of catchment areas of karst springs is still a challenge because of the usually unknown location of large-scale heterogeneities, such as karst conduits, within the aquifer. Common approaches for catchment delineation in porous aquifers like the mapping of geomorphological and topographical features and water balance approaches (Goldscheider and Drew, 2007) are only of limited use in karst systems. Delineating catchment areas from hydraulic head contour lines requires an observation well network, which covers the highly conductive conduit system. On groundwater catchment scale these data are scarce in carbonate areas (Sauter, 1992). Artificial tracer tests provide information about point-to-point connections, but the practical restrictions of tracer investigations prevent using them for completely defining the catchment area.

In addition, catchment areas may change under different hydrological conditions further complicating the issue.

Numerical groundwater flow simulations are process-based tools that can be used for combining results from different investigation methods (Geyer et al., 2013) and for augmenting them with physical equations (Birk et al., 2005). There are numerous simulation approaches, which are applicable for karst aquifers. Single continuum models assume the aquifer to be a porous medium that can be divided into representative elementary volumes (REV) (Bachmat and Bear, 1986). The dual flow characteristics of karst aquifers are directly addressed by hybrid or double continuum modeling approaches. Double continuum models simulate groundwater flow in two separate overlapping continua: a matrix continuum and a conduit continuum, linked via a linear exchange term (Teutsch, 1989; Mohrlok and Sauter, 1997). Hybrid models include the spatial distribution of local discrete pipe elements representing the major karst conduits coupled to a matrix continuum which represents the properties of the low permeability fissured matrix blocks (Liedl et al., 2003; Birk et al., 2005). Due to the required detailed information and the relatively high numerical effort, the application of hybrid modeling approaches to real karst systems is rare (Reimann et al., 2011a). The highest accuracy regarding the description of aquifer heterogeneities is achieved by discrete multiple fracture set models which represent the fissured system as well as the conduit system as a set of discrete fissures. Due to the intense investigation effort required for characterizing the discrete pathways they are practically not applicable for catchment studies (Teutsch and Sauter, 1991). Thus, the question which degree of complexity within the numerical model is necessary for achieving the aim of the investigation is of primary importance since more complex models require more specific information about the model area and higher numerical effort.

This work analyzes how distributive numerical models can be used to support the delineation of catchment areas of karst springs. The proposed novel approach is illustrated using a karst area in southwestern Germany. It is based on the evaluation of the influence of different types of aquifer heterogeneity on the karst flow system. More specifically, the interdependencies between hydraulic head distribution, hydraulic parameters and spring discharges are examined. For this purpose, a homogeneous continuum model and hybrid modeling approaches for flow simulation of a large-scale karst system were set up employing the finite element simulation software Comsol Multiphysics®. These two different modeling approaches were chosen since the geometry of the highly conductive conduits was of special interest in this study because of their potential impact on the delineation of the catchment areas. Simulating the conduit geometry with the single continuum approach would have required intense meshing along the karst conduits needing a very flexible mesh and being numerically highly demanding. Steady state flow equations were implemented for both model types.

The three-dimensional geometry of the aquifer system was geologically modeled with the software Geological Objects Computer Aided Design® (GoCAD®) and transferred to the Comsol® software.

2.2 Methods and Approach

Comsol Multiphysics® is a software that conducts multiphysical simulations using the Finite Element Method (FEM). The different physical properties and equations are stored in different modules, which can be coupled and adapted as required. The interfaces used in this work belong to the Subsurface Flow Module, which provides equations for modeling flow in porous media, and to the basic module. The basic module includes interfaces, where mathematical equations can be defined by the user and employed for any physical application. This concept is described in more detail for scenario 3 (Chapter 2.2.3). All simulations were performed in the stationary mode, thus neglecting storage effects. Simulations were performed three-dimensionally. To examine the effects of different types of heterogeneity several scenarios were set up including more and more characteristic features of karst catchments. Figure 2.1 schematically shows the simulated scenarios. Catchment areas were derived by importing the simulated water tables from Comsol® to ArcGIS® 10.0 and using the default hydrology tools. Generally, those are used for deriving catchment areas from topographic lines. Since the concept of water flowing towards the lower potential is true for groundwater as well as for surface water, they can be likewise used for delineating groundwater catchments from groundwater contour maps.

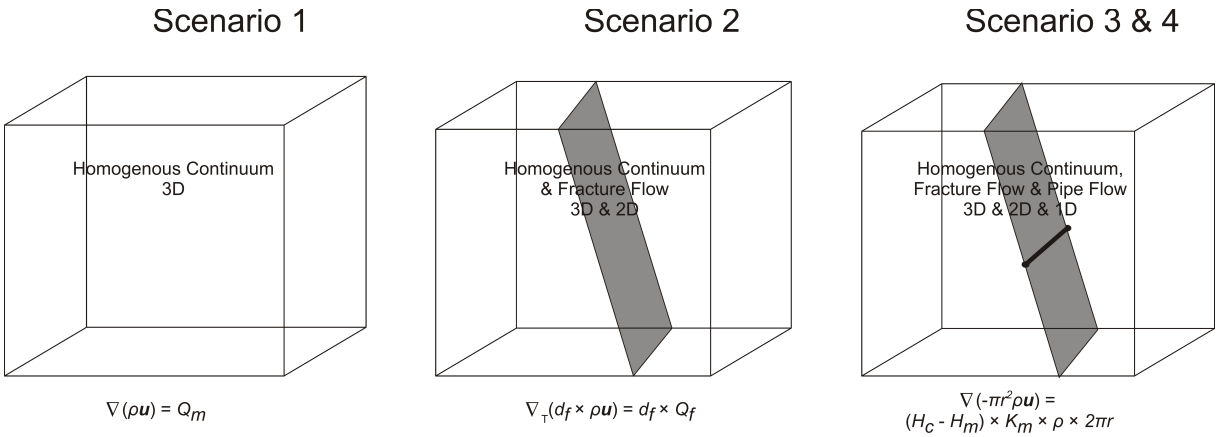

Figure 2.1. Conceptual geometry of the simulated scenarios. For explanation of the flow equations see scenario description in Chapter 2.

2.2.1 Scenario 1

Scenario 1 simulates a completely homogenous case. It takes into account the thickness of the aquifer and boundary conditions given by rivers and surface water divides. Recharge and hydraulic conductivity were kept constant throughout the area. For the flow simulation the Darcy's Law Interface of the Subsurface Flow Module was used. It calculates the fluid pressure p [M $L^{-1} T^{-2}$] within the model domain with the Darcy equation (Eq. 2.1a and b).

$$Q_m = \nabla(\rho \boldsymbol{u}) \tag{2.1a}$$

$$\boldsymbol{u} = -\frac{K_m}{\rho g}(\nabla p + \rho g \nabla D) \tag{2.1b}$$

In these equations Q_m is the mass source term [M $L^{-3} T^{-1}$], ρ is the density of the fluid [M L^{-3}], K_m is the hydraulic conductivity of the matrix [L T^{-1}] and $\boldsymbol{u}$ the Darcy velocity [L T^{-1}]. g is the magnitude of gravitational acceleration [L T^{-2}] and ∇D is a unit vector in the direction over which the gravity acts. The hydraulic conductivity K_m is the only calibration parameter in this scenario.

2.2.2 Scenario 2

Scenario 2 includes a highly conductive fracture simulated as a discrete vertical 2D element embedded in the three-dimensional continuum model. The 2D element, in this case, represents a large-scale fault zone observed from geological mapping within the area of investigation. The continuum represents the fissured matrix of the karst aquifer. Groundwater flow in the fracture was simulated with the Fracture Flow Interface of the Subsurface Flow Module implemented in Comsol®. The module requires the definition of the fracture aperture d_f [L] and hydraulic conductivity K_f [LT^{-1}] inside the fracture. Comsol® assumes that flow processes in the fracture are basically the same as in the surrounding matrix and calculates flow along the fracture with the tangential version of the Darcy equation. The Fracture Flow Module does not allow the application of different flow laws in the two regions. To simulate two-dimensional fracture flow the term for the fracture aperture is multiplied with both sides of Eq. (2.1):

$$d_f \times Q_f = \nabla_{\mathrm{T}}(d_f \rho \boldsymbol{u}) \tag{2.2a}$$

$$\boldsymbol{u} = -\frac{K_f}{\rho g}(\nabla_{\mathrm{T}} p + \rho g \nabla_{\mathrm{T}} D) \tag{2.2b}$$

with Q_f being the mass source term for the fracture [M $L^{-3} T^{-1}$] and ∇_{T} the tangential gradient operator. The hydraulic conductivity of the fracture K_f is the second calibration parameter beside the matrix conductivity K_m (Eq. 2.1b) in scenario 2.

2.2.3 Scenario 3

In scenario 3, highly conductive conduits were included along the positions of dry valleys, which are believed to be former riverbeds that have dried up during karstification. For these, 1D structures are the most fitting representation. Since the Subsurface Flow Module does not offer a similar functionality as Fracture Flow for 1D elements in 3D domains, a hybrid model was set up employing Comsol's PDE Interfaces for simulation of one-dimensional pipes. The interface chosen is called Coefficient Form Edge PDE because it allows calculations along the edges (1D elements) of a 3D model. The interface offers a partial differential equation (PDE) (Eq. 2.3) for which coefficients have to be defined.

$$f = \nabla(-c\nabla v + \gamma) \tag{2.3}$$

In Eq. (2.3), c is defined as the diffusion coefficient, γ as the conservative flux source and f as the source term. By default, the source term is dimensionless. Its unit can be defined in the interface and the units of the coefficients are then calculated accordingly. v is the dependent variable in this equation. In the application using Darcy Flow, v corresponds to the pressure p [M L^{-1} T^{-2}]. The source term f equals the mass source term Q_m of the Darcy equation (Eq. 2.1a). The first of the remaining terms describes the effect of water pressure gradients, the other the effect of gravitation (compare Eq. 2.1b). In this case the diffusion coefficient c depends on the hydraulic conduit conductivity K_c, which is normalized for a unit cross-sectional area. Thus, after multiplying with the conduit area πr^2 Eq. (2.3) translates to Eq. (2.4). The conduit area term replaces the two missing dimensions while performing simulations in 1D elements in a 3D domain.

$$\pi r^2 \times Q_m = \nabla\left(-\pi r^2 \frac{K_c}{g}\nabla p - \pi r^2 \rho K_c \nabla D\right) \tag{2.4}$$

The source term multiplied with the conduit area $\pi r^2 \times Q_m$ is equal to the mass exchange of water per unit length between the matrix and the conduit [M L^{-1} T^{-1}]. Reimann et al. (2011b) define the exchange term between a karst conduit and the rock matrix as

$$q_{ex} = \frac{K\prime}{b\prime} \times P_{ex} \Delta h_{ex}. \tag{2.5}$$

q_{ex} is the exchange flow per unit length [L^2 T^{-1}], Δh_{ex} is the difference between the hydraulic head in the matrix and the hydraulic head in the conduit [L], P_{ex} the exchange perimeter [L] and K′/b′ the leakage coefficient [T^{-1}]. For this simulation the equation was simplified by assuming the exchange perimeter equal to the pipe perimeter. Assuming there is no barrier between the conduit and the matrix, the leakage coefficient is equal to the hydraulic conductivity of the matrix divided by the theoretical distance b' [L] over which the hydraulic head difference is calculated. b' is kept at unit

length throughout the simulation. The equation given by Reimann et al. (2011b) is multiplied by the density for obtaining the mass exchange term. The resulting exchange equation is defined in Eq. (2.6):

$$\pi r^2 \times Q_m = (H_c - H_m) \times \frac{K_m}{b'} \times \rho \times 2\pi r \quad (2.6)$$

with H_c being the hydraulic head in the conduit and H_m being the hydraulic head in the matrix [L]. $2\pi r$ is the perimeter of the pipe [L]. The exchange term is used as mass flux for the matrix and as mass source for the conduits with a changed algebraic sign. Dirichlet conditions were set as boundary conditions at the springs.

2.2.4 Scenario 4

Scenario 4 was based on the same structure of the conduit system as scenario 3 but differed in the assumption for the conduit radius. While for scenario 3 the radius is constant within the entire conduit system, for scenario 4 a change in conduit radius towards the spring was introduced. Liedl et al. (2003) showed with their karst genesis simulations that for a conduit derived from solution processes a change in diameter is likely to occur along its extent. They introduced several simulations with different boundary conditions and derived different types of solutional widening and resulting conduit shapes.

For situations where diffuse recharge prevails, Liedl et al. (2003) showed a nearly linear increase in conduit diameters towards a karst spring. Thus, in scenario 4 a linear widening function was applied to each conduit along its length. At each intersection the radii of both branches were added to account for the larger volume of water flowing there. The largest simulated radius is 4.6 m at the main karst spring.

2.3 Field site

Simulations were performed for several karst springs located at the Swabian Alb in southwestern Germany (Figure 2.2). The Gallusquelle spring is the largest of the springs located within the investigation area of approximately 150 km^2 (Figure 2.3). The size of its catchment area is estimated to be 45 km^2 based on a water balance approach and artificial tracer tests (Sauter, 1992) (Figure 2.3). The spring is used for drinking water supply of approximately 40 000 people and has an average annual discharge of 0.5 m^3 s^{-1}. It is a suitable location for distributive karst modeling due to the extensive studies that have been conducted in the area before (e.g. Sauter, 1992; Geyer et al., 2007; Hillebrand et al., 2012).

Geologically the area consists of Upper Jurassic limestone and marlstone. The main aquifer is composed primarily of massive and layered limestone of the Kimmeridgian 2 and 3 (ki2/3), which are dominated by an algal sponge bioherm facies (Sauter, 1992). Beneath those rocks there are marly limestones and marlstones of the Kimmeridgian 1 (ki1) which mainly act as aquitards due to their lower hydraulic conductivity. The whole sequence dips with approximately 1.2° to the southeast (Sauter, 1992).

Two major fault zones cross the model area. The Hohenzollerngraben strikes northwest to southeast, the Lauchertgraben crosses the area in the east striking north to south (Figure 2.2). While there is no information about the hydraulic conductivity of the Lauchertgraben fault zones, the Hohenzollerngraben was crossed by tunneling work related to the construction of a regional water pipeline (Albstollen, Bodensee-Wasserversorgung). The northern boundary fault was found to be highly conductive from the significant amount of water entering the tunnel while crossing it (Gwinner et al., 1993). A high hydraulic conductivity of this zone can further be assumed from the fact that the Gallusquelle spring lies exactly at the extension of this fault where it meets the river Lauchert (Figure 2.2). Parts of the area show intense fracturing. There are two main fracture directions, one with a strike of 0–30° and one with a strike of 100–140° parallel to the Hohenzollerngraben (Sauter, 1992).

The average hydraulic heads in the area were derived by Sauter (1992) for the period 1965–1990. The total range of hydraulic head variations during this time differs between 6 m and 20 m depending on the observation well (Sauter, 1992). The monthly rainfall varied from less than 10 mm to more than 180 mm and the annual rainfall from about 600 mm a^{-1} to 1 200 mm a^{-1}. Even though these variations are high, Villinger (1977) deduced, that the boundaries of the catchment area for the Gallusquelle spring do not change significantly throughout the year. His analysis is based on equipotential maps constructed from hydraulic head measurements for high and low water levels in the area. Furthermore, several artificial tracer tests especially in the west of the area were repeated under different flow conditions and showed little to no alteration in flow directions.

2.4 Model design and calibration

The model area is constrained by fixed head boundaries at the rivers Lauchert, Fehla and Schmiecha (Dirichlet boundaries). No flow boundaries are derived from the dip of the aquifer base and artificial tracer test information (Figure 2.3). The size of the model area is about 150 km^2. The assumed catchment area of the Gallusquelle spring lies completely within the model area (Figure 2.2). The positions of dry valleys were adapted after Gwinner et al. (1993). Highly conductive pipes connected

to the Gallusquelle spring were implemented according to Mohrlok and Sauter (1997) and Doummar et al. (2012). The lateral positions of model boundaries, highly conductive faults and the pipe network along dry valleys were constructed in ArcGIS® 10.0 and imported to Comsol® as 2D dxf-files or interpolation curves. Vertically, the highly conductive conduits were positioned approximately at the elevation of the water table simulated in scenario 1. Lacking other information, it was assumed that the homogeneously simulated water table roughly represents the one existing during the onset of karstification. Therefore, the conduits lie between 710 m and 600 m a.s.l. with a dip towards the springs. The highly conductive 2D fracture for scenario 2 was positioned along the northern fault of the Hohenzollerngraben. The documented fault was linearly extended to the east to cross the river Lauchert at the position of the Gallusquelle spring (compare Figure 2.5a and c).

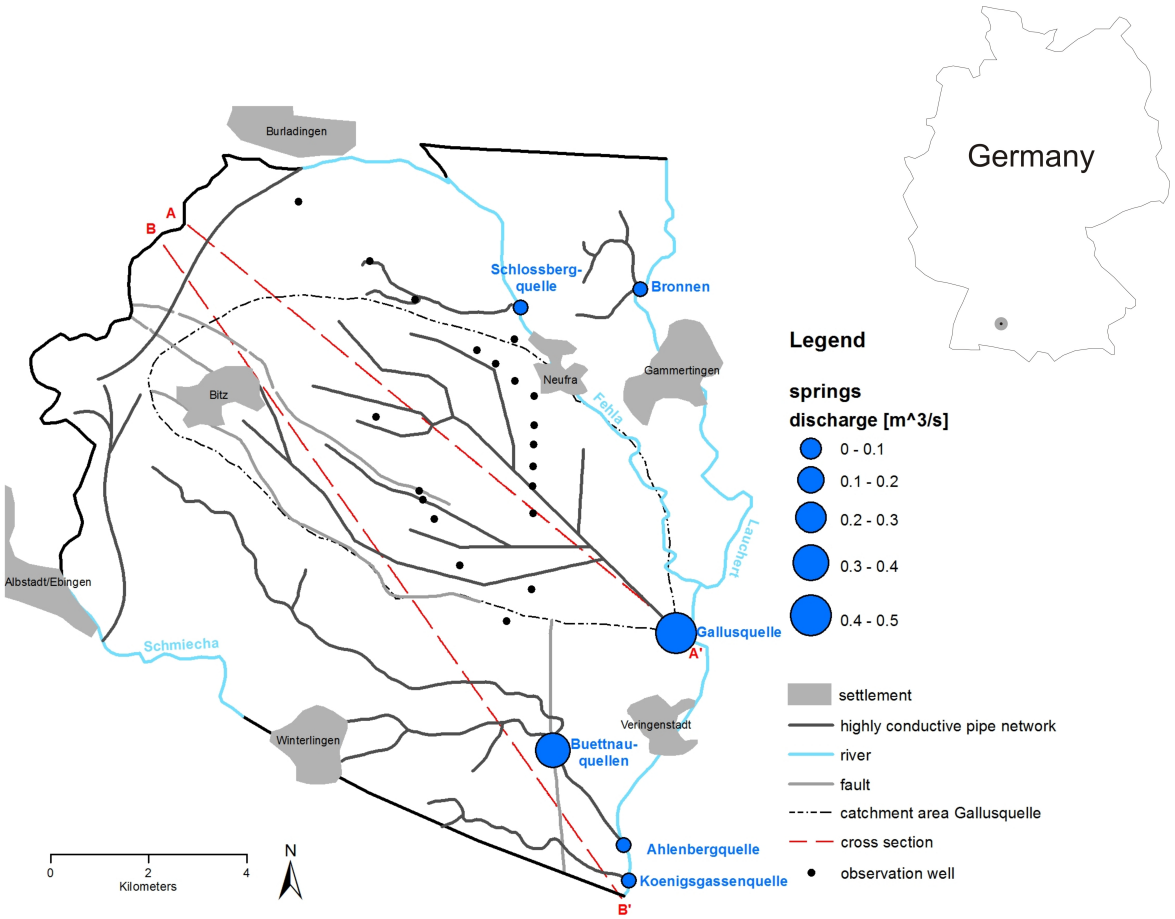

Figure 2.2. Model area, including the catchment of the Gallusquelle spring and positions of all simulated springs. The highly conductive elements feeding the Gallusquelle spring were modeled after Doummar et al. (2012) and the ones along the dry valleys after Gwinner et al. (1993).

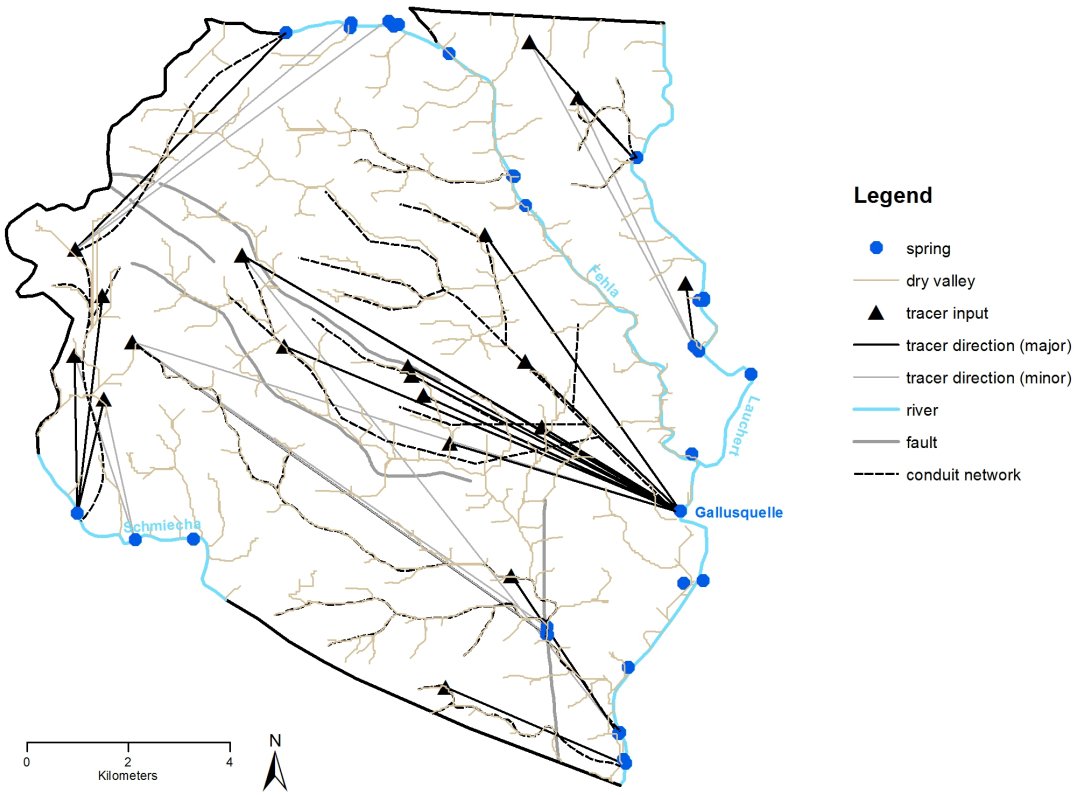

Figure 2.3. Top view of the model area. Tracer tests within the area are illustrated with their major and minor registration points (excluded: uncertain registrations and registration points in rivers) after information from the Landesamt für Geologie, Rohstoffe und Bergbau (LGRB). Dry valleys were simulated with ArcGIS® 10.0 and counterchecked with field observations of Gwinner et al. (1993).

Vertically the model consists of two layers. The upper one represents the aquifer. In the east it stretches from ground surface to the base of the Kimmeridgian 2 (ki2). The formation is tapering out in the west of the area but reaches a thickness of over 200 m in the east where the Gallusquelle spring is located. In the west the underlying Kimmeridgian 1 (ki1) approaches the surface until it crops out. In that region it shows karstification and thus is part of the aquifer. The depth of the karstification was derived from drilling cores. The unkarstified ki1 acts as aquitard and composes the second layer of the model. It was simulated down to a horizontal depth of 300 m a.s.l. since its lower boundary is not expected to influence the simulation. The ground surface is defined by a digital elevation model (DEM) with a cell size of 40 m. The position of the ki2 base was derived from boreholes and a base map provided in Sauter (1992). Two cross sections were constructed through the model area for illustrating the geology (Figure 2.4). Their positions are illustrated in Figure 2.2.

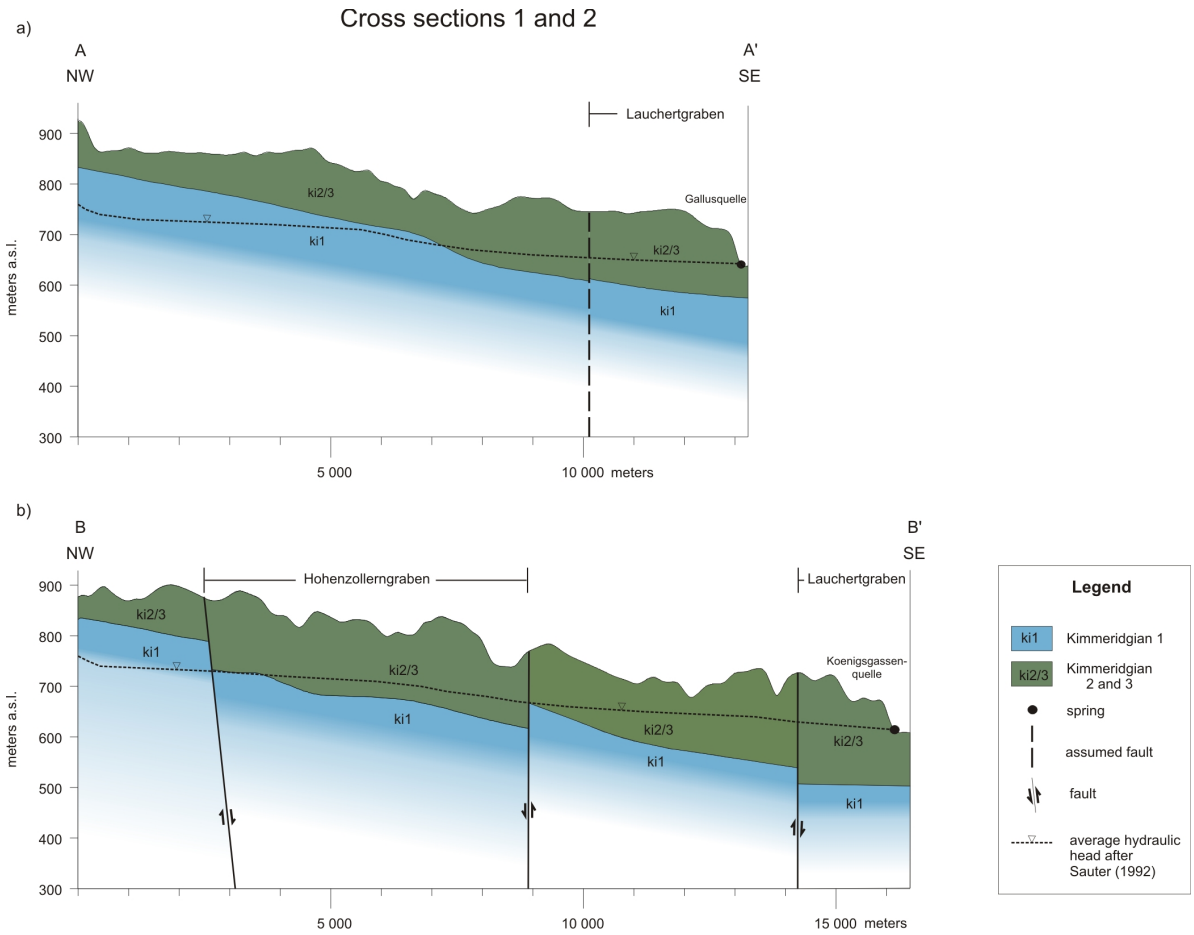

Figure 2.4. Cross sections of the study area as constructed in GoCAD® from northwest to southeast with a vertical exaggeration of 10:1. (a**) cross section 1 through the Lauchertgraben and the Gallusquelle spring. (**b**) cross section 2 through the Hohenzollerngraben, the Lauchertgraben and the Königsgassenquelle spring.**

Current Comsol® software has major difficulties interpolating irregular surfaces that cannot be described by analytical functions. Therefore, the three-dimensional position of these layers, including displacement by faults and dip of the aquifer base, were constructed with the geologic modeling software Geological Objects Computer Aided Design (GoCAD®). The surface points were imported to Comsol® as text files and used to constrain parametric surfaces. Those were converted to solid objects for defining 3D domains. At the ground surface a constant recharge was applied as a Neumann condition. The recharge was derived by Sauter (1992) as long-term average for the years 1965–1990. Geyer at al. (2011) derived the same value for the extended period 1955–2006. The base of the model was defined as a no flow boundary, while the base of the aquifer was set as a continuity boundary, which assures a continuous pressure gradient across the boundary, allowing undisturbed water transfer. The exact values for all model parameters are provided in Table 2.1.

Table 2.1. Input and calibration values of the different scenarios. The root mean square error of the hydraulic head distribution is given as an index for the quality of the model fit.

	Scenario 1: homogeneous	Scenario 2: single fracture	Scenario 3: conduit network with constant radius	Scenario 4: conduit network with increasing radius
R (mm d^{-1})	1	1	1	1
K_m (m s^{-1})	5.1×10^{-5}	3.1×10^{-5}	2.3×10^{-5}	2.6×10^{-5}
K_l (m s^{-1})	1.0×10^{-10}	1.0×10^{-10}	1.0×10^{-10}	1.0×10^{-10}
K_f / K_c (m s^{-1})	–	2.7	6.5	2.0
d_z (m)	–	aquifer thickness	–	–
d_y (m) / radius (m)	–	0.129	1.282	linear with slope 1.18×10^{-4}, maximum: 4.6 m
RMSE (m)	15.0	13.3	13.4	7.7

R = groundwater recharge by precipitation, K_m = hydraulic conductivity of matrix, K_l = hydraulic conductivity of lowly conductive ki1, K_f = hydraulic conductivity of fracture, K_c = hydraulic conductivity of conduits, d_z = fracture depth, d_y = fracture aperture, RMSE = root mean square error for the hydraulic head distribution.

The model was calibrated employing Comsol Multiphysics® Parametric Sweep option, which calculates several model runs considering different parameter combinations. The focus of the calibration lay on the hydraulic head distribution. The measured hydraulic head values are long-term averages derived from twenty exploration or observation wells that were drilled within the model area (Figure 2.2).

For the calibration of spring discharges five smaller springs were included in the model besides the Gallusquelle spring. Other springs within the investigation area are either very small or have not been measured on a regular basis for reliably estimating their average annual discharges. The Gallusquelle spring and three of the other springs considered in the model calibration, the Bronnen spring, the Ahlenbergquelle spring and the Königsgassenquelle spring, are located at the river Lauchert; the Schlossbergquelle spring is situated at the river Fehla; a group of springs called the Büttnauquellen springs is located at a dry valley (Gwinner et al., 1993; Golwer et al., 1978) (Figure 2.2). The Büttnauquellen springs and the Ahlenbergquelle spring probably share most of their catchment area and are likely to be fed by the same karst conduit network (Figure 2.2). Localized discharge was also simulated into the rivers Fehla and Schmiecha in the west of the area, where several springs exist (Figure 2.3). The highly conductive karst conduits used in the simulation connect points in the proximity of the Hohenzollerngraben with the Fehla-Ursprung spring at the Fehla and the Balinger Quelle spring at the Schmiecha. The karst conduits were identified by tracer tests (Figure 2.3). However, there is not enough data for the discharges of the Fehla-Ursprung spring and the

Balinger Quelle spring to calibrate the model in this area. Since the Gallusquelle spring is the most intensively investigated spring in the area and thus not only has the most discharge measurements but the most tracer tests as well, the main weight during calibration was laid on this spring. The simulation had to fit the Gallusquelle spring discharge within a range of 10 l s^{-1}, if this could be achieved with a reasonable fit for the hydraulic head distribution.

The radii of the highly conductive conduits were calibrated for a conduit volume of 200 000 m^3 for the Gallusquelle catchment that was deduced from an artificial tracer test (Geyer et al., 2008). For the other springs in the model area, there was no such information. For scenario 3 a systematic approach for relating the cross-sectional areas of the conduits connected to each spring to the one of the Gallusquelle spring was employed. The conduit area for each spring was defined as the area for the Gallusquelle spring multiplied by the ratio of the spring discharge to the discharge of the Gallusquelle spring. For scenario 4 where a linear relationship between the arc length and the conduit diameter was defined, it was assumed that the shorter conduits of the smaller springs lead to accordingly smaller cross-sectional areas without any further adjustments. At the springs, fixed head boundary conditions were set at the conduits.

2.5 Results and Discussion

The four scenarios were evaluated and compared regarding hydraulic head distribution, hydraulic parameters, spring discharges and catchment area delineations. Figure 2.5 shows the simulated hydraulic head distributions for all scenarios. They are compared to a hydraulic head contour map that Sauter (1992) constructed based on field measurements (Figure 2.5a). Figure 2.6 gives a detailed overview of the measured and simulated hydraulic heads and hydraulic gradients. The calibration parameters can be found in Table 2.1. Table 2.2 and Figure 2.7 compare the simulated and observed spring discharges.

2.5.1 Hydraulic head distribution

The model can approximate the hydraulic head distribution in all scenarios. However, there is a significant difference of the model fit between scenario 1 with a root mean square error (RMSE) of 15 m and the best fit (scenario 4) with a RMSE of 7.7 m. Scenarios 2 and 3 show similar RMSE of about 13 m. The measured hydraulic head values in the observation wells and the difference between measured and simulated head for each scenario are given in Table 2.3.

The measured hydraulic heads show a lateral change in hydraulic gradients. In accordance with observations in the karst aquifer of Mammoth Cave (Kentucky, USA) reported by Worthington

(2009), the Gallusquelle catchment shows lower hydraulic gradients in the east towards the spring than in the rest of the area. This is probably caused by the higher hydraulic conductivity due to the higher karstification in the vicinity of the karst spring. After Worthington (2009) this is one of the typical characteristics of karst areas. The observation is also supported by Liedl et al. (2003) who found a widening of karst conduits in spring direction. At the field site, the steepest hydraulic head gradients were observed in the central area.

Scenario 1 cannot reproduce this behavior of the hydraulic gradient (Figure 2.5b and Figure 2.6a). It shows the opposite of the observed gradient distribution with steeper gradients close to the river Lauchert, where most of the springs are located. This effect usually occurs in homogeneous aquifers with evenly distributed recharge conditions. The highly conductive fracture in scenario 2 crosses the model area completely from west to east. Therefore, it mainly lowers the hydraulic head values in the central and western part, thus opposing the observed gradient distribution. In the west, where the fault starts to drain the area, its very high transmissivity leads to a strong distortion of hydraulic head contour lines (Figure 2.5c).

The conduit network in scenario 3 drains the area predominantly in the central part. This results in a much lower hydraulic gradient than actually observed in the field (Figure 2.5d and Figure 2.6c). This effect is due to the constant and relatively high conduit diameter of 2.56 m for the conduits connected to the Gallusquelle spring. This allows large amounts of water to flow into the conduits in the central part of the catchment. While the low hydraulic conductivity of the matrix is limiting groundwater flow in this part of the catchment, the ability of the conduits to conduct water becomes limiting close to the Gallusquelle spring and causes water to flow out of the conduits and back into the matrix. According to the classification after Kovács et al. (2005) the flow regime in this part of the model area thus is conduit influenced.

Scenario 4 shows a significantly better fit for the hydraulic gradient distribution (Figure 2.5e and Figure 2.6d). The increase of conduit diameters towards the spring represents the higher degree of karstification and thus higher transmissivity close to the spring. As a consequence, the hydraulic gradient is steeper in the central part of the catchment than close to the spring (Figure 2.5e). This corresponds to the matrix-influenced flow regime according to Kovács et al. (2005), where the discharge is controlled by the matrix rather than by the conduits. The effect is not strong enough to completely avoid an overestimation of hydraulic heads in the east and an underestimation in the central part and in the west (Figure 2.6d). This leads to the assumption that the change in gradient is not purely derived from the higher karstification but that other, probably geologic factors contribute to the lateral differences in hydraulic conductivity. A more dendritic and farther extended conduit system could also lower the hydraulic head in the east. Due to the gradual widening of the conduits,

the troughs in the hydraulic head contour lines are less pronounced in scenario 4 than in scenario 3 and occur further east.

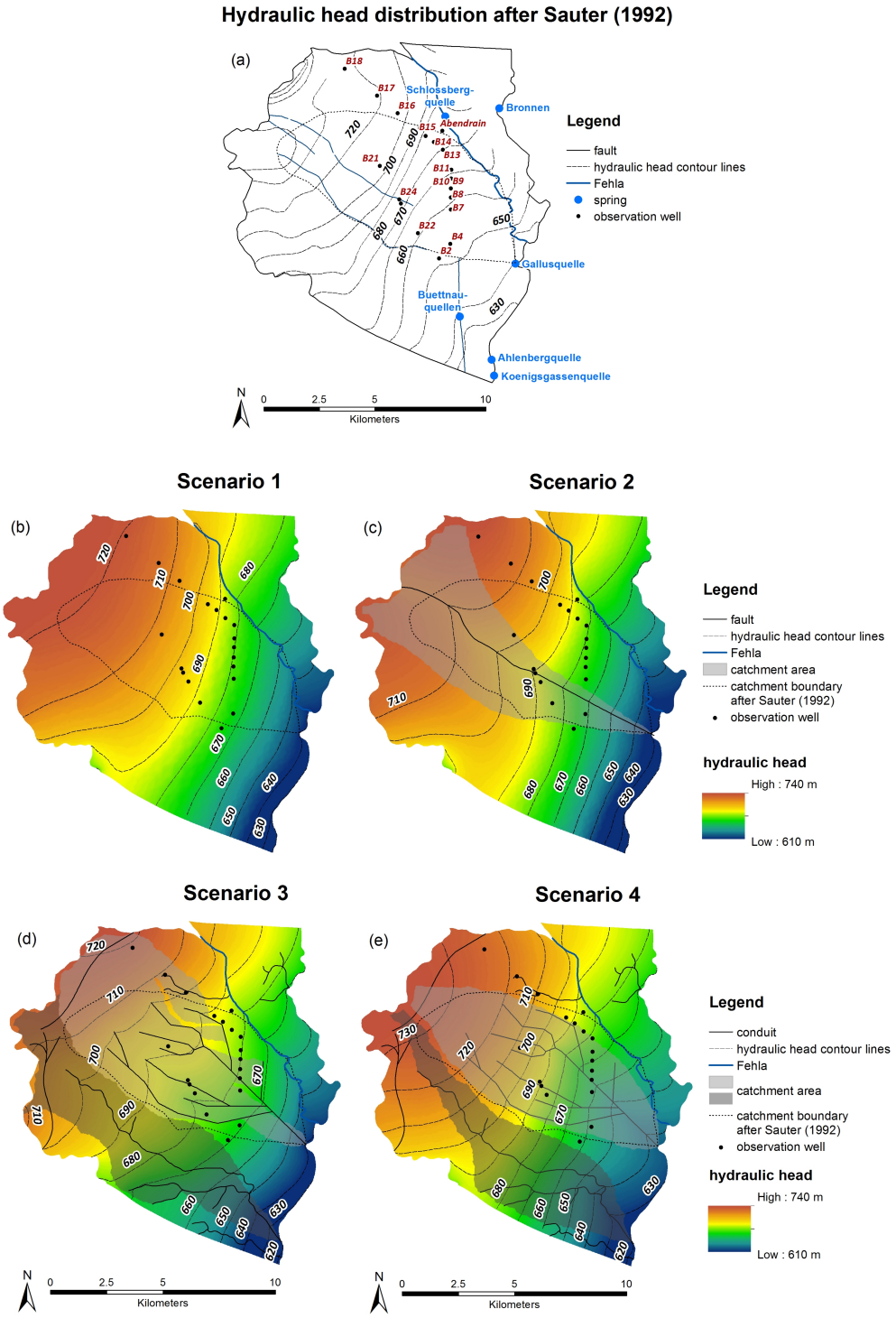

Figure 2.5. Hydraulic head distributions and simulated catchment areas. (a) after Sauter (1992), derived from borehole measurements. (b) after the homogeneous simulation. (c) after the simulation with fracture flow along the northern fault of the Hohenzollerngraben. (d) after the simulation with a 1D conduit network with constant radius. (e) after the simulation with a 1D conduit network with increasing radius.

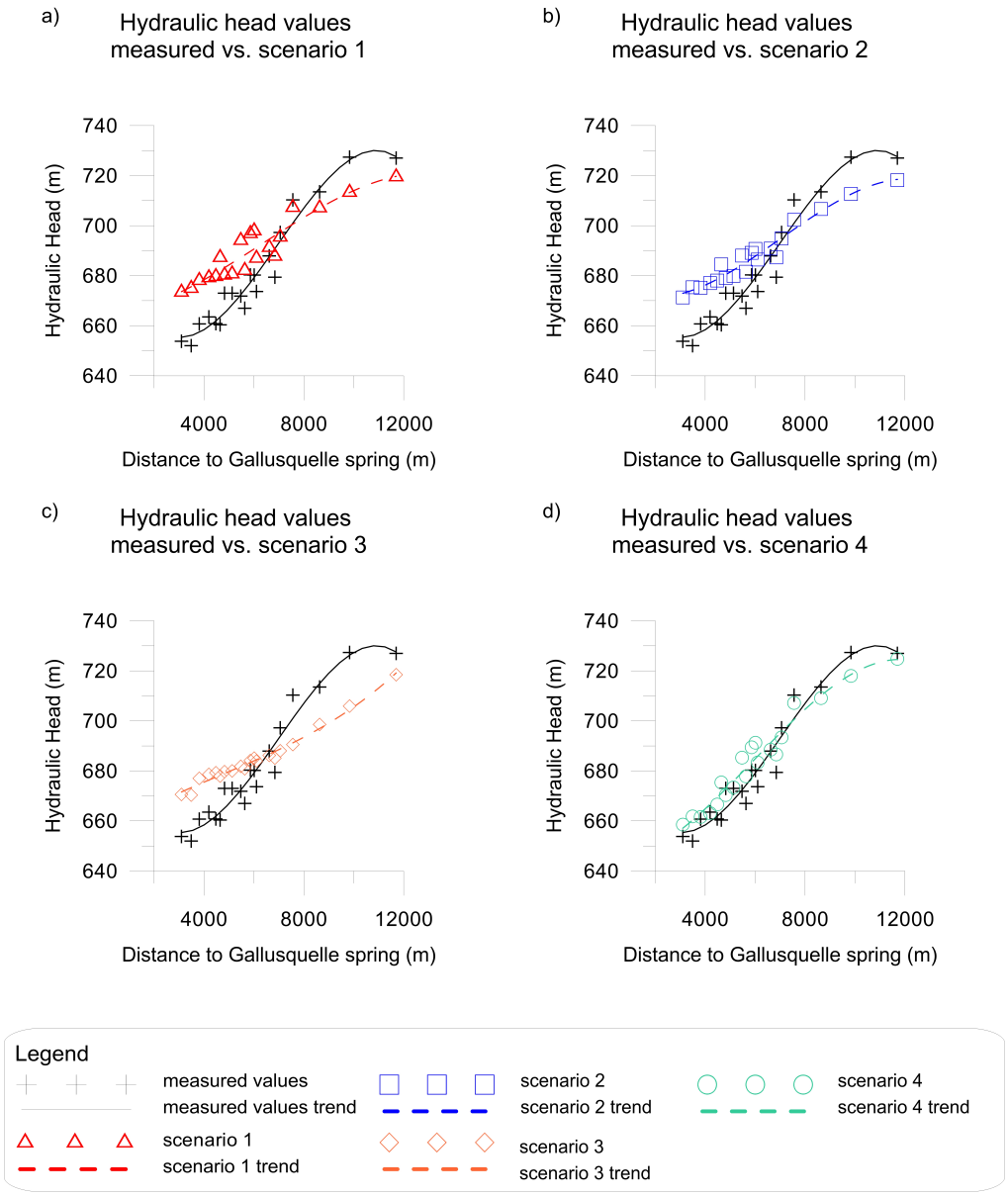

Figure 2.6. Comparison of the hydraulic head values measured in the observation wells and those simulated at the well positions. (a) after the homogeneous simulation. (b) after the simulation with fracture flow along the northern fault of the Hohenzollerngraben. (c) after the simulation with a 1D conduit network with constant radius. (d) after the simulation with a 1D conduit network with increasing radius.

2.5.2 Hydraulic parameters

In heterogeneous aquifers the hydraulic conductivity strongly depends on the scale of investigation of the applied method (Geyer et al., 2013). Sauter (1992) employed several approaches to determine the hydraulic conductivity in the catchment area of the Gallusquelle spring from local to regional scale. Regional methods like the gradient (Darcy) approach or the baseflow recession method average over the whole aquifer system and yielded values between 2×10^{-5} m s^{-1} and 2×10^{-4} m s^{-1}.

Values obtained with local borehole methods such as pumping or slug tests ranged approximately from 1×10^{-6} m s^{-1} to 1×10^{-5} m s^{-1}.

The simulated K_m values for all scenarios are well within the aforementioned ranges. The highest K_m value is obtained in scenario 1 with 5.1×10^{-5} m s^{-1}. This is due to the fact that K_m for the homogeneous case averages the hydraulic conductivities of all structures in the area, since none of the discrete features is considered individually. Therefore, the calibrated K_m is within the range given by Sauter (1992) for the regional scale. The highly conductive fracture in scenario 2 allows rapid local flow and therefore lower hydraulic heads can be achieved with a lower value for the matrix conductivity of 3.1×10^{-5} m s^{-1}. This trend continues for scenarios 3 and 4, where K_m drops to 2.3×10^{-5} m s^{-1} and 2.6×10^{-5} m s^{-1}, respectively. In these scenarios the hydraulic conductivity values approach those obtained by Sauter (1992) with borehole tests, suggesting that most of the highly conductive features in the area are explicitly taken into account.

The fracture conductivity K_f is introduced in scenario 2. Despite being in the typical range of literature of 2–10 m s^{-1} (Sauter, 1992) the obtained value of 2.7 m s^{-1} probably is too low, because all other karst features, which can drain water from the Gallusquelle spring catchment towards other springs, are neglected. If additional highly conductive features are included, higher fracture conductivities will be necessary to provide the observed average spring discharge of the Gallusquelle spring. This effect is partly responsible for the relatively high conduit conductivity K_c of 6.5 m s^{-1} in scenario 3. Even though the discharge at the Gallusquelle spring is the same as well as the integrated conduit volume, the conduit conductivity of 2 m s^{-1} obtained for scenario 4 is significantly lower than the value of 6.5 m s^{-1} obtained for scenario 3. This is because the karst conduit system with constant diameter needs a higher overall transmissivity to transport the same amount of water due to limiting flow capacity of the conduits close to the spring.

The conduit diameter in scenario 3 corresponds to a representative constant diameter for the Gallusquelle spring. Birk et al. (2005) used artificial tracer tests for calculating the representative diameter. The authors calculated a diameter of about 5 m, which is higher than the 2.56 m simulated with scenario 3. This is probably due to the fact that these tracer tests were conducted approximately 3 km northwest of the spring while in the model the conduits extend approximately 10 km to the northwest. Thus, this supports the idea that the diameters of the conduits closer to the spring are higher than those farther away (see Chapter 2.2.4).

2.5.3 Spring discharge

Scenario 1 fails to simulate the locally increased discharge at the karst springs (Table 2.2). Since there are no areas of focused flow, there is only diffuse groundwater discharge into the rivers, mainly the Lauchert. In scenario 2 fracture flow along the fault allows the simulation of increased discharge at the Gallusquelle spring (Table 2.2). The other springs that were not connected to highly conductive elements show no locally increased discharge (Table 2.2). The slightly raised discharge of the Schlossbergquelle spring compared to scenario 1 results from generally increased water flow into the river Fehla, not from locally raised discharge at the spring location. The local discharges at all springs can only be represented by scenarios 3 and 4. The simulation is satisfactory for both scenarios. The simulated discharge of the scenarios is very similar for the Gallusquelle spring, the Schlossbergquelle spring and the Königsgassenquelle spring (compare Table 2.2 and Figure 2.7). The fit for these springs is good, even though the discharge is slightly overestimated for the Königsgassenquelle spring and underestimated for the Schlossbergquelle spring. Since the Schlossbergquelle spring is the only spring included at the river Fehla and no registration of discharge values of the river itself was conducted, it cannot be distinguished, if the underestimation at the Schlossbergquelle spring is due to an inexact karst conduit network or to an underestimated discharge into the river. For the Bronnen spring, different results can be observed for the two scenarios. While scenario 3 has a very good fit, scenario 4 underestimates the discharge. This suggests that the conduits leading to the spring are assumed too short in the simulation leading to underestimated conduit diameters in scenario 4.

The most pronounced difference between the two simulations occurs at the Büttnauquellen and Ahlenbergquelle springs. Both simulations underestimate their discharge with a significantly stronger underestimation in scenario 4 (Figure 2.7). This is probably due to the simplified approach of treating them like a single spring and attaching them to the same conduit. While the Ahlenbergquelle spring is perennial, the Büttnauquellen springs are intermittent. This suggests that there are karst conduits in at least two different depths and thus that the representation with a conduit network in a single depth is not adequate. A too short conduit system with too little side branches has a stronger impact on scenario 4 because of the dependence of diameters on the total length and amount of intersections leading to a stronger underestimation of conduit volumes than in scenario 3.

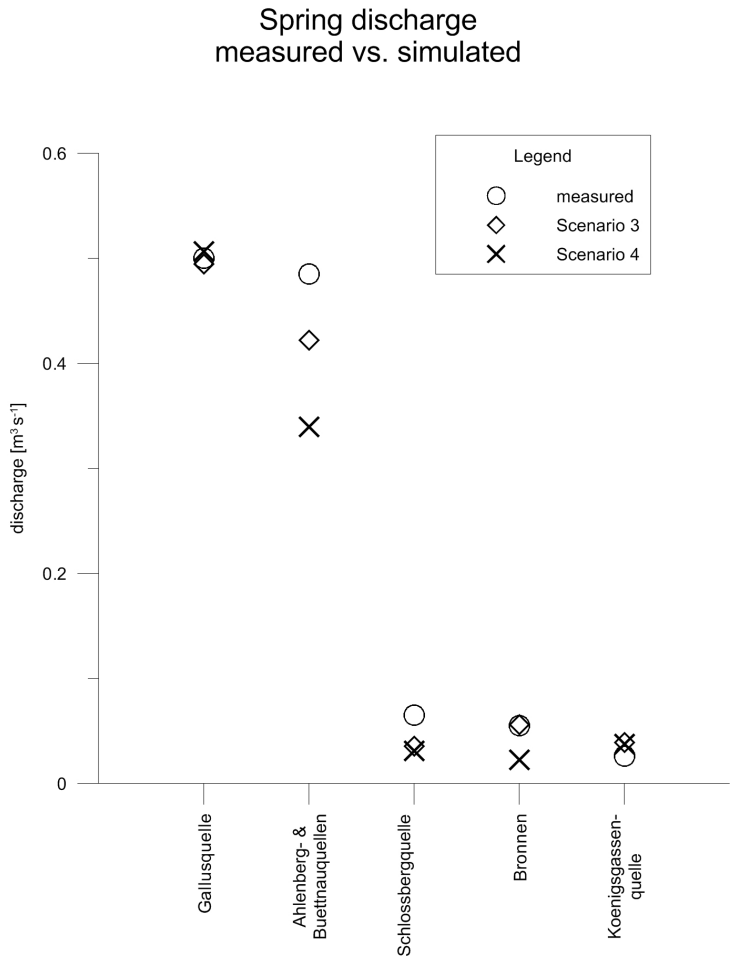

Figure 2.7. Spring discharge: measured and simulated values using a conduit network with constant radius (scenario 3) and with linearly increasing radius (scenario 4).

Table 2.2. Simulated spring discharges ($m^3 s^{-1}$) for all scenarios.

Spring	Measured discharge	Scenario 1: homogeneous	Scenario 2: single fracture	Scenario 3: conduit network with constant radius	Scenario 4: conduit network with linear radius
Gallusquelle	0.500	4.0×10^{-4}	0.500	0.495	0.506
Büttnauquellen and Ahlenbergquelle	0.485	4.4×10^{-4}	3.5×10^{-4}	0.422	0.340
Schlossbergquelle	0.065	2.5×10^{-4}	0.004	0.036	0.031
Bronnen	0.055	2.7×10^{-4}	2.1×10^{-4}	0.056	0.022
Königsgassenquelle	0.026	4.3×10^{-4}	3.4×10^{-4}	0.039	0.038

Table 2.3. Measured hydraulic head values that were used for calibration. For each scenario the difference of the simulated to the measured hydraulic heads is given in meters. The positions of the observation wells are given in Figure 2.5a.

Well	Measured	Scenario 1	Scenario 2	Scenario 3	Scenario 4
	m a.s.l.	m	m	m	m
B2	652.0	22.9	23.4	18.4	9.8
B4	653.8	19.6	17.5	16.8	4.7
B7	660.7	17.4	14.5	16.3	0.9
B8	663.5	15.7	13.5	15.1	–0.4
B9	660.8	18.9	17.3	18.5	5.8
B10	673.0	7.2	6.1	6.7	–2.7
B11	673.0	7.7	6.9	7.0	0.4
B12	667.0	15.1	14.6	13.9	10.8
B13	673.7	13.3	12.8	10.3	9.7
B14	687.9	3.4	2.9	–1.7	0.6
B15	697.3	–1.8	–2.4	–9.2	–3.8
B16	713.5	–6.4	–6.9	–14.9	–4.4
B17	727.4	–14.0	–14.7	–21.4	–9.4
B18	727.0	–7.5	–8.8	–8.6	–2.2
B19	680.3	16.5	8.8	3.8	9.1
B22	660.4	26.9	24.1	17.6	15.1
B21	710.3	–3.0	–8.0	–19.8	–3.1
B24	680.2	17.8	10.5	4.9	11.1
B25	671.9	22.2	16.2	10.0	13.5
Abendrain	679.4	8.4	7.9	5.7	7.2

2.5.4 Catchment area delineation

The spring catchment areas were delineated according to the hydraulic heads within the matrix. For the delineation a bending of contour lines towards the springs is required, meaning they can only be generated with localized discharge at the spring positions. Therefore no catchment areas can be delineated in scenario 1. In scenario 2 a catchment area for the Gallusquelle spring can be delineated. It has approximately the size that can be expected from water balance calculations, but does not include all injection locations of tracer tests with recovery at the Gallusquelle spring. Since the hydraulic conductivity of the fault is assumed to be constant, it receives most of the inflow in the west and cannot receive more water close to the spring. Thus, the catchment area mainly includes the western part of the model area (Figure 2.5c).

In scenario 3 catchment areas can be simulated for the Gallusquelle spring and for the Büttnauquellen and Ahlenbergquelle springs (Figure 2.5d). The unusually looking shape of the areas is caused by the filling of the conduits with water in the west of the model domain which prevents drainage of the fissured matrix by the conduit system in the east of the area. Therefore the Gallusquelle spring mainly receives water from the western part of the area, where its conduits drain enormous water volumes due to their relatively large diameter. Due to outflow of water into the matrix in the east, only part of the water from the shown catchment area is transported to the springs. In the west it can be observed that the catchment areas of the Gallusquelle spring and the Büttnauquellen and Ahlenbergquelle springs reach across karst conduits leading to other springs (Figure 2.5d). In this case the catchment areas of the springs overlap. The catchment areas were constructed in 2D according to surface values, so that they envision the flow above the smaller conduits in the west. In the east it can be observed that the catchment areas do not include all parts of the respective karst conduit network. In these areas the conduits cannot accommodate more water and outflow occurs. The catchment area for the Gallusquelle spring that was delineated in scenario 3 includes all but one tracer test conducted. The Gallusquelle spring drains nearly all water from the springs at the river Fehla. The hydraulic heads in the west are lowered leading to influent flow conditions along parts of the western Fehla. This contradicts the development of several springs in this area and makes this scenario highly unlikely (compare Figure 2.3).

Scenario 4 is the only simulation leading to reasonable results regarding the catchment areas (Figure 2.5e). The size of the Gallusquelle spring catchment area is in accordance with water balance calculations and includes all tracer tests conducted in the catchment of the Gallusquelle spring. The size of the catchment area for the Büttnauquellen and Ahlenbergquelle springs is probably underestimated due to the underestimation of spring discharge (Table 2.2). Since the underestimation is more pronounced for scenario 4 than for scenario 3, the catchment area is

significantly smaller (compare Figure 2.5d and Figure 2.5e). A small overlap of catchment areas can still be observed in the west but in scenario 4 the Gallusquelle only drains small amounts of water from the western part, so that the western Fehla is completely effluent. Since the simulation was performed stationary, the delineated catchment areas are only valid for the average hydraulic head distribution. As known from literature (Chapter 2.3) they should be representative for the usually observed variations in the Gallusquelle area. For reliably simulating possible shifts in the catchment areas during extreme flow conditions, more detailed information on recession behavior of the aquifer and lateral and temporal recharge distribution should be included. This is beyond the scope of this paper.

For the smaller springs, no catchment areas could be generated in either of the scenarios. They produce a very small ratio of the total discharge of the model area (<5%) and the resolution of the simulation was not fine enough to reliably draw their catchment boundaries.

2.6 Conclusion

The results show that distributive numerical simulation is a useful tool for approaching the complex subject of subsurface catchment delineation in karst aquifers as long as effects of karstification are sufficiently taken into account. Even though the Gallusquelle area is significantly less karstified than for example the Mammoth Cave (Kentucky, USA) (Worthington, 2009) and does not show significant troughs in the hydraulic head contour lines, it cannot be simulated with a homogeneous hydraulic parameter field. The geometry of the conduits is of major importance for the simulation. Although the Gallusquelle spring is positioned on the linear extension of the northern fault of the Hohenzollerngraben the hydraulic conditions cannot correctly be simulated without consideration of dry valleys. For catchment delineation, the approach of using conduits with constant geometric parameters is not satisfactory, either. While it is possible to fit spring discharges with a double continuum model (e.g. Kordilla et al., 2012) or a single continuum model with a highly conductive zone with constant hydraulic properties (e.g. Doummar et al., 2012) the hydraulic head distribution and hydraulic conductivities cannot be correctly approximated with these approaches.

Using numerical models for catchment delineation allows for the combination of several methods and observations under consideration of the geological and hydrogeological properties of the area. The model can be used for advanced simulations of transient groundwater flow and transport and can also account for heterogeneous distributions of recharge or aquifer properties. It therefore represents a flexible tool for risk assessment and prediction in heterogeneous flow systems.

The uncertainty of the results depends mainly on the available input data. The modeling approach allows an integrated analysis of data from different sources. Theoretically, the method requires average annual spring discharge and hydraulic head measurements in the catchment. Nonetheless, the measurement of the discharge of several springs in the proximity of the investigated spring catchment is advisable for the simulation of catchment boundaries. In addition, deriving some knowledge about the location and properties of the karst conduit network from natural or artificial tracers, groundwater contour lines, direct investigations or the morphology of the land surface is highly recommended.

To improve simulation results, future work includes the implementation and simulation of solute transport, e.g. simulation of artificial tracer tests. Since the hydraulic head distribution and the spring discharges were found to be strongly dependent on the selected geometry of the highly conductive elements it seems unavoidable to better constrain their positions and sizes in the area. In case of the Gallusquelle area the smooth hydraulic gradients do not allow the localization of conduits by troughs in the hydraulic head contour lines like in some other karst areas (e.g. Joodi et al., 2010). Karst genesis simulation would provide process-based information about conduit widening towards a karst spring. Such simulations were employed for instance by Kaufmann and Braun (1999), Liedl et al. (2003), Bauer et al. (2003), and Hubinger and Birk (2011). They simulate the temporal evolution of a small fracture or fracture network due to solution with coupled transport and hydraulic models. Under the constraints of recharge conditions and initial geometries they derive the conduit size distribution. A detailed overview of the basic techniques and processes is given by Dreybrodt et al. (2005). The implementation of a karst genesis module would be possible with Comsol Multiphysics®, given sufficient input data.

Acknowledgements

The presented study was funded by the German Federal Ministry of Education and Research (promotional reference no. 02WRS1277A, AGRO, “Risikomanagement von Spurenstoffen und Krankheitserregern in ländlichen Karsteinzugsgebieten”) and by the Austrian Science Fund (FWF): L576-N21. Tracer test data was provided by the Landesamt für Geologie, Rohstoffe und Bergbau (LGRB).

References

Bachmat, Y. and Bear, J., 1986. Macroscopic Modelling of Transport Phenomena in Porous Media. 1: The Continuum Approach. Transport in Porous Media 1, 213–240.

Bauer, S., Liedl, R., and Sauter, M., 2003. Modeling of karst aquifer genesis: Influence of exchange flow. Water Resources Research 39(10), 1285, doi:10.1029/2003WR002218.

Birk, S., Geyer, T., Liedl, R., and Sauter, M., 2005. Process-Based Interpretation of Tracer Tests in Carbonate Aquifers. Ground Water 43, 381–388.

Doummar, J., Sauter, M., and Geyer, T., 2012. Simulation of flow processes in a large scale karst system with an integrated catchment model (Mike She) – Identification of relevant parameters influencing spring discharge. Journal of Hydrology 426–427, 112–123, doi:10.1016/j.jhydrol.2012.01.021.

Dreybrodt, W., Gabrovšek, F., and Romanov, D., 2005. Processes of speleogenesis: a modeling approach. Carsologica, 4, Založba ZRC, Postojna – Ljubljana, 357 pp.

Geyer, T., Birk, S., Licha, T., Liedl, R., and Sauter, M., 2007. Multi-tracer test approach to characterize reactive transport in karst aquifers. Ground Water 45(1), 36–45.

Geyer, T., Birk, S., Liedl, R., and Sauter, M., 2008. Quantification of temporal distribution of recharge in karst systems from spring hydrographs. Journal of Hydrology 348, 452–463.

Geyer, T., Selg, M., Gudera, T., and Sauter, M., 2011. Langzeitabflussverhalten der Gallusquelle und des Blautopfs – relative Bedeutung der Matrix und des Karströhrensystems. Laichinger Höhlenfreund 46, 63–74.

Geyer, T., Birk, S., Reimann, T., Dörfliger, N., and Sauter, M., 2013. Differentiated characterization of karst aquifers: some contributions. Carbonates and Evaporites 28, 41–46, doi:10.1007/s13146-013-0150-9.

Goldscheider, N. and Drew, D., 2007. Combined use of methods. In: Methods in Karst Hydrogeology, International contributions to hydrogeology 26, Taylor & Francis, London, 223–228.

Golwer, A., Koerner, U., Villinger, E., and Werner, J., 1978. Erläuterungen zu Blatt 7821 Veringenstadt, Geologische Karte 1 : 25 000 von Baden-Württemberg. Geologisches Landesamt Baden-Württemberg, Stuttgart, 151 pp.

Gwinner, M. P., Villinger, E., and Schreiner, A., 1993. Erläuterungen zu Blatt 7721 Gammertingen, Geologische Karte 1 : 25 000 von Baden-Württemberg. Geologogisches Landesamt Baden-Württemberg, Freiburg/Stuttgart, 78 pp.

Hillebrand, O., Nödler, K., Licha, T., Sauter, M., and Geyer, T., 2012. Identification of the attenuation potential of a karst aquifer by an artificial dualtracer experiment with caffeine. Water Research 46 (16), 5381–5388.

Hubinger, B. and Birk, S., 2011. Influence of initial heterogeneities and recharge limitations on the evolution of aperture distributions in carbonate aquifers. Hydrology and Earth System Sciences 15, 3715-3729, doi:10.5194/hess-15-3715-2011.

Joodi, A. S., Sizaret, S., Binet, S., Bruand, A., Alberic, P., and Lepiller, M., 2010. Development of a Darcy-Brinkman model to simulate water flow and tracer transport in a heterogenous karstic aquifer (Val d'Orléans, France). Hydrogeology Journal 18, 295–309, doi:10.1007/s10040-009-0536-x.

Kaufmann, G. and Braun, J., 1999. Karst aquifer evolution in fractured rocks. Water Resources Research 35 (11), 3223–3238.

Kordilla, J., Sauter, M., Reimann, T., and Geyer, T., 2012: Simulation of saturated and unsaturated flow in karst systems at catchment scale using a double continuum approach. Hydrology and Earth System Sciences 16, 3909–3929, doi:10.5194/hess-16-3909-2012.

Kovács, A., Perrocket, P., Király, L., and Jeannin, P. Y., 2005. A quantitative method for the characterisation of karst aquifers based on spring hydrograph analysis. Journal of Hydrology 303, 152–164.

Liedl, R., Sauter, M., Hückinghaus, D., Clemens, T., and Teutsch, G., 2003. Simulation of the development of karst aquifers using a coupled continuum pipe flow model. Water Resources Research 39(3), 1057, doi:10.1029/2001WR001206.

Mohrlok, U. and Sauter, M., 1997. Modelling groundwater flow in a karst terraine using discrete and double-continuum approaches: importance of spatial and temporal distribution of recharge. In: Proceedings of the 12th International Congress of Speology, 2/6th Conference on Limestone Hydrology and Fissured Media, La Chaux-de-Fonds, Switzerland, 10–17 August 1997, 167–170.

Reimann, T., Rehrl, C., Shoemaker, W. B., Geyer, T., and Birk, S., 2011a. The significance of turbulent flow representation in single-continuum models. Water Resources Research 47, W09503, doi:10.1029/2010WR010133.

Reimann, T., Geyer, T., Shoemaker, W. B., Liedl, R., and Sauter, M., 2011b. Effects of dynamically variable saturation and matrix-conduit coupling of flow in karst aquifers. Water Resources Research 47, W11503, doi:10.1029/2011WR010446.

Sauter, M., 1992. Quantification and Forecasting of Regional Groundwater Flow and Transport in a Karst Aquifer (Gallusquelle, Malm, SW Germany). Tübinger Geowissenschaftliche Arbeiten C13, Tübingen.

Teutsch, G., 1989. Groundwater Models in Karstified Terrains: Two practical Examples from the Swabian Alb (S. Germany). In: Proceedings of the 4th Conference – Solving Groundwater Problems with Models, Indianapolis, USA, 7–9 February 1989, 11 pp.

Teutsch, G. and Sauter, M., 1991. Groundwater modeling in karst terranes: scale effects, data aquisition and field validation. In: Proceedings of the 3rd Conference on Hydrogeology, Ecology, Monitoring and Management of Ground Water in Karst Terranes, 4–6 December 1991, Nashville, USA, 17–34.

Villinger, E., 1977. Über die Potentialverteilung und Strömungssysteme im Karstwasser der Schwäbischen Alb (Oberer Jura, SW-Deutschland). Geologisches Jahrbuch., C18, Hannover.

Worthington, S. R. H., 2009. Diagnostic hydrogeologic characteristics of a karst aquifer (Kentucky, USA). Hydrogeology Journal 17, 1665–1678, doi:10.1007/s10040-009-0489-0.

Chapter 3

3 Reducing the ambiguity of karst aquifer models by pattern matching of flow and transport on catchment scale

Sandra Oehlmann[a], Tobias Geyer[a,b], Tobias Licha[a], Martin Sauter[a]

Citation:

Oehlmann, S., Geyer, T., Licha, T., and Sauter, M., 2015. Reducing the ambiguity of karst aquifer models by pattern matching of flow and transport on catchment scale. Hydrology and Earth System Sciences 19, 893–912, doi:10.5194/hess-19-893-2015.

[a]Geoscience Center, University of Göttingen, Göttingen, Germany

[b]Landesamt für Geologie, Rohstoffe und Bergbau, Regierungspräsidium Freiburg, Freiburg, Germany

Abstract

Assessing the hydraulic parameters of karst aquifers is a challenge due to their high degree of heterogeneity. The unknown parameter field generally leads to a high ambiguity for flow and transport calibration in numerical models of karst aquifers. In this study, a distributed numerical model was built for the simulation of groundwater flow and solute transport in a highly heterogeneous karst aquifer in south-western Germany. Therefore, an interface for the simulation of solute transport in one-dimensional pipes was implemented into the software COMSOL Multiphysics® and coupled to the three-dimensional solute transport interface for continuum domains. For reducing model ambiguity, the simulation was matched for steady-state conditions to the hydraulic head distribution in the model area, the spring discharge of several springs and the transport velocities of two tracer tests. Furthermore, other measured parameters such as the hydraulic conductivity of the fissured matrix and the maximal karst conduit volume were available for model calibration. Parameter studies were performed for several karst conduit geometries to analyse the influence of the respective geometric and hydraulic parameters and develop a calibration approach in a large-scale heterogeneous karst system.

Results show that it is possible not only to derive a consistent flow and transport model for a 150 km^2 karst area but also to combine the use of groundwater flow and transport parameters thereby greatly reducing model ambiguity. The approach provides basic information about the conduit network not accessible for direct geometric measurements. The conduit network volume for the main karst spring in the study area could be narrowed down to approximately 100 000 m^3.

3.1 Introduction

Karst systems play an important role in water supply worldwide (Ford and Williams, 2007). They are characterized as dual-flow systems where flow occurs in the relatively lowly conductive fissured matrix and in highly conductive karst conduits (Reimann et al., 2011). There are a number of process-based modelling approaches available for simulating karst aquifer behaviour. Overviews on the various types of distributed process and lumped-parameter models are provided by several authors (Teutsch and Sauter, 1991; Jeannin and Sauter, 1998; Kovács and Sauter, 2007; Hartmann et al., 2014). In most cases, lumped-parameter models are applied, since they are less demanding on input data (Geyer et al., 2008; Perrin et al., 2008; Hartmann et al., 2013; Schmidt et al., 2014). These models consider neither the actual flow process nor the heterogeneous spatial distribution of aquifer parameters, but are able to simulate the integral aquifer behaviour, e.g. karst spring responses. The spatial distribution of model parameters and state variables, e.g. the hydraulic head distribution,

need to be addressed with distributed numerical models should the necessary field data be available (e.g. Oehlmann et al., 2013; Saller et al., 2013). A distributed modelling approach suited for the simulation of strongly heterogeneous and anisotropic aquifers with limited data availability is the hybrid modelling approach. The approach simulates the fast flow component in the highly conductive karst conduit system in discrete one-dimensional elements and couples it to a two- or three-dimensional continuum representing the fissured matrix of the aquifer (Oehlmann et al., 2013). Hybrid models are rarely applied to real karst systems because they have a high demand of input data (Reimann et al., 2011). They are, however, regularly applied in long-term karst genetic simulation scenarios (e.g. Clemens et al., 1996; Bauer et al., 2003; Hubinger and Birk, 2011). In these models not only groundwater flow but also solute transport is coupled in the fissured matrix and in the karst conduits. Aside from karst evolution such coupling enables models to simulate tracer or contaminant transport in the karst conduit system (e.g. Birk et al., 2005). In addition to serving for predictive purposes, such models can be used for deriving information about the groundwater catchment itself (Rehrl and Birk, 2010).

A major problem for characterizing the groundwater system with numerical models is generally model ambiguity. The large number of calibration parameters is usually in conflict with a relatively low number of field observations, e.g. different hydraulic parameter fields and process variables may give a similar fit to the observed data but sometimes very different results for prognostic simulations (Li et al., 2009). Especially the geometric and hydraulic properties of the karst conduit system are usually unknown and difficult to characterize with field experiments for a whole spring catchment (Worthington, 2009). With artificial tracer test data the maximum conduit volume can be estimated but an unknown contribution of fissured matrix water prevents further conclusions on conduit geometry (Birk et al., 2005; Geyer et al., 2008). It is well known that the use of several objective functions, i.e. several independent field observations, can significantly reduce the number of plausible parameter combinations (Ophori, 1999). Especially in hydrology (e.g. Khu et al., 2008; Hunter et al., 2005) and also for groundwater systems (e.g. Ophori, 1999; Hu, 2011; Hartmann et al., 2013) this approach has been successfully applied with a wide range of observation types, e.g. groundwater recharge, hydraulic heads, remote sensing and solute transport. Particularly, the simulation of flow and transport is known to reduce model ambiguity and yield information on karst conduit geometry (e.g. Birk et al., 2005; Covington et al., 2012; Luhmann et al., 2012; Hartmann et al., 2013). Usually, automatic calibration schemes performing a multi-objective calibration for several parameters are used for this purpose (Khu et al., 2008). However, for complex modelling studies calculation times might be large due to the high number of model runs needed (Khu et al., 2008) and a precise conceptual model is essential as basis for the automatic calibration (Madsen, 2003). In general, numerical models of karst aquifers are difficult to build because of their highly developed

heterogeneity (Rehrl and Birk, 2010). Thus, automatic calibration procedures are better suited for conceptual and lumped-parameter models, where calibration parameters include effective geometric properties and no spatial representation of the hydraulic parameter field and conduit geometry is necessary. Complex distributed numerical approaches generally require longer simulation times due to the necessary spatial resolution. Long simulation times limit the number of model runs that can reasonably be performed and manual calibration based on hydrogeological knowledge is necessary (e.g. Saller et al., 2013). Therefore, applied distributed numerical models in karst systems usually focus on a smaller number of objective functions. They generally cannot simulate the hydraulic head distribution in the area, spring discharge and tracer breakthrough curves simultaneously on catchment scale. Some studies combine groundwater flow with particle tracking for tracer directions (e.g. Worthington, 2009; Saller et al., 2013) without simulating tracer velocities. On the other hand there are studies simulating breakthrough curves without calibrating for measured hydraulic heads (e.g. Birk et al., 2005). For developing process-based models which can be used as prognostic tools, e.g. for the delineation of protection zones, the simulation should be able to reproduce groundwater flow and transport within a groundwater catchment. Especially in complex hydrogeological systems, this approach would reduce model ambiguity, which is a prerequisite in predicting groundwater resources and pollution risks.

This study shows how the combination of groundwater flow and transport simulation can be used not only to develop a basis for further prognostic simulations in a heterogeneous karst aquifer with a distributed modelling approach on catchment scale but also to reduce model ambiguity and draw conclusions on the spatially distributed karst network geometries and the actual karst conduit volume. The approach shows the kind and minimum number of field observations needed for this aim. Furthermore, a systematic calibration strategy is presented to reduce the number of necessary model runs and the simulation time compared to standard multi-objective calibrations. For this purpose a hybrid model was built and a pattern matching procedure was applied for a well-studied karst aquifer system in south-western Germany. The model was calibrated for three major observed parameters: the hydraulic head distribution derived from measurements in 20 boreholes, the spring discharge of six springs and the tracer breakthrough curves of two tracer tests.

3.2 Modelling approach

The simulations are based on the mathematical flow model discussed in detail by Oehlmann et al. (2013). The authors set up a three-dimensional hybrid model for groundwater flow with the software COMSOL Multiphysics®. As described by Oehlmann et al. (2013) the simulations are conducted simultaneously in the three-dimensional fissured matrix, in an individual two-dimensional fault zone

and in one-dimensional karst conduit elements to account for the heterogeneity of the system. Results showed that the karst conduits widen towards the springs and therefore, a linear relationship between the conduit radius and the conduit length *s* [L] was established. Values for *s* start with zero at the point farthest away from the spring and increase towards the respective karst spring. In agreement with these results and karst genesis simulations by Liedl et al. (2003), the conduit radius is calculated as

$$r_c = ms + b \,, \tag{3.1}$$

where r_c [L] is the radius of a conduit branch and *m* and *b* are the two parameters defining the conduit size. *b* [L] is the initial radius of the conduit at the point farthest away from the spring and *m* [–] is the slope with which the conduit radius increases along the length of the conduit *s*.

In the following the equations used for groundwater flow and transport are described. The subscript *m* denotes the fissured matrix, *f* the fault zone and *c* the conduits hereby allowing a clear distinction between the respective parameters. Parameters without a subscript are the same for all karst features in the model.

3.2.1 Groundwater flow

Groundwater flow was simulated for steady-state conditions. This approach seems appropriate since this work focuses on the simulation of tracer transport in the conduit system during tracer tests, which are ideally conducted under quasi-steady-state flow conditions. Therefore, the simulations refer to periods with a small change of spring discharge, e.g. base flow recession, and are not designed to predict conditions during intensive recharge / discharge events. The groundwater flow in the three-dimensional fissured matrix was simulated with the continuity equation and the Darcy equation (Eqs. 3.2a and b).

$$Q_m = \nabla(\rho \boldsymbol{u}_m) \,, \tag{3.2a}$$

$$\boldsymbol{u}_m = -K_m \, \nabla H_m \,, \tag{3.2b}$$

where Q_m is the mass source term [M L^{-3} T^{-1}], ρ the density of water [M L^{-3}] and $\boldsymbol{u}_m$ the Darcy velocity [L T^{-1}]. In Eq. 3.2b K_m is the hydraulic conductivity of the fissured matrix [L T^{-1}] and H_m the hydraulic head [L].

Two-dimensional fracture flow in the fault zone was simulated with the COMSOL® Fracture Flow Interface. The interface only allows for the application of the Darcy equation inside of fractures, so

laminar flow in the fault zone was assumed. In order to obtain a process-based conceptualization of flow, the hydraulic fault conductivity K_f was calculated by the cubic law (Eq. 3.3):

$$K_f = \frac{d_f^2 \rho g}{12\mu}, \tag{3.3}$$

where d_f is the fault aperture [L], ρ the density of water [M L^{-3}], g the gravity acceleration [L T^{-2}] and μ the dynamic viscosity of water [M T^{-1} L^{-1}].

For groundwater flow in the karst conduits, the Manning equation was used (Eq. 3.4).

$$\boldsymbol{u}_c = \frac{1}{n}\left(\frac{r_c}{2}\right)^{\frac{2}{3}} \sqrt{\frac{\mathrm{d}H_c}{\mathrm{d}x}}, \tag{3.4}$$

where $\boldsymbol{u}_c$ is the specific discharge in this case equalling the conduit flow velocity [L T^{-1}], n the Manning coefficient [T $L^{-1/3}$], $r_c/2$ the hydraulic radius [L] and $\mathrm{d}H_c/\mathrm{d}x$ the hydraulic gradient [–]. The Manning coefficient is an empirical value for the roughness of a pipe with no physical nor measurable meaning. The hydraulic radius is calculated by dividing the cross section of flow by the wetted perimeter, which in this case corresponds to the total perimeter of the pipe (Reimann et al., 2011).

The whole conduit network was simulated for turbulent flow conditions. Due to the large conduit diameters (0.01 m – 6 m, Chapter 3.5) this assumption is a good enough approximation. Hereby, strong changes in flow velocities due to the change from laminar to turbulent flow can be avoided. At the same time, the model does not require an estimation of the critical Reynolds number, which is difficult to assess accurately.

The three-dimensional flow in the fissured matrix and the one-dimensional conduit flow were coupled through a linear exchange term that was defined according to Barenblatt et al. (1960) as

$$q_{ex} = \frac{\alpha}{L}(H_c - H_m), \tag{3.5}$$

where q_{ex} is the water exchange between conduit and fissured matrix [L^2 T^{-1}] per unit conduit length L [L], H_m the hydraulic head in the fissured matrix [L], H_c the hydraulic head in the conduit [L] and α the leakage coefficient [L^2 T^{-1}]. The leakage coefficient was defined as:

$$\alpha = 2\pi r_c K_m, \tag{3.6}$$

where $2\pi r_c$ is the conduit perimeter [L]. Other possible influences e.g. the lower hydraulic conductivity at the solid-liquid interface of the pipe and the fact that water is not exchanged along the whole perimeter but only through the fissures are not considered. The exact value of these influences is unknown and the exchange parameter mainly controls the reaction of the karst conduits

and the fissured matrix to hydraulic impulses. Since the flow simulation is performed for steady-state conditions this simplification is not expected to exhibit significant influence on the flow field.

3.2.2 Solute transport

Transient solute transport was simulated based on the steady-state groundwater flow field. COMSOL Multiphysics® offers a general transport equation with its Solute Transport Interface. This interface was applied for the three-dimensional fissured matrix. In this work saturated, conservative transport was simulated, with an advection-dispersion equation (Eq. 3.7)

$$\frac{\partial}{\partial t}(\theta_m c_{\mathrm{m}}) + \nabla(\boldsymbol{u}_m c_m) = \nabla[\theta_m(\mathbf{D}_{\mathrm{Dm}} + \mathbf{D}_{\mathrm{em}})\nabla c_m] + S_m \,, \tag{3.7}$$

where θ_m is the matrix porosity [–], c_m the solute concentration [M L^{-3}], $\mathbf{D}_{\mathrm{Dm}}$ the mechanical dispersion tensor [L^2 T^{-1}] and $\mathbf{D}_{\mathrm{em}}$ the effective molecular pore diffusion coefficient [L^2 T^{-1}]. S_m is the source term [M L^{-3} T^{-1}].

The Solute Transport Interface cannot be applied to one-dimensional elements within a three-dimensional model. COMSOL® offers a so-called Coefficient Form Edge PDE Interface to define one-dimensional mathematical equations. There, a partial differential equation is provided (COMSOL AB, 2012) which can be adapted as needed and leads to Eq. (3.8) in its application for solute transport in karst conduits:

$$\theta_c \frac{\partial c_c}{\partial t} + \nabla(-\mathbf{D}_{\mathrm{c}}\nabla c_c + \boldsymbol{u}_c c_c) = f \,, \tag{3.8}$$

where c_c [M L^{-3}] is the solute concentration inside the conduit, θ_c the conduit porosity which is set equal to 1, $\mathbf{D}_c$ [L^2 T^{-1}] the diffusion-dispersion coefficient $\mathbf{D}_c = (\mathbf{D}_{Dc} + \mathbf{D}_{ec})$, f [M L^{-3} T^{-1}] the source term and $\boldsymbol{u}_c$ [L T^{-1}] the flow velocity inside the conduits, which corresponds to the advective transport component. Flow divergence cannot be neglected, as is often the case in other studies (e.g. Hauns et al., 2001; Birk et al., 2006; Coronado et al., 2007). Different conduit sizes and in- and outflow along the conduits lead to significant velocity divergence in the conduit system. This needs to be considered for mass conservation during the simulation. The mechanical conduit dispersion coefficient $\mathbf{D}_{Dc}$ was calculated with Eq. (3.9) (Hauns et al., 2001).

$$\mathbf{D}_{Dc} = \varepsilon \boldsymbol{u}_c \tag{3.9}$$

where ε is the dispersivity in the karst conduits [L].

The source term f [M T^{-1} L^{-3}] in Eq. (3.8) equals in this case the mass flux of solute per unit conduit volume V [L^3] due to matrix-conduit exchange of solute c_{ex} [M L^{-1} T^{-1}]:

$$\pi r_c^2 \, f = c_{ex} = -\mathbf{D}_{\mathrm{em}} \frac{2\pi \mathrm{r_c}}{L} (c_m - c_c) - q_{\mathrm{ex}} \, c_i \, . \tag{3.10}$$

The first term of the right-hand side of Eq. (3.10) defines the diffusive exchange due to the concentration difference between conduit and fissured matrix. The second term is a conditional term adding the advective exchange of solute due to water exchange. The concentration of the advective exchange c_i is defined as

$$c_{\mathrm{i}} = \begin{cases} c_c \text{ if } q_{ex} > 0 \\ c_m \text{ if } q_{ex} \leq 0 \end{cases}. \tag{3.11}$$

When q_{ex} is negative, the hydraulic head in the fissured matrix is higher than in the conduit (Eq. 3.5) and water with the solute concentration of the fissured matrix c_m enters the conduit. When it is positive, water with the solute concentration c_c of the conduit leaves the conduit and enters the fissured matrix. Since one-dimensional transport is simulated in a three-dimensional environment, the left-hand side of Eq. (3.8) is multiplied with the conduit cross section πr_c^2 [L^2]. These considerations lead to the following transport equation for the karst conduits:

$$\pi r_c^2 \frac{\partial c_c}{\partial t} + \pi r_c^2 \, \nabla(-\mathbf{D}_{\mathrm{c}} \nabla c_c + \boldsymbol{u}_c c_c) = -\mathbf{D}_{\mathrm{e}} \frac{2\pi r_c}{L} (c_m - c_c) - q_{ex} \, c_i \, . \tag{3.12}$$

3.3 Field site and model design

The field site is the Gallusquelle spring area on the Swabian Alb in south-western Germany. The size of the model area is approximately 150 km^2, including the catchment area of the Gallusquelle spring and surrounding smaller spring catchments (Oehlmann et al., 2013). The Gallusquelle spring is the main point outlet with a long-term average annual discharge of 0.5 $m^3 \, s^{-1}$. The model area is constrained by three rivers and no-flow boundaries derived from tracer test information and the dip of the aquifer base (Oehlmann et al., 2013) (Figure 3.1).

The aquifer consists of massive and bedded limestone of the stratigraphic units Kimmeridgian 2 and 3 (ki2/3) (Golwer, 1978; Gwinner, 1993). The marly limestones of the underlying Kimmeridgian 1 (ki1) mainly act as an aquitard. In the west of the area where they get close to the surface, they are partly karstified and contribute to the aquifer (Sauter, 1992; Villinger, 1993). The Oxfordian 2 (ox2) that lies beneath the ki1 consists of layered limestones. It is more soluble than the ki1 but only slightly karstified because of the protective effect of the overlying geological units. In the catchment areas of the Fehla-Ursprung and the Balinger springs close to the western border (Figure 3.1a) the ox2 partly contributes to the aquifer. For simplicity, only two vertical layers were differentiated in the model: the aquifer and the underlying aquitard.

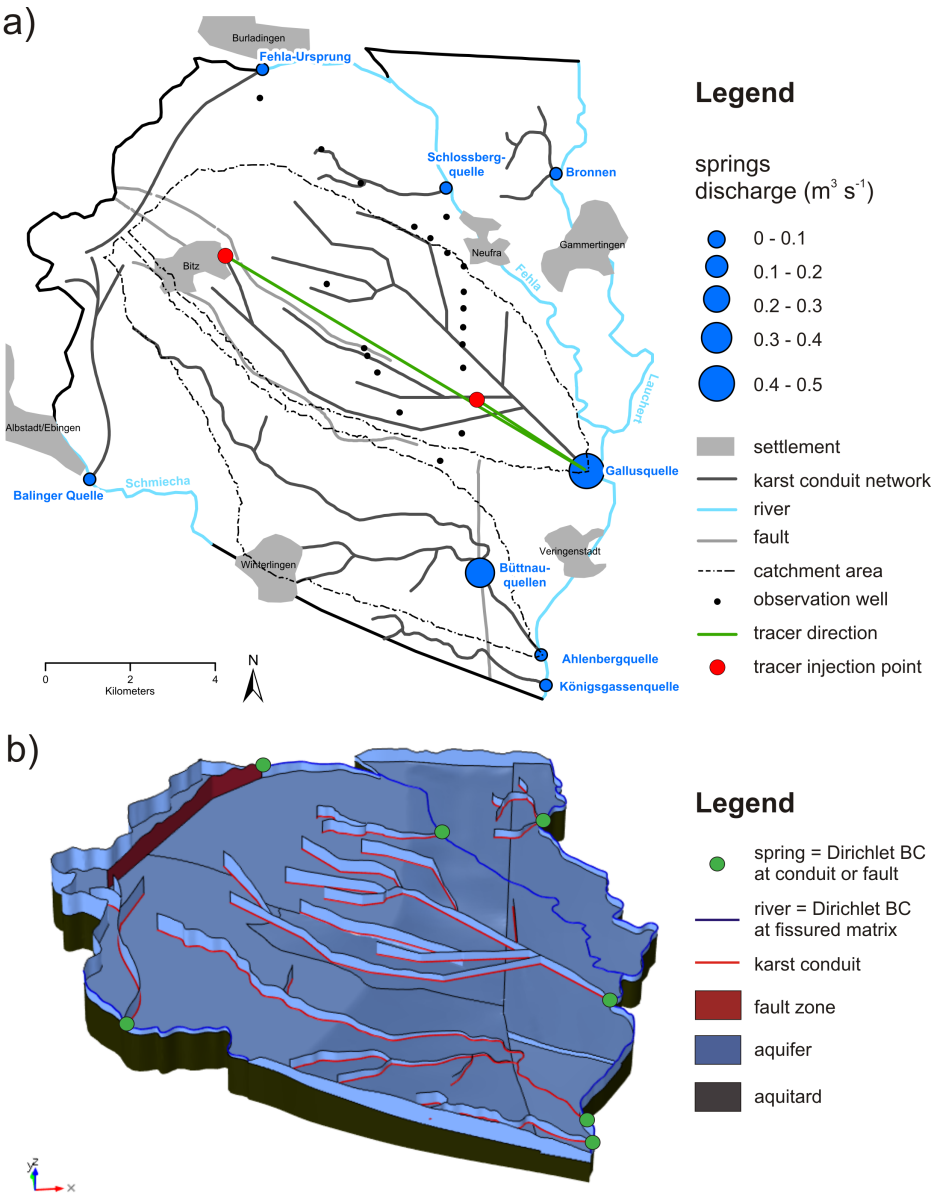

Figure 3.1. (a**) Plan view of the model area. Settlements, fault zones and rivers in the area are plotted, as well as the 20 observation wells used for hydraulic head calibration, the six springs used for spring discharge calibration and the two tracer tests employed for flow velocity calibration. Catchment areas for the Gallusquelle spring and the Ahlenberg and Büttnauquellen springs were simulated according to Oehlmann et al. (2013). (**b**) Three-dimensional view of the model. The upper boundary is hidden to allow a view of the karst conduit system and the aquifer base. The abbreviation BC stands for boundary condition. At the hidden upper boundary, a constant recharge Neumann BC is applied.**

The geometry of the conduit system was transferred from the COMSOL® model calibrated for flow by Oehlmann et al. (2013). It is based on the occurrence of dry valleys in the investigation area and artificial tracer test information (Gwinner, 1993). The conduit geometry for the Gallusquelle spring was also employed for distributed flow simulations by Doummar et al. (2012) and Mohrlok and

Sauter (1997) (Figure 3.1). In this work, all highly conductive connections identified by tracer tests in the field were simulated as discrete one-dimensional karst conduit elements. The only exception is a connection in the west of the area that runs perpendicular to the dominant fault direction and reaches the Fehla-Ursprung spring at the northern boundary (Figure 3.1). While the element was regarded as a karst conduit by Oehlmann et al. (2013) it is more likely that the water crosses the graben structure by a transversal cross-fault (Strayle, 1970). Therefore, the one-dimensional conduit element was replaced by a two-dimensional fault element (Figure 3.1b). This leads to a small adjustment in the catchment areas compared to the results of Oehlmann et al. (2013) (Figure 3.1a). While the discharge data for the Fehla-Ursprung spring are not as extensive as for the other simulated springs, it is approximated to 0.1 $m^3 s^{-1}$, the annual average ranging from 0.068 $m^3 s^{-1}$ to 0.135 $m^3 s^{-1}$. The fault zone aperture was calibrated accordingly (Chapter 3.5).

Table 3.1. Calibrated parameters and model fit for the best-fit simulations. Literature values are given if available. TT1 and TT2 refer to the two tracer tests. For the definition of the parameters m_h and b_h see Chapter 3.4.2.

Parameter	Simulated values scenario 2	Simulated values scenario 5	Literature values
K_m ($m\ s^{-1}$)	8×10^{-6}	1.5×10^{-5}	1×10^{-6}–2×10^{-5} (local scale)[e] 2×10^{-5}–1×10^{-4} (regional scale)[e]
m_h ($m^{-2/3}\ s^{-1}$)	0.3	0.3	–
b_h ($m^{1/3}\ s^{-1}$)	0.22	0.18	–
n ($s\ m^{-1/3}$)	1.04 – 4.55	1.05–5.56	0.03 – 1.07[a]
b (m)	0.01	0.01	–
m (–)	2.04×10^{-4}	1.42×10^{-4}	–
ε_1 (m) for TT 1	7.15	7.5	4.4 – 6.9[f], 10[e]
ε_2 (m) for TT 2	30	23	20[g]
A[h] (m^2)	11.9	13.4	13.9[f]
V_c (m^3)	109 351	89 286	≤ 200 000[b]
RMSE H (m)	5.61	5.91	–
Peak offset TT 1 (h)	-0.28[c]	-0.28[c]	–
Peak offset TT 2 (h)	2.5[d]	-1.39[d]	–

[a]Jeannin (2001); [b]Geyer et al. (2008); [c]measurement interval 1 min, simulation interval 2.7 h; [d]measurement interval 6 h, simulation interval 2.7 h; [e]Sauter (1992); [f]Birk et al. (2005); [g]Merkel (1991); [h]average for the interval between tracer test 1 and the spring

Due to a large number of studies conducted in the area during the last decades (e.g. Villinger, 1977; Sauter, 1992; Geyer et al., 2008; Kordilla et al., 2012; Mohrlok, 2014) many data for pattern matching are available even though the karst conduit network itself is not accessible. Since the groundwater flow simulation was performed for steady–state conditions, direct recharge, which is believed to play an important role during event discharge (Geyer et al., 2008), was neglected. It is not expected that recharge dynamics exhibit significant influence on the flow field during recession periods. From Sauter (1992) the long-term average annual recharge, ranges of hydraulic parameters and the average annual hydraulic head distribution derived from 20 observation wells (Figure 3.1a) are available. Villinger (1993) and Sauter (1992) provided data on the geometry of the aquifer base. Available literature values for the model parameters are given in Table 3.1.

The observed hydraulic gradients in the Gallusquelle area are not uniform along the catchment. Figure 3.2 shows an S-shaped distribution with distance to the Gallusquelle spring. The gradient at each point of the area depends on the combination of the respective transmissivity and total flow. The amount of water flowing through a cross sectional area increases towards the springs due to flow convergence. In the Gallusquelle area, the transmissivity rises in the vicinity of the springs leading to a low hydraulic gradient. In the central part of the area discharge is relatively high while the transmissivities are lower leading to the observed steepening of the gradient starting in a distance of 4 000 m to 5 000 m from the Gallusquelle spring. Towards the boundary of the catchment area in the west the water divide reduces discharge in the direction of the Gallusquelle spring leading to a smoothing of hydraulic gradients.

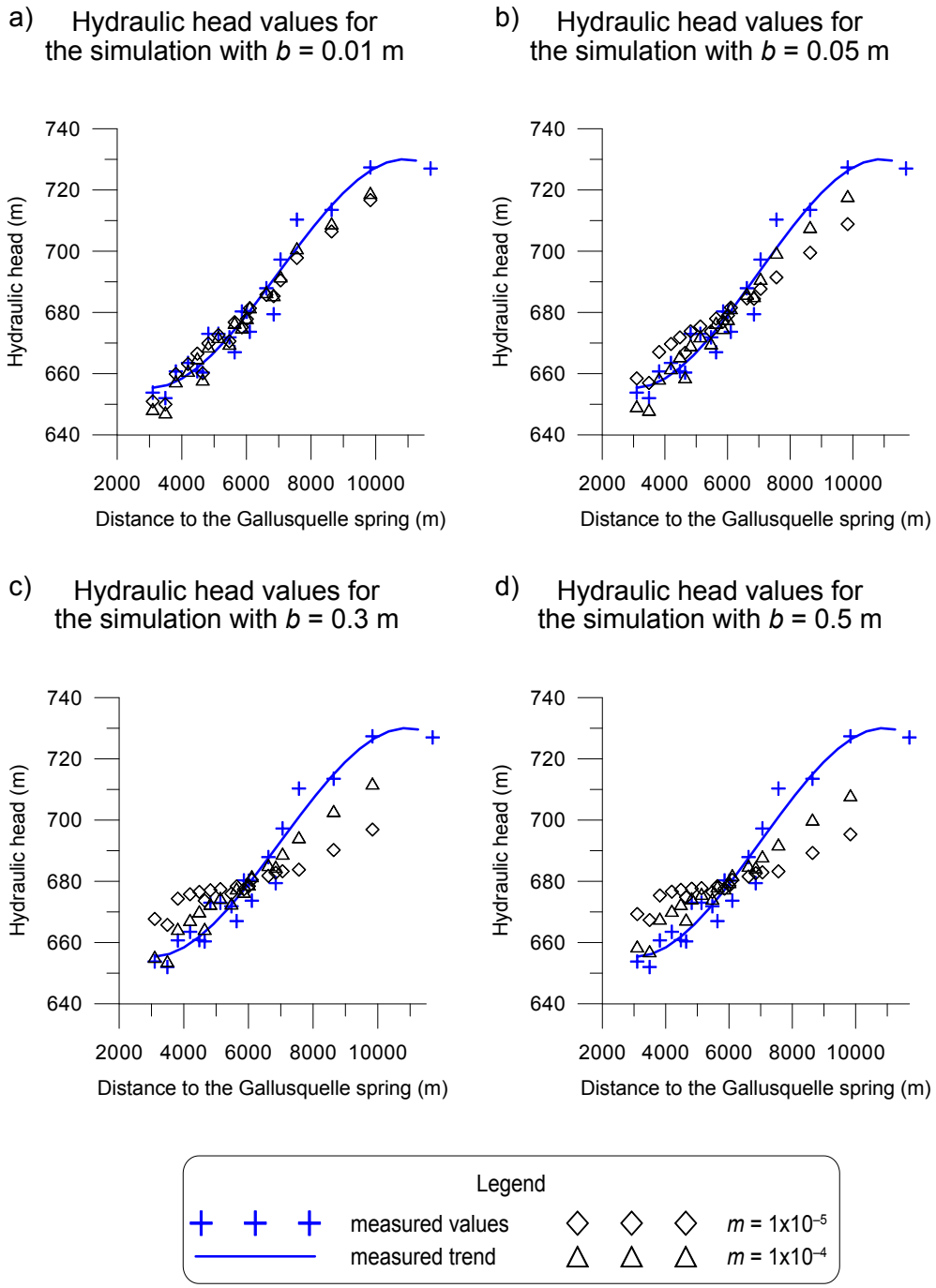

Figure 3.2. Hydraulic head distributions for different combinations of geometric conduit parameters for scenario 1 (Chapter 3.4). b is the lowest conduit radius and m the radius increase along the conduit. For comparison, a trend line is fitted to the measured hydraulic head values showing the distribution of hydraulic gradients from the Gallusquelle spring to the western border of its catchment area.

Geyer et al. (2008) calculated the maximum conduit volume for the Gallusquelle spring V_c [L^3] with information from the tracer test that will be referred to as tracer test 2 in the following. Since the injection point of the tracer test is close to the catchment boundary, it is assumed that it covers the whole length of the conduit system. The authors calculated the maximum volume at 218 000 m^3. Their approach assumes the volume of the conduit corresponds to the total volume of water

discharged during the time between tracer input and tracer arrival neglecting the contribution of the fissured matrix.

The six springs that were monitored and therefore simulated are shown in Figure 3.1. Except for the Balinger spring, their discharges were fitted to long-term average annual discharge data. For the Balinger spring discharge calibration was not possible due to lack of data. It was included as a boundary condition because several tracer tests provided a valuable basis for the conduit structure leading to the spring.

Tracer directions were available for 32 tracer tests conducted at 20 different tracer injection locations (Oehlmann et al., 2013). In all, 16 of the tracer tests were registered at the Gallusquelle spring. For this work two of them were chosen for pattern matching of transport parameters. Both of them were assumed to have a good and direct connection to the conduit network. Tracer test 1 (Geyer et al., 2007) has a tracer injection point at a distance of three kilometres to the Gallusquelle spring. Tracer test 2 (MV746 in Merkel, 1991; Reiber et al., 2010) was conducted at 10 km distance to the Gallusquelle spring (Figure 3.1a). Due to the flow conditions (Figure 3.1a) it can be assumed that tracer test 2 covers the total length of the conduit network feeding the Gallusquelle spring. The recovered tracer mass was chosen as input for the tracer test simulation. The basic information about the tracer tests is given in Table 3.2.

Since the tracer tests were not performed at average flow conditions, the model parameters for groundwater flow were calibrated first for the long-term average annual recharge of 1 mm d^{-1} and the long-term average annual discharge of 0.5 m^3 s^{-1}. For the transport simulations, the recharge was then adapted to produce the respective discharge observed during the tracer experiment (Table 3.2).

Table 3.2. Field data of the simulated tracer tests.

	Tracer test 1	**Tracer test 2**
input mass (kg)	0.75	10
recovery (%)	72	50
distance to spring (km)	3	10
spring discharge (m^3 s^{-1})	0.375	0.76
sampling interval	1 min	6 h
peak time (h)	47	79.5

3.4 Parameter analysis

An extensive parameter analysis was performed in order to identify parameters determining the hydraulic parameter field in the model area, as well as their relative contributions to the discharge and conduit flow velocities. The fitting parameters include the parameters controlling the respective transmissivities of the fissured matrix and the karst conduit system, i.e. the geometry and roughness of the conduit system, the hydraulic conductivity of the fissured matrix and the fracture aperture for the Fehla-Ursprung spring. Furthermore, the apparent dispersivities for the two artificial tracer tests were calibrated (Table 3.1). Since all model runs were performed for steady-state conditions parameters controlling the temporal distribution of recharge were not considered. The parameter analysis was performed with COMSOL Multiphysics® Parametric Sweep tool, which sweeps over a given parameter range. Parameter ranges were chosen according to literature values (Table 3.1). For the conduit geometry parameters, lowest conduit radius *b* and slope of radius increase *m*, no literature values are available. Therefore, the ranges were chosen so that conduit volumes ranged below the maximum volume given by Geyer et al. (2008). In addition to the variation of the fitting parameters, five basic scenarios were compared. They correspond to different conceptual representations of the area and are summarized in Figure 3.3 and Table 3.3.

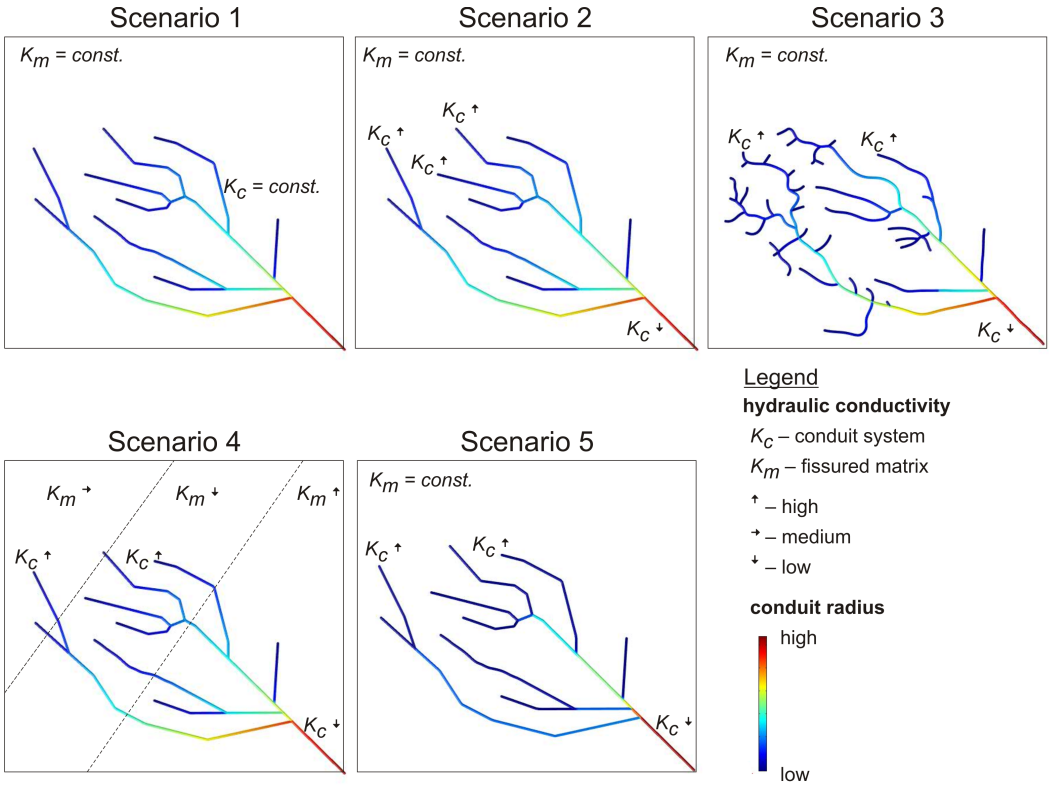

Figure 3.3. Conceptual overview of the simulated scenarios. The conduit geometry and the varying parameters are shown.

Table 3.3. Specifics of the different scenarios. The bold writing indicates the parameter that is analysed in the respective scenario. The results are indicated by comparative markers. "+" means good, "o" means average and "-" means bad compared to the other scenarios. Details to the scenarios and results evaluation can be found in Chapter 3.4.

Parameter	Scenario 1	Scenario 2	Scenario 3	Scenario 4	Scenario 5
K_c	constant	**linear increase**	linear increase	linear increase	linear increase
lateral network	minimal	minimal	**extended**	minimal	minimal
K_m	constant	constant	constant	**variable**	constant
intersection radius r_{c2}	r_{c0}	r_{c0}	r_{c0}	r_{c0}	$\sqrt{\boldsymbol{r_{c0}^2 + r_{c1}^2}}$
main results					
hydraulic head fit	+	+	+	+	+
tracer test fit	-	+	+	+	+
model applicability	+	o	-	-	o

Three objective functions were employed for pattern matching: spring discharge, hydraulic head distribution and flow velocities of the two tracer tests (Chapter 3.3). The average spring discharge of the Gallusquelle spring was set by the difference between simulated and the measured discharge. A difference of 10 L s^{-1} was considered as acceptable. Parameter sets, which could not fulfil this criterion, were not considered for parameter analysis. The other low-discharge and less-investigated springs (Chapter 3.3) were used to inspect the flow field and water balance in the modelling area, i.e. they were only considered after parameter fitting to check the plausibility of the deduced parameter set.

The fit of the tracer tests was determined by comparing the arrival times of the highest peak concentration of the simulation with the measured value (peak offset). Since tracer experiments conducted in karst conduits usually display very narrow breakthrough curves, this procedure appears to be justified. The quality of the fit was judged as satisfactory if the peak offset was lower than either the simulation interval or the measurement interval.

The fit of the hydraulic head distribution was determined by calculating the root mean square error (RMSE) between the simulated and the observed heads at the respective locations of the observation wells. Since the fit at local points with a large-scale modelling approach generally shows large uncertainties due to low-scale heterogeneities, an overall fit of < 10 m RMSE was accepted. Furthermore, a qualitative comparison with the hydraulic gradients in the area was performed (e.g.

Figure 3.2) to ensure that the general characteristics of the area were represented instead of only the statistical value.

3.4.1 Scenario 1 – standard scenario

In scenario 1 all features were implemented as described in Chapters 3.2 and 3.3. The parameter analysis shows that for each conduit geometry, defined by their smallest conduit radii *b* and their slopes of radius increase along the conduit length *m* (Eq. 3.1), only one value of the Manning coefficient *n* allows a simulated discharge for the Gallusquelle spring of 0.5 $m^3 s^{-1}$. The *n*-value correlates well with that for the total conduit volume due to the fact that the spring discharge is predominantly determined by the transmissivity of the karst conduit system. The transmissivity of the conduit system at each point in space is the product of its hydraulic conductivity, which is proportional to 1/*n*, and the cross sectional area of the conduit *A*. Thus, to keep the spring discharge at 0.5 $m^3 s^{-1}$ a higher conduit volume requires a higher calibrated *n*-value (Eq. 3.4).

With scenario 1 it is possible to achieve a hydraulic head fit resulting in an RMSE of 6 m that can be judged as adequate on catchment scale. Regarding the conduit geometry, a good hydraulic head fit can be achieved with small *b*-values independently of the chosen *m*-value (Figure 3.2a). The higher the *b*-value, the higher the *m*-value to reproduce the hydraulic gradients of the area (Figure 3.2). This implies that the hydraulic head fit is independent of the conduit volume during steady-state conditions but depends on the *b*/*m*-ratio. The influence of the *b*/*m*-ratio on the hydraulic head fit depends on the hydraulic conductivity of the fissured matrix K_m. For low K_m values of ca. 1×10^{-6} m s^{-1} the hydraulic head fit is completely independent of the conduit geometry and the RMSE is very high (Figure 3.4a). For high K_m values of ca. 5×10^{-4} m s^{-1} (Figure 3.4a) the dependence is also of minor importance and the RMSE is relatively stable at ca. 11 m. Due to the high hydraulic conductivity of the fissured matrix the hydraulic gradients do not steepen in the vicinity of the spring even for high *b*/*m*-ratios. For K_m values between the above values the RMSE significantly rises for *b*/*m*-ratios above 1000 m. For the range of acceptable errors, i.e. lower than 10 m, it is apparent in Figure 3.4a that the best-fit K_m value is approximately 1×10^{-5} m s^{-1} independent of the conduit geometry. However, no distinct best-fit conduit geometry can be derived. There are several parameter combinations providing a good fit for the Gallusquelle spring discharge and the hydraulic head distribution.

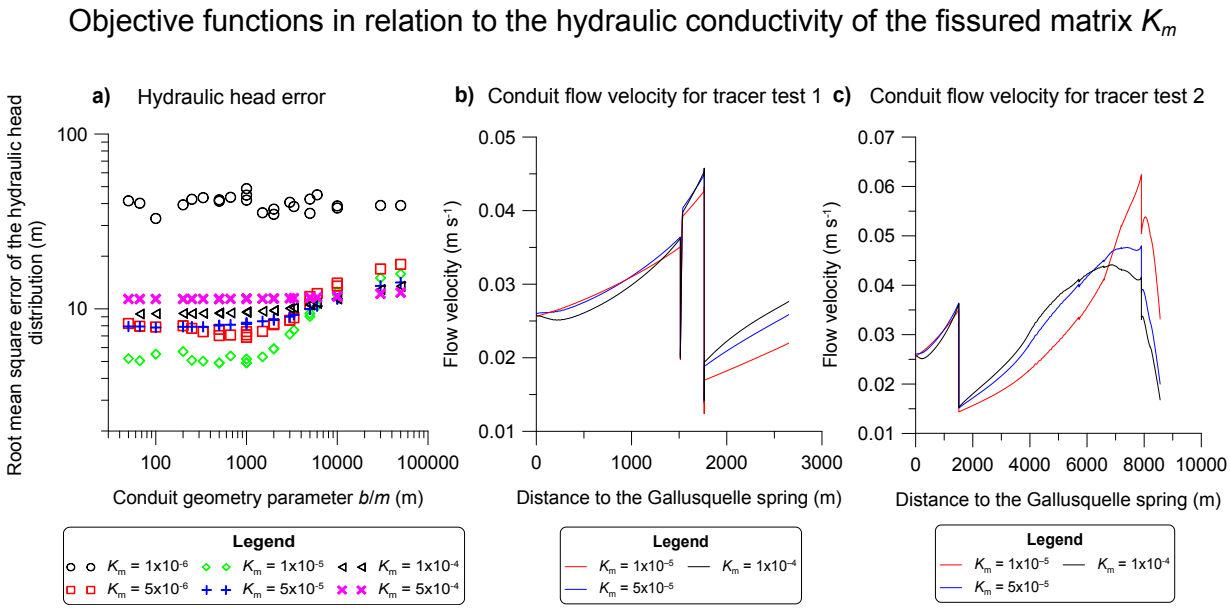

Figure 3.4. Influence of the hydraulic conductivity of the fissured matrix on the objective functions. (a) Influence on the root mean square error of the hydraulic head distribution in relation to the conduit geometry. The conduit geometry is represented by the parameter b/m (Eq. 3.1), which is the ratio of the smallest radius to the slope of radius increase along the conduit length. (b) Influence on the conduit flow velocity for tracer test 1. (c) Influence on the conduit flow velocity for tracer test 2.

The goodness of the fit of the simulation of the tracer breakthrough is mainly determined by the conduit geometry. The influence of the hydraulic conductivity of the fissured matrix K_m on flow velocities inside the karst conduits is comparatively low and decreases even further in the vicinity of the springs (Figure 3.4b and c) leading to minor influences on tracer travel times. Instead, the quality of the fit mainly depends on the conduit volume and accordingly on the Manning coefficient *n* (Figure 3.5). It is possible to simulate only one of the two tracer experiments with this scenario (Figure 3.5). Given the broad range of geometries for which an adequate hydraulic head fit can be achieved (Figure 3.2 and Figure 3.4) it is possible to simulate one of the two tracer peak velocities and the hydraulic head distribution with the same set of parameters. While the simulation of the breakthrough of tracer test 1 requires relatively high *n*-values, of ca. 2.5 s $m^{-1/3}$, that of tracer test 2 can only be calibrated with lower values of ca. 1.7 s $m^{-1/3}$ (cf. Figure 3.5a and b). For every parameter set, where the travel time of the simulated tracer test 2 is not too long, that of tracer test 1 is too short. For the simulation of tracer test 2, the velocities at the beginning of the conduits must be relatively high. To avoid the flow velocities from getting too high in downgradient direction, the conduit size would have to increase drastically due to the constant additional influx of water from the fissured matrix. In the given geometric range, the conduit system has a dominant influence on spring discharge. Physically, this situation corresponds to the conduit-influenced flow conditions (Kovács et al., 2005). Thus, conduit transmissivity is a limiting factor for conduit-matrix exchange and a positive feedback mechanism is triggered, if the conduit size is increased. A higher conduit size

leads to higher groundwater influx from the fissured matrix and spring discharge is overestimated. Therefore, parameter analysis shows that scenario 1 is too strongly simplified to correctly reproduce the complex nature of the aquifer.

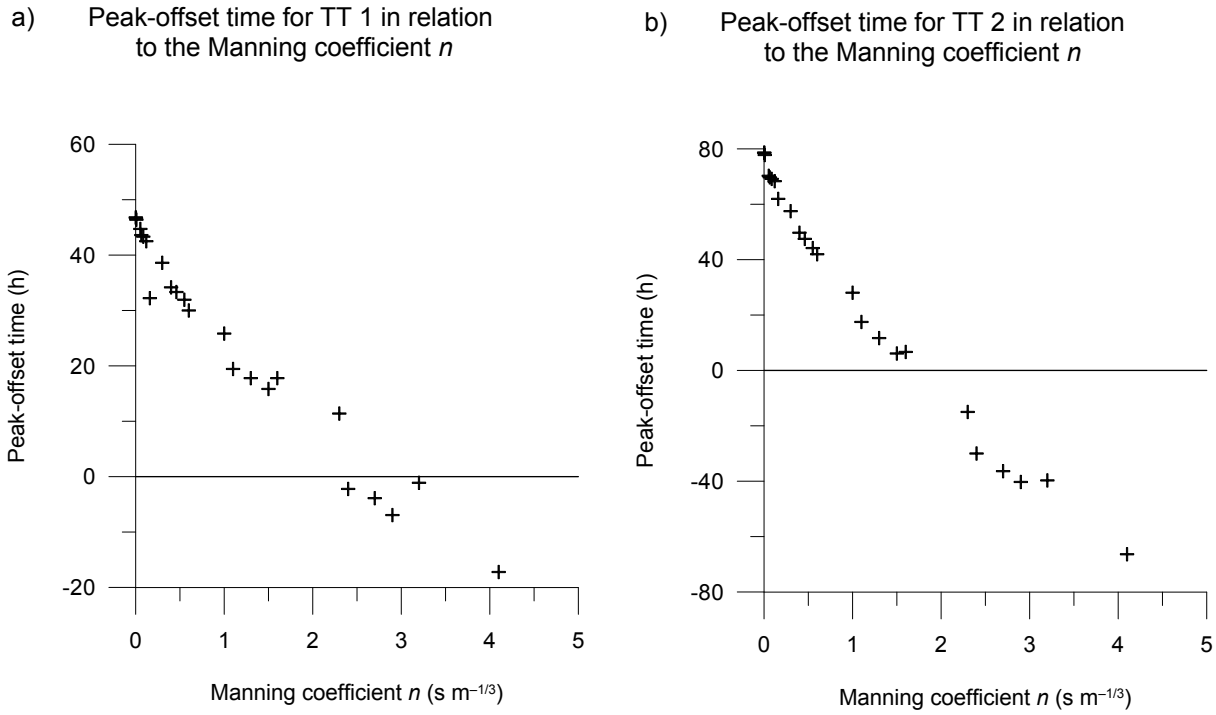

Figure 3.5. Difference between peak concentration times vs. the Manning n-value for scenario 1. High n-values correspond to high conduit volumes and high cross-sectional areas at the spring (a**) for tracer test 1 (**b**) for tracer test 2.**

3.4.2 Scenario 2 – conduit roughness coefficient K_c

In scenario 2 the Manning coefficient *n* was changed from constant to laterally variable. In the literature, *n* is generally kept constant throughout the conduit network (e.g. Jeannin, 2001; Reimann et al., 2011) for lack of information on conduit geometry. However, it is assumed that the Gallusquelle spring is not fed by a single large pipe. Rather there is some evidence in the spring area that a bundle of several small-interconnected pipes feed the spring. Since the number of individual conduits per bundle is unknown and the regional modelling approach limits the resolution of local details, the small diameter conduits, which the bundle consists of, cannot be simulated individually. Therefore, each single pipe in the model represents a bundle of conduits in the field.

It can be assumed that the increase in conduit cross section is at least partly provided by additional conduits added to the bundle rather than a single individual widening conduit. Therefore, while the

cross section of the simulated conduit, i.e. the total effective cross section of the conduit bundle, increases towards the springs, it is not specified how much of this increase is due to the individual conduits widening and how much is due to additional conduits, not distinguishable in the simulation. If the simulated effective cross sectional area increase is mainly due to additional conduits being included in the bundle, the surface / volume ratio increases with the cross section, contrary to what would be observed, if a single conduit in the model would represent a single conduit in the field. The variation in surface area / volume ratio implicitly leads to a larger roughness in the simulation, even further enhanced by exchange processes between the individual conduits. This effect again leads to an increase in the Manning coefficient n in the downgradient direction towards the spring for a simulated single conduit. Since the number and size of the individual conduits is unknown, it is impossible to calculate the change of n directly from the geometry. Thus, a simple scenario was assumed where the roughness coefficient K_c, which is the reciprocal of n, was linearly and negatively coupled to the rising conduit radius (Eq. 3.13).

$$K_c = \frac{1}{n} = -m_h\, r_c + m_h\, r_{c,max} + b_h\ , \tag{3.13}$$

where r_c [L] is the conduit radius and $r_{c,max}$ [L] the maximum conduit radius simulated for the respective spring, which COMSOL® calculates from Eq. (3.1). m_h [$L^{-2/3}$ T^{-1}] and b_h [$L^{1/3}$ T^{-1}] are calibration parameters determining the slope and the lowest value of the roughness coefficient respectively.

For every conduit geometry several combinations of m_h and b_h lead to the same spring discharge. However, hydraulic head fit and tracer velocities are different for each m_h – b_h combination even if spring discharge is the same. With the new parameters a higher variation of velocity profiles is possible. This allows for the calibration of the tracer velocities of both tracer tests. The dependence of tracer test 2 on m_h is much higher than that of tracer test 1 since it is injected further upgradient towards the beginning of the conduit (Figure 3.6). Therefore, tracer test 2 is influenced more strongly by the higher velocities far away from the spring introduced by high m_h-values and always shows a significant positive correlation with m_h (Figure 3.6).

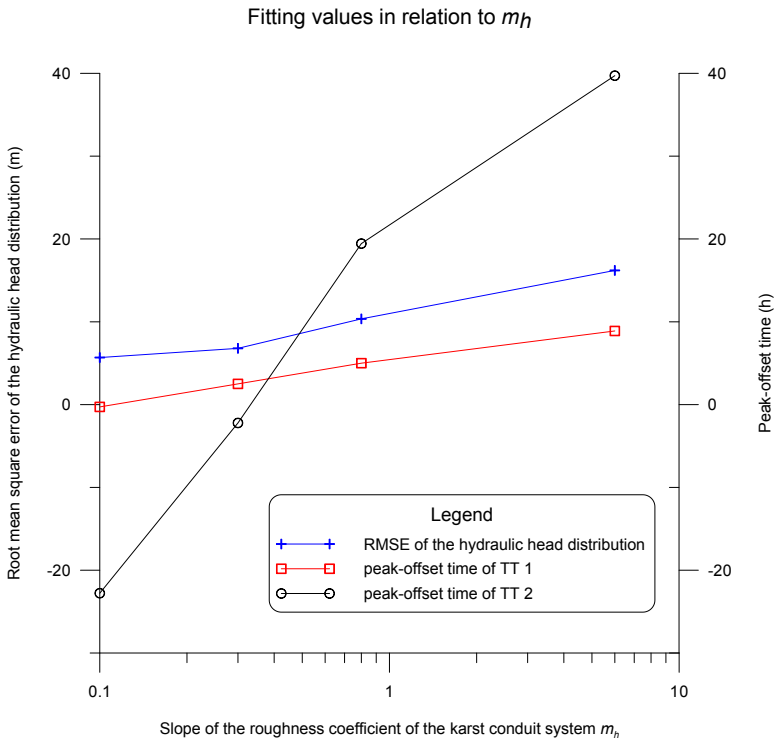

Figure 3.6 Hydraulic head errors and differences between peak concentration times for both tracer tests for scenario 1. The example is shown for a conduit geometry with a starting value b = 0.01 ($m^{1/3}$ s^{-1}) and a radius increase of m = 2×10^{-4} ($m^{-2/3}$ s^{-1}). Each m_h-value corresponds to a respective value of the highest conduit roughness b_h and each combination results in the same spring discharge.

Since the slope of K_c is negative with respect to the conduit length, the variable K_c leads to a slowing down of water towards the springs. As discussed in detail by Oehlmann et al. (2013) a rise of transmissivity towards the springs is observed in the Gallusquelle area. Therefore, adequate hydraulic head fits can only be obtained, if the decrease of K_c towards the spring is not too large and compensates the effect of the increase in conduit transmissivity due to the increasing conduit radius. This effect reduces the number of possible and plausible parameter combinations. From these considerations a best-fit model can be deduced capable of reproducing all objective functions within the given error ranges (Figure 3.7a). According to the model simulations, karst groundwater discharge and flow velocities significantly depend on the total conduit volume as is to be expected. It can be deduced from the parameter analysis that the conduit volume can be estimated at ca. 100 000 m^3 for the different parameters to match equally well (Figure 3.7a).

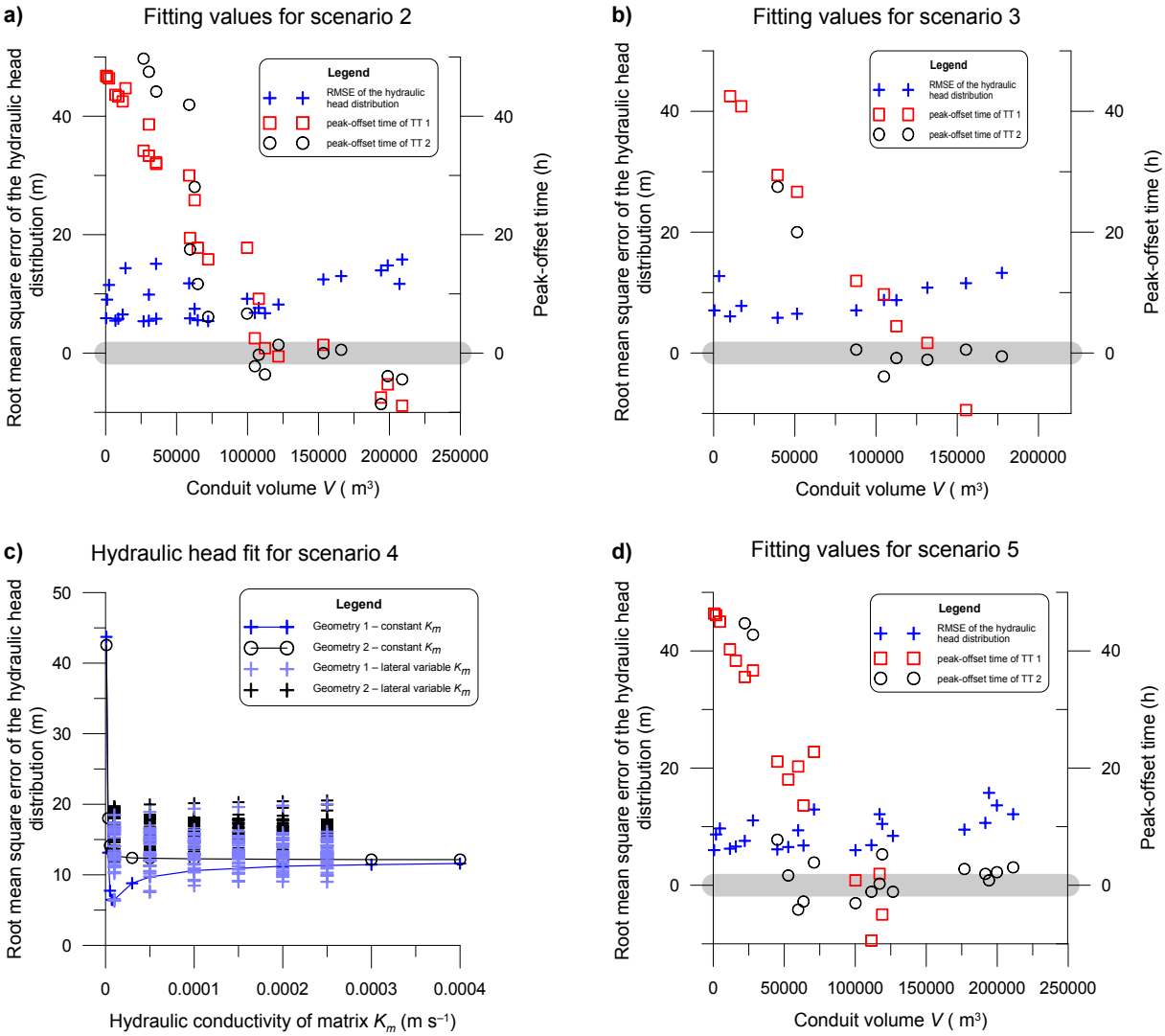

Figure 3.7. Calibrated values for the simulated scenarios. For scenarios 2, 3 and 5 (Figure (a), (b) and (d)) hydraulic head fit and the peak-offset times of both tracer tests (referred to as TT 1 and TT2) are shown in relation to conduit volume. The thick grey bar marks the target value of zero. For scenario 4 (Figure (c)) the root mean square error of the hydraulic heads is given for two different conduit geometries in relation to the hydraulic conductivity of the fissured matrix K_m. For the version with laterally variable matrix conductivity the axis shows as an example the hydraulic conductivity of the north-western part. The parameters for the two geometries are given in Table 3.4.

3.4.3 Scenario 3 – extent of conduit network

In scenario 3, a laterally further extended conduit system was employed, assuming the same maximum conduit volume as in scenarios 1 and 2 but with different spatial distribution along the different total conduit lengths. The original conduit length for the Gallusquelle spring in scenarios 1 and 2 is 39 410 m, for scenario 3 it is 63 490 m; therefore, the total length was assumed to be larger by ca. 50% (Figure 3.8). The geometry of the original network was mainly constructed along dry valleys where point-to-point connections are observed based on qualitative evaluation from artificial

tracer tests. Of the dry valleys without tracer tests, only the larger ones were included, where the assumption of a high karstification is backed up by the occurrence of sinkholes (Mohrlok and Sauter, 1997). Therefore, it represents the minimal extent of the conduit network. For scenario 3 the network was extended along all dry valleys within the catchment, where no tracer tests were conducted.

The results of the parameter variations are comparable to those of scenario 2 (cf. Figure 3.7a and b). While the hydraulic head contour lines are smoother than for the original conduit length the general hydraulic head fit is the same (Figure 3.7b). It seems possible to obtain a good fit for all model parameters but the scenario is more difficult to handle numerically. Calculation times are up to 10 times larger compared to the other scenarios and goodness of convergence is generally lower. Since the calibrated parameters are not significantly different from those deduced in scenario 2 it is concluded that the ambiguity introduced by the uncertainty in total conduit length is small if hydraulic conduit parameters and total conduit volumes are the aim of investigation.

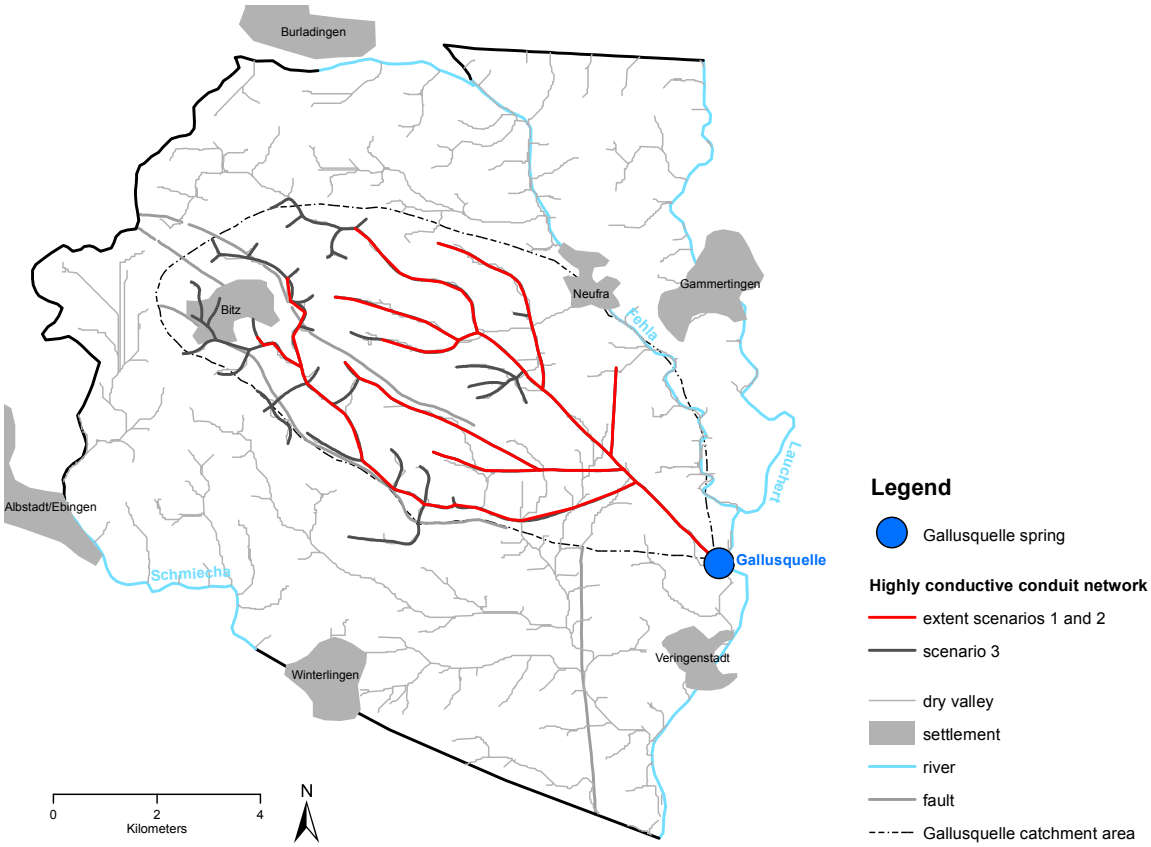

Figure 3.8. Extended conduit system for scenario 3. The conduit configuration (extent) that is used for the other scenarios is marked in red.

3.4.4 Scenario 4 – matrix hydraulic conductivity K_m

In scenario 4, the homogeneously chosen hydraulic conductivity of the fissured matrix K_m was changed into a laterally variable conductivity based on different types of lithology and the spatial distribution of the groundwater potential. Sauter (1992) found from field measurements that the area can be divided into three parts with different hydraulic conductivities. Oehlmann et al. (2013) discussed that the major influence is the conduit geometry leading to higher hydraulic transmissivities close to the springs in the east of the area. It is also possible that not only the conduit diameters change towards the spring but the hydraulic conductivity of the fissured matrix as well, since the aquifer cuts through three stratigraphic units (Chapter 3.3). These geologic changes are likely to affect the lateral distribution of hydraulic conductivities (Sauter, 1992). Figure 3.9 shows the division into three different areas. K_m values were varied in the range of the values measured by Sauter (1992).

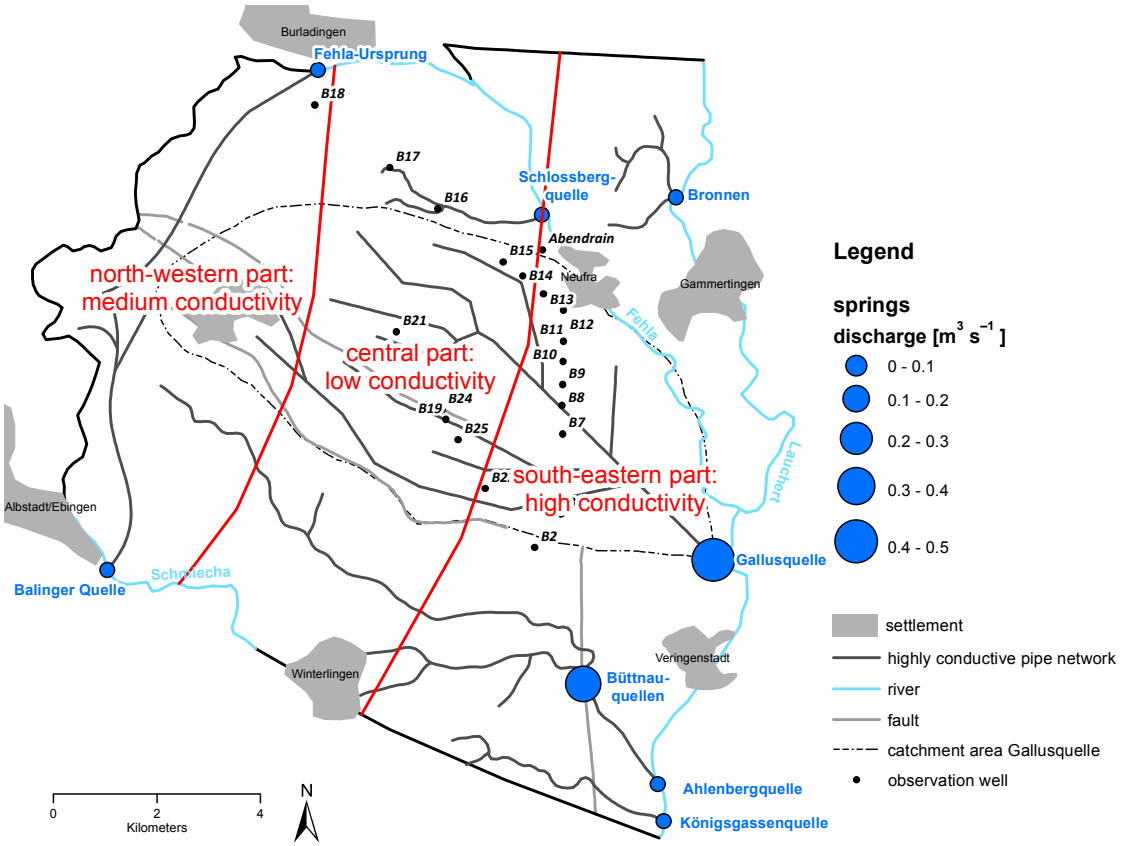

Figure 3.9. Model catchment with spatially distributed hydraulic conductivities. The model area is divided into three parts after geologic aspects. For each segment different values of the hydraulic conductivity were examined during parameter analysis in scenario 4.

It was expected that a laterally variable K_m value has a major influence on the hydraulic head distribution. All variations of scenario 2 that produce good results for both tracer tests and have a high total conduit volume above 100 000 m^3 yield poor results for hydraulic head errors and spatial distributions of the hydraulic heads (Figure 3.7). For scenario 4, two different conduit configurations (geometries) were chosen that achieve good results with respect to conduit flow velocities. Geometry G1 has a conduit volume of 112 000 m^3. G2 has a higher *b*-value which leads to the maximum conduit volume of ca. 150 000 m^3. All parameters for the two simulations are given in Table 3.4.

Table 3.4. Parameters for the two different conduit configurations compared in scenario 4. *b* is the minimum conduit radius, *m* the slope of radius increase towards the springs, b_h the highest conduit roughness, m_h the slope of roughness decrease away from the spring and V_c the conduit volume.

	Geometry 1	**Geometry 2**
b (m)	0.01	0.5
m (–)	2.07×10^{-4}	1.5×10^{-4}
b_h (s^{-1} $m^{1/3}$)	0.17	0.15
m_h (s^{-1} $m^{-2/3}$)	0.4	0.6
V_c(m^3)	112 564	153 435

It was found that while the maximum root mean square error of the hydraulic head fit is similar for both geometries, the minimum RMSE for the hydraulic head is determined by the conduit system. It is not possible to compensate an unsuitable conduit geometry with suitable K_m values (Figure 3.7c), which assists in the independent conduit network and fissured matrix calibration. This observation increases the confidence in the representation of the conduits and improves the possibility to deduce the conduit geometry from field measurements. For an adequate conduit geometry, laterally variable matrix conductivities do not yield any improvement. The approach introduces additional parameters and uncertainties because the division of the area into three parts is not necessarily obvious without detailed investigation. From the distribution of the exploration and observation wells (Figure 3.1a) it is apparent that especially in the south and west the boundaries are not well defined.

3.4.5 Scenario 5 – conduit intersections

In scenario 5, the effect of the conduit diameter change at intersections was investigated. In the first four scenarios the possible increase in cross sectional area at intersecting conduits was neglected. In nature however, the influx of water from another conduit is likely to influence conduit evolution and therefore its diameter. In general, higher flow rates lead to increased dissolution rates because dissolution products are quickly removed from the reactive interface. If conditions are turbulent the solution is limited by a diffusion dominated layer that gets thinner with increasing flow velocities (Clemens, 1998). Clemens (1998) simulated karst evolution in simple Y-shaped conduit networks and found higher diameters for the downstream conduit even after short simulation times. Preferential conduit widening at intersections could further be enhanced by the process of mixing corrosion (Dreybrodt, 1981). However, Hückinghaus (1998) found during his karst network evolution simulations that the water from other karst conduits has a very high saturation with respect to Ca^{2+} compared to water entering the system through direct recharge. Thus, if direct recharge is present, the mixing with nearly saturated water from an intersecting conduit could hamper the preferential evolution of the conduit downstream slowing down the aforementioned processes. In scenario 5 the influence of an increase in diameter at conduit intersections was investigated. Since the amount of preferential widening at intersections is unknown, the cross sections of two intersecting conduits were added and used as starting cross section for the downstream conduit. The new conduit radius was then calculated according to Eq. (3.14) at each intersection.

$$r_{c2} = \sqrt{r_{c0}^2 + r_{c1}^2} \tag{3.14}$$

where r_{c2} is the conduit radius downstream of the intersection and r_{c0} and r_{c1} the conduit radii of the two respective conduits before their intersection.

Results are very similar to those of scenario 2 (cf. Figure 3.7a and d). Both simulations result in nearly the same set of parameters (Table 3.1). The estimated conduit volume is even a little smaller for scenario 5 since larger cross sections in the last conduit segment near the spring are reached for a lower total conduit volume. The drastic increase of conduit cross sections at the network intersections leads to higher variability in the cross sections along the conduit segments. The differences between the peak offsets of both tracer tests are higher compared to those of scenario 2. While the peak time of tracer test 2 can be calibrated for large conduit volumes, i.e. conduit volumes above 120 000 m^3 (Figure 3.7d), the peak time of tracer test 1 is too late for large conduit volumes. This is due to the fact that the injection point for tracer test 1 is much closer to the spring than that for tracer test 2. In scenario 5 the conduit volume is spatially differently distributed from that of scenario 2 for the identical total conduit volume. The drastic increase in conduit diameters

downgradient of conduit intersections leads to rather high conduit diameters in the vicinity of the spring. Therefore, while tracer transport in tracer test 2 occurs in relatively small conduits with high flow velocities and larger conduits with lower velocities, the tracer in tracer test 1 is only transported through the larger conduits whose flow velocities are restricted by the spring discharge. In Figure 3.7d the parameter values for the best fit would lie well below the lower boundary of the diagram at negative values below -10 h. However, since the fit for conduit volumes around 100 000 m^3 is similar to that of scenario 2, the two scenarios can in this case not be distinguished based on field observations.

3.4.6 Conclusions of the parameter analysis

Table 3.3 provides a comparison, i.e. the characteristics for all scenarios. The parameter analysis shows that there is only a limited choice of parameters with which the spring discharges (water balance), the hydraulic head distribution and the tracer velocities can be simulated. Scenario 1 is the only scenario that cannot reproduce the peak travel times observed in both tracer tests simultaneously (Chapter 3.4.1). It underestimates the complexity of the geometry and internal surface characteristics (e.g. roughness) of the conduit system.

Scenario 4 introduces two additional model parameters. The best fit for this scenario is, however, still achieved with all three K_m values being equal, which basically results in the parameter set of scenario 2. This implies that the major influence leading to the differences in hydraulic gradients observed throughout the area is the conduit system and not the variability of the fissured matrix hydraulic conductivity. It was also shown by Saller et al. (2013) that for the Madison aquifer (USA), a better representation of the hydraulic head distribution can be achieved by including a discrete conduit system even for reduced variability in the hydraulic conductivity of the fissured matrix. Their conclusion complies very well with the findings for scenario 4.

Scenario 3 simulates the presence of a couple of additional smaller dendritic branches. The deduced parameter values and the fit of the objective functions are similar to those of scenarios 2 and 5. Because of long calculation times without additional advantage for the presented study, scenario 3 is not considered for further analysis.

Scenarios 2 and 5 are both judged as suitable. Their parameters and the quality of the fit are similar. Therefore, it is not possible to decide which one is the better representation of reality. Regarding the different processes interacting during karst evolution (Chapter 3.4.5) it is most likely that the actual geometry ranges somewhat in between these two scenarios. Table 3.1 summarizes all parameters of

both simulations and Figure 3.10 shows the simulated tracer breakthrough curves and spring discharges.

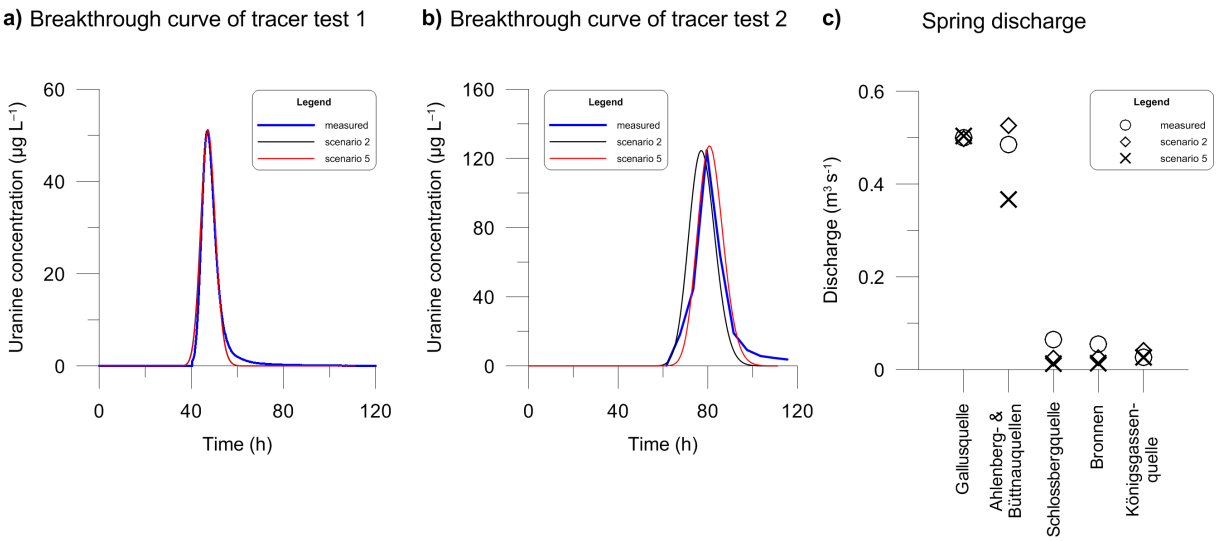

Figure 3.10 Comparison of the best-fit simulations with field data for scenarios 2 and 5. (a) breakthrough curve of tracer test 1, (b) breakthrough curve of tracer test 2, (c) spring discharge.

3.5 Discussion

3.5.1 Plausibility of the best-fit simulations

The main objective of the model simulation is not only to reproduce the target values but also to provide insight into dominating flow and transport processes, sensitive parameters and to check the plausibility of the model set-up. Possible ambiguities in parameterizations can also be checked, i.e. different combinations of parameters producing identical model output.

For these aims model parameters and aquifer properties simulated with scenarios 2 and 5 are compared to those observed in the field. As seen in Table 3.1 most of the calibrated parameters range well within values provided in the literature. The calibrated Manning coefficients are relatively high compared to other karst systems. Jeannin (2001) lists effective conductivities for several different karst networks that translate into *n*-values of between 0.03 s $m^{-1/3}$ and 1.07 s $m^{-1/3}$, showing that the natural range of *n*-values easily extends across 2 orders of magnitude and the minimum *n*-values of the simulation lie within the natural range. The maximum *n*-values are significantly higher than those given by Jeannin (2001). This is not surprising since the calibrated *n*-value reflects the

total roughness of the conduit bundles and therefore includes geometric conduit properties in addition to the wall roughness that it was originally defined for. This effect is specific for the Gallusquelle area but it might be important to consider for other moderately karstified areas as well where identification of conduit geometries is especially difficult.

The total conduit volume of the Gallusquelle spring derived from scenarios 2 and 5 is only 50% of that estimated with traditional methods (Geyer et al., 2008). Since the conduit transmissivity increases towards the spring water enters the conduits preferably in the vicinity of the spring in the Gallusquelle area. Therefore, the matrix contribution is high. In addition, the travel time at peak concentration of tracer test 2, which was used for the volume estimation by Geyer et al. (2008), is longer than 3 days, during which time matrix-conduit water exchange can readily take place. Based on the results of a tracer test conducted in a distance of 3 km to the Gallusquelle spring Birk et al. (2005) estimated the error incurred by deducing the conduit volume without taking conduit-matrix exchange fluxes into account with a very simple numerical model. The authors found a difference in conduit volumes of approximately 50%. This fits well with the results of the present simulation. Birk et al. (2005) also estimated the simulated equivalent conduit cross sectional area between their tracer injection point and the spring to be 13.9 m^2. For scenario 2 the simulated average cross sectional area is 11.9 m^2 and for scenario 5 13.4 m^2, which compares very well with the results of Birk et al. (2005).

It was not possible to match the shape of both breakthrough curves with the same dispersivity. The apparent dispersion in the tracer test 2 breakthrough is much higher compared to that of tracer test 1, while the breakthrough of tracer test 1 shows a more expressed tailing (Figure 3.10a and b). This corresponds to the effect observed by Hauns et al. (2001). The authors found scaling effects in karst conduits: the larger the distance between input and observation point, the more mixing occurred. The tailing is generally induced by matrix diffusion or discrete geometric changes such as pools, where the tracer can be held back and released more slowly. Theoretically, every water drop employs medium and slow flow paths if the distance is large enough, leading to a more or less symmetrical, but broader, distribution and therefore a higher apparent dispersion (Hauns et al., 2001). To quantify this effect, exact knowledge of the geometric conduit shape such as the positions and shapes of pools would be necessary. Furthermore, an additional unknown possibly influencing the observed retardation and dispersion effects is the input mechanism. The simulation assumes that all introduced tracers immediately and completely enter the conduit system, which neglects effects of the unsaturated zone on tracer breakthrough curves. In addition, the shape of the breakthrough curve of tracer test 2 is difficult to deduce since the 6 h sampling interval can be considered as rather low leading to a breakthrough peak which is described by only seven measurement points.

Therefore, the apparent dispersivity was calibrated for both breakthrough curves separately. Calibrated dispersivity ranges well within those quoted in literature (Table 3.1). The mass recovery during the simulation was determined to range between 98.4% and 99.9% in all simulations. The slight mass difference results from a combination of diffusion of the tracer into the fissured matrix and numerical inaccuracies.

The spring discharge of the minor springs in the area (Chapter 3.3) was slightly underestimated in most cases (Figure 3.10c). For most springs the models of scenarios 2 and 5 provide similar results. The underestimation of discharge is in the order of <0.05 $m^3 s^{-1}$ and is not expected to significantly influence the general flow conditions. It probably results from the unknown conduit geometry in the catchments of the different minor springs. The only case in which the two scenarios give significantly different results is the spring discharge of the spring group consisting of the Ahlenberg and Büttnauquellen springs (Figure 3.10c). Scenario 2 overestimates and scenario 5 underestimates the discharge. This is due to the fact that the longest conduit of the Ahlenberg and Büttnauquellen springs is longer than the longest one of the Gallusquelle spring but the conduit network has less intersections (Figure 3.1). Therefore the conduit volume of the Ahlenberg and Büttnauquellen springs is 134 568 m^3 in scenario 2 and only 75 085 m^3 in scenario 5 leading to the different discharge values. It is reasonable to assume that a better fit for the spring group can be achieved, if more variations of conduit intersections are tested. An adequate fit for the Fehla-Ursprung spring of 0.1 $m^3 s^{-1}$ was achieved for both scenarios with a fault aperture of 0.005 m.

3.5.2 Uncertainties and limitations

The most important uncertainties regarding the reliability of the simulation include the assumptions that were made prior to modelling. First, flow dynamics were neglected. This approach was chosen because tracer tests are supposed to be conducted during quasi-steady-state flow conditions. However, this is only the ideal case. During both tracer tests spring discharge declined slightly. The influence of transient flow on transport velocities inside the conduits was estimated by a very simple transient flow simulation for the best-fit models in which recharge and storage coefficients were calibrated to reproduce the observed decline in spring discharges. The transient flow only slightly affected peak velocities but led to a larger spreading of the breakthrough curves and therefore lower calibrated dispersion coefficients. This effect occurred because the decline in flow velocities is not completely uniform inside the conduits and depending on where the tracer is at which time it experiences different flow velocities in the different parts of the conduits, which leads to a broader distribution at the spring. The same breakthrough curves can be simulated under steady-state flow conditions with slightly higher dispersivity coefficients. So, the calibrated dispersivities do not only

represent geometrical heterogeneities but also temporal effects as is the case for all standard evaluations of dispersion from tracer breakthrough curves.

The influence of rapid recharge is not considered in the simulation of baseflow conditions. However, there might be an influence on flow velocities during the actual recharge events, i.e. if rapid recharge is intensive and strong enough to lead to a reversal of the flow gradients between conduit and fissured matrix. Therefore, an alternative simulation was performed for tracer test 2, which was conducted during high flow conditions (Table 3.2) after a recharge event. The maximum percentage of direct recharge of 10% estimated by Sauter (1992) and Geyer et al. (2008) was used for this simulation. Neither for scenario 2 nor for scenario 5 a gradient reversal between conduit and matrix occurred and the influence on flow velocities was negligible (Figure 3.11).

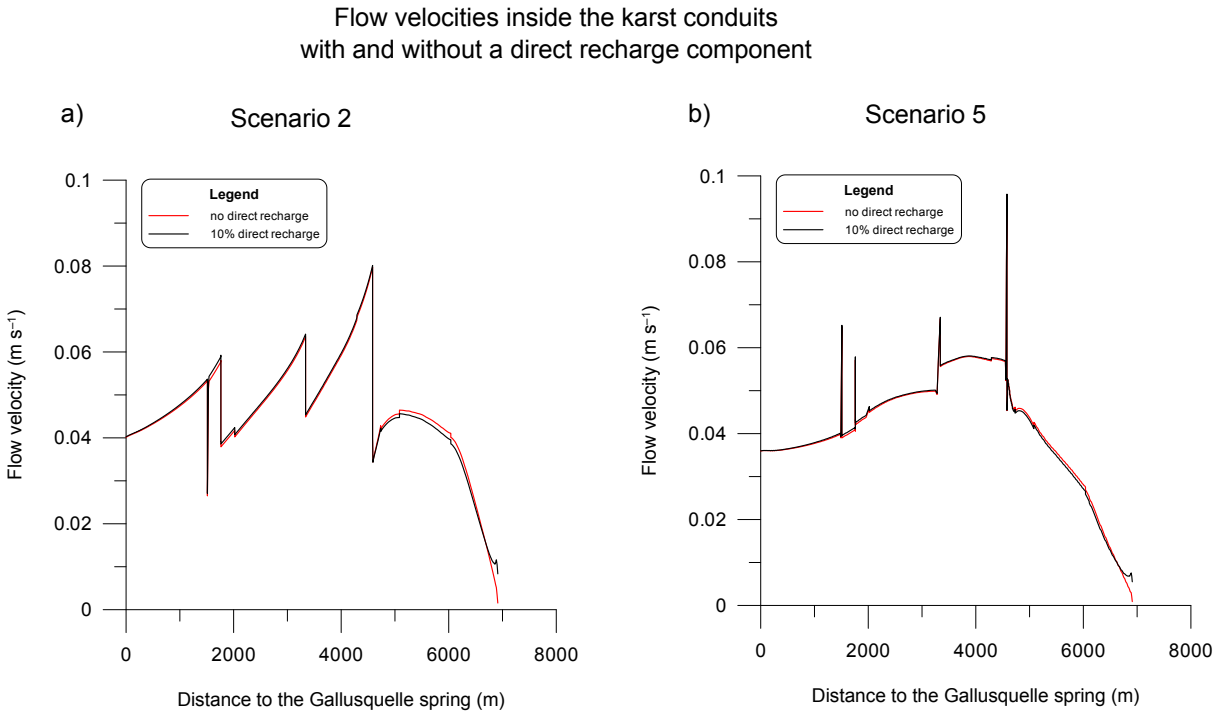

Figure 3.11. Flow velocities inside the main conduit branch of the Gallusquelle spring during the simulation of tracer test 2. The best-fit simulations for scenarios 2 and 5 are compared to simulations where a direct recharge of 10% is introduced.

Furthermore, flow in all karst conduits was simulated for turbulent conditions. Turbulent conditions can be generally assumed in karst conduits (Reimann et al., 2011) and also apply to all calibrated model conduit cross sections. Since the conduit cross section presents the total cross section of the conduit bundle, the cross sections of the individual tubes are uncertain, though. The high *n*-values suggest that the surface / volume ratio is relatively high, which implies that the individual conduit

cross sections are rather small. Therefore, laminar flow in some conduits is likely. While laminar flow conditions in the conduits influence hydraulic gradients considerably, this fact is believed not to influence the overall results and conclusions of this study, i.e. the relative significance of the parameters deduced from parameter analysis and the deduced conduit volume, especially since flow is simulated for steady-state conditions.

For all distributed numerical karst simulations, uncertainties regarding the exact positions and interconnectivities of the conduit branches still remain. Due to the extensive investigations already performed in previous work (Chapter 3.3) these uncertainties are reduced in the Gallusquelle area and the above scenarios include the most probable ones. However, the flexibility of the modelling approach allows for the integration of any future information that might enhance the numerical model further.

3.5.3 Calibration strategy

For a successful calibration of a distributed groundwater flow and transport model for a karst area on catchment scale certain constraints have to be set a priori. The geometry of the model area, i.e. locations / types of boundary conditions and aquifer base, fixed during calibration, has to be known with sufficient certainty. Furthermore, the objective functions for calibration have to be defined, i.e. the hydraulic response of the system and transport velocities. In a karst groundwater model, these consist of measurable variables, i.e. spring discharges, hydraulic heads in the fissured matrix and two tracer breakthrough curves. The hydraulic head measurements should be distributed across the entire catchment and preferably close to the conduit system, should geometric conduit parameters be calibrated for as well. It is expected that the influence of the conduits on the hydraulic head decreases and the influence of matrix hydraulic conductivities increases with distance to the conduit system. In the design of the tracer experiment, the following criteria should be observed: for a representative calibration, the dye should be injected at as large a distance to each other as possible with one of them including the length of the whole conduit system. Each tracer test gives integrated information about its complete flow path. If the injection points lie close together, no information about the development of conduit geometries from water divide to spring can be obtained. Further, the dye should be injected as directly as possible into the conduit system, e.g. via a flushed sinkhole, to obtain information on the conduit flow regime and to minimize matrix interference. To ease interpretation a constant spring discharge during the tests is desirable.

In this study, the flow field was simulated not only for the catchment area of the Gallusquelle spring, but also for a larger area including the catchment areas of several smaller springs (Figure 3.1). This is in general not essential for deducing conduit volumes and setting up a flow and transport model.

Simulating several catchments, however, helps to increase the reliability of the simulation. The positions of water divides are majorly determined by the hydraulic conductivity of the fissured matrix K_m, so that the simulated catchment areas of the different springs can be used to estimate how realistic the simulated flow field is and decrease the range of likely K_m values. In this study, high K_m values above ca. 3×10^{-5} m s^{-1} made the simulation of the spring discharge of the Fehla-Ursprung spring (Figure 3.1) impossible because the water divide in the west could not be simulated and most of the water in the area discharged to the east towards the river Lauchert resulting in a very narrow and long catchment area for the Gallusquelle spring.

There are eight parameters available for model calibration in this study. Two of these parameters define the conduit geometry: b is the lowest conduit radius and m the slope with which the conduit radius increases. One parameter, d_f, defines the aperture of the fault zone. The hydraulic conductivity of the fissured matrix is represented by the parameter K_m and the roughness of the conduit system by two parameters: b_h represents the highest roughness and m_h the slope of roughness decrease in upgradient direction from the spring. The last two parameters ε_1 and ε_2 are the respective conduit dispersivities obtained from the two artificial tracer experiments (Table 3.1).

For efficiency reasons it is important to know which of these parameters can be calibrated independently. The apparent transport dispersivities ε_1 and ε_2 are pure transport parameters, which influence only the shape of the breakthrough curves and not the flow field. The hydraulic model parameters influence the shape of the tracer breakthrough curves as well. Therefore, dispersivities ε_1 and ε_2 should be calibrated separately after calibrating the hydraulic model parameters.

Only for hydraulically dominant fault zones knowledge of the fault zone aperture d_f is required. For the model area this parameter was required for one fault zone lying in the west of the area feeding the Fehla-Ursprung spring (Figure 3.1). Since the Fehla-Ursprung spring has its own catchment area the fault zone has only minor influence on the flow regime in the Gallusquelle catchment. Its hydraulic parameters were calibrated at the beginning of the simulation procedure to reproduce the catchment and the discharge of the Fehla-Ursprung spring adequately and kept constant throughout all the simulations. In the final calibrated models it was rechecked, but the calibrated value was still acceptable.

The hydraulic conductivity of the fissured matrix K_m can be calibrated independently in principle as well. The influence on spring discharge is relatively small. The best-fit K_m value depends on the conduit parameters, i.e. geometry and roughness, since the hydraulic conductivities of the conduit system and of the fissured matrix define the total transmissivity of the catchment area together. Nonetheless, the best-fit value lies in the same range for different conduit geometries (Figure 3.4a

and Figure 3.7c). The greater the difference between the simulated conduit geometries, the more likely is a slight shift of the best-fit K_m value. Therefore, it is advisable to calibrate it anew for significant model changes, e.g. different scenarios, but to keep it constant during the rest of the calibrations. For the best-fit configuration, potentially used as a prognostic tool, the K_m value needs to be checked and adapted if necessary. This observation is, however, only valid for steady-state flow conditions. The dynamics of the hydraulic head and spring discharge might be highly sensitive to the matrix hydraulic conductivity, the conduit-matrix exchange coefficient and the lateral conduit extent. This work focuses on the conduits as highly conductive pathways for e.g. contaminant transport, but the calibration of matrix velocities, e.g. by use of environmental tracers, would likely be sensitive to the K_m values as well. Therefore, the choice of the flow regime and the objective functions determines the strength of the interdependencies between fissured matrix and conduit system parameters and therefore whether K_m can be calibrated independently.

The conduit parameters for geometry and roughness, here four parameters (lowest conduit radius b, slope of radius increase m, highest roughness b_h and slope of roughness decrease m_h), have to be varied simultaneously. All of them have a major influence on spring discharge and cannot be varied separately without introducing discharge errors. For each conduit geometry, there are a number of possible b_h–m_h combinations that result in the observed spring discharge. In general, the slowest transport velocities are achieved with an m_h value of zero. So, to deduce the range of geometric parameters that reproduce the objective functions, it is advisable to check the minimum conduit volume for which the tracer tests are not too fast for a value of m_h equal to zero. For the Gallusquelle area, transmissivities significantly increase towards the springs, which is characteristic for most karst catchments. Therefore low b_h values oppose the general hydraulic head trend: they increase the conduit roughness at the spring leading to slower flow and higher gradients. The higher the conduit volume, the higher b_h is required to reproduce the observed transport velocities. Therefore, the best-fit model likely has the smallest conduit volume for which both tracer tests can be reproduced. In Figure 3.7 this condition can be seen to clearly range in the order of 100 000 m^3 for the Gallusquelle area. While the four conduit parameters allow for a good model fit, they are pure calibration parameters. They show that the karst conduit system has a high complexity, which cannot be neglected for distributed velocity and hydraulic head representation. A systematic simulation of the heterogeneities, e.g. with a karst genesis approach, would be a process-based improvement to the current method and give more physical meaning to the parameters.

3.6 Conclusion

The study presents a large-scale catchment-based distributed hybrid karst groundwater flow model capable of simulating groundwater flow and solute transport. For flow recession conditions this model can be used as a predictive tool for the Gallusquelle area with relative confidence. The approach of simultaneous pattern matching of flow and transport parameters provides new insight into the hydraulics of the Gallusquelle conduit system. The model ambiguity was significantly reduced to the point where an estimation of the actual karst conduit volume for the Gallusquelle spring could be made. This would not have been possible simulating only one or two of the three objective functions, i.e. the spring discharge, the hydraulic head distribution and two tracer tests.

The model allows for the identification of the relevant parameters affecting karst groundwater discharge and transport in karst conduits and the examination of the respective overall importance in a well-investigated karst groundwater basin for steady-state flow conditions. While a differentiated representation of the roughness values in the karst conduits is substantial for buffering the lack of knowledge of the exact conduit geometry, e.g. local variations in cross section and the number of interacting conduits, variable matrix hydraulic conductivities cannot improve the simulation. It was shown that the effect of the unknown exact lateral extent of the conduit system and the change in conduit cross section at conduit intersections is of minor importance for the overall karst groundwater discharge. This is important since these parameters are usually unknown and difficult to measure in the field.

For calibration purposes, this study demonstrates that for a steady-state flow field and the observed objective functions the hydraulic conductivities of the fissured matrix can practically be calibrated independently of the conduit parameters. Furthermore, a strategy for the simultaneous calibration of conduit volumes and conduit roughness in a complex karst catchment was developed.

As discussed in Chapter 3.5 the major limitation of the simulation is the neglect of flow dynamics, which limits the applicability to certain flow conditions. Therefore, transient flow simulation is the focus of on-going work. This will enhance the applicability of the model as a prognostic tool to all essential field conditions and lead to further conclusions regarding the important karst system parameters, their influences on karst hydraulics and their interdependencies. It can be expected that some parameters, which are of minor importance in a steady-state flow field, e.g. the lateral conduit extent and the percentage of recharge entering the conduits directly, will exhibit significant influence for transient flow conditions.

Acknowledgements

The presented study was funded by the German Federal Ministry of Education and Research (promotional reference no. 02WRS1277A, AGRO, Risikomanagement von Spurenstoffen und Krankheitserregern in ländlichen Karsteinzugsgebieten).

References

Barenblatt, G. I., Zheltov, I. P., and Kochina, I. N., 1960. Basic concepts in the theory of seepage in fissured rocks (strata). Journal of Applied Mathematics and Mechanics, English translation, 24 (5), 1286-1303.

Bauer, S., Liedl, R., and Sauter, M., 2003. Modeling of karst aquifer genesis: Influence of exchange flow. Water Resources Research 39 (10), 1285, doi:10.1029/2003WR002218.

Birk, S., Geyer, T., Liedl, R., and Sauter, M., 2005. Process-Based Interpretation of Tracer Tests in Carbonate Aquifers. Ground Water 43, 381-388.

Birk, S., Liedl, R., and Sauter, M., 2006. Karst Spring responses examined by process-based modeling. Ground Water 44 (6), 832-836.

Clemens, T., 1998. Simulation der Entwicklung von Karstaquiferen. Ph.D. thesis, Eberhard-Karls-Universität zu Tübingen, Tübingen.

Clemens, T., Hückinghaus, D., Sauter, M., Liedl, R., and Teutsch, G., 1996. A combined continuum and discrete network reactive transport model for the simulation of karst development. In: Proceedings of the ModelCARE 96 Conference, 24.-26. September 1996, Golden, Colorado, USA, 237, 309-318.

COMSOL AB, 2012. COMSOL Multiphysics® User's Guide v4.3, 1292 pp.

Coronado, M., Ramírez-Sabag, J., and Valdiviezo-Mijangos, O., 2007. On the boundary conditions in tracer transport models for fractured porous underground formations. Revista Mexicana Física 53 (4), 260-269.

Covington, M. D., Luhmann, A. J., Wicks, C. M., and Saar, M. O., 2012. Process length scales and logitudinal damping in karst conduits. Journal of Geophysical Research 117, F01025, doi:10.1029/2011JF002212.

Doummar, J., Sauter, M., and Geyer, T., 2012. Simulation of flow processes in a large scale karst system with an integrated catchment model (Mike She) – Identification of relevant parameters influencing spring discharge. Journal of Hydrology 426, 112-123, doi:10.1016/j.jhydrol.2012.01.021.

Dreybrodt, W., 1981. Mixing in $CaCO_3$–CO_2–H_2O systems and its role in the karstification of limestone areas. Chemical Geology 32, 221-236.

Ford, D.C. and Williams, P.W., 2007. Karst geomorphology and hydrology. Wiley, West Sussex, 562 pp.

Geyer, T., Birk, S., Licha, T., Liedl, R., and Sauter, M., 2007. Multi-tracer test approach to characterize reactive transport in karst aquifers. Ground Water 45, 36-45.

Geyer, T., Birk, S., Liedl, R., and Sauter, M., 2008. Quantification of temporal distribution of recharge in karst systems from spring hydrographs. Journal of Hydrology, 348, 452-463.

Golwer, A., 1978. Erläuterungen zu Blatt 7821 Veringenstadt, Geologische Karte 1 : 25 000 von Baden-Württemberg. Geologisches Landesamt Baden-Württemberg, Stuttgart, 151 pp.

Gwinner, M. P., 1993. Erläuterungen zu Blatt 7721 Gammertingen, Geologische Karte 1 : 25 000 von Baden-Württemberg. Geologisches Landesamt Baden-Württemberg, Freiburg/Stuttgart, 78 pp.

Hartmann, A., Weiler, M., Wagener, T., Lange, J., Kralik, M., Humer, F., Mizyed, N., Rimmer, A., Barberá, J. A., Andreo, B., Butscher, C., and Huggenberger, P., 2013. Process-based karst modelling to relate hydrodynamic and hydrochemical characteristics to system properties. Hydrology and Earth System Sciences 17, 3305-3321, doi:10.5194/hess-17-3305-2013.

Hartmann, A., Goldscheider, N., Wagener, T., Lange, J., and Weiler, M., 2014. Karst water resources in a changing world: Review of hydrological modeling approaches. Reviews of Geophysics 52, 1-25, doi:10.1002/2013RG000443.

Hauns, M., Jeannin, P.-Y., and Atteia, O., 2001. Dispersion, retardation and scale effect in tracer breakthrough curves in karst conduits. Journal of Hydrology 241, 177-193.

Hu, R., 2011. Hydraulic tomography: A new approach coupling hydraulic travel time, attenuation and steady shape inversions for high-spatial resolution aquifer characterization. Ph.D. thesis, University of Göttingen, Göttingen, 116 pp.

Hubinger, B. and Birk, S., 2011. Influence of initial heterogeneities and recharge limitations on the evolution of aperture distributions in carbonate aquifers. Hydrology and Earth System Sciences 15, 3715-3729, doi:10.5194/hess-15-3715-2011.

Hückinghaus, D., 1998. Simulation der Aquifergenese und des Wärmetransports in Karstaquiferen. Tübinger Geowissenschaftliche Arbeiten C42, Tübingen.

Hunter, N. M., Bates, P. D., Horritt, M. S., De Roo, P. J., and Werner, M. G. F., 2005. Utility of different data types for calibrating flood inundation models with a GLUE framework. Hydrology and Earth System Sciences 9 (4), 412-430.

Jeannin, P.-Y., 2001. Modeling flow in phreatic and epiphreatic karst conduits in the Hölloch cave (Muotatal, Switzerland). Water Resources Research 37 (2), 191-200.

Jeannin, P.-Y. and Sauter, M., 1998. Modelling in karst systems. Bulletin d'Hydrogéologie 16, Université de Neuchâtel, Neuchâtel.

Khu, S.-T., Madsen, H., and di Pierro, F., 2008. Incorporating multiple observations for distributed hydrologic model calibration: An approach using a multi-objective evolutionary algorithm and clustering. Advances in Water Resources 31, 1387-1398.

Kordilla, J., Sauter, M., Reimann, T., and Geyer, T., 2012. Simulation of saturated and unsaturated flow in karst systems at catchment scale using a double continuum approach. Hydrology and Earth System Sciences 16, 3909-3929, doi:10.5194/hess-16-3909-2012.

Kovács, A. and Sauter, M., 2007. Modelling karst hydrodynamics. In: Methods in karst hydrogeology, International contributions to hydrogeology 26, editors: Goldscheider, N. and Drew, D., 201–222, Taylor and Fracis, London.

Kovács, A., Perrochet, P., Király, L., and Jeannin, P.-Y., 2005. A quantitative method for the characterisation of karst aquifers based on spring hydrograph analysis. Journal of Hydrology 303, 152-164.

Liedl, R., Sauter, M., Hückinghaus, D., Clemens, T., and Teutsch, G., 2003. Simulation of the development of karst aquifers using a coupled continuum pipe flow model. Water Resources Research 39 (3), 1057, doi:10.1029/2001WR001206.

Li, H. T., Brunner, P., Kinzelbach, W., Li, W. P., and Dong, X.G., 2009. Calibration of a groundwater model using pattern information from remote sensing data. Journal of Hydrology 377, 120-130, doi:10.1016/j.jhydrol.2009.08.012.

Luhmann, A. J., Covington, M. D., Alexander, S. C., Chai, S. Y., Schwartz, B. F., Groten, J. T., and Alexander, E. C., 2012. Comparing conservative and nonconservative tracers in karst and using them to estimate flow path geometry. Journal of Hydrology 448-449, 201-211, doi:10.1016/j.jhydrol.2012.04.044.

Madsen, H., 2003. Parameter estimation in distributed hydrological catchment modelling using automatic calibration with multiple objectives. Advances in Water Resources 26, 205-216.

Merkel, P., 1991. Karsthydrologische Untersuchungen im Lauchertgebiet (westl. Schwäbische Alb). Diplom thesis, University of Tübingen, Tübingen, 108 pp.

Mohrlok, U., 2014. Numerische Modellierung der Grundwasserströmung im Einzugsgebiet der Gallusquelle unter Festlegung eines Drainagesystems. Grundwasser 19, 73-85, doi:10.1007/s00767-013-0249-x.

Mohrlok, U. and Sauter, M., 1997. Modelling groundwater flow in a karst terraine using discrete and double-continuum approaches: importance of spatial and temporal distribution of recharge. In: Proceedings of the 12th International Congress of Speology, 2/6th Conference on Limestone Hydrology and Fissured Media, La Chaux-de-Fonds, Switzerland, 10-17 August 1997, 167-170.

Oehlmann, S., Geyer, T., Licha, T., and Birk, S., 2013. Influence of aquifer heterogeneity on karst hydraulics and catchment delineation employing distributive modeling approaches. Hydrology and Earth System Sciences 17, 4729-4742, doi:10.5194/hess-17-4729-2013.

Ophori, D. U., 1999. Constraining permeabilities in a large-scale groundwater system through model calibration. Journal of Hydrology 224, 1-20.

Perrin, C., Andréassian, V., Serna, C. R., Mathevet, T., and Le Moine, N., 2008. Discrete parameterization of hydrological models: Evaluating the use of parameter sets libraries over 900 catchments. Water Resources Research 44, W08447, doi:10.1029/2007WR006579.

Rehrl, C. and Birk, S., 2010. Hydrogeological characterisation and modelling of spring catchments in a changing environment. Austrian Journal of Earth Sciences 103 (2), 106-117.

Reiber, H., Klein, F., Selg, M., and Heidland, S., 2010. Hydrogeologische Erkundung Baden-Württemberg – Mittlere Alb 4 – Markierungsversuche, Abwassereinleitungen. Landesamt für Umwelt, Messungen und Naturschutz Baden-Württemberg, Tübingen, 71 pp.

Reimann, T., Rehrl, C., Shoemaker, W. B., Geyer, T., and Birk, S., 2011. The significance of turbulent flow representation in single-continuum models. Water Resources Research 47, W09503, doi:10.1029/2010WR010133.

Saller, S. P., Ronayne, M. J., and Long, A. J., 2013. Comparison of a karst groundwater model with and without discrete conduit flow. Hydrogeology Journal 21 (7), 1555-1566, doi:10.1007/s10040-013-1036-6.

Sauter, M., 1992. Quantification and Forecasting of Regional Groundwater Flow and Transport in a Karst Aquifer (Gallusquelle, Malm, SW Germany). Tübinger Geowissenschaftliche Arbeiten C13, Tübingen.

Schmidt, S., Geyer, T., Guttman, J., Marei, A., Ries, F., and Sauter, M., 2014. Characterisation and modelling of conduit restricted karst aquifers – Example of the Auja spring, Jordan Valley. Journal of. Hydrology 511, 750–763.

Strayle, G., 1970. Karsthydrologische Untersuchungen auf der Ebinger Alb (Schwäbischer Jura). In: Jahreshefte des Geologischen Landesamtes Baden-Württemberg 12, Freiburg im Breisgau, 109-206.

Teutsch, G. and Sauter, M., 1991. Groundwater Modeling in karst terranes: scale effects, data aquisition and field validation. In: Proceedings of the 3rd Conference on Hydrogeology, Ecology, Monitoring and Management of Ground Water in Karst Terranes, 4-6 December 1991, Nashville, USA, 17-34.

Villinger, E., 1977. Über Potentialverteilung und Strömungssysteme im Karstwasser der Schwäbischen Alb (Oberer Jura, SW-Deutschland). Geologisches Jahrbuch C18, Bundesanstalt für Geowissenschaften und Rohstoffe und Geologische Landesämter der Bundesrepublik Deutschland, Hannover.

Villinger, E., 1993. Hydrogeologie, in: Erläuterungen zu Blatt 7721 Gammertingen, Geologische Karte 1 : 25 000 von Baden-Württemberg. In: Gwinner, M. P., Geologisches Landesamt Baden-Württemberg, Freiburg/Stuttgart, 30-57.

Worthington, S. R. H., 2009. Diagnostic hydrogeologic characteristics of a karst aquifer (Kentucky, USA). Hydrogeology Journal 17, 1665-1678, doi:10.1007/s10040-009-0489-0.

Chapter 4

4 Groundwater residence time distributions in heterogeneous karst aquifers

Sandra Oehlmann[a], Tobias Geyer[a,b], Martin Sauter[a]

Manuscript:

Oehlmann, S., Geyer, T., and Sauter, M. Groundwater residence time distributions in heterogeneous karst aquifers. In preparation for submission to Journal of Hydrology.

[a]Geoscience Center, University of Göttingen, Göttingen, Germany

[b]Landesamt für Geologie, Rohstoffe und Bergbau, Regierungspräsidium Freiburg, Freiburg, Germany

Abstract

Groundwater residence time data provide important information for the management of groundwater resources. Together with data on the protective overburden the vulnerability of groundwater resources to anthropogenic pollution can be assessed. Furthermore, they can provide basic information on groundwater recharge. Because of the highly heterogeneous nature and the complex flow regime (triple porosity) of karst aquifers, the determination of their residence times is very challenging.

In this study, numerical modelling is employed as a tool for the understanding of the interaction between the three karst aquifer compartments, i.e. conduits, fractures and rock matrix, and the relative importance of different parameters and recharge events on residence time distributions. The modelling approach is based on a hybrid model including discrete conduits coupled to a three-dimensional fissured system. A double continuum approach is employed for the porous and the fissured systems of the aquifer. For the assessment of the effect of the conduit structure two model setups are simulated: one with a single conduit and one with a dendritic system.

Results show that the dendritic conduits lead to a better mixing and a more evenly distributed residence time field. The residence times in the dendritic conduit system are considerably more sensitive to parameter changes than the single conduit system. The highest influence on the observed residence times can be attributed to the ratio between direct and diffuse recharge, with the total recharge, the porosities of the fissured and porous systems and the aquifer thickness as secondary factors. Important hydraulic parameters such as the hydraulic conductivities of the fissured and conduit systems do not show a noticeable influence on average groundwater residence times.

4.1 Introduction

Groundwater ages and residence times are essential parameters for water resources management and the delineation of well head protection areas (Molson and Frind, 2012; Morgenstern and Daughney, 2012). Groundwater ages can be derived from environmental tracers, which enter the aquifer with recharge water and which are measured at a respective discharge location, e.g. a spring or a groundwater abstraction well (e.g. Maloszewski et al., 2002; Geyer, 2008). Generally, an analytical (e.g. Doyon and Molson, 2012) or a lumped-parameter (e.g. Long and Putnam, 2009) model is used to infer the water age from the tracer measurement. Those models do not consider specific aquifer parameters or structural features. They apply highly simplified weighting functions that rely on simplified conceptual assumptions to generate average residence times or residence

time distributions at the spring. There are specialized lumped-parameter approaches for karst aquifers that combine several simplified assumptions, e.g. piston flow in the conduit system and diffusive flow in the fissured matrix (e.g. Maloszewski et al., 2002). This type of approach can give indications for the vulnerability and turnover times of an aquifer and can be employed to draw conclusions about the structure of the conduit system and to separate old and young components of discharge water (Einsiedl, 2005; Long and Putnam, 2009; Maloszewski et al., 2002). Since these approaches treat the aquifer as a lumped system, they cannot provide any quantitative information on the spatial distribution of groundwater residence times. This distribution is important for groundwater protection purposes since it allows the delineation of sensitive areas of the aquifer system, e.g. drinking water protection zones (e.g. Frind et al., 2002).

Goode (1996) developed an approach for simulating groundwater ages distributively at each point within the aquifer based on an advection-dispersion equation. Hereby, the groundwater age is considered as a water property that is carried along with the water molecules as e.g. a solute would be. Therefore, groundwater age can be represented by a concentration variable whose value is increasing with time (Goode, 1996). This approach is able to consider the structure and the hydraulic parameter field of the aquifer and does not suffer the same drawbacks as advective particle-tracking approaches in highly heterogeneous media (Frind et al., 2002; Goode, 1996; Varni and Carrera, 1998). It is also possible to apply Goode's (1996) equation backward and to track the migration of the "age" from the outlet to the recharge area. This backward age is called "life expectancy" and yields the time required for groundwater to reach the outlet (Cornaton and Perrochet, 2006a). Such a distribution can be used for the determination of well or spring protection zones (e.g. Frind et al., 2002, 2006). For porous aquifer systems, extensive studies of age and life expectancy distributions have been successfully performed and were found to match field data (e.g. Molson and Frind, 2012).

The high heterogeneity and large contrast in hydraulic conductivity between conduits and matrix in karst aquifers make it difficult to define well head or spring protection zones. Karst aquifers can generally be described as triple porosity systems (Worthington, 2007). The primary porosity consists of the pore space that was generated during rock formation. It is usually not considered separately in groundwater flow simulations since water inside the small pores is quasi not relevant with respect to flow. It can have an influence on groundwater residence times and attenuation of solutes since water and solute can migrate into the pores by diffusion processes (Worthington, 2007). Therefore, transit times can differ largely between facies of different porosities or between different solutes (Einsiedl and Mayer, 2005). The secondary porosity consists of small fissures and fractures that are distributed throughout the rock and mainly develop due to mechanical or thermal stresses. The water inside the fissures actively contributes to groundwater flow but can take several years to reach the respective

outlet, depending on the distance. The tertiary porosity is built by solutionally enlarged conduits or caves, in which water can cover a distance of several kilometres within hours to days (Worthington, 2007). These highly conductive pathways make karst springs highly vulnerable to contamination but are especially difficult to locate and to characterise in the field, since they only comprise a small percentage of the aquifer (Sauter, 1992; Worthington, 2009).

Only few attempts were made so far at simulating residence times in karst aquifers distributively. Cornaton (2004, p. 57) presents a 3D-hybrid model of a hypothetical karst aquifer simulating capture zones for a karst spring. The approach couples a discrete conduit system to a continuum representing the combination of the fissured and the porous system of the aquifer. The author simulates spring catchments for different time intervals with the life expectancy approach and was able to show the importance of the karst conduits for the distribution of groundwater transit times. Cornaton (2004) did not include the effects of the porous system separately, however, so that the triple-porosity nature of the aquifer was not accounted for. Geyer (2008) presented a block model, which included the fissured and porous systems and investigated differences between the age and life expectancy in the saturated and unsaturated zone, focusing on the long-term component of the karst aquifer. Both authors simulate flow towards a single point outlet, i.e. a karst spring, and do not include the duality of recharge and discharge that is often observed in karst systems (Király, 2002).

This study presents a distributed groundwater residence time simulation in a highly simplified karst system. The work focuses on three points: 1) the development of an effective modelling approach to represent all three porosities in the model and to gain differentiated information on travel times of groundwater in hydrogeologically highly heterogeneous systems 2) the comparison of transit time distributions at the outlet generated by the numerical model with those calculated by lumped-parameter approaches, and 3) a parameter sensitivity study to determine the relative influence of model parameters on the transit times. The parameter study serves two purposes: a) gaining information on the kind of measurements most important for calibrating groundwater residence times for actual field sites and b) assessing the potential of groundwater age measurements as a tool for karst aquifer characterisation. Groundwater ages are already known to provide estimates for hydraulic parameters in lumped-parameter models (e.g. Maloszewski et al., 2002) and can therefore be assumed to have a potential for parameter calibration in distributed models as well.

4.2 Methods and approach

4.2.1 Numerical implementation

Groundwater flow and residence times are simulated with the finite element software COMSOL Multiphysics®, that couples multiple equations of different physical processes in multiple dimensions. For groundwater flow, two different karst features were considered with a hybrid modelling approach. The fissured system is simulated as a three-dimensional continuum. For the karst conduit network, discrete one-dimensional elements are introduced. The simulation approach of Oehlmann et al. (2015) is used for the implementation. For the three-dimensional fissured system, the Darcy equation combined with the continuity equation (Eq. 4.1) is applied. Conduit flow is simulated fully turbulent with the Manning equation (Eq. 4.2) and the left-hand side of this equation is multiplied by the conduit cross section A [L^2] to account for the lateral dimension of the conduit.

$$S_f \frac{\partial H_f}{\partial t} + \nabla\left(K_f \nabla H_f\right) = Q_f \tag{4.1}$$

$$A \frac{1}{n} \left(\frac{r_c}{2}\right)^{\frac{2}{3}} \sqrt{\frac{dH_c}{dx}} = -\alpha\left(H_c - H_f\right) \tag{4.2}$$

where S_f [L^{-1}] is the storage coefficient of the fissured system, H_f and H_c [L] are the hydraulic heads in the fissured system and in the conduit system respectively, K_f [$L\ T^{-1}$] is the hydraulic conductivity of the fissured system, Q_f [T^{-1}] is the source term of the fissured system, n [$T\ L^{-1/3}$] is the Manning coefficient for conduit roughness and r_c [L] is the conduit radius. The right hand side of Eq. (4.2) is the source term of the conduit system due to exchange of water between the conduit and the fissures (Bauer et al., 2003). α [$L^2\ T^{-1}$] is the conduit-matrix exchange coefficient. The exchange is calculated per unit conduit length L [L]. For the fissured system, the exchange term is applied along the conduit with a changed algebraic sign.

For groundwater transport, i.e. the simulation of ages and life expectancies, all three porosities were considered. The fissured and the porous system were implemented with a double-continuum approach, i.e. both systems fill the same space and are linked via an exchange term (Teutsch and Sauter, 1991). Following the approach of Goode (1996) the average groundwater age was treated as a concentration variable in the transport equation (Chapter 4.1) with a zero order source term equalling the porosity of the respective system (Goode, 1996). A_f, A_p and A_c [T] are the ages of water in the fissured, porous and conduit systems respectively. A_f and A_c are simulated with advection-dispersion equations (Eqs. 4.3 and 4.4).

$$\theta_f \frac{\partial A_f}{\partial t} + \nabla\left(A_f q_f\right) - \nabla\left(\theta_f D_f \nabla A_f\right) - \theta_f = \beta(A_p - A_f) \tag{4.3}$$

$$A\left(\frac{\partial A_c}{\partial t} + \nabla\,(A_c q_c) - \nabla\,(D_c\,\nabla A_c) - 1\right) = -q_{ex}\,A_{f,c} \tag{4.4}$$

where θ_f is the porosity of the fissured system [-], with the porosity of the conduit system set to unity. q_f [L T^{-1}], q_c [L T^{-1}] and q_{ex} [L^2 T^{-1}] are the Darcy flow velocities in the fissured and conduit system and the water exchange between fissured and conduit system calculated with Eq. (4.2), respectively. As for flow, the cross section of the conduit *A* is included to account for the lateral dimensions. D_f and D_c [L^2 T^{-1}] are the coefficients of hydrodynamic dispersion. The dispersion coefficients depend on the respective dispersivities ε_f and ε_c [L] and flow velocities. The expression $A_{f,c}$ in the exchange term on the right hand side of the equation refers to either the variable A_f or A_c, depending on the direction of fissured-conduit exchange. For the fissured system, the analogous exchange term is again applied locally at the discrete element representing the karst conduit. Eq. (4.3) includes an additional exchange term for the diffusive exchange with the porous system. The flow in the conduit system is expected to be too fast for significant diffusive exchange processes. β [T^{-1}] is the diffusive exchange coefficient between the fissured and the porous system. It depends on the porosity of the porous and the geometric properties of the fissured system, i.e. the fissure spacing, as well as on the diffusion coefficient of the porous system (Cook et al., 2005; Maloszeski and Zuber, 1985). Fissure spacing and geometry cannot be defined in a double-continuum model because the fissures are not considered as individual discontinuities. Therefore, β is treated as a calibration parameter during the simulation.

Groundwater movement within the porous system is considered as purely diffusive due to low hydraulic conductivities (Doyon and Molson, 2012). Therefore, Eq. (4.3) is reduced to Eq. (4.5) in the porous system.

$$\theta_p\,\frac{\partial A_p}{\partial t} - \nabla\,(\theta_p D_p\,\nabla A_p) - \theta_p = -\beta(A_p - A_f) \tag{4.5}$$

For the porous system, the hydrodynamic dispersion only consists of the diffusive component, which exclusively depends on the porosity θ_p. Since no temperature variations are included, molecular diffusion is constant.

Life expectancy was simulated with the same equations for a reversed flow field (Cornaton and Perrochet, 2006a), i.e. the signs of the advective flow components and the advective exchange terms are reversed and boundary conditions are adapted (Chapter 4.2.2). The residence time distribution was derived during post-processing by summing up the age and the life expectancy at each simulation point (Cornaton and Perrochet, 2006a).

4.2.2 Model scenarios and parameterization

Since this study focuses on groundwater residence times within the aquifer, i.e. the saturated zone, the influences of the overburden and unsaturated zone are neglected in the model setup and the aquifer is simulated as confined. The effect this simplification might have for an actual field site application is discussed in Chapter 4.4. Two basic model configurations are used for studying the residence time distributions (Figure 4.1). Both configurations are three-dimensional with a lateral extent of 5×5 km^2 and an aquifer thickness of 100 m. An observation well is inserted south of the conduit system at a depth of 50 m to simulate sampling in the field (Figure 4.1). The conduit volume is identical for both configurations, but in configuration 1 it is distributed on a 3 km long single conduit, while for configuration 2 a dendritic conduit system with a total length of 16 km is employed. The conduit diameter for configuration 1 is kept constant along the conduit length. In configuration 2 a widening of the karst conduits towards the spring is assumed. With a constant diameter conduit velocities would increase drastically at the intersections, which is not only unrealistic since higher flow velocities enhance karst dissolution processes (e.g. Clemens, 1998), but also numerically difficult to solve in the transport simulation. For the increase in radius, the empirical approach of Oehlmann et al. (2015) was employed (Eq. 4.6).

$$r_{c,0} = m\,s + b \tag{4.6a}$$

$$r_{c,i} = m\,s + 2\sqrt{{r_{c,i-1}}^2 + {r_{c,i-2}}^2 + {r_{c,i-3}}^2} \tag{4.6b}$$

where r_c [L] is the conduit radius, s [L] is the conduit length and m [-] is the slope of linear radius increase along the conduit length. For the smallest conduit branches an initial radius b [L] is defined (Eq. 4.6a). At the conduit intersections, the cross-sectional areas of the intersecting conduits are added as initial cross-section for the downgradient conduit (Eq. 4.6b). The factor 2 was derived empirically to ensure that flow velocities are as uniform as possible during the simulations. The intersections of three conduit branches at the same points lead to a significant increase in flow velocities, if the factor of 1 (Oehlmann et al., 2015) is used.

For selection of parameter values and ranges for sensitivity analysis, the area of the Gallusquelle spring in south-western Germany was used. The Gallusquelle is a medium sized karst spring with an average annual discharge of 0.5 $m^3\ d^{-1}$. The aquifer is characterized as a mixed system, where both, conduit flow and diffuse matrix flow occur and are of significant importance (Sauter, 1992). Extensive field investigations and model studies provide a good database for model parameters (e.g. Sauter, 1992; Oehlmann et al., 2015). Average groundwater transit times in the saturated zone were determined by Geyer (2008) with the ^{85}Kr method to range between 3 and 4 years. Table 4.1 shows the chosen parameters for the reference simulations and the variation ranges. The relative

parameter sensitivity was calculated by using the Root Square Error (RSE) of the average age and life expectancy values with respect to the reference scenario. For a relative difference below 0.5 years the parameter was considered as insensitive with respect to the objective function, i.e. age or life expectancy. For the spring discharge the same value was set as by Oehlmann et al. (2015) and a difference of 10 L s^{-1} was counted as significant.

For the porous system, all boundaries are zero-flux Neumann boundaries. In and out flux for the system is only provided by exchange with the fissured system. The fissured system is bounded by no-flux boundaries everywhere except for the top. The whole upper boundary is defined as a Neumann boundary with the value of groundwater recharge as defined in Table 4.1. For the transport equation of groundwater age (Eq. 4.3), top of the domain is a zero-flux Neumann condition as well. By definition, groundwater age cannot enter the aquifer from the outside but is only produced inside of it. For the life expectancy the sign of the recharge is reversed and multiplied with the expectancy value to remove the water that reached the inlet boundary. The upper eastern edge of the domain is set as a Dirichlet boundary condition for groundwater flow and a Neumann condition for transport representing a river (Figure 4.1). The conduit system has the same kind of boundary condition for the karst spring. Recharge to the conduit is provided by exchange with the fissured system and by a source term representing the direct recharge component, i.e. recharge reaching the conduit system directly through vertical shafts, if present. For both, river and spring, Neumann conditions are zero flux for the life expectancy and equal to the groundwater discharge multiplied by the age for groundwater age, analogous to the recharge boundary.

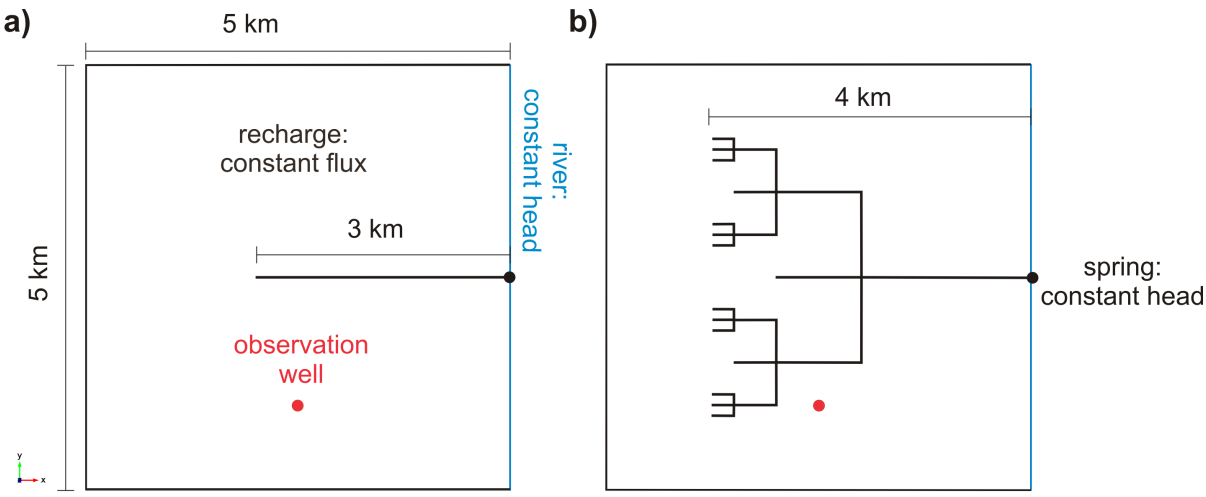

Figure 4.1. Conceptual model scenarios. (a) configuration 1 with a single conduit, (b) configuration 2 with a dendritic conduit network. Boundary conditions are the same for both scenarios.

Table 4.1. Parameters for the numerical simulation and variation range for the parameter analysis. The corresponding equations are given in Chapter 4.2. The *z*-axis points upwards.

Parameter description	Parameter name	Reference setup 1	Reference setup 2	Variation range
Porous system				
porosity	θ_p (%)	1	1	1 – 10
porous–fissured exchange coefficient	β (s^{-1})	3.3×10^{-12}	3.3×10^{-12}	1×10^{-14} – 1×10^{-8}
Fissured system				
total recharge	r (mm d^{-1})	1.5	1.5	0.5 – 50
porosity	θ_f (%)	1	1	1 – 10
hydraulic conductivity	K_f (m s^{-1})	5×10^{-5}	5×10^{-5}	1×10^{-6} – 1×10^{-3}
dispersivity	ε_f (m)	50	50	5 - 100
aquifer thickness	m_{af} (m)	100	100	10 – 100
Conduit system				
vertical position	z_c (m)	100	100	0 – 100
direct recharge	r_d (%)	0	0	0 – 95
conduit-matrix exchange coefficient	α (m^2 s^{-1})	6.1×10^{-4}	6.1×10^{-4}	1×10^{-8} – 1×10^{-3}
cross-section	A (m^2)	12	2.24[a]	0.6 - 35
roughness	n (s $m^{-1/3}$)	3	3	0.01 - 20
dispersivity	ε_c (m)	7	7	2 - 50
initial radius	b (m)	1.95	0.1	0.001 – 2
radius increase	m (-)	0	1×10^{-4}	0 – 1×10^{-3}

[a]average value

The reference simulations and parameter analysis were performed for steady-state conditions. Steady-state conditions are useful for protection zone delineation and required as initial values for transient modelling. In order to assess the influence of discrete groundwater recharge events on the residence time distribution, an additional simulation was performed introducing a hypothetical recharge event with the duration of one week. Contrary to the steady-state reference simulation (Table 4.1) a direct recharge component of 10% was assumed for the transient simulation to include the influence of the duality of aquifer recharge. Furthermore, the dispersivity of the conduit system was set to 50 m. It was found to be insensitive during the parameter analysis (Chapter 4.3.2) and a

higher dispersion coefficient leads to a higher numerical stability of the fast transport in the karst conduit system.

4.2.3 Evaluation and comparison with lumped-parameter approaches

Besides the average age of spring water, it is important to know its composition with respect to transit times. This composition can be visualized with the transit time distribution *g(t)* of the spring water and can be used for assessing the concentration and duration of possible contaminations. It corresponds to the breakthrough curve at the outlet for a Dirac input function (Maloszewski and Zuber, 1982). Maloszewski and Zuber (1982) provided the basis for simplified lumped-parameter simulations of transit time distributions. Three of those models are considered in this work for comparison of the distribution curves.

The dispersion model (DM) (Eq. 4.7) is generally considered as the appropriate model for long-term studies, i.e. longer than 2-3 years, in karst systems (e.g. Einsiedl, 2005; Einsiedl et al., 2009), since it represents the fissured and porous systems (Maloszewski et al., 2002).

$$g(t) = \left(\frac{4\pi tD}{vxT}\right)^{-0.5} EXP\left[-T\ \left(1-\frac{t}{T}\right)^2\ \frac{vx}{4Dt}\right]\ t^{-1}\ , \qquad (4.7)$$

where *t* is the time [T], *T* is the average transit time [T], *D* is the dispersion coefficient [$L^2\ T^{-1}$], *v* is the average velocity [$L\ T^{-1}$] and *x* is the average distance between recharge area and outlet [L]. The parameters *D*, *v* and *x* are usually combined to a single parameter: the apparent dispersion parameter $P_D = D/(v\ x)$ (Maloszewski and Zuber, 1982). A high P_D value suggests a dispersion controlled flow regime.

The dispersion model neglects the influence of the conduit system. After Maloszewski et al. (2002) it is possible to approximate the conduit component with a piston flow model (PFM) so that the karst system can be characterized as a combination of both. The piston flow model assumes that the Dirac impulse entering the system is transmitted without any mixing or dispersion effects to the spring, leading to a unit concentration pulse at the average transit time *T* (Maloszewski and Zuber, 1982) (Eq. 4.8).

$$g(t) = \delta(t-T)\ , \qquad (4.8)$$

where δ is the Dirac function.

The third model considered for comparison is the combined exponential and piston flow model (EPM) (Eq. 4.9) of Maloszewski and Zuber (1982). The model assumes part of the system to behave as a well-mixed reservoir and part to behave like a piston flow reservoir (Maloszewski and Zuber,

1982). Therefore, it might also be suited for modelling the heterogeneous behaviour of karst aquifers.

$$g(t) = \begin{cases} \frac{\eta}{T}\, EXP\left(-\eta\frac{t}{T} + \eta - 1\right) & for\ t \geq T(1-\eta^{-1}) \\ 0 & for\ t < T(1-\eta^{-1}) \end{cases}, \quad (4.9)$$

where η [-] is the ratio of the total aquifer volume to the volume showing exponential flow behaviour, i.e. behaving like a well-mixed reservoir.

For comparison of the transit time curves, a transient transport simulation was performed in Comsol Multiphysics®, introducing a concentration impulse at the first day of the simulation and removing the source terms on the left-hand sides of Eqs. (4.3)–(4.5). The breakthrough curves at the spring and the observation well (Figure 4.1) were normalized by the recovered mass to ensure comparability. The similarity of the distribution curves generated with the lumped-parameter models and with the distributed approach is assessed by calculating the root mean square error (RMSE) between the two curves.

4.3 Results

4.3.1 Reference Models – steady-state

Table 4.2 lists the simulated averages and ranges for the age and the life expectancy variables for both model configurations. Figure 4.2 shows top views of the groundwater age, life expectancy and residence times for all three porosities. In all cases, the distribution in the porous matrix follows that in the fissured system with significantly higher values, as can be expected. The only route on which water leaves the porous matrix is by diffusive exchange with the fissured system.

The age in the fissured system A_f increases towards the river (Figure 4.2b and k). In the vicinity of the conduit system, groundwater ages are significantly higher than in the surrounding area differing from this pattern. The conduits draw older water from greater depth that mixes with the newly recharged water (Figure 4.3a). These results complement the findings of Cornaton (2004), who observed higher average ages inside the conduit system than inside the surrounding fissured matrix during his simulations. Therefore, the vertical component of the aquifer system has a high importance for groundwater age simulations compared to pure groundwater flow, which can often be approximated with a two-dimensional horizontal aquifer (e.g. Mohrlok, 2014).

The vertical layering of the system largely depends on the boundary conditions. The groundwater recharge boundary extends two-dimensionally across the whole aquifer leading to a mixing of older water with new recharge water at the top of the domain and increasing ages with depth (Figure 4.3a). For the life expectancy, groundwater flow is reversed so that the "inlet" boundary of the fissured system is the river, which is a one-dimensional element positioned at the eastern edge of the system. Therefore, no mixing with water with life expectancy zero occurs within the domain and no distinct vertical layering is observed (Figure 4.3b). The lateral layering is much more pronounced, however, and maximum values are higher since no extensive dilution with newly recharged water occurs (cf. Figure 4.2b and e or Figure 4.2k and n).

The ages and life expectancies in the fissured and porous systems are very similar for the two model configurations, i.e. the single and the dendritic conduit. However, the maximum life expectancy in the conduit system is 3.6 days for configuration 1, while the smaller branches of the dendritic system show life expectancies of up to two years. The large difference is caused by two effects. First, the flow velocities in the smaller conduit branches are lower. Their smaller volumes draw less water than the large single conduit. This leads to higher life expectancies and lower ages compared to the single conduit (Figure 4.2i and o). Second, at conduit intersections three branches meet and their water volumes are added, drastically increasing the hydraulic head in the conduit branch. For a short distance, the hydraulic head in the conduit system exceeds that of the fissured system and exchange flow is reversed. Therefore, the life expectancy in the smallest branches in the central part of the area includes water that will have considerably longer residence times since it travels part of the distance in the fissured systems with its lower flow velocities. Even though the ages and life expectancies inside the conduit system are both more heterogeneous for the dendritic conduits in configuration 2, average ages at the spring are approximately the same (Table 4.2).

While the residence time is derived as the sum of both, the groundwater age and its life expectancy, its distributions in the fissured and porous system are clearly dominated by the life expectancy. The life expectancy in those compartments has both, the generally higher values and the more heterogeneous distribution (Figure 4.2h and q, Figure 4.2g and p). In the direct vicinity of the conduit system, the influence of the groundwater age on the residence time increases due to its relatively high values (Figure 4.2b and k). Therefore, the lowest values of the residence time do not occur inside the conduit system as they do for the life expectancy, but in the fissured system a few meters away from the conduit, where both, age and life expectancy, are relatively low (Figure 4.2h and q).

Table 4.2. Statistical values of groundwater age, life expectancy and residence time for the reference simulations of both model configurations. The value of the residence time at the spring is equal to that of the age and the value at the observation well is the sum of the age and the time span of the life expectancy.

	Configuration 1			Configuration 2		
	A_p (a)	A_f (a)	A_c (a)	A_p (a)	A_f (a)	A_c (a)
average	99.9	3.6	3.6	100.0	3.7	3.0
range	97.2 – 102.9	0.9 – 6.6	3.0 – 3.6	97.3 – 102.6	0.9 – 6.3	2.1 – 3.6
spring	100.7	4.4	3.6	100.7	4.4	3.6
observation well	100.1	3.7		100.1	3.8	
	E_p	E_f	E_c	E_p	E_f	E_c
average	99.9	3.6	0.0	100.0	3.7	0.3
range	96.3 – 118.6	0.0 – 22.3	0.0 – 0.01	96.3 – 117.0	0.0 – 20.6	0.0 – 2.0
observation well	101.1	4.7		100.6	4.3	
	T_p	T_f	T_c	T_p	T_f	T_c
average	199.9	7.2	3.6	199.9	7.3	3.3
range	195.5 – 220.6	2.8 – 28.0	3.0 – 3.6	195.5 – 218.7	2.8 – 26.1	2.1 – 4.4

Figure 4.2 also shows the simulated spring catchment areas delineated after Oehlmann et al. (2013). Furthermore, it shows the 50-days life expectancy contour lines. These lines are examples for the delineation of time dependent spring capture zones. A travel time of 50 days is assumed to be large enough for bacteria to be removed in groundwater and is therefore used for protection area delineation in Germany (Birkholz et al., 2013). The 50-days contour lies close to the conduit system and the river itself. For the dendritic case, not all branches of the conduit system are part of this protection zone (Figure 4.2n).

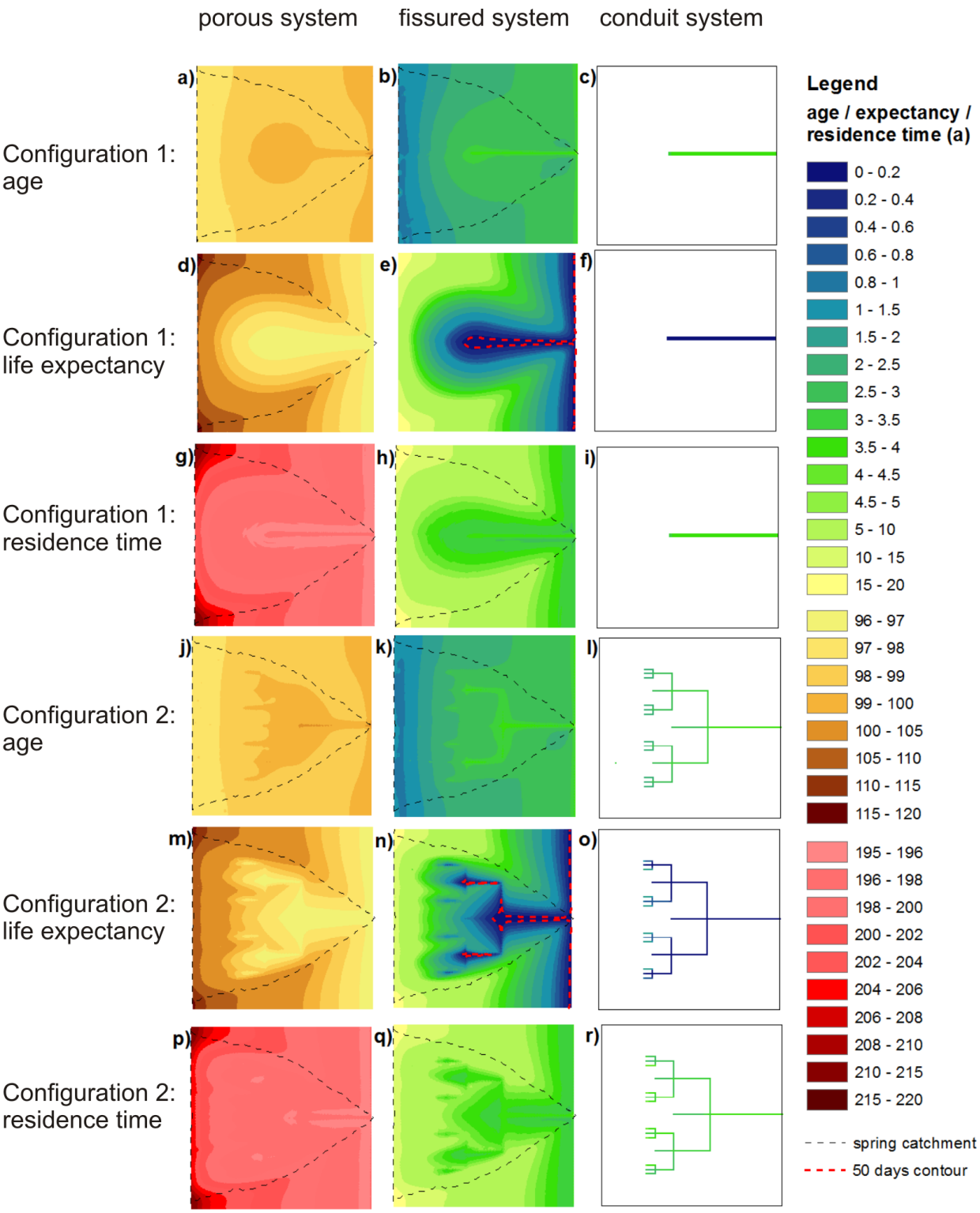

Figure 4.2. Plan view of ages and life expectancies of the reference simulations for all objectives and both model configurations in the three compartments.

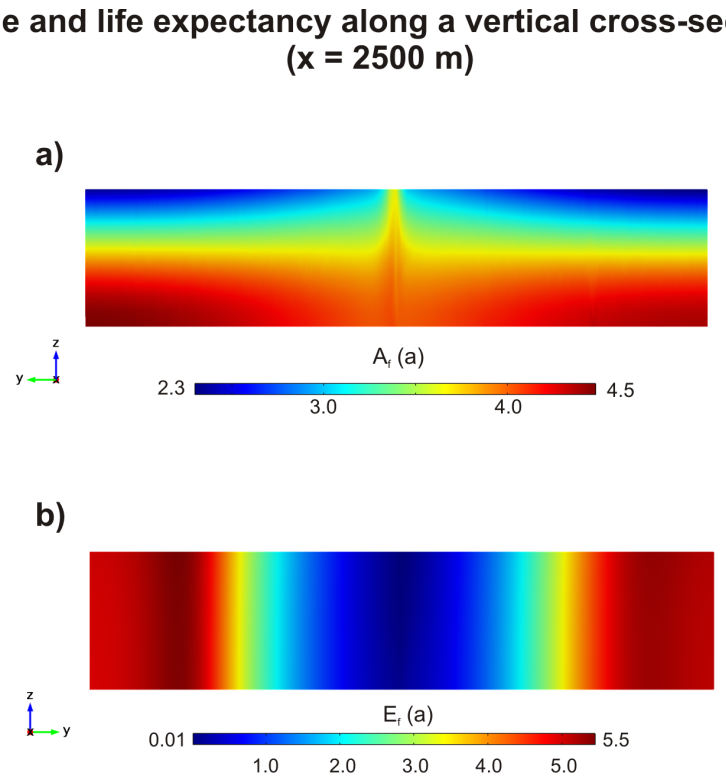

Figure 4.3 Vertical layering of groundwater age (a) and life expectancy (b) for the single conduit reference model.

4.3.2 Parameter sensitivity

4.3.2.1 Parameter influence on average values

Figure 4.4 summarizes the highest calculated RSE values for all parameter variations. The trends of the age and life expectancy changes with the parameter variations are illustrated in the Appendix Figure 4.A1 to Figure 4.A4. For all parameters except the porous-fissured exchange coefficient β the trends in the porous system are the same as in the fissured system. β has a large influence on the porous age and life expectancy A_p and E_p, which increase with decreasing β, with no influence on the remaining variables. The exchange flux between fissured and porous system linearly depends on β and on the age difference between porous and fissured ages A_p-A_f (Eq. 4.5). Therefore, a lower β-value leads to an increased age difference, i.e. a higher water age in the porous system, with the age in the fissured system remaining the same. A_p and E_p reach an asymptotic value for a β of ca. 1×10^{-9} s^{-1}. Above that value A_p-A_f is small enough to limit the exchange flux and an increased β value has no further influence.

The only other parameter changing the age difference A_p-A_f is the porosity of the porous system θ_p, since these are the only two varied parameters that are part of the age equation for the porous

system (Eq. 4.5). The increase of both A_p and A_f with θ_p is linear, with A_p showing a steeper increase. The effect of a change in porosity of the fissured system θ_f on all variables except for A_p and E_p is the same as for a change of θ_p. This is consistent with the findings of Varni and Carrera (1998) who stated that the average groundwater ages only depend on the total porosity of the system and not on the volumetric distribution between fissures and pores. The porosities are two of the most influential parameters with respect to average values (Figure 4.4), as already empathized by Cornaton and Perrochet (2006b) for porous aquifers.

The life expectancy of water in the conduit system E_c is generally the least sensitive to parameter changes. For the dendritic conduit, a slight influence can be observed for most parameter changes (Figure 4.4). For most cases, however, the influence on E_c is significantly smaller than the influence on the other variables. Since flow velocities inside the conduit system are high and E_c is usually in the order of seconds to a few days maximum, parameter variations must have a strong influence on flow velocities to lead to a noticeable change in life expectancy. Such changes only occur for reversed flow conditions at some point of the conduit, i.e. with groundwater flow directed into the fissured system. For those conditions the parameters of the fissured system can influence E_c. This is always the case for the dendritic conduit, since the combination of several conduit branches locally increases the hydraulic head in the conduit system. E_c generally rises for parameters, which increase conduit-fissured exchange flow, e.g. large values of the exchange coefficient α. Also the conduit cross-section A, the conduit roughness n and the fissured hydraulic conductivity K_f belong to that group of parameters. They do not influence any of the other residence time objectives significantly, only E_c of the dendritic system and the spring discharge (Figure 4.4). For the single conduit, flow from the conduit into the fissured system is only observed for high percentages of direct recharge r_{dir} of more than 70% of the total recharge. Therefore, r_{dir} is the only parameter significantly influencing E_c in the single conduit configuration (Figure 4.4).

All other variables are highly sensitive with respect to r_{dir} as well. The parameter r_{dir} controls the distribution of water between the fissured and the conduit system. In general, an increase in groundwater volume in the conduit system leads to higher spring discharge and increased ages and life expectancies in the fissured system, due to lower flow velocities. This effect is to some degree controlled by several parameters, i.e. the hydraulic conductivity of the fissured system K_f, the roughness coefficient of the conduit system n, the conduit-matrix exchange coefficient α and the conduit cross-section A. For most of these parameters, the age at the spring A_c closely follows the age of the groundwater in the fissured matrix A_f. High r_{dir} values result in very young groundwater recharged directly into the conduit system, however, leading to a significant decrease of the conduit groundwater age A_c. The fact that the increase of A_f is significantly higher for the single conduit

compared to that of the dendritic conduit shows that the dendritic conduit reaches its capacity at higher discharge rates and a significant amount of water flows from the conduit into the fissured system instead of being channelled directly to the spring. This is also documented in the smaller increase in spring discharge for the dendritic system (Figure 4.4).

The effect of the total recharge r is in the same order as that of r_{dir}, except for the single conduit fissured system, where it is lower. r is the only parameter that has the same influence on all objective functions, i.e. age and life expectancy in all three compartments. Ages and life expectancies decrease with higher recharge rates since a higher total discharge is generating increasing flow velocities in the fissured and the conduit system. The decrease in ages and life expectancies shows an asymptotic behaviour tending against zero. For r values above ca. 20–30 mm d^{-1} the changes are not significant anymore.

Besides the two porosities and the two recharge parameters, the thickness of the aquifer m_{af} is the only other parameter leading to high effects of several years (Figure 4.4). The increase of ages and life expectancies is linear with increasing thickness. Only for high thicknesses above 1 000 m (not shown) the behaviour becomes exponential when the draining influence of the conduit system does not reach to the aquifer base anymore.

Besides r_{dir}, the vertical position of the conduit system z_c is the only parameter that increases average groundwater ages in the fissured system while simultaneously lowering the age at the spring. The influence is not significant, however. The effect is slightly higher for the dendritic conduit system, because the single conduit is large enough to homogenise water ages across the whole vertical depth. If z_c is high, the dendritic conduits lie close to the aquifer top and draw predominately younger water from the upper layers. The older water at larger depths is not drained as efficiently, thereby increasing the average ages. The influence of z_c is expected to increase with a higher total aquifer thickness.

The dispersivities of the fissured and the conduit system have only minor influence. Especially, the dispersivity of the conduit system ε_c has only a slight influence on the average life expectancies of the dendritic conduit network. Groundwater ages and life expectancies in the other compartments as well as the life expectancy in the single conduit are completely independent of ε_c. The life expectancy in the single conduit is not distributed heterogeneously enough for a change in dispersivity to have a noticeable effect. The effect of a change in the fissured system dispersivity ε_f is also minor and becomes asymptotic for dispersivity values above ca. 40 m. Below that value, average age and life expectancy in the fissured system decrease with increasing dispersivity.

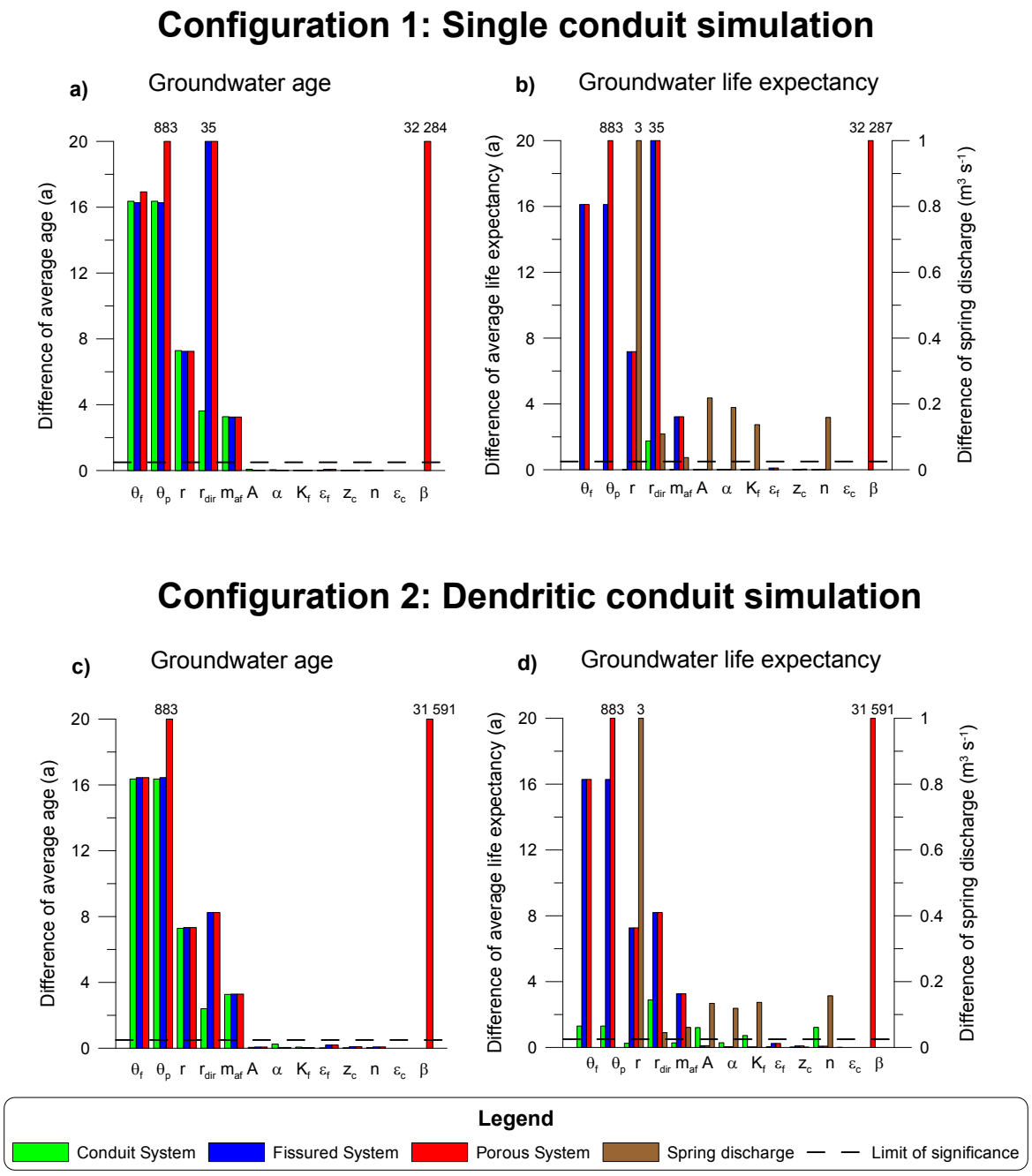

Figure 4.4. Maximum relative differences between average age, life expectancy and spring discharge in the reference simulation and the results of the parameter variations. For presentation purposes, the *y*-axis was cut off at 20 years and 1 $m^3 s^{-1}$ and the maximum differences are written above the respective columns.

4.3.2.2 Representativeness of local values

The average values of the groundwater age and life expectancy were compared with the values of the groundwater age simulated at the spring and the age and life expectancy in the observation well, since these are the locations where field values could be measured in an actual catchment area. Therefore, it is important to know how well these "measurements" represent the average values and which parameters have a large influence on spatial heterogeneity of the groundwater ages and life

expectancies. For assessing the difference between the "local" and the average values, deviations from the average value are provided in per cent. Figure 4.5 shows the range of deviations for each parameter. For the reference simulation (Chapter 4.3.1), the difference between A_f and E_f at the observation well and the average values are 3.3% and 27.3% for the single conduit (configuration 1) and 2.5% and 12.2% for the dendritic simulation (configuration 2). The smaller diameter but more evenly distributed dendritic conduits lead to a more homogeneous distribution of groundwater ages and even more so of groundwater life expectancies. Since life expectancy cannot be measured in the field, the difference between the age values is the more important parameter which lies with 2–4% well within the range of other uncertainties in the field.

The percentage of direct recharge r_{dir}, which showed the largest overall influence on average values, has the largest influence on the spatial distribution. The maximum differences between the average age and the age in the observation well of 31.5% for configuration 1 and 89.5% for configuration 2 were reached for high r_{dir} values above 90%. For high r_{dir} values the newly recharged water does not enter the fissured system evenly distributed, i.e. as diffuse recharge at the top, but indirectly via the conduit system due to gradient inversion. Therefore, lower velocities are observed in the fissured system and the average age increases. For configuration 2 the observation well is situated significantly closer to the conduit system due to its overall higher lateral extent (Figure 4.1). It receives a high amount of young water from the conduit system which leads to the large differences in groundwater age compared to the average age. For configuration 1, the ages in the observation well tend to higher values compared to the average age until a critical value of 95% direct recharge is reached and the water flux from the conduit system is high enough to reach the observation well.

Further, small ε_f values of 5 m have a relatively high influence of 13.5% for configuration 2 and 8.9% for configuration 1. The parameter m_{af} can lead to a significant homogenization due to the smaller variety of different paths the water can take. For small m_{af} values, the differences of A_f and E_f between the observation well and the average value decrease to 0.1% and 2.3%, respectively, for configuration 1. For configuration 2, the age difference also decreases to 0.1%. The difference in life expectancies increases with decreasing aquifer thickness, however. Since the observation well is vertically positioned in the middle of the aquifer, it lies closer to the aquifer top and therefore the conduit system for a reduced vertical extent. Therefore, the life expectancy is reduced more strongly in the observation well. For a thickness of 10 m the water in the observation well has less than half the life expectancy of the average groundwater in the aquifer.

As can be expected, the groundwater ages at the spring represent a significantly better approximation of the average values than the individual local observation well age measurements. For the reference simulation the age difference is only 0.7% for the single conduit and 0.4% for the

dendritic conduit configuration. For configuration 1 the only parameter that induces a significant difference of over 2% between the spring and the average age value is the percentage of direct recharge r_{dir} (Figure 4.5c). The dendritic conduit simulation (configuration 2) shows higher sensitivities to most parameters. The two porosities θ_p and θ_f, the conduit system dispersivity ε_c and the porous-fissured exchange coefficient β do not influence the spatial distributions for either setup. r_{dir} and the total recharge r have a slightly higher influence for configuration 1 since the single conduit transmits water more efficiently (see also Chapter 4.3.3). All other parameters have higher influences on the difference between average fissured system age and spring water age for configuration 2. Only four of these influences are significant, however. A decrease in the vertical conduit position z_c or in the fissured-conduit exchange coefficient α leads to slightly higher spring water ages and slightly lower average ages in the fissured system (Chapter 4.3.2.1). Decreasing values of the conduit roughness n or the fissured system dispersivity ε_f both increase the average age inside the fissured system and the spring water age simultaneously. Since the influence of both parameters on the average ages is higher, however, they also increase the difference between spring water and average age significantly.

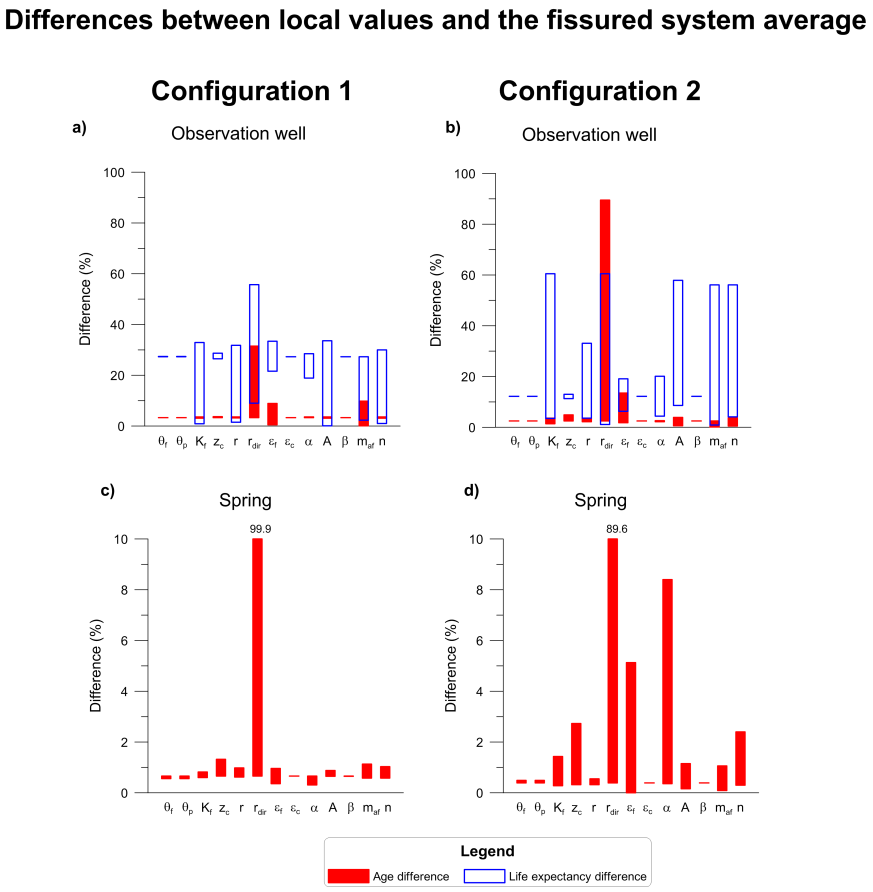

Figure 4.5. Differences in age and life expectancy between the fissured system average and: (a) the observation well for the single conduit simulation (configuration 1) (b) the observation well for the dendritic conduit simulation (configuration 2) (c) the spring water for configuration 1 (d) the spring water for configuration 2.

4.3.3 Transient age simulations – influence of recharge events

As described in Chapter 4.2.2 a theoretical recharge event was introduced into the model. Figure 4.6 shows the event and the corresponding groundwater age responses in the fissured system and at the spring. Initially, the spring water age represents the average age of the water in the fissured system. While the response of the groundwater age at the spring is rapid and intense, the fissured system average age only decreases slightly and with a lag time of several days. For configuration 1 the minimum for the average fissured age will be reached after 26 days and for configuration 2 after 27.4 days (not shown) and only differ from the initial age by ca. 0.16 years. The influence on the age in the porous system (not shown) is in the order of $1x10^{-4}$ years and is not significant. Diffusive exchange processes are too slow to significantly react to the relatively short-term recharge event. It is noticeable that the spring age recovers much faster back to average values than the spring discharge. For both configurations, the spring water age is higher than the fissured system average after the simulation period of 20 days, even though the spring water age is still ca. 0.1-0.2 years younger than at the beginning of the recharge event (Figure 4.6). This is due to a slight decrease in the average age of groundwater in the fissured system. The young recharge water is stored in the upper regions of the aquifer, while the conduits drain an important amount of water from greater depths (Figure 4.3). Therefore, this effect is stronger for the single conduit than for the dendritic system.

The change of groundwater ages at the spring is significantly less pronounced for the dendritic conduit than for the single conduit configuration (Figure 4.6b). The dendritic conduit pattern results in flow regimes where conduit water flows into the fissured system for head gradient conditions directed towards the fissured system immediately after direct recharge events. The direct recharge pulse is not transmitted completely and directly to the spring, as is the case for the single conduit. This effect also dampens spring discharge but this dampening is comparatively less well developed. The variation in spring water age for the dendritic system is less than 50%, while the variation in discharge is almost 80% of that of the single conduit configuration. This shows the relatively large amount of fissured matrix water mobilized by the new recharge mixed into the spring discharge.

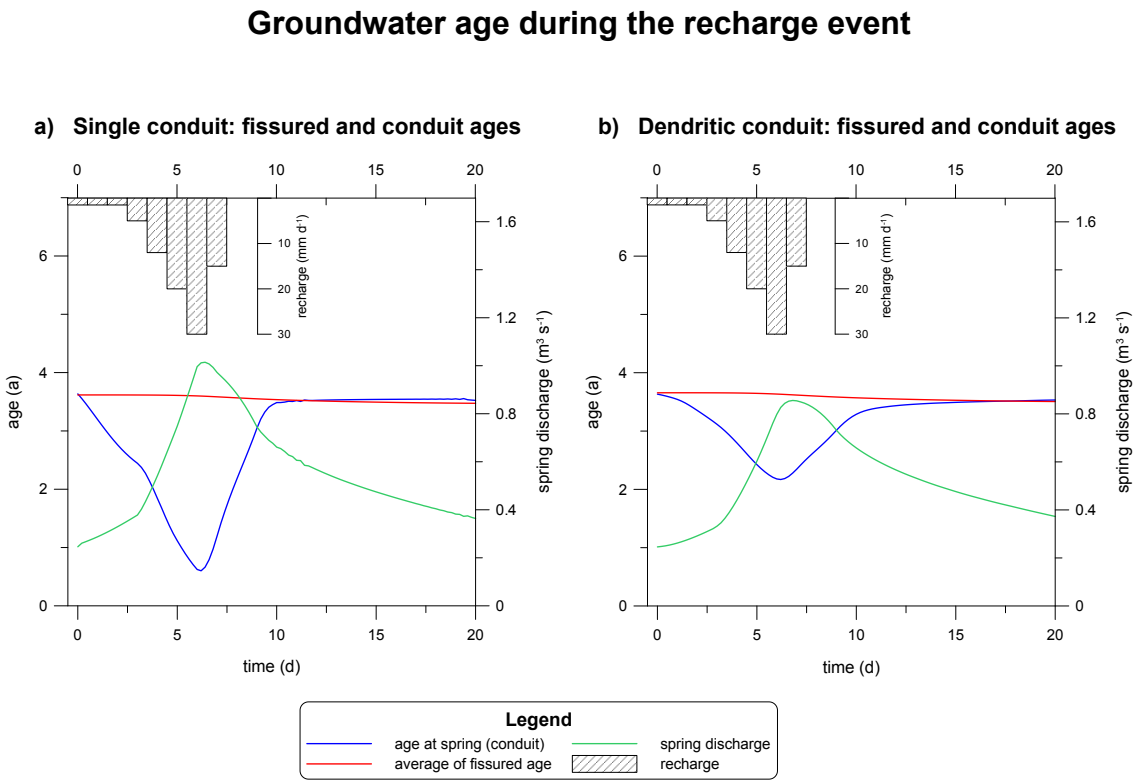

Figure 4.6. Simulated groundwater recharge event for single conduit and dendritic conduit system configurations. The change in average ages and spring discharge is shown.

4.3.4 Comparison of transit time distribution curves

Figure 4.7 shows the comparison between the transit time distribution curves monitored at the spring and at the observation well with the distributed simulation and the curves simulated with the chosen lumped-parameter approaches (Chapter 4.2.3). The transit time distribution curves for the two model configurations (single and dendritic conduit system) are very similar. The signal at the spring shows a slightly higher first peak and steeper decline at the beginning of the simulation period for the dendritic conduit configuration. No direct recharge was considered in this simulation. The first peak consists of the diffusely recharged water in the immediate vicinity of the conduit system, which is captured quickly and transferred to the spring. The larger lateral extent of the dendritic system increases the contact area between the fissured and the conduit system compared to the single conduit configuration leading to the observed higher amplitude of the first peak.

The lumped-parameter models were calibrated to fit the Comsol® curves. For all simulations, the EPM model showed the best fit with RMSEs in the order of 1×10^{-4} to 1×10^{-3} years giving a good approximation of the middle part of the curve, which mainly results from the fissured system. However, for simulating the age of the spring discharge, it fails to reproduce the amplitude of the peak of young water introduced by the conduit. For the observation well located in the fissured

system, the amplitude of the maximum is well met, but the timing of the peak, which is a consequence of the spatial aquifer extent, is not reproduced (Figure 4.7). The calibrated parameter η (Eq. 4.9) has in all cases the value 1, which implies that the piston flow component of the model is switched off and a simple exponential model would have given the same goodness of fit. The simulated average transit time is with ca. 1.8 years significantly shorter than that of the numerical model with ca. 3.6 years. The exponential curves drop below those of the numerical model after ca. 70 years and do, therefore, not include the very old components of the porous system significantly contributing to longer average ages. The PFM fails in all cases to simulate the transit time curves because even the first peak could not be described by piston flow behaviour. The fit of the first peak can possibly be improved if direct recharge is considered in the simulation.

The DM fails to approximate the transit time curves at the spring. The fit is improved considerably if only the last part of the curve is considered for calibration, i.e. water with ages higher than 2.5 years as already suggested by Maloszewski et al. (2002). Nevertheless, average transit times are still underestimated by more than one year. For the fissured system ages monitored at the observation well, the statistical fit of the DM is with a difference of ca. 4×10^{-4} years only slightly worse than that of the EPM. The DM can nonetheless be viewed as superior since it approximates the average transit time at the observation well very well with only differences of 0.06 and 0.09 years for the dendritic and the single conduit system, respectively. The apparent dispersion parameter P_D (Chapter 4.2.3) is in both cases ca. 1.9 showing a high importance of the dispersive component.

The transit time distribution for the porous system monitored at the observation well is very flat and broad due to the slow diffusion processes. Both, the EPM and the DM estimate the average transit time of the distributed model of 101.1 years almost correctly with a difference of 1.1 years for DM and only 0.3 years for EPM.

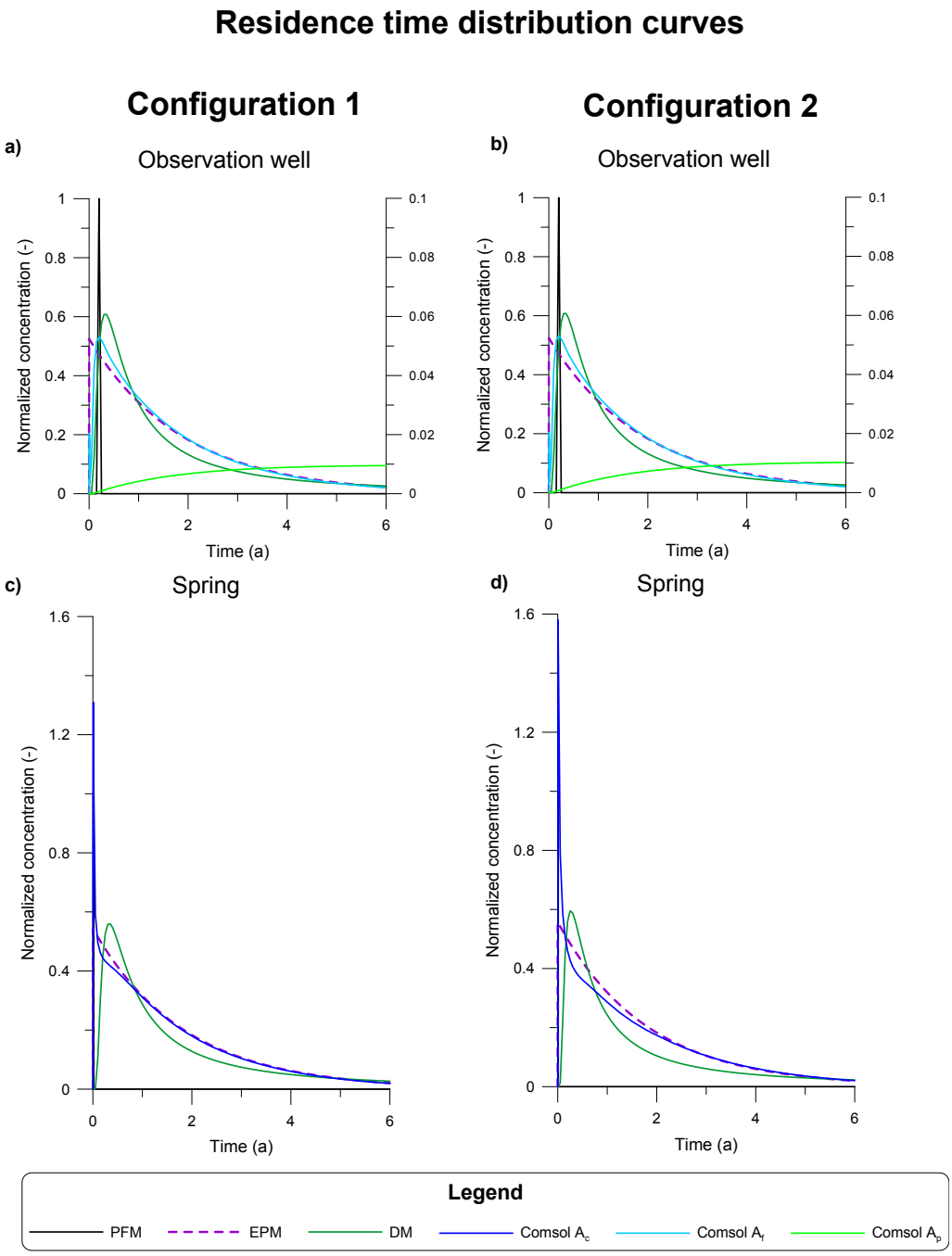

Figure 4.7. Simulated transit time distribution curves at the spring with the presented distributed model and several lumped-parameter approaches. The age distribution in the porous system is plotted on the secondary y-axis, all others on the primary axis. Figure (b): the A_c-curve is cut at 1.6 for representation reasons. The maximum value is 1.9. Abbreviations: PFM = Piston Flow Model, EPM = Exponential Piston Flow Model, DM = Dispersion Model; A_c = Age in the conduit system, A_f = Age in the fissured system, A_p = Age in the porous system.

4.4 Discussion

4.4.1 Model applicability

In this study, the modelling approach is applied for generating age and life expectancy distributions for two synthetic, highly simplified karst systems. It is easily applicable to more complex models, as long as the computer capacity is not limiting due to the high number of degrees of freedom. Flow and transport can be solved separately but the three objective functions simulated with the transport equation, i.e. age or life expectancy in the porous, fissured and conduit system, have to be solved synchronously easily leading to high system requirements for large meshes. For application to actual field situations, the effect of the overburden and unsaturated zone has to be considered, depending on the environmental tracer used for model calibration. Geyer (2008) compared different tracers for the Gallusquelle area and found a difference in calculated ages of more than 15 years between tracers including the unsaturated zone, i.e. ^{3}H, and ^{85}Kr and SF_6. For the modelling of ^{3}H data, the model would have to be extended to an unsaturated model. A comparison of different types of field tracers can possibly assist to independently identify the effect of flow in unsaturated and saturated zone on travel time distributions.

The comparison with age distributions generated by lumped-parameter models showed that the transit time distribution at the observation well can partly be represented with dispersion or exponential models. The dispersion model is better suited for catching the tailing and therefore the average ages, while the exponential model is superior in reproducing the middle part of the distribution curve, i.e. ages between 1 and 4 years (Figure 4.7). Simulating the whole breakthrough curve at the spring is not possible with the lumped-parameter approaches. Maloszewski et al. (2002) showed that age distributions in karst aquifers can be approximated with a combination of a piston flow and a dispersion model. This is supported by the numerical model distribution curves (Figure 4.7c and d) presented here. The calculation of Maloszewski et al. (2002) is based on the amount of direct recharge, while direct recharge was not simulated in this study. Water recharged close to the conduit system is still fast enough to create a visible peak with young ages. The consideration of flow through the unsaturated zone would considerably change this picture since diffuse recharge usually experiences an important delay in the unsaturated zone. Therefore, the shape of the age distribution curve also depends on the type of tracer that is measured and the kind of travel time required.

4.4.2 Model parameters

The parameters can be subdivided into four groups regarding their sensitivity: parameters which both, spring discharge and groundwater residence times are sensitive to, those which only the spring discharge is sensitive to, those which only the residence times are sensitive to and parameters which no objective function is sensitive to. Totally non-influential parameters cannot be deduced by the above simulations and respective field measurements. The knowledge that they do not have an important effect reduces the amount of parameters to be considered though. The non-influential parameters include the two dispersivities ε_f and ε_c and the vertical conduit position z_c. z_c only becomes significant, for very large aquifer thicknesses, i.e. if the drainage effect of the conduit does not reach down to the base of the aquifer.

The first group includes the recharge parameters. Total recharge and the ratio between diffuse and direct recharge strongly influence all objective functions. Especially the percentage of direct recharge greatly influences not only the absolute values of residence times but significantly increases the heterogeneity of the residence time distribution within the aquifer. Furthermore, the location of recharge, e.g. in large catchment areas with differences in elevation, influences the local velocity field and the distribution of residence times. Therefore, a good estimation of the recharge distribution is an essential precondition for a meaningful calibration.

The parameters that influence the spring discharge but with only minor effect on residence times comprise the hydraulic conductivity of the fissured matrix K_f and basically all conduit parameters, i.e. cross-section A, exchange coefficient α and roughness n. For the single conduit configuration, these parameters have no real influence on residence times at all. For the dendritic conduit configuration, their influence on life expectancy distributions inside the conduit system increases. So, it can be assumed that they gain significance in weakly or moderately karstified systems, where the conduit system consists of many different interacting branches and includes passages where outflow from the conduit into the fissured system occurs.

The group of parameters, which only the residence times are sensitive to, is especially interesting within the context of efforts to reduce model ambiguity. When groundwater flow is not sensitive to a certain parameter, additional objectives have to be included in a model to assess it (e.g. Hartmann et al., 2013; Oehlmann et al., 2015). Residence time distributions are especially sensitive to the porosities of the fissured and the porous systems θ_f and θ_p. However, the influences of these two porosities on ages in the fissured system are the same and therefore difficult to distinguish in the field. Assessing the diffusive exchange coefficient β could be helpful for solving this issue. In this study, it was viewed as a pure calibration parameter. In real field situations, the parameter β

depends on the properties of the interfacial area between the two exchanging systems. These properties are generally unknown, but it can be expected that a larger pore space increases the effective exchange area. Doyon and Molson (2012) derived an analytical solution for a system consisting of an immobile matrix and parallel discrete fractures, where they define the flux of age mass at the interface as:

$$J_{f\to m} = -\theta_m \rho D_m \frac{\partial A_m}{\partial x}, \tag{4.10}$$

where ρ is the density of water [M L^{-3}]. As apparent from Eq. (4.10), the exchange coefficient depends on the molecular diffusion coefficient and on the porosity. Since a double continuum approach is used in this work to represent the fissured and the porous systems, the coefficient can be assumed to depend on both porosities and the degree of connectivity between them. Without geometric information or laboratory experiments, the exact value cannot be derived. An increased exchange with increasing porosities would produce non-linear dependencies and provide information on how to distinguish and quantify the effects of individual changes in the two porosities in the field.

The thickness of the aquifer m_{af} also slightly influences the spring discharge, but the influence on residence times is higher. Furthermore, spring discharge is largely controlled by the properties of the highly conductive conduit system, which are often challenging to derive independently, e.g. by field measurements. The simulations in this study showed, that the conduit system has only a minor influence on the groundwater age, especially during recession flow conditions. Therefore, for known recharge conditions and estimated porosities, the groundwater residence time can be a good indicator for aquifer thickness. In catchments with highly variable aquifer thicknesses, distributive age measurements might also indicate which area the water predominately comes from. The effects of increased aquifer thickness and increased porosity are in the same order of magnitude, if calculated with respect to a change in total water volume within the aquifer. The thickness further influences the mixing and the flow distance leading not only to lower average ages and expectancies for lower thicknesses but also to a lower difference between maximum and minimum values, even though the number of mesh elements was approximately the same for each simulation.

The transient simulation shows the short effect of the direct recharge on groundwater ages. Between 3 to 7 days after the event, the spring water age has already returned to the fissured system average even though the spring discharge is still slightly higher due to the influence of event water. Further, the dampening effect of the dendritic conduit system is much higher on the age signal than on the discharge. This is due to the fact that the increased discharge is a function of the higher water

volume within the catchment area while the age signal is easily dampened by diffusion, dispersion and mixing processes.

4.5 Conclusion

This study presents an approach for the simulation of the complete residence time distribution, i.e. lateral distribution in the porous, fissured and conduit systems, in a karst aquifer. It is successfully applied to two process studies. Common lumped-parameter simulations only derive the distribution of residence times at a certain point under highly simplified assumptions. The comparison of the derived distribution curves shows, that the lumped-parameter models cannot represent the whole distribution curve. The exponential-piston flow model gives a valid approximation of the middle part of the curve, which is generated by the fissured system. However, it fails to reproduce the rising limp and the pronounced tailing that result of the conduit and the porous systems. This shows the importance of including the effects of the triple porosity nature of karst aquifers for the simulation of groundwater residence times. Even in the absence of a direct recharge component, a significant peak with very young age of 5 days was observed at the spring showing the effect of the conduit system.

The approach further allows for the identification of important parameters in residence time distributions. The parameter analysis showed that the measurement of groundwater ages can be a useful tool for estimating the aquifer thickness, since the other influential parameters, i.e. the porosity and the recharge, can be approximated independently with different approaches. The relatively less expressed influence of conduit parameters on the average spring water age seems promising for using the recession flow age to characterize the fissured-porous part of the aquifer system.

To further improve the understanding of the groundwater residence time distribution in karst aquifers, the use of a field study with groundwater age measurements in observation wells and at one or several springs would be ideal. For a better understanding of the influence of the porous system, experiments regarding the diffusive exchange coefficient and its dependence on the porosities in the fissured and porous system would be the key investigation required.

Acknowledgement

The presented study was funded by the German Federal Ministry of Education and Research (promotional reference No. 02WRS1277A, AGRO, “Risikomanagement von Spurenstoffen und Krankheitserregern in ländlichen Karsteinzugsgebieten”).

References

Bauer, S., Liedl, R., and Sauter, M., 2003. Modeling of karst genesis: Influence of exchange flow. Water Resources Research 39 (10), 1285, doi:10.1029/2003WR002218.

Birkholz, T., Burg, D., Carl, F., Eckl, H., Frühauf, A., Karfusehr, C., Krugmann, E.-H., Meggeneder, M., Präkelt, E.-F., Rausch, A., Sander, L., Sütering, U., Uhlen, M., and Wehr, M., 2013. Praxisempfehlung für Niedersächsische Wasserversorgungsunternehmen und Wasserbehörden; Handlungshilfe Ausweisung von Wasserschutzgebieten für Grundwasserentnahmen. Wasserverbandstag e.V. Bremen, Niedersachsen, Sachen-Anhalt, Hannover.

Clemens, T., 1998. Simulation der Entwicklung von Karstaquiferen. Ph.D. thesis, Eberhard-Karls-Universität zu Tübingen, Tübingen.

Cook, P. G., Love, A. J., Robinson, N. I., and Simmons, C. T., 2005. Groundwater ages in fractured rock aquifers. Journal of Hydrology 308, 284-301, doi:10.1016/j.jhydrol.2004.11.005.

Cornaton, F., 2004. Deterministic models of groundwater age, life expectancy and transit time distributions in advective-dispersive systems. Ph.D. thesis, University of Neuchâtal.

Cornaton, F. and Perrochet, P., 2006a. Groundwater age, life expectancy and transit time distributions in advective-dispersive systems: 1. Generalized reservoir theory. Advances in Water Resources 29, 1267-1291.

Cornaton, F. and Perrochet, P., 2006b. Groundwater age, life expectancy and transit time distributions in advective-dispersive systems: 2. Reservoir theory for sub-drainage basins. Advances in Water Resources 29, 1292-1305.

Doyon, B. and Molson, J. W., 2012. Groundwater age in fractured porous media: Analytical solution for parallel fractures. Advances in Water Resources 37, 127–135, doi:10.1016/j.advwatres.2011.11.008.

Einsiedl, F., 2005. Flow system dynamics and water storage of a fissured-porous karst aquifer characterized by artificial and environmental tracers. Journal of Hydrology 312, 312–321, doi:10.1016/j.jhydrol.2005.03.031.

Einsiedl, F. and Mayer, B., 2005. Sources and processes affecting sulfate in a karstic groundwater system of the Franconian Alb, southern Germany. Environmental Science & Technology 39, 7118-7125.

Einsiedl., F., Maloszewski, P., and Stichler, W., 2009. Multiple isotope approach to the determination of the natural attenuation potential of a high-alpine karst system. Journal of Hydrology 365, 113-121, doi:10.1016/j.jhydrol.2008.11.042.

Frind, E. O., Muhammad, D. S., and Molson, J. W., 2002. Delineation of Three-Dimensional Well Capture Zones for Complex Multi-Aquifer Systems. Ground Water 40 (6), 586–598.

Frind, E. O., Molson, J. W., and Rudolph, D. L., 2006. Well Vulnerability: A quantitative approach for source water protection. Ground Water 44 (5), 732–742.

Geyer, T., 2008. Process-based characterisation of flow and transport in karst aquifers at catchment scale. Ph.D. thesis, University of Göttingen.

Goode, D. J., 1996. Direct simulation of groundwater age. Water Resources Research 32 (2), 289–296.

Hartmann, A., Wagener, T., Rimmer, A., Lange, J., Brielmann, H., and Weiler, M., 2013. Testing the realism of model structures to identifying karst system processes using water quality and quantity signatures. Water Resources Research 49, 3345–3358, doi:10.1002/wrcr.20229.

Király, L., 2002. Karstification and groundwater flow. In: Gabrovšek, F. (Ed.), Proceedings of the Conference on Evolution of Karst: From Prekarst to Cessation, Postojna-Ljubljana, 155-190.

Long, A. J. and Putnam, L. D., 2009. Age-distribution estimation for karst groundwater: Issues of parameterization and complexity in inverse modeling by convolution. Journal of Hydrology 376, 579-588.

Maloszewski, P. and Zuber, A., 1982. Determining the turnover time of groundwater systems with the aid of environmental tracers 1. Models and their Applicability. Journal of Hydrology 57, 207-231.

Maloszewski, P., Stichler, W., Zuber, A., and Rank, D., 2002. Identifying the flow systems in a karstic-fissured-porous aquifer, the Schneealpe, Austria, by modelling of environmental ^{18}O and ^{3}H isotopes. Journal of Hydrology 256, 48-59.

Mohrlok U., 2014. Numerische Modellierung der Grundwasserströmung im Einzugsgebiet der Gallusquelle unter Festlegung eines Drainagesystems. Grundwasser, 19, 73-85, doi:10.007/s00767-013-0249-x.

Molson, J. W. and Frind, E. O., 2012. On the use of mean groundwater age, life expectancy and capture probability for defining aquifer vulnerability and time-of-travel zones for source water protection, Journal of Contaminant Hydrology 127, 76-87.

Morgenstern, U. and Daughney, C. J., 2012. Groundwater age for identification of baseline groundwater quality and impacts of land-use intensification – The National Groundwater Monitoring Programme of New Zealand. Journal of Hydrology 456-457, 79-93.

Oehlmann, S., Geyer, T., Licha, T., and Birk, S., 2013. Influence of aquifer heterogeneity on karst hydraulics and catchment delineation employing distributive modeling approaches. Hydrology and Earth System Sciences 17, 4729-4742, doi:10.5194/hess-17-4729-2013.

Oehlmann, S., Geyer, T., Licha, T., and Sauter, M., 2015. Reducing the ambiguity of karst aquifer models by pattern matching of flow and transport on catchment scale. Hydrology and Earth System Sciences 19, 893–912, doi:10.5194/hess-19-893-2015.

Sauter, M., 1992. Quantification and Forecasting of Regional Groundwater Flow and Transport in a Karst Aquifer (Gallusquelle, Malm, SW Germany). Tübinger Geowissenschaftliche Arbeiten C13, Tübingen.

Teutsch, G. and Sauter, M., 1991. Groundwater Modeling in karst terranes: scale effects, data aquisition and field validation. In: Proceedings of the 3rd Conference on Hydrogeology, Ecology, Monitoring and Management of Ground Water in Karst Terranes, 4-6 December 1991, Nashville, USA, 17-34.

Varni, M. and Carrera, J., 1998. Simulation of groundwater age distributions. Water Resources Research 34 (12), 3271-3281.

Worthington, S. R. H., 2007. Groundwater residence times in unconfined carbonate aquifers. Journal of Cave and Karst studies 69 (1), 94-102.

Worthington, S. R. H., 2009. Diagnostic hydrogeologic characteristics of a karst aquifer (Kentucky, USA). Hydrogeology Journal 17, 1665-1678.

Appendix A

Age and life expectancy trends for the parameter analysis

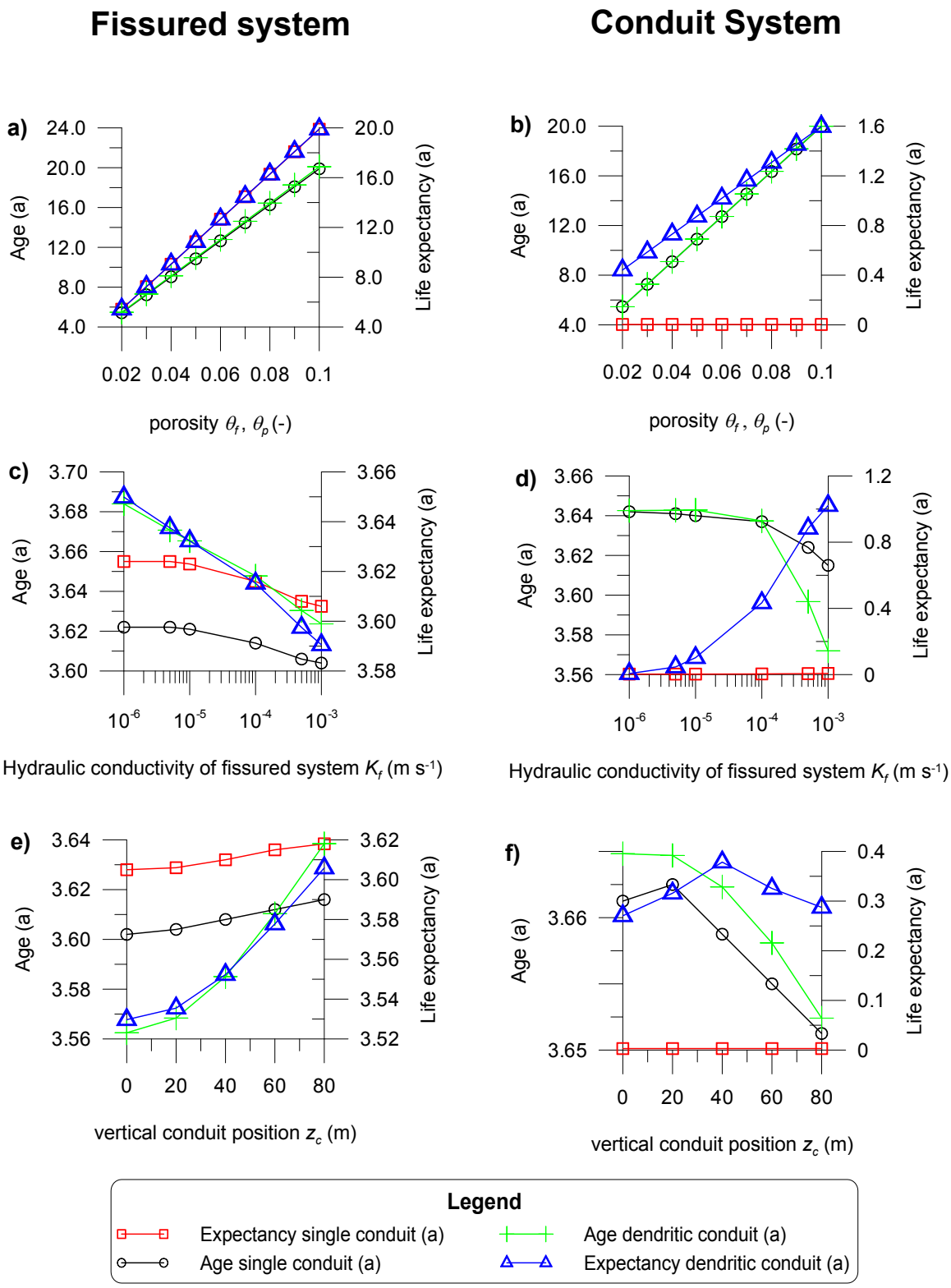

Figure 4.A1. Trends of average age and life expectancy in different model compartments during parameter analysis. The maximum differences with respect to the reference simulations can be found in Figure 4.4

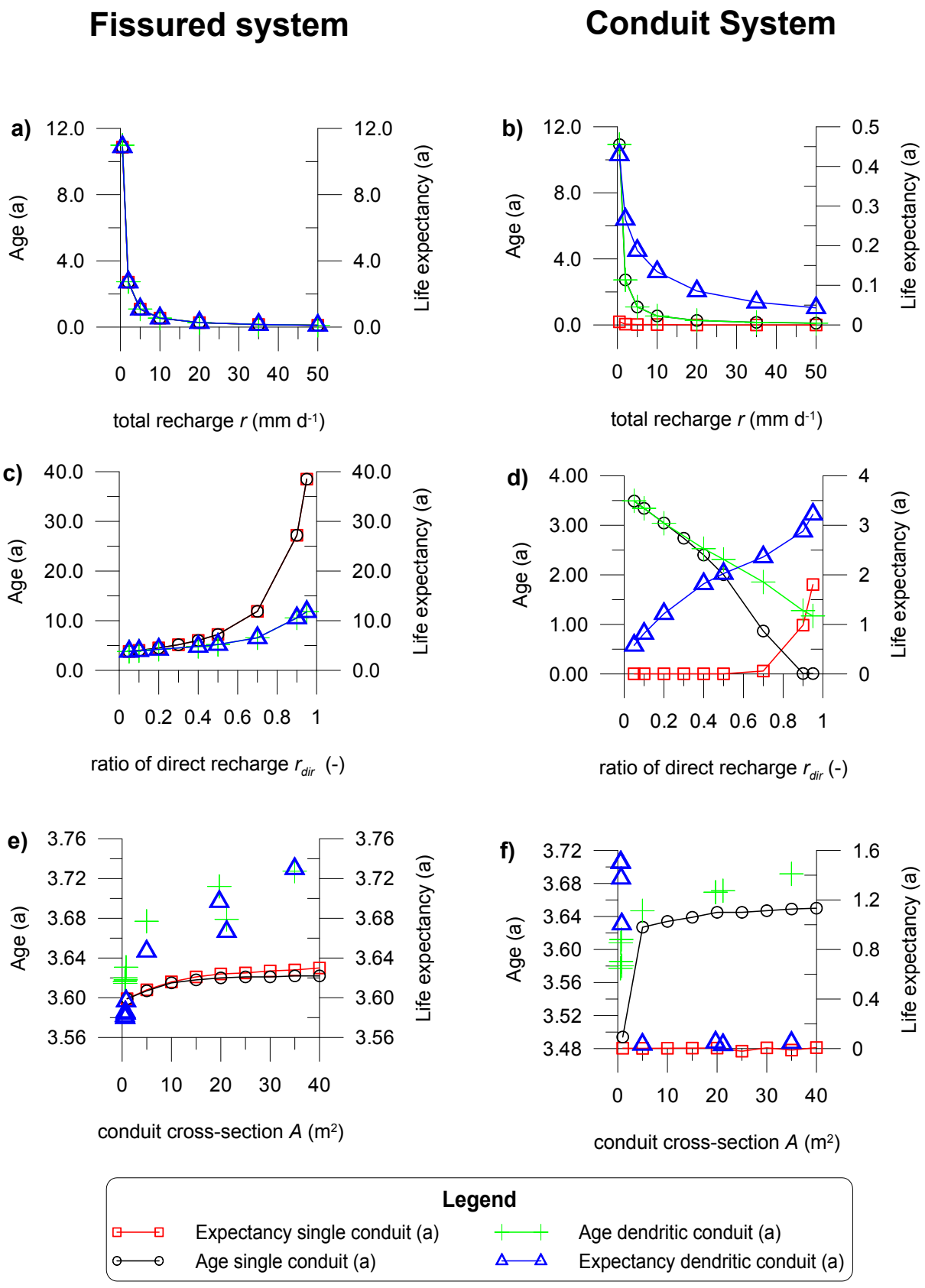

Figure 4.A2. Trends of average age and life expectancy in different model compartments during parameter analysis. The maximum differences with respect to the reference simulations can be found in Figure 4.4.

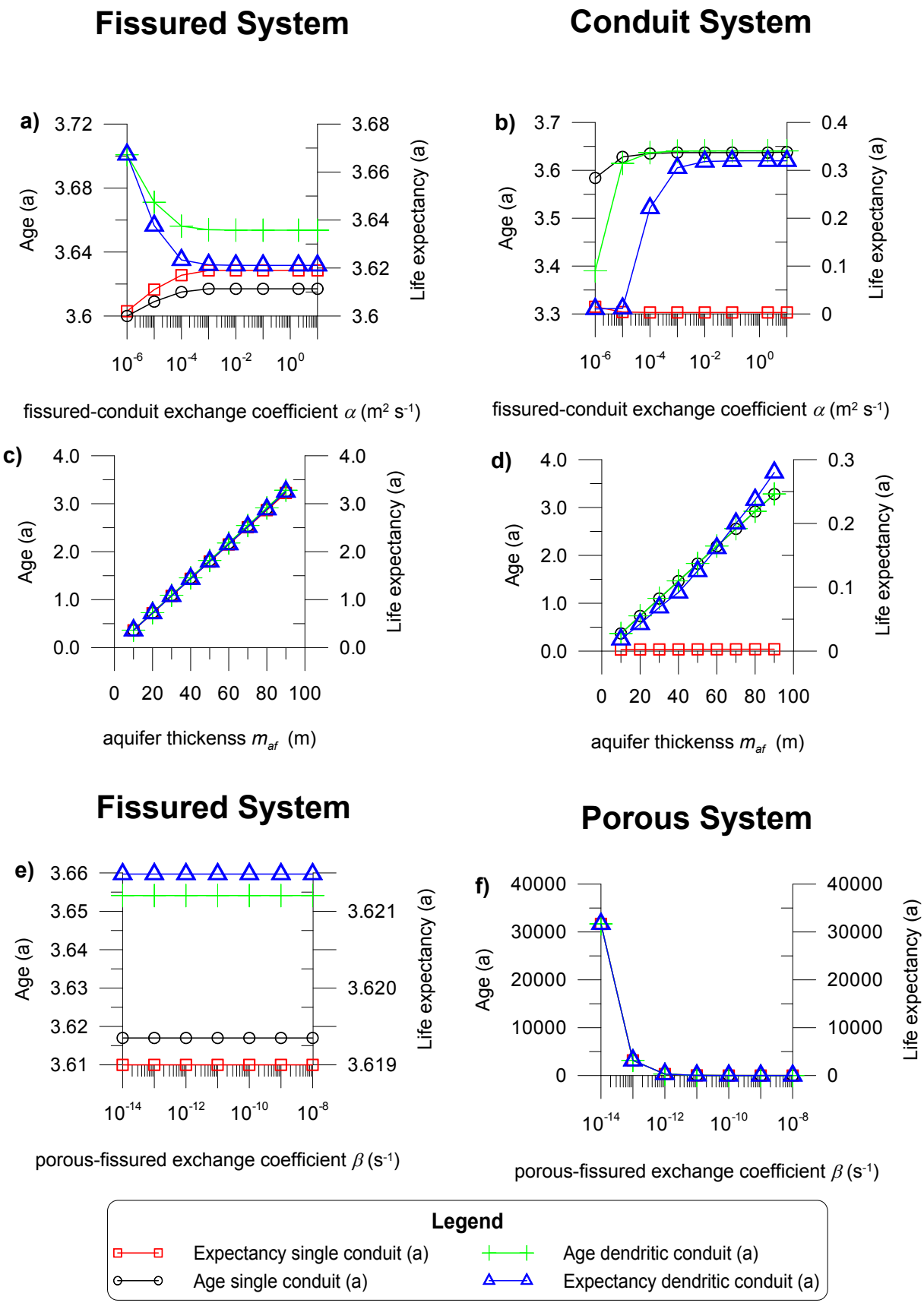

Figure 4.A3. Trends of average age and life expectancy in different model compartments during parameter analysis. The maximum differences with respect to the reference simulations can be found in Figure 4.4.

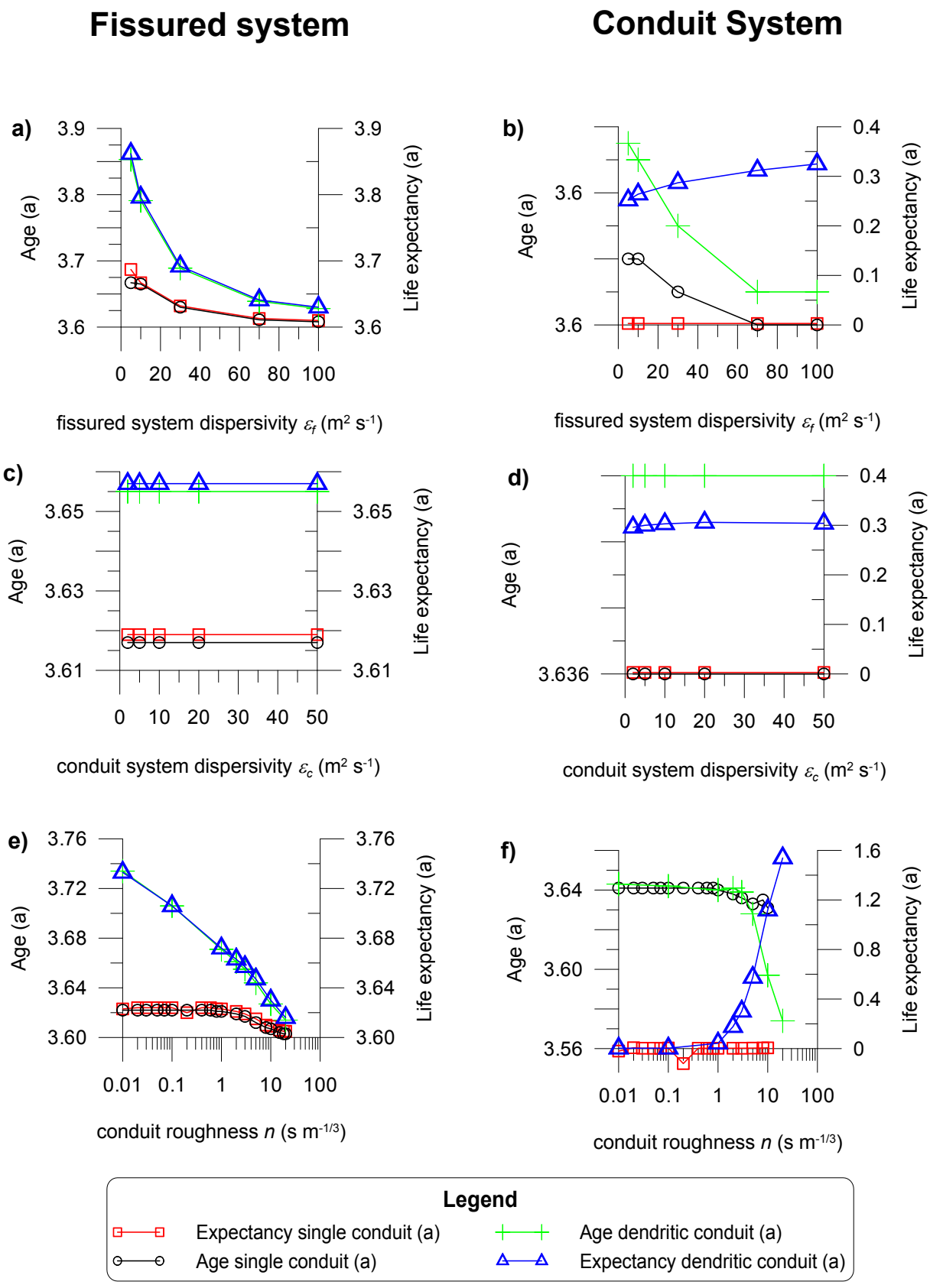

Figure 4.A4. Trends of average age and life expectancy in different model compartments during parameter analysis. The maximum differences with respect to the reference simulations can be found in Figure 4.4.

Chapter 5

5 Application outlook: distributed numerical simulation of groundwater residence times in the Gallusquelle aquifer

5.1 Background and approach

The presented approach for simulating the groundwater ages, life expectancies and residence times (Chapter 4) is applied to the numerical model of the Gallusquelle developed in Chapters 2 and 3. The aim of the simulation is to generate an average residence time distribution under recession flow conditions for the whole aquifer. Further, a transient transport simulation was performed for the steady-state flow field for deriving the transit time distribution curves at the different karst springs in the area as described in Chapter 4.2.3. The model geometry and parameters were principally chosen as discussed in Chapter 3 (Table 3.1: Scenario 2). The only difference is the representation of the upper boundary of the aquifer. The Gallusquelle aquifer is unconfined and, therefore, the water-saturated thickness is determined by the position of the groundwater table. While it was demonstrated in Chapters 2 and 3 that the regional flow field and the conduit velocities can be calibrated without explicitly taking this into account, the groundwater residence times have a high dependency on the water-saturated thickness (Chapter 4) and might be influenced significantly. Therefore, the model was adapted for including the unconfined conditions and the aquifer top was placed directly at the water table.

Since COMSOL Multiphysics® does not provide an interface for the simulation of unconfined aquifers, the *Moving Mesh* interface was employed for aligning the aquifer top with the water table. This module provides an arbritary Lagrangian-Eulerian (ALE) interface, where a new geometric environment (spatial domain) is calculated from a reference environment (material domain) with defined mesh displacement values (Jin et al., 2014). Every model equation can either be solved in the spatial or in the material domain. Jin et al. (2014) showed how this interface can be applied for the simulation of unconfined aquifers. The ALE interface is coupled to the Darcy flow interface by the upper boundary condition that sets the *z*-component of the upper aquifer boundary at the position of the hydraulic head of the fissured matrix, i.e. at zero pressure. The interface does not remesh the

domain but deforms the mesh elements reducing simulation time compared to remeshing after every step (COMSOL AB, 2012). The disadvantage of this approach for hybrid modelling is, that the deformation of the mesh leads to slight changes in the positions and shapes of the discrete elements. Especially since the conduit radius is calculated based on the conduit length (Chapter 2) a slight distortion of the discrete elements can lead to changes in conduit geometry and numerical problems. Therefore, the conduit flow and transport equations were solved in the material domain, where they are not influenced by the distortion, while the equations for the fissured and porous systems were solved in the spatial domain. This introduces slight inaccuracies because the calculation frames for the systems are different. However, since the vertical conduit position does not have a large influence on the residence time distribution (Chapter 4) and a steady-state flow field was used for the simulation this effect is assumed to be negligible.

Field data on groundwater ages are scarce in the Gallusquelle area as in most karst aquifers. Geyer (2008) analysed several environmental tracers and estimated the groundwater ages with three lumped-parameter models. Since the presented numerical model is limited to the saturated zone of the aquifer, tracers that include the travel time through the unsaturated zone, e.g. ^{3}H, cannot be employed for calibration purposes. Sulfurhexafluoride (SF_6) and ^{85}Kr only document the passage through the saturated zone, since they are gaseous tracers, which are expected to be in equilibrium with the atmosphere while they are above the water table (Geyer, 2008). Geyer (2008) took samples of both tracers at the Gallusquelle at three different days, each time after a dry period of at least 12 days. The SF_6 and ^{85}Kr ages all lay between 3 and 4 years with an estimated error of ca. 0.5 years. Geyer (2008) also performed $^{3}H/^{3}He$ sampling in two pumping wells within the area. The results varied between the same age as spring water to more than 50 years. Since pumping from wells probably induces the mobilization of otherwise stagnant water in the aquifer, these ages can be considered as a mixture of the age in the fissured system and that in the porous system. They were therefore not included for direct calibration but for checking whether the model reproduces the correct range of ages.

Therefore, only age data directly at the Gallusquelle spring are available for calibration and the simulated spatial distribution of the groundwater ages cannot be validated at this stage. However, the simulation is used for checking the applicability of the residence time approach and the investigated parameter effects for the more complex model. Furthermore, the ability of the model to reproduce the groundwater age at the Gallusquelle and the observed ranges in the aquifer is a further clue to the plausibility of the already calibrated flow field.

In addition to the parameters already described in Chapter 3 (Table 3.1) the porosities of the fissured and the porous system, the dispersivitiy in the fissured system and the fissured-porous exchange

coefficient have to be defined. The porosity of the fissured system θ_f was set to 1% after the results of Sauter (1992). The dispersivities were found in Chapter 4 to show only slight or no sensitivity and were set to 25 m for the conduit and 200 m for the fissured system. The porous-fissured exchange coefficient β was set to 4×10^{-12} m^2 s^{-1} in accordance with the reference value of Chapter 4. Since neither the dispersivities nor β significantly influence the spring water age (Chapter 4) and all other values were either estimated by field measurements or calibrated during the previous steps, the residence times were then calibrated for the spring water age at the Gallusquelle by adjusting the matrix porosity θ_p.

5.2 Results and discussion

Figure 5.1 shows the simulated age and life expectancy distributions. A groundwater age of 3.8 years is reached at the Gallusquelle for a θ_p value of 2%. This is in a realistic range for Jurassic limestone (e.g. Seiler et al., 1989; Worthington et al., 2000; Einsiedl, 2005) but seems a little low for the study area. Weiß (1987) analysed porosities in core samples of the neighbouring Franconian Alb and found values between ca. 1% and 12%. However, the porosities of the massive facies tended to be higher than that for the layered facies, so that values above 4-5% could have been expected for the Gallusquelle area, which predominantly consists of the massive limestone of the Kimmeridgium 2 and 3. This suggests that the aquifer thickness is slightly overestimated by the model. This is probably due to the rough estimation of the aquifer base in the south and west of the model area, where no borehole information is available (Figure 1.3).

Simulated groundwater ages in the porous matrix have average values in the range of 160 to 167 years. At the borehole locations of Geyer (2008) the age of the water in the fissured system is slightly older than spring water age with 4.3 years and the age of the water in the porous system is ca. 162 years. Therefore, the simulated old water component easily covers the 50 years of Geyer (2008). Besides the results of Geyer (2008), there is a measurable concentration of atrazine still discharged at the Gallusquelle, especially during low-flow conditions (Hillebrand et al., 2014). Hillebrand et al. (2014) conclude that the atrazine is kept in the porous matrix of the aquifer since it is diluted during recharge events contradicting an input from the soil or unsaturated zone. Atrazine is forbidden in Germany since 1991, indicating that the corresponding groundwater component has an age of at least 25 years. However, Hillebrand et al. (2014) suggest that the majority of the atrazine probably still remains in the aquifer, which hints at significantly higher residence times. The simulated average residence times in the porous matrix are ca. twice as long as the age and range between 319 and 345 years. However, the transit time distribution for the porous matrix is very broad (e.g. Figure 4.7), which reduces the significance of the average values. For the well locations of

Geyer (2008), the concentration maximum of the transit time distribution curve is reached at ca. 5.5 years. The high average age results from the very strong tailing, which is still significant at the end time of the transient simulation at 450 years.

In general, the residence time simulation for the Gallusquelle spring shows the same features as in Chapter 4. Since the porosities and the recharge were distributed uniformly the groundwater age distribution follows the aquifer thickness. Especially the southern Lauchertgraben in the south-east of the area where the aquifer base is lowered by up to 50 m (Figure 1.3) is visible by the higher ages surrounding the Königsgassenquelle and the Ahlenbergquelle springs (Figure 5.1a). In the conduit system, the mixing of water with different ages can be observed where smaller branches tend to carry younger water as already suggested in Chapter 4 (Figure 5.1b). For the life expectancy in the conduit system, a different behaviour is observed for the different springs (Figure 5.1d). The relatively large conduits for the Gallusquelle and the Ahlenberg- and Büttnauquellen show a relatively smooth distribution with decreasing values towards the springs. The conduits for the Balinger Quelle, the Schlossbergquelle and the Königsgassenquelle show significantly higher life expectancies in the smallest branches. Here, influent flow conditions occur for short distances where the branches meet, increasing life expectancies in the up-gradient branches. The life expectancy in the fissured system follows the conduit systems and the rivers with low values as could be expected. The highest values trace the water divides, where the flow velocities are lowest, giving a good overview over the different catchment areas (Figure 5.1c). Total residence times in the fissured system of the aquifer vary between 2 and 29 years with the lowest values close to the conduit system in the central part of the area and the highest values along the water divide between the Fehla-Ursprung and the Gallusquelle springs (Figure 5.1e). Due to the very low life expectancies, the age and the residence times in the conduit system are practically identical (Figure 5.1f).

Spring water ages are approximately the same for all springs lying in the range of 3.8 to 4.8 years with the lowest value at the Gallusquelle and the highest at the Bronnen. The only exception is the Königsgassenquelle, which receives its water mainly from the southern Lauchertgraben leading to an age of more than 6 years. The Ahlenberg- and Büttnauquellen receive water from the Lauchertgraben as well, but it is mixed with very young water of 1 to 2 years from the central area, where the aquifer thickness is low (Figure 5.1a and b). An increase of groundwater ages in flow direction as it was seen in Chapter 4 cannot be observed because of the dominating influence of the varying aquifer thickness. Furthermore, the high conduit density removes water from the fissured system after relatively low travel distances. On local scale, e.g. next to the Fehla-Ursprung conduit where conduit density is lower, a slight increase of age in flow direction, i.e. towards the conduit, is still observed.

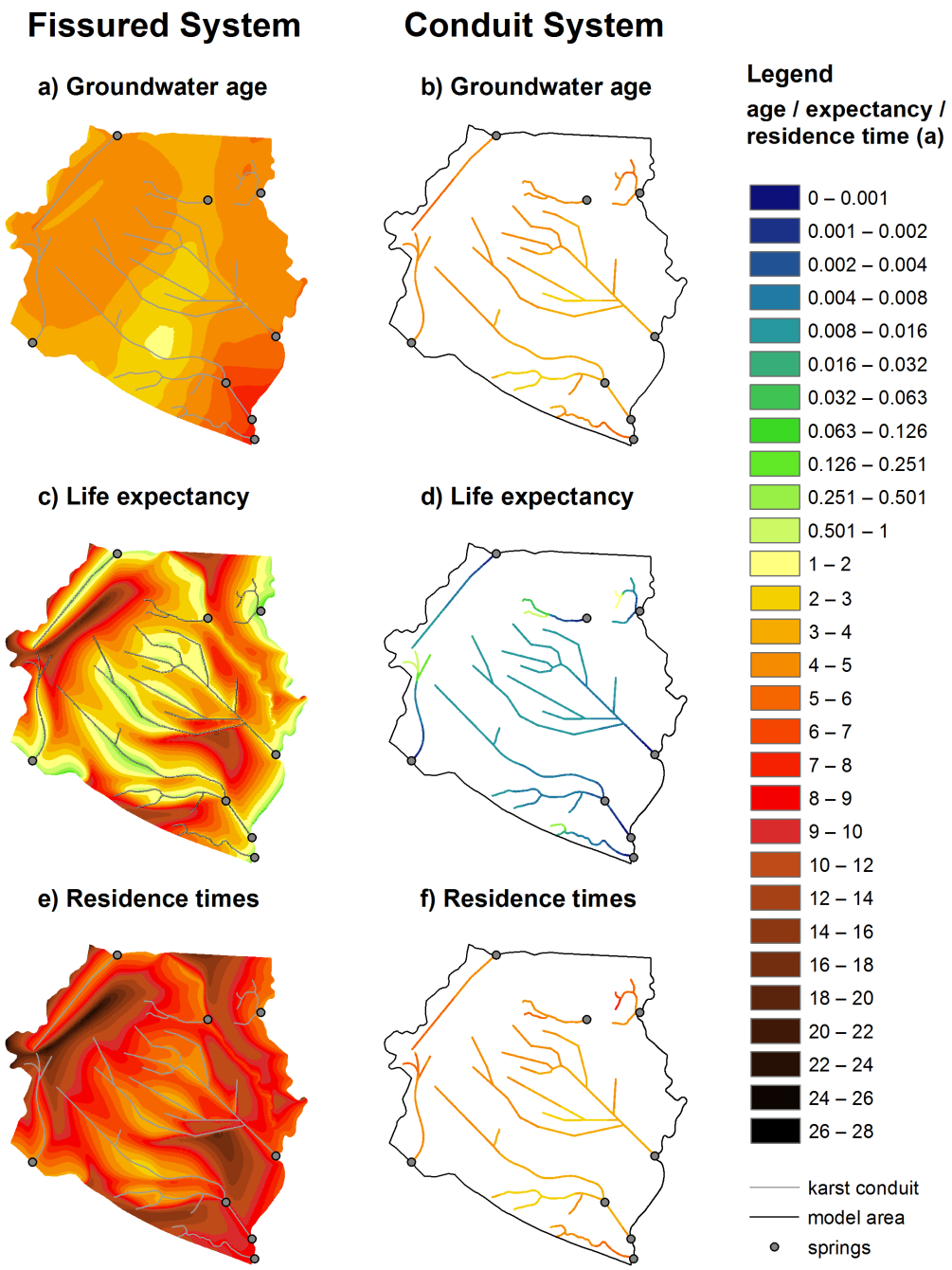

Figure 5.1. Top view of the model area showing the ages, life expectancies and residence times in the fissured and the conduit systems.

The transit time distribution curves at the springs show the same shape with three phases that was found for the simplified block model in Chapter 4. The curve shapes of the different springs only differ slightly, with the exception of the Königsgassenquelle, whose significantly higher age is accompanied by a very sharp initial decline, a low decline on medium time-scales and a more

pronounced tailing (Figure 5.2). For the other springs, only a very small initial peak is observed showing the quick drainage of water in the immediate vicinity of the conduit systems (Figure 5.2a) and the decline on medium time-scales is relatively smooth and close to an exponential function (Figure 5.2b). All curves show a significant tailing on long time-scales, i.e. more than 100 years (Figure 5.2c). The differences in the transit time curves result from a combination of the conduit size and the aquifer thickness. The magnitude of the initial peak is more pronounced for the smaller springs since their relatively low cross-sections and water volumes reduce the mixing effect inside the conduits. The magnitude of the tailing depends on both, the conduit size and the aquifer thickness. Generally, the springs show a higher tailing, if their conduits are shorter and therefore also have smaller cross-sections (Chapter 3.2). However, the curves at the Königsgassenquelle and the Schlossbergquelle do not follow this trend. Whereas the high aquifer depth at the Königsgassenquelle increases the tailing, the Schlossbergquelle lies in a relatively shallow part of the aquifer (Figure 5.1a) leading to a tailing that is very similar to that of the much larger Büttnau- and Ahlenbergquellen (Figure 5.2c). The overall different transit time curve of the Königsgassenquelle is a consequence of the high aquifer thickness in its catchment as well. The water that is recharged close to the conduit system is quickly discharged but the rest of the catchment is not drained as efficiently as for the other springs with larger conduits and shallower catchments. The dependence of the curve shape on the aquifer thickness was verified with the simple conceptual model employed in Chapter 4 by varying the aquifer depth for the same conduit system (Figure 5.3). It can be seen that the decline of the transit time distribution curves is smooth on medium time-scales for an aquifer thickness of 10 m, but shows two distinct phases for higher thicknesses. The higher the aquifer thickness, the deeper the drop in the first phase while the second phase shows a lower and more linear decline. The curve shape at 150 m is very similar to that of the Königsgassenquelle (cf. Figure 5.2b and Figure 5.3d)

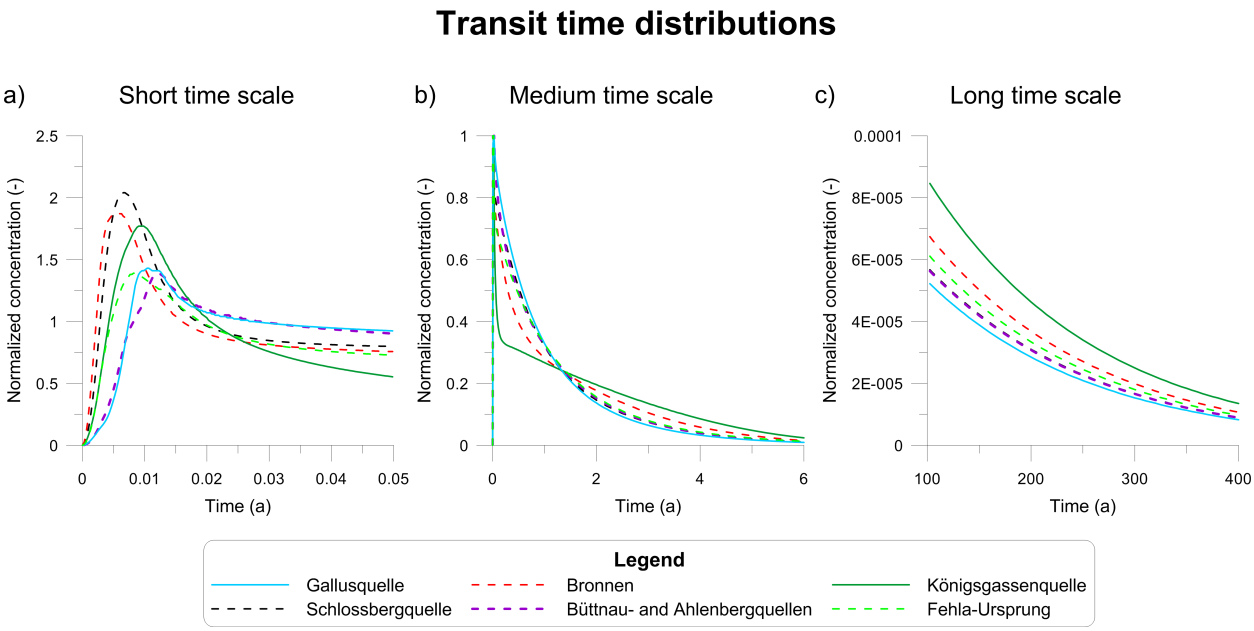

Figure 5.2. Transit time distributions for the simulated springs in the model area normalized for a recovery of 1.

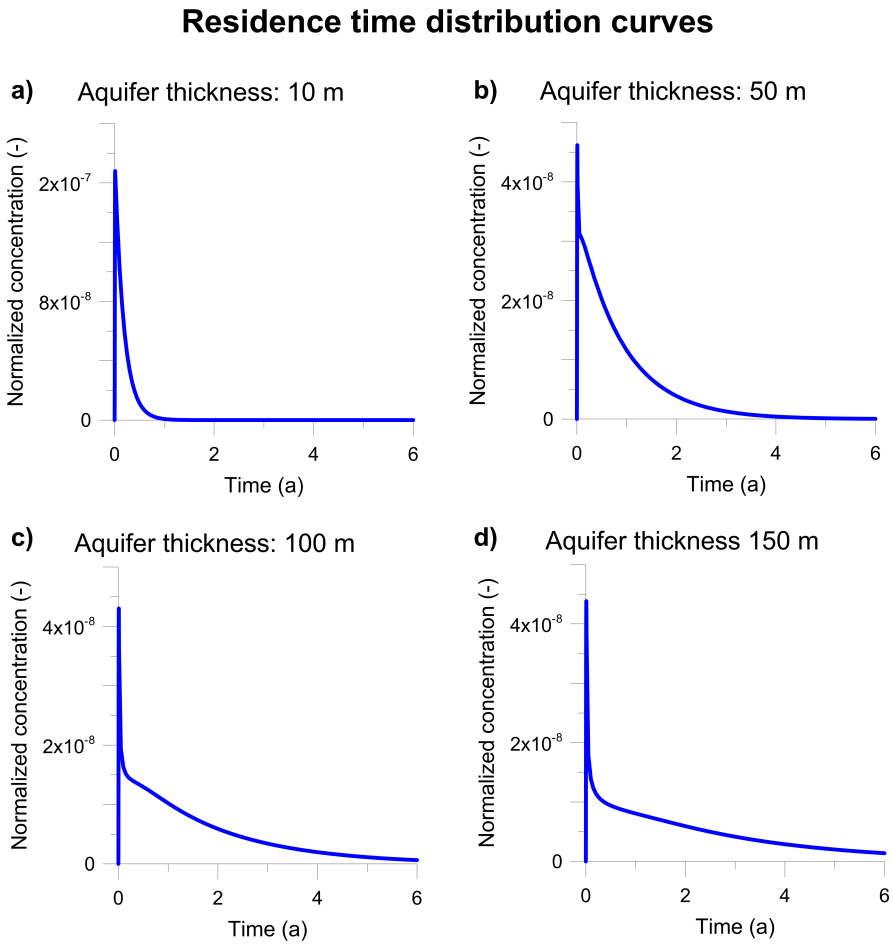

Figure 5.3. Normalized residence time distribution curves at the spring for the conceptual single conduit model presented in Chapter 4 for different depth of the aquifer.

5.3 Conclusion and Outlook

It is concluded that the model gives reasonable results. To check the plausibility of the values, more thorough investigations would be necessary. Groundwater age measurements at the other karst springs would be ideal, since the influence of local scale heterogeneities is lower than for borehole measurements. Aside from that, spring discharge represents the free outflow of the system and no mobilization of stagnant water due to pumping has to be considered.

Laboratory investigations of rock samples could give more information about the matrix porosity and the matrix-porous exchange coefficient. Such measurements could verify whether the calibrated matrix porosity of 2% is lower than the average porosity in the field and therefore show whether the aquifer thickness is truly overestimated in the model. A spatially distributed characterization of porosities might also be important for the Gallusquelle aquifer. The aquifer cuts through three lithological units of massive and layered limestones (e.g. Sauter, 1992), which might differ significantly in porosity. Porosity measurements for the different units could assist in estimating this influence.

References

COMSOL AB, 2012. COMSOL Multiphysics® User's Guide v4.3. 1292 pp.

Geyer, T., 2008. Process-based characterisation of flow and transport in karst aquifers at catchment scale. Ph.D. thesis, University of Göttingen.

Einsiedl, F., 2005. Flow system dynamics and water storage of a fissured-porous karst aquifer characterized by artificial and environmental tracers. Journal of Hydrology 312, 312–321, doi:10.1016/j.jhydrol.2005.03.031.

Hillebrand, O., Nödler, K., Geyer, T., and Licha, T., 2014. Investigating the dynamics of two herbicides at a karst spring in Germany: Consequences for sustainable raw water management. Science of the Total Environment 482–483, 193–200.

Jin, Y., Holzbecher, E., and Sauter, M., 2014. A novel approach using arbritary Lagrangian-Eularian (ALE) method for the flow simulation in unconfined aquifers. Computers and Geosciences 62, 88–94.

Sauter, M., 1992. Quantification and Forecasting of Regional Groundwater Flow and Transport in a Karst Aquifer (Gallusquelle, Malm, SW Germany). Tübinger Geowissenschaftliche Arbeiten C13, Tübingen.

Seiler, K.-P., Maloszewski, P., and Behrens, H., 1989. Hydrodynamic dispersion in karstified limestones and dolomites in the Upper Jurassic of the Franconian Alb, F.R.G.. Journal of Hydrology 108, 235–247.

Weiß, E.G., 1987. Porositäten, Permeabilitäten und Verkarstungserscheinungen im Mittleren und Oberen Malm der südlichen Frankenalb. Ph.D. thesis, University of Erlangen-Nürnberg.

Worthington, S.R.H., Ford, D.C., and Beddows, P.A., 2000. Porosity and Permeability Enhancement in Unconfined Carbonate Aquifers as a Result of Solution. In: Speleogenesis — Evolution of Karst Aquifers, edited by Klimchouk et al., 463–472, Natl. Geol. Soc., Huntsville, Alabama.

Chapter 6

6 General conclusions

Karst aquifers are highly vulnerable and complex systems which can transport contaminants to springs within hours but also store them for decades leading to a highly heterogeneous residence time distribution. This makes the residence time distribution of karst aquifers difficult to assess, which is, however, essential for spring protection measures. While there have been many studies concerning themselves with the dynamics of karst aquifers and their effective integral hydraulic parameters, the spatial distribution of hydraulic parameters and objective functions is usually not considered. This results primary from lack of input data for distributed numerical models. Especially the location and geometry of the highly conductive karst conduit system is challenging to derive in the field. Further, current distributed numerical modelling approaches only consider one or two porosities, while many karst aquifers act as triple porosity system.

This thesis shows how distributed numerical models can be applied for the characterization of karst aquifers and the derivation of the spatial distribution of groundwater residence times in all three porosities. The required field data and the benefit for aquifer characterization differ for the different modelling steps. Generally, the higher the complexity of the model and the simulation objectives, the more field data are required and the more information can be derived with respect to aquifer characterization. In this thesis, three modelling steps are presented: the delineation of catchment areas, the representation of conduit flow velocities and the simulation of the complete residence time distribution. This chapter summarizes the conclusions that were drawn with respect to the modelling approaches, their input data and their use for aquifer characterization. In addition, the new information derived from this study regarding the Gallusquelle aquifer is discussed. At the end of the chapter, future research perspectives are outlined.

6.1 Modelling strategy

Software

In this thesis, the simulation software COMSOL Multiphysics® is used for distributed numerical modelling. The choice of the software was mainly determined by its high flexibility. It makes use of the *Finite Element Method* discretization scheme, which allows for the representation of irregularly shaped objects. Furthermore, it is specialized on the coupling of different physical processes in

different spatial dimensions and enables the user to define own modelling equations. These abilities were exploited for coupling the calculation of conduit geometries in one-dimensional elements, the groundwater flow with a hybrid modelling approach in one-, two- and three-dimensional elements and the solute transport with the hybrid and a double-continuum approach.

The main drawback of the software with respect to the performed simulations is the problematic representation of unconfined aquifer conditions (Chapter 5). COMSOL® was developed for technical applications and is no specialized hydrogeological software. Therefore, there is no interface for explicitly considering the variable aquifer thickness under unconfined conditions. The *Moving Mesh* interface, which deforms the whole modelling domain, can be used as an alternative (Jin et al., 2014). The deformation can lead to the distortion of discrete elements, which are placed within the model domain, however. The produced discrepancies might be negligible for small deformations, but need to be taken in consideration for transient groundwater flow simulations with changes in water table position of several meters.

Catchment delineation

For the delineation of spring catchments, a *hybrid modelling approach* is recommended. The employed single continuum approach did not only fail to simulate the spring discharges but also the hydraulic head distribution (Chapter 2). An adaption of the single continuum model with spatially varying hydraulic conductivities, i.e. tracing the karst conduits with highly conductive cells, might have improved the simulation results. However, the conduit geometry was found to be one of the most sensitive parameters for reproducing the observed flow field and would have been difficult to derive with a single continuum model. Especially, since the widening of the karst conduits towards the springs had to be taken into account. In a single continuum model this change of geometry would possibly have to be mimicked by an increase of hydraulic conductivity towards the springs.

The required input data includes the *average recharge*, *average spring discharges* and *hydraulic head* observations. The number of hydraulic head measurements is the most crucial part of the field data. While spring discharge data is usually available or relatively easy to measure, hydraulic head measurements require drilling and not only the number of observations but also their distribution are of high importance. The hydraulic head measurements do not only help calibrating the hydraulic conductivity of the fissured matrix but also the geometry of the conduit network. Besides the approximation of the *location of the main conduits*, which can often be derived from landscape features ideally combined with tracer tests, no other information on the conduit parameters and geometries is required.

With respect to aquifer characterization, this kind of model is able to provide an estimation of the *hydraulic conductivity of the fissured matrix* and of the *lateral change of conduit geometries*. The ambiguity is too high for deriving more detailed information about conduit geometry, due to the strong interdependency between conduit conductivity/roughness and conduit size.

Derivation of conduit flow velocities

The employed *hybrid modelling* approach is also suitable for simulating conduit flow velocities. Since flow velocities are highly sensitive to the conduit size, if spring discharge is given, the correct representation of conduit geometries is especially important. As input data, at least *two artificial tracer* tests are needed in addition to the data for the previous model step. The two tracer tests should be conducted in as great a distance to each other as possible with one of them including the whole length of the conduit system. The maximum length of the conduit system can usually be estimated by localizing the nearest water divide. Since each tracer test gives integral information over its whole flow path, the use of two tracer tests allows for the distinction between flow velocities in different parts of the conduit system. It is important that the tracer substances arrive in the conduit system as directly as possible, e.g. by injection in a sinkhole with throughout flushing, for minimizing the influence of the unsaturated zone.

The ambiguity of conduit parameters is greatly reduced by the conduit velocity calibration so that the *conduit volume* and *roughness* can be estimated. The roughness is hereby an integral parameter including all aspects of conduit geometry that can lead to higher hydraulic gradients and slowdown of flow, e.g. wall roughness, conduit tortuosity, back-flow or small-scale changes of conduit diameter. Therefore, the parameter does not correspond to a single physical property of the system but serves as a proxy for a number of geometrical unknowns. The empirically based Manning equation, which is used for turbulent flow simulation in this thesis, is suited for representing this fact. It is of special significance that the hydraulic conductivity of the fissured matrix and the transmissivity of the conduit system, i.e. its size and roughness, only show limited interdependencies for the steady-state simulation. Even spatially variable fissured matrix conductivities cannot compensate an inadequate conduit system geometry or roughness, which leads to a high parameter identifiability in the model and make it an efficient tool for the characterization of the karst conduit system.

Residence time distributions

For the simulation of the residence time distribution, the hybrid modelling approach is only partly adequate. While it may serve for karst aquifers with very limited primary porosity, it is not suited for those acting as triple porosity systems. The very heterogeneous residence times in the Gallusquelle area indicate that the primary matrix porosity is of significant importance at the field site (Chapter 5).

Therefore, a new modelling approach was developed, which combines a *hybrid model* for the conduit and fissured systems with a *double continuum model* for fissured system and the porous matrix. This approach can successfully simulate the processes in all three porosities and therefore the large differences in residence times. The drawback of the method is the higher demand on input data caused by the high number of model parameters. *Measurements of groundwater age* are required in addition to the previously mentioned observations. Hereby, including measurements of water pumped from observation wells is challenging, since pumping can mobilize practically stagnant water form the porous matrix (Geyer, 2008) and the derived values therefore represent a mixture of the water ages in the fissured and the porous systems. Spring water samples are more suited for calibrating the numerical model and should ideally be taken at several springs.

Especially, if only water samples from a single spring are available, as is the case in the Gallusquelle area, the ambiguity of the residence time model with respect to the spatial distribution is high. A good prior estimation of the model parameters can assist the model calibration. The most sensitive parameters are the *porosities* of the fissured system and the porous matrix as well as the *total recharge*, its distribution and the *percentage of direct recharge*, and the *aquifer thickness*. Effective fissured system porosities can be derived by local scale pumping or slug tests, matrix porosity can be measured on rock samples in a laboratory and there are several methods available for deriving the average recharge and the percentage of direct recharge (e.g. Sauter, 1992; Geyer, 2008). Therefore, the simulation of groundwater residence times is a promising approach for approximating the aquifer thickness. The advantage of the groundwater age compared to other objective functions derivable at karst springs is the comparatively low influence of the parameters of the karst conduit system and the hydraulic conductivity of the fissured system. These parameters are often insufficiently known and can lead to high uncertainties, if their influence is high.

Parameter calibration

Since distributed numerical models are often not suited for automatic multi-parameter calibration (Chapter 3), special attention was paid to the calibration strategy during all simulations. The model

was calibrated for steady-state conditions, which reduces the complexity of the parameter interdependencies. The influence of the hydraulic conductivity of the fissured system K_f on spring discharge and conduit flow velocities is low and it can be calibrated nearly independently from the conduit system. The only interdependency between K_f and the conduit parameters occurs for the hydraulic head distribution. The influence of the conduit system on the hydraulic heads decreases for high or low K_f values and shows a maximum in between (Chapter 3, Figure 3.4). With respect to the conduit geometry, the hydraulic heads depend only on the lateral change in conduit cross-section, not on the conduit size itself. This dependency results in a limited range of plausible conduit geometries for which the best-fit K_f values are found to be very similar in this study. Therefore, K_f can be calibrated first and then kept at a fixed value during further calibration of conduit parameters.

The conduit size and roughness are the main parameters controlling the spring discharge and conduit flow velocities and can be calibrated in the next step. They have to be varied synchronously to always reproduce the correct spring discharge. In this work, the distribution of the laterally variable conduit size and roughness is controlled by four parameters (Chapter 3). A high conduit roughness close to the springs contradicts the observation of increasing transmissivities in the vicinity of karst springs (Chapter 2). Therefore the maximum roughness at the spring is controlled by the hydraulic head distribution. The degree of lateral roughness change inside the conduits controls the ratio of flow velocities of the two tracer tests and the conduit size controls the total velocity, i.e. higher conduit volumes lead to slower flow for both tracer tests. In general the lowest conduit volume for which both tracer tests can be matched gives the best fit for the hydraulic head distribution (Chapter 3).

The dispersivities inside the conduit system can be calibrated independently after the calibration of flow parameters. They only influence the shape of the tracer breakthrough curves, their influence on the residence times is negligible. Generally, each tracer test has to be calibrated with an individual dispersivity value and the calibrated dispersivities increase with the distance of the tracer injection point to the outlet. The fissured system dispersivity shows too little sensitivity to be calibrated with the imposed objective functions. A numerically reasonable value can be chosen and kept constant during all simulations (Chapter 4). The same goes for the conduit-fissured exchange coefficient, which will probably only be sensitive to transient flow simulations.

For steady-state simulations, the porosity does not influence the flow field but only the groundwater age. Therefore, the porosities of the fissured and porous system and the fissured-porous exchange coefficient can be calibrated in the last step. If the groundwater age in the porous system is unknown, the porosities of the fissured and the porous system cannot be distinguished during the calibration process, since their influence on conduit and fissured ages is identical. Therefore, independent measurements of at least one of the two porosities as input parameter are essential for

a meaningful calibration. The porous-fissured exchange coefficient can only be calibrated, if an estimate of porous system age is available, as well.

6.2 Gallusquelle area

The application of the developed modelling strategy to the Gallusquelle catchment did not only serve for testing the approach, but also provided new information about the catchment area itself. The conduit system in the area was located by several tracer tests but no geometric information besides the maximum conduit volume was available. The distributed numerical model shows, that the conduit size increases towards the karst springs. This is important to consider for the drainage behaviour and the origin of spring water. Further, the model suggests that the conduit system consists of several pipes forming conduit bundles. At least part of the cross-section increase towards the spring is provided by the addition of more conduits to the bundle. This effect leads to an increase in conduit roughness towards the springs having a high influence on flow velocities. This concept might be applicable to other moderately karstified areas and help the interpretation of measurements and the modelling of such systems. Besides the spatial changes of conduit size and roughness, the total conduit volume of the Gallusquelle can be estimated. Before, a volume of up to 200 000 m^3 was considered, but the simulation shows that the actual volume is only ca. 50% of that. This also emphasizes how strongly conduit volumes can be overestimated, if the influence of the fissured system is not included in the calculations. An increasing conduit size towards the spring favours this effect, since the higher transmissivity and exchange area drains a high amount of water from the area close to the spring.

With the simulation of the residence time distribution, a matrix porosity of 2% was derived. While porosities in the range of a few per cent are usual in limestone, 2% seems too low for the area. After Geyer (2008) porosities of at least 4% can be expected for the massive limestone that constitutes most of the aquifer. This implies that the current model slightly overestimates the aquifer thickness. This is not surprising due to the relatively rough estimate of the aquifer base, especially in the south of the area where drilling information is rare (Figure 1.3). Further, the porosity value is averaged over different lithologic layers. While the consideration of different rock properties for the different stratigraphic layers did not improve the simulation of the hydraulic head distribution (Chapter 3), treating the different layers explicitly for the porosities and residence times might be significant.

6.3 Future research perspectives

There are several ways of improving and extending the shown methods. A few suggestions for the next steps are listed below.

(1) The presented models were established for reproducing field observations. It would be useful to also approach the matter from a karst genesis point of view. Since the main structures in the Gallusquelle area, i.e. main fault systems and fracture directions, are known, the area appears suited for a *karst genesis simulation*. The derived conduit structures could be compared with the ones derived in this study to close the gap between karst development and field observations.

(2) General understanding of the interaction between the different porosities could be improved by measurements on several scales. For the *exchange coefficient between the porous and the fissured* system, small-scale laboratory experiments might help establishing clear relationships between the coefficient and the porosities thereby reducing the number of independent model parameters and the model ambiguity. For the *exchange coefficient between the conduits and the fissured system*, detailed analyses of large-scale pumping tests and transient distributed numerical modelling would provide more information.

(3) The presented model can be used as a prognostic tool for the Gallusquelle area for long-term development. Extending the steady-state modelling approach into a dynamic one would extend its applicability to the highly variable flow conditions during recharge events. In addition to that, a *dynamic flow simulation* would enable the model to also simulate dynamic transport, e.g. of environmental tracers, and therefore extend the ranges of objective functions that can be employed. Further, a dynamic calibration might help reducing the ambiguity regarding the extent of the conduit network and the conduit-matrix exchange coefficient, which were insensitive for the steady-state simulations.

(4) For the residence time distribution, the simulation of the *lateral recharge distribution* including the *unsaturated zone* would be valuable. This work focuses on processes within the aquifer, while most threats to groundwater quality occur at the ground surface. Including the different travel times through the unsaturated zone might be of great importance for estimating the effect of pollution. One method for distinguishing between the travel times in the saturated and in the unsaturated zone is the use of several environmental tracers with different behaviour as shown by Geyer (2008). For validating the model, further groundwater age measurement will be needed. Especially measurements at the other springs within the model area would greatly improve the calibration.

(5) Finally, it would be worthwhile to apply the shown modelling approach to other karst areas to further explore the possibility for aquifer characterization and assist in aquifer management issues.

References

Geyer, T., 2008. Process-based characterisation of flow and transport in karst aquifers at catchment scale. Ph.D. thesis, University of Göttingen.

Jin, Y., Holzbecher, E., and Sauter, M., 2014. A novel approach using arbritary Lagrangian-Eularian (ALE) method for the flow simulation in unconfined aquifers. Computers and Geosciences 62, 88–94.

Sauter, M., 1992. Quantification and Forecasting of Regional Groundwater Flow and Transport in a Karst Aquifer (Gallusquelle, Malm, SW Germany). Tübinger Geowissenschaftliche Arbeiten C13, Tübingen.

Sandra Oehlmann

Persönliche Daten

geboren am	28.08.1986
in	Hannover
Nationalität	deutsch
Familienstand	ledig

Hochschulausbildung

04/2012 – 09/2015	Georg-August-Universität Göttingen Promotionsstudiengang Geowissenschaften Geowissenschaftliches Zentrum Göttingen Abteilung Angewandte Geologie, Prof. Dr. Martin Sauter
10/2009 – 09/2011	Leibniz-Universität Hannover M.Sc. Geowissenschaften Masterarbeit: Geologische 3D-Untergrundmodellierung als Beitrag zum Verständnis der Heilquellen von Bad Nenndorf
10/2006 – 09/2009	Leibniz-Universität Hannover B.Sc. Geowissenschaften Bachelorarbeit: Niederschlags- und Flusswasserisotopie im ostafrikanischen Riftsystem

---

Beruflicher Werdegang

seit 02/2012	Georg-August-Universität Göttingen Wissenschaftliche Mitarbeiterin am Geowissenschaftlichen Zentrum, Abteilung Angewandte Geologie
11/2009 – 03/2010	Bundesanstalt für Geowissenschaften und Rohstoffe, Hannover Studentische Hilfskraft im Referat Ingenieurgeologie, Baugrunddynamik

Hydrol. Earth Syst. Sci., 17, 4729–4742, 2013
www.hydrol-earth-syst-sci.net/17/4729/2013/
doi:10.5194/hess-17-4729-2013

Hydrology and Earth System Sciences
Open Access

Influence of aquifer heterogeneity on karst hydraulics and catchment delineation employing distributive modeling approaches

S. Oehlmann[1], T. Geyer[1], T. Licha[1], and S. Birk[2]

[1]Geoscience Center, University of Göttingen, Göttingen, Germany
[2]Institute for Earth Sciences, University of Graz, Graz, Austria

Correspondence to: S. Oehlmann (sandra.oehlmann@geo.uni-goettingen.de)

Received: 12 June 2013 – Published in Hydrol. Earth Syst. Sci. Discuss.: 11 July 2013
Revised: 1 October 2013 – Accepted: 16 October 2013 – Published: 3 December 2013

Abstract. Due to their heterogeneous nature, karst aquifers pose a major challenge for hydrogeological investigations. Important procedures like the delineation of catchment areas for springs are hindered by the unknown locations and hydraulic properties of highly conductive karstic zones.

In this work numerical modeling was employed as a tool in delineating catchment areas of several springs within a karst area in southwestern Germany. For this purpose, different distributive modeling approaches were implemented in the finite element simulation software Comsol Multiphysics®. The investigation focuses on the question to which degree the effect of karstification has to be taken into account for accurately simulating the hydraulic head distribution and the observed spring discharges.

The results reveal that the representation of heterogeneities has a large influence on the delineation of the catchment areas. Not only the location of highly conductive elements but also their geometries play a major role for the resulting hydraulic head distribution and thus for catchment area delineation. The size distribution of the karst conduits derived from the numerical models agrees with knowledge from karst genesis. It was thus shown that numerical modeling is a useful tool for catchment delineation in karst aquifers based on results from different field observations.

1 Introduction

Karst aquifers are strongly heterogeneous systems due to a local development of large-scale discontinuities such as conduit systems. This heterogeneity also causes a large anisotropy in the hydraulic parameter field. Conceptually, karst aquifers can be described as dual-flow systems consisting of a fissured matrix with a relatively low hydraulic conductivity and highly conductive karst conduits (Liedl et al., 2003). A characteristic attribute of many karst aquifers is their high discharge focused to large springs. This makes them especially interesting as drinking water resources. However, the delineation of catchment areas of karst springs is still a challenge because of the usually unknown location of large-scale heterogeneities, such as karst conduits, within the aquifer. Common approaches for catchment delineation in porous aquifers like the mapping of geomorphological and topographical features and water balance approaches (Goldscheider and Drew, 2007) are only of limited use in karst systems. Delineating catchment areas from hydraulic head contour lines requires an observation well network, which covers the highly conductive conduit system. On groundwater catchment scale these data are scarce in carbonate areas (Sauter, 1992). Artificial tracer tests provide information about point-to-point connections, but the practical restrictions of tracer investigations prevent using them for completely defining the catchment area. In addition, catchment areas may change under different hydrological conditions further complicating the issue.

Numerical groundwater flow simulations are process-based tools that can be used for combining results from different investigation methods (Geyer et al., 2013) and for augmenting them with physical equations (Birk et al., 2005). There are numerous simulation approaches, which are applicable for karst aquifers. Single continuum models assume the aquifer to be a porous medium that can be divided into representative elementary volumes (REV) (Bachmat and Bear, 1986). The dual flow characteristics of karst aquifers are

directly addressed by hybrid or double continuum modeling approaches. Double continuum models simulate groundwater flow in two separate overlapping continua: a matrix continuum and a conduit continuum, linked via a linear exchange term (Teutsch, 1989; Mohrlok and Sauter, 1997). Hybrid models include the spatial distribution of local discrete pipe elements representing the major karst conduits coupled to a matrix continuum which represents the properties of the low permeability fissured matrix blocks (Liedl et al., 2003; Birk et al., 2005). Due to the required detailed information and the relatively high numerical effort, the application of hybrid modeling approaches to real karst systems is rare (Reimann et al., 2011a). The highest accuracy regarding the description of aquifer heterogeneities is achieved by discrete multiple fracture set models which represent the fissured system as well as the conduit system as a set of discrete fissures. Due to the intense investigation effort required for characterizing the discrete pathways they are practically not applicable for catchment studies (Teutsch and Sauter, 1991). Thus, the question which degree of complexity within the numerical model is necessary for achieving the aim of the investigation is of primary importance since more complex models require more specific information about the model area and higher numerical effort.

This work analyzes how distributive numerical models can be used to support the delineation of catchment areas of karst springs. The proposed novel approach is illustrated using a karst area in southwestern Germany. It is based on the evaluation of the influence of different types of aquifer heterogeneity on the karst flow system. More specifically, the interdependencies between hydraulic head distribution, hydraulic parameters and spring discharges are examined. For this purpose, a homogeneous continuum model and hybrid modeling approaches for flow simulation of a large-scale karst system were set up employing the finite element simulation software Comsol Multiphysics®. These two different modeling approaches were chosen since the geometry of the highly conductive conduits was of special interest in this study because of their potential impact on the delineation of the catchment areas. Simulating the conduit geometry with the single continuum approach would have required intense meshing along the karst conduits needing a very flexible mesh and being numerically highly demanding. Steady state flow equations were implemented for both model types. The three-dimensional geometry of the aquifer system was geologically modeled with the software Geological Objects Computer Aided Design®(GoCAD®) and transferred to the Comsol®software.

2 Methods and approach

Comsol Multiphysics®is a software that conducts multiphysical simulations using the finite element method (FEM). The different physical properties and equations are stored in different modules, which can be coupled and adapted as required. The interfaces used in this work belong to the Subsurface Flow Module, which provides equations for modeling flow in porous media, and to the basic module. The basic module includes interfaces, where mathematical equations can be defined by the user and employed for any physical application. This concept is described in more detail for scenario 3 (Sect. 2.3). All simulations were performed in the stationary mode, thus neglecting storage effects. Simulations were performed three-dimensionally. To examine the effects of different types of heterogeneity several scenarios were set up including more and more characteristic features of karst catchments. Figure 1 schematically shows the simulated scenarios. Catchment areas were derived by importing the simulated water tables from Comsol®to ArcGIS®10.0 and using the default hydrology tools. Generally, those are used for deriving catchment areas from topographic lines. Since the concept of water flowing towards the lower potential is true for groundwater as well as for surface water, they can be likewise used for delineating groundwater catchments from groundwater contour maps.

2.1 Scenario 1

Scenario 1 simulates a completely homogenous case. It takes into account the thickness of the aquifer and boundary conditions given by rivers and surface water divides. Recharge and hydraulic conductivity were kept constant throughout the area. For the flow simulation the Darcy's Law Interface of the Subsurface Flow Module was used. It calculates the fluid pressure p ($\mathrm{ML^{-1}T^{-2}}$) within the model domain with the Darcy equation (Eq. 1a and b).

$$Q_\mathrm{m} = \nabla(\rho u) \tag{1a}$$

$$\boldsymbol{u} = -\frac{K_\mathrm{m}}{\rho \mathrm{g}}(\nabla p + \rho g \nabla D) \tag{1b}$$

In these equations Q_m is the mass source term ($\mathrm{ML^{-3}T^{-1}}$), ρ is the density of the fluid ($\mathrm{ML^{-3}}$), K_m is the hydraulic conductivity of the matrix ($\mathrm{LT^{-1}}$) and $\boldsymbol{u}$ the Darcy velocity ($\mathrm{LT^{-1}}$). g is the magnitude of gravitational acceleration ($\mathrm{LT^{-2}}$) and ∇D is a unit vector in the direction over which the gravity acts. The hydraulic conductivity K_m is the only calibration parameter in this scenario.

2.2 Scenario 2

Scenario 2 includes a highly conductive fracture simulated as a discrete vertical 2-D element embedded in the three-dimensional continuum model. The 2-D element, in this case, represents a large-scale fault zone observed from geological mapping within the area of investigation. The continuum represents the fissured matrix of the karst aquifer. Groundwater flow in the fracture was simulated with the Fracture

Flow Interface of the Subsurface Flow Module implemented in Comsol®. The module requires the definition of the fracture aperture d_f (L) and hydraulic conductivity K_f (LT^{-1}) inside the fracture. Comsol®assumes that flow processes in the fracture are basically the same as in the surrounding matrix and calculates flow along the fracture with the tangential version of the Darcy equation. The fracture flow module does not allow the application of different flow laws in the two regions. To simulate two-dimensional fracture flow the term for the fracture aperture is multiplied with both sides of Eq. (1):

$$d_f \times Q_f = \nabla_T(d_f \rho \boldsymbol{u}) \tag{2a}$$

$$\boldsymbol{u} = -\frac{K_f}{\rho g}(\nabla_T p + \rho g \nabla_T D), \tag{2b}$$

with Q_f being the mass source term for the fracture ($ML^{-3}T^{-1}$) and ∇_T the tangential gradient operator. The hydraulic conductivity of the fracture K_f is the second calibration parameter beside the matrix conductivity K_m (Eq. 1b) in scenario 2.

2.3 Scenario 3

In scenario 3, highly conductive conduits were included along the positions of dry valleys, which are believed to be former riverbeds that have dried up during karstification. For these, 1-D structures are the most fitting representation. Since the Subsurface Flow Module does not offer a similar functionality as fracture flow for 1-D elements in 3-D domains, a hybrid model was set up employing Comsol's PDE Interfaces for simulation of one-dimensional pipes. The interface chosen is called Coefficient Form Edge PDE because it allows calculations along the edges (1-D elements) of a 3-D model. The interface offers a partial differential equation (PDE) (Eq. 3) for which coefficients have to be defined.

$$f = \nabla(-c\nabla v + \gamma) \tag{3}$$

In Eq. (3), c is defined as the diffusion coefficient, γ as the conservative flux source and f as the source term. By default, the source term is dimensionless. Its unit can be defined in the interface and the units of the coefficients are then calculated accordingly. v is the dependent variable in this equation. In the application using Darcy Flow, v corresponds to the pressure p ($ML^{-1}T^{-2}$). The source term f equals the mass source term Q_m of the Darcy equation (Eq. 1a). The first of the remaining terms describes the effect of water pressure gradients, the other the effect of gravitation (compare Eq. 1b). In this case the diffusion coefficient c depends on the hydraulic conduit conductivity K_c which is normalized for a unit cross-sectional area. Thus, after multiplying with the conduit area πr^2 Eq. (3) translates to Eq. (4). The conduit area term replaces the two missing dimensions while performing simulations in 1-D elements in a 3-D domain.

$$\pi r^2 \times Q_m = \nabla(-\pi r^2 \frac{K_c}{g}\nabla p - \pi r^2 \rho K_c \nabla D) \tag{4}$$

The source term multiplied with the conduit area $\pi r^2 \times Q_m$ is equal to the mass exchange of water per unit length between the matrix and the conduit ($ML^{-1}T^{-1}$). Reimann et al. (2011b) define the exchange term between a karst conduit and the rock matrix as

$$q_{ex} = \frac{K'}{b'} \times P_{ex} \triangle h_{ex}. \tag{5}$$

q_{ex} is the exchange flow per unit length ($L^2\ T^{-1}$), Δh_{ex} is the difference between the hydraulic head in the matrix and the hydraulic head in the conduit (L), P_{ex} the exchange perimeter (L) and K'/b' the leakage coefficient (T^{-1}). For this simulation the equation was simplified by assuming the exchange perimeter equal to the pipe perimeter. Assuming there is no barrier between the conduit and the matrix, the leakage coefficient is equal to the hydraulic conductivity of the matrix divided by the theoretical distance b' (L) over which the hydraulic head difference is calculated. b' is kept at unit length throughout the simulation. The equation given by Reimann et al. (2011b) is multiplied by the density for obtaining the mass exchange term. The resulting exchange equation is defined in Eq. (6):

$$\pi r^2 \times Q_m = (H_c - H_m) \times \frac{K_m}{b'} \times \rho \times 2\pi r \tag{6}$$

with H_c being the hydraulic head in the conduit and H_m being the hydraulic head in the matrix (L). $2\pi r$ is the perimeter of the pipe (L). The exchange term is used as mass flux for the matrix and as mass source for the conduits with a changed algebraic sign. Dirichlet conditions were set as boundary conditions at the springs.

2.4 Scenario 4

Scenario 4 was based on the same structure of the conduit system as scenario 3 but differed in the assumption for the conduit radius. While for scenario 3 the radius is constant within the entire conduit system, for scenario 4 a change in conduit radius towards the spring was introduced. Liedl et al. (2003) showed with their karst genesis simulations that for a conduit derived from solution processes a change in diameter is likely to occur along its extent. They introduced several simulations with different boundary conditions and derived different types of solutional widening and resulting conduit shapes.

For situations where diffuse recharge prevails, Liedl et al. (2003) showed a nearly linear increase in conduit diameters towards a karst spring. Thus, in scenario 4 a linear widening function was applied to each conduit along its arc length.

At each intersection the radii of both branches were added to account for the larger volume of water flowing there. The largest simulated radius is 4.6 m at the main karst spring.

3 Field site

Simulations were performed for several karst springs located at the Swabian Alb in southwestern Germany (Fig. 2). The Gallusquelle spring is the largest of the springs located within the investigation area of approximately 150 km^2 (Fig. 3). The size of its catchment area is estimated to be 45 km^2 based on a water balance approach and artificial tracer tests (Sauter, 1992) (Fig. 3). The spring is used for drinking water supply of approximately 40 000 people and has an average annual discharge of 0.5 $m^3 s^{-1}$. It is a suitable location for distributive karst modeling due to the extensive studies that have been conducted in the area before (e.g., Sauter, 1992; Geyer et al., 2007; Hillebrand et al., 2012).

Geologically the area consists of Upper Jurassic limestone and marlstone. The main aquifer is composed primarily of massive and layered limestone of the Kimmeridgian 2 and 3 (ki2/3), which are dominated by an algal sponge bioherm facies (Sauter, 1992). Beneath those rocks there are marly limestones and marlstones of the Kimmeridgian 1 (ki1) which mainly act as aquitards due to their lower hydraulic conductivity. The whole sequence dips with approximately 1.2° to the southeast (Sauter, 1992).

Two major fault zones cross the model area. The Hohenzollerngraben strikes northwest to southeast, the Lauchertgraben crosses the area in the east striking north–south (Fig. 2). While there is no information about the hydraulic conductivity of the Lauchertgraben fault zones, the Hohenzollerngraben was crossed by tunneling work related to the construction of a regional water pipeline (Albstollen, Bodensee-Wasserversorgung). The northern boundary fault was found to be highly conductive from the significant amount of water entering the tunnel while crossing it (Gwinner et al., 1993). A high hydraulic conductivity of this zone can further be assumed from the fact that the Gallusquelle spring lies exactly at the extension of this fault where it meets the river Lauchert (Fig. 2). Parts of the area show intense fracturing. There are two main fracture directions, one with a strike of 0–30° and one with a strike of 100–140° parallel to the Hohenzollerngraben (Sauter, 1992).

The average hydraulic heads in the area were derived by Sauter (1992) for the period 1965–1990. The total range of hydraulic head variations during this time differs between 6 m and 20 m depending on the observation well (Sauter, 1992). The monthly rainfall varied from less than 10 mm to more than 180 mm and the annual rainfall from about 600 mm a^{-1} to 1200 mm a^{-1}. Even though these variations are high, Villinger (1977) deduced, that the boundaries of the catchment area for the Gallusquelle spring do not change significantly throughout the year. His analysis is based on equipotential maps constructed from hydraulic head measurements for high and low water levels in the area. Furthermore, several artificial tracer tests especially in the west of the area were repeated under different flow conditions and showed little to no alteration in flow directions.

4 Model design and calibration

The model area is constrained by fixed head boundaries at the rivers Lauchert, Fehla and Schmiecha (Dirichlet boundaries). No flow boundaries are derived from the dip of the aquifer base and artificial tracer test information (Fig. 3). The size of the model area is about 150 km^2. The assumed catchment area of the Gallusquelle spring lies completely within the model area (Fig. 2). The positions of dry valleys were adapted after Gwinner et al. (1993). Highly conductive pipes connected to the Gallusquelle spring were implemented according to Mohrlok and Sauter (1997) and Doummar et al. (2012). The lateral positions of model boundaries, highly conductive faults and the pipe network along dry valleys were constructed in ArcGIS® 10.0 and imported to Comsol® as 2-D dxf-files or interpolation curves. Vertically, the highly conductive conduits were positioned approximately at the elevation of the water table simulated in scenario 1. Lacking other information, it was assumed that the homogeneously simulated water table roughly represents the one existing during the onset of karstification. Therefore, the conduits lie between 710 m and 600 m a.s.l. with a dip towards the springs. The highly conductive 2-D fracture for scenario 2 was positioned along the northern fault of the Hohenzollerngraben. The documented fault was linearly extended to the east to cross the river Lauchert at the position of the Gallusquelle spring (compare Fig. 5a and c).

Vertically the model consists of two layers. The upper one represents the aquifer. In the east it stretches from ground surface to the base of the Kimmeridgian 2 (ki2). The formation is tapering out in the west of the area but reaches a thickness of over 200 m in the east where the Gallusquelle spring is located. In the west the underlying Kimmeridgian 1 (ki1) approaches the surface until it crops out. In that region it shows karstification and thus is part of the aquifer. The depth of the karstification was derived from drilling cores. The unkarstified ki1 acts as aquitard and composes the second vertical layer of the model. It was simulated down to a horizontal depth of 300 m a.s.l. since its lower boundary is not expected to influence the simulation. The ground surface is defined by a digital elevation model (DEM) with a cell size of 40 m. The position of the ki2 base was derived from boreholes and a base map provided in Sauter (1992). Two cross sections were constructed through the model area for illustrating the geology (Fig. 4). Their positions are illustrated in Fig. 2.

Current Comsol® software has major difficulties interpolating irregular surfaces that cannot be described by

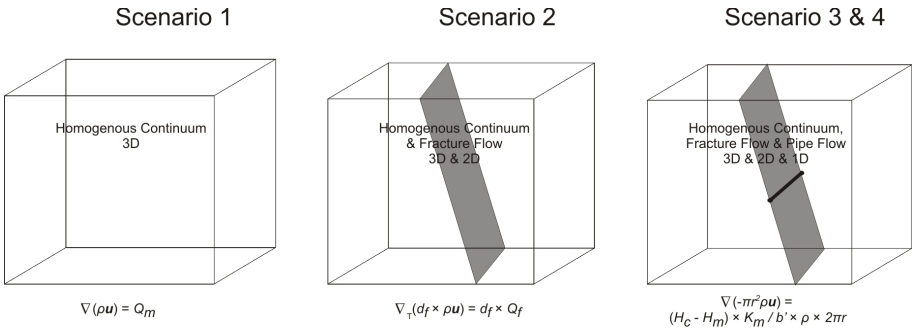

Fig. 1. Conceptual geometry of the simulated scenarios. For explanation of the flow equations see scenario description in Sect. 2.

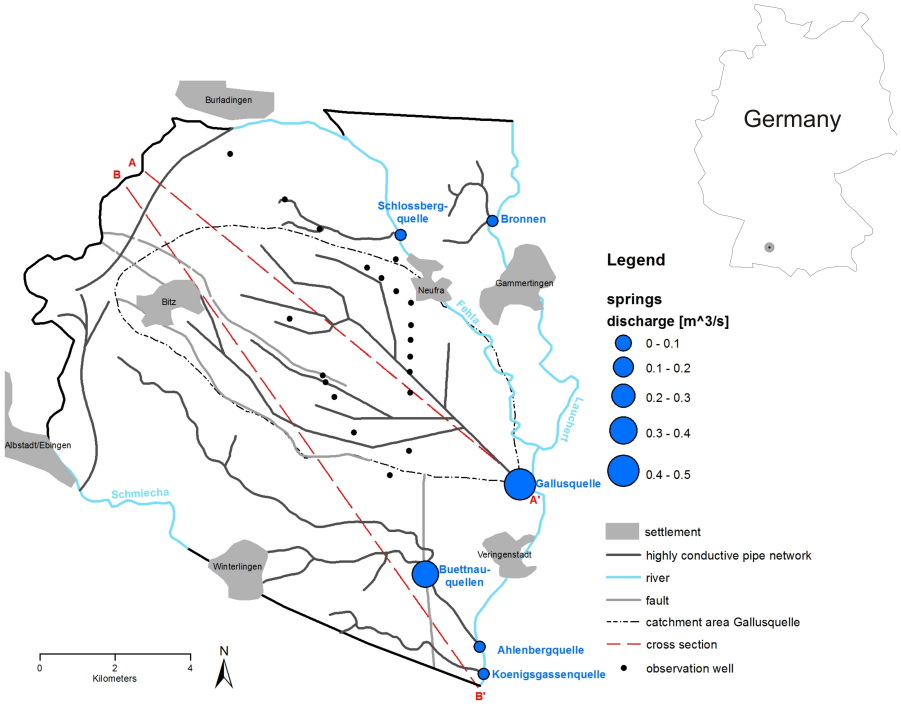

Fig. 2. Model area, including the catchment of the Gallusquelle spring and positions of all simulated springs. The highly conductive elements feeding the Gallusquelle spring were modeled after Doummar et al. (2012) and the ones along the dry valleys after Gwinner et al. (1993).

analytical functions. Therefore, the three-dimensional position of these layers, including displacement by faults and dip of the aquifer base, were constructed with the geologic modeling software Geological Objects Computer Aided Design (GoCAD®). The surface points were imported to Comsol® as text files and used to constrain parametric surfaces. Those were converted to solid objects for defining 3-D domains. At the ground surface a constant recharge was applied as a Neumann condition. The recharge was derived by Sauter (1992) as long-term average for the years 1965–1990. Geyer at al. (2011) derived the same value for the extended period 1955–2006. The base of the model was defined as a no flow boundary, while the base of the aquifer was set as a continuity boundary allowing undisturbed water transfer. The exact values for all model parameters are provided in Table 1.

The model was calibrated employing Comsol Multiphysics® Parametric Sweep option, which calculates several model runs considering different parameter combinations. The focus of the calibration lay on the hydraulic head distribution. The measured hydraulic head values are long-term averages derived from twenty exploration or observation wells that were drilled within the model area (Fig. 2).

For the calibration of spring discharges five smaller springs were included in the model besides the Gallusquelle spring. Other springs within the investigation area are either very small or have not been measured on a regular basis for reliably estimating their average annual discharges. The

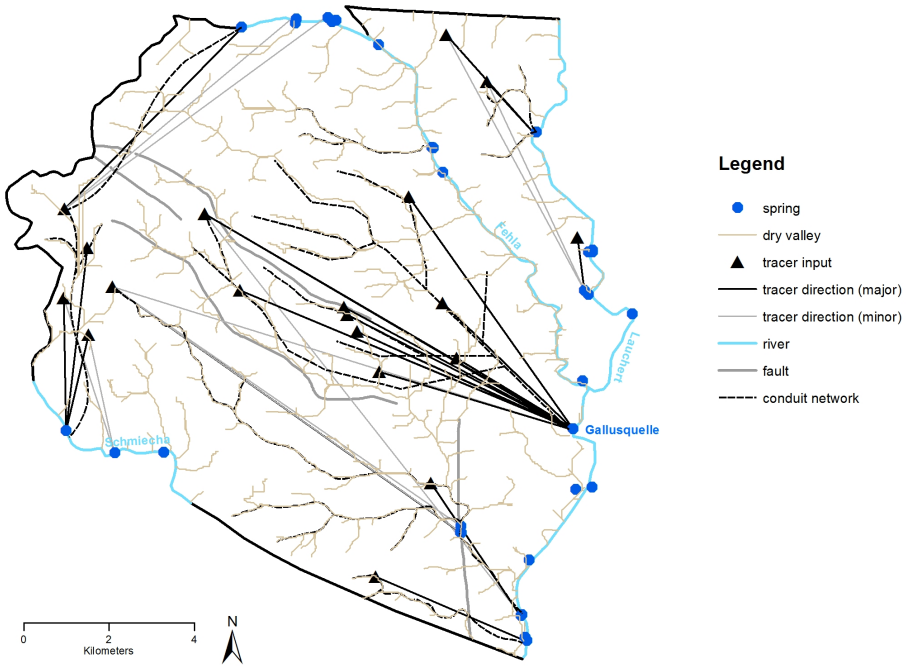

Fig. 3. Top view of the model area. Tracer tests within the area are illustrated with their major and minor registration points (excluded: uncertain registrations and registration points in rivers) after information from the Landesamt für Geologie, Rohstoffe und Bergbau (LGRB). Dry valleys were simulated with ArcGIS® 10.0 and counterchecked with field observations of Gwinner et al. (1993).

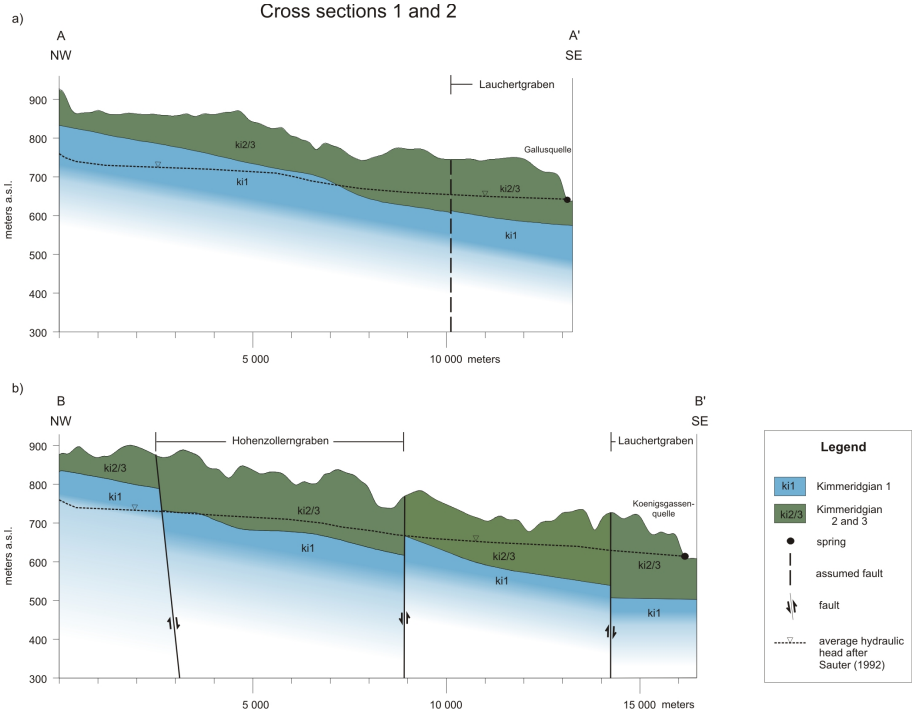

Fig. 4. Cross sections of the study area as constructed in GoCAD® from northwest to southeast with a vertical exaggeration of 10 : 1. **(a)** cross section 1 through the Lauchertgraben and the Gallusquelle spring. **(b)** cross section 2 through the Hohenzollerngraben, the Lauchertgraben and the Königsgassenquelle spring.

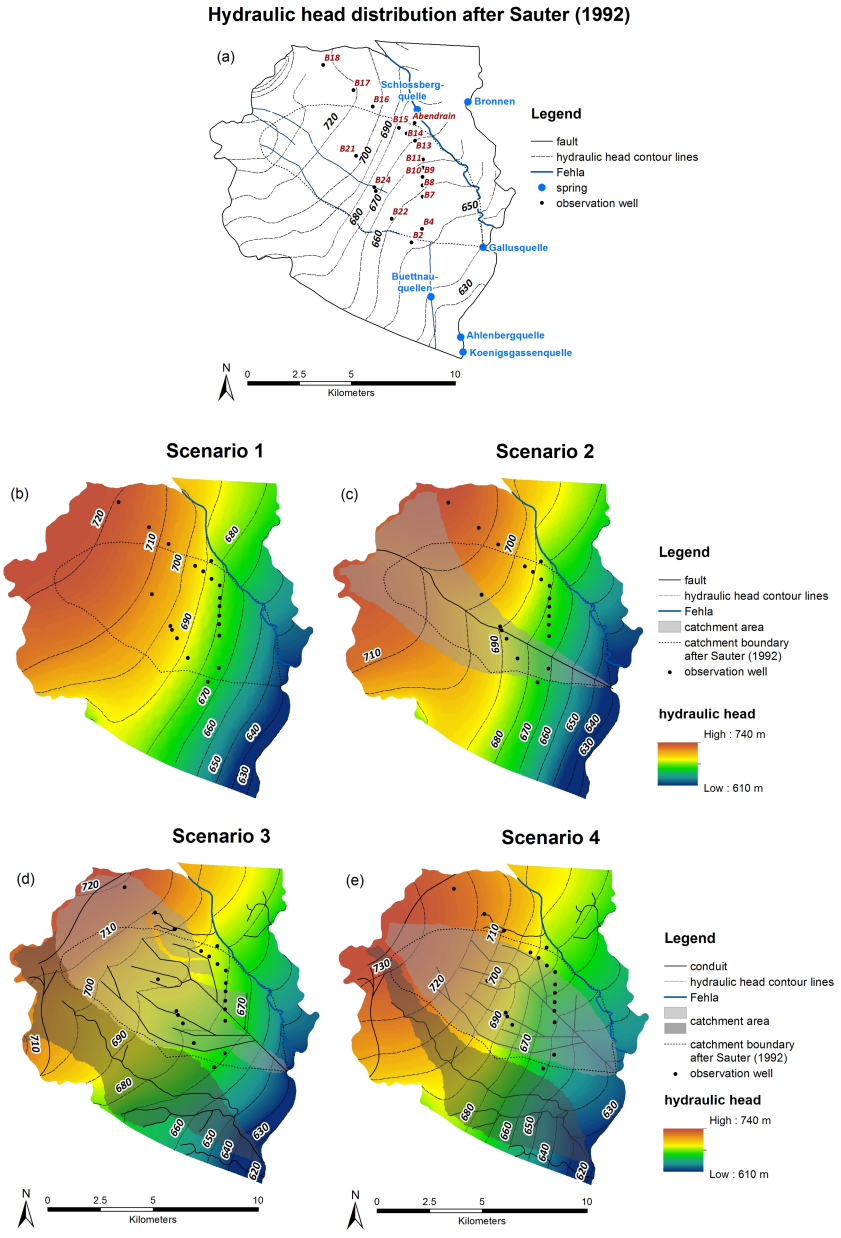

Fig. 5. Hydraulic head distributions and simulated catchment areas. **(a)** after Sauter (1992), derived from borehole measurements. **(b)** after the homogeneous simulation. **(c)** after the simulation with fracture flow along the northern fault of the Hohenzollerngraben. **(d)** after the simulation with a 1-D conduit network with constant radius. **(e)** after the simulation with a 1-D conduit network with increasing radius.

Gallusquelle spring and three of the other springs considered in the model calibration, the Bronnen spring, the Ahlenbergquelle spring and the Königsgassenquelle spring, are located at the river Lauchert; the Schlossbergquelle spring is situated at the river Fehla; a group of springs called the Büttnauquellen spring is located at a dry valley (Gwinner et al., 1993; Golwer et al., 1978) (Fig. 2). The Büttnauquellen springs and the Ahlenbergquelle spring probably share most of their catchment area and are likely to be fed by the same karst conduit network (Fig. 2). Localized discharge was also simulated into the rivers Fehla and Schmiecha in the west of the area, where several springs exist (Fig. 3). The highly conductive karst conduits used in the simulation connect points in the proximity of the Hohenzollerngraben with the Fehla-Ursprung spring at the Fehla and the Balinger Quelle spring at the Schmiecha. The karst conduits were identified by tracer tests (Fig. 3). However, there is not enough data for the discharges of the Fehla-Ursprung spring and the

Table 1. Input and calibration values of the different scenarios. The root mean square error of the hydraulic head distribution is given as an index for the quality of the model fit.

	Scenario 1: homogenous	Scenario 2: single fracture	Scenario 3: conduit network with constant radius	Scenario 4: conduit network with increasing radius
R (mm d^{-1})	1	1	1	1
K_m (m s^{-1})	5.1×10^{-5}	3.1×10^{-5}	2.3×10^{-5}	2.6×10^{-5}
K_l (m s^{-1})	1.0×10^{-10}	1.0×10^{-10}	1.0×10^{-10}	1.0×10^{-10}
K_f / K_c (m s^{-1})	–	2.7	6.5	2.0
d_z (m)	–	aquifer thickness	–	–
d_y (m)/ radius (m)	–	0.129	1.282	linear with slope 1.18×10^{-4}, maximum: 4.6 m
RMSE (m)	15.0	13.3	13.4	7.7

R = groundwater recharge by precipitation, K_m = hydraulic conductivity of matrix, K_l = hydraulic conductivity of lowly conductive ki1, K_f = hydraulic conductivity of fracture, K_c = hydraulic conductivity of conduits, dz = fracture depth, dy = fracture aperture, RMSE = root mean square error for the hydraulic head distribution.

Balinger Quelle spring to calibrate the model in this area. Since the Gallusquelle spring is the most intensively investigated spring in the area and thus not only has the most discharge measurements but the most tracer tests as well, the main weight during calibration was laid on this spring. The simulation had to fit the Gallusquelle spring discharge within a range of 10 L s^{-1}, if this could be achieved with a reasonable fit for the hydraulic head distribution.

The radii of the highly conductive conduits were calibrated for a conduit volume of 200 000 m^3 for the Gallusquelle spring catchment that was deduced from an artificial tracer test (Geyer et al., 2008). For the other springs in the model area, there was no such information. For scenario 3 a systematic approach for relating the cross-sectional areas of the conduits connected to each spring to the one of the Gallusquelle spring was employed. The conduit area for each spring was defined as the area for the Gallusquelle spring multiplied by the ratio of the spring discharge to the discharge of the Gallusquelle spring. For scenario 4 where a linear relationship between the arc length and the conduit diameter was defined, it was assumed that the shorter conduits of the smaller springs lead to accordingly smaller cross-sectional areas without any further adjustments. At the springs, fixed head boundary conditions were set at the conduits.

5 Results and discussion

The four scenarios were evaluated and compared regarding hydraulic head distribution, hydraulic parameters, spring discharges and catchment area delineations. Figure 5 shows the simulated hydraulic head distributions for all scenarios. They are compared to a hydraulic head contour map that Sauter (1992) constructed based on field measurements (Fig. 5a). Figure 6 gives a detailed overview of the measured and simulated hydraulic heads and hydraulic gradients. The calibration parameters can be found in Table 1. Table 2 and Fig. 7 compare the simulated and observed spring discharges.

5.1 Hydraulic head distribution

The model can approximate the hydraulic head distribution in all scenarios. However, there is a significant difference of the model fit between scenario 1 with a root mean square error (RMSE) of 15 m and the best fit (scenario 4) with a RMSE of 7.7 m. Scenario 2 and 3 show similar RMSE of about 13 m. The measured hydraulic head values in the observation wells and the difference between measured and simulated head for each scenario are given in Table 3.

The measured hydraulic heads show a lateral change in hydraulic gradients. In accordance with observations in the karst aquifer of Mammoth Cave (Kentucky, USA) reported by Worthington (2009), the Gallusquelle spring catchment shows lower hydraulic gradients in the east towards the spring than in the rest of the area. This is probably caused by the higher hydraulic conductivity due to the higher karstification in the vicinity of the karst spring. After Worthington (2009) this is one of the typical characteristics of karst areas. The observation is also supported by Liedl et al. (2003) who found a widening of karst conduits in spring direction. At the field site, the steepest hydraulic head gradients were observed in the central area.

Scenario 1 cannot reproduce this behavior of the hydraulic gradient (Fig. 5b and Fig. 6a). It shows the opposite of the observed gradient distribution with steeper gradients close to the river Lauchert, where most of the springs are located. This effect usually occurs in homogeneous aquifers with evenly distributed recharge conditions. The highly conductive fracture in scenario 2 crosses the model area completely from west to east. Therefore, it mainly lowers the hydraulic head values in the central and western part, thus opposing the observed gradient distribution. In the west, where the fault starts to drain the area, its very high transmissivity leads to a strong distortion of hydraulic head contour lines (Fig. 5c).

The conduit network in scenario 3 drains the area predominantly in the central part. This results in a much lower hydraulic gradient than actually observed in the field (Fig. 5d

Table 2. Simulated spring discharges ($m^3\ s^{-1}$) for all scenarios.

Spring	Measured discharge	Scenario 1: homogeneous	Scenario 2: single fracture	Scenario 3: conduit network with constant radius	Scenario 4: conduit network with linear radius
Gallusquelle	0.500	4.0×10^{-4}	0.500	0.495	0.506
Büttnauquellen and Ahlenbergquelle	0.485	4.4×10^{-4}	3.5×10^{-4}	0.422	0.340
Schlossbergquelle	0.065	2.5×10^{-4}	0.004	0.036	0.031
Bronnen	0.055	2.7×10^{-4}	2.1×10^{-4}	0.056	0.022
Königsgassenquelle	0.026	4.3×10^{-4}	3.4×10^{-4}	0.039	0.038

Table 3. Measured hydraulic head values that were used for calibration. For each scenario the difference of the simulated to the measured hydraulic heads is given in meters. The positions of the observation wells are given in Fig. 5a.

Well	Measured	Scenario 1	Scenario 2	Scenario 3	Scenario 4
	m a.s.l.	m	m	m	m
B2	652.0	22.9	23.4	18.4	9.8
B4	653.8	19.6	17.5	16.8	4.7
B7	660.7	17.4	14.5	16.3	0.9
B8	663.5	15.7	13.5	15.1	−0.4
B9	660.8	18.9	17.3	18.5	5.8
B10	673.0	7.2	6.1	6.7	−2.7
B11	673.0	7.7	6.9	7.0	0.4
B12	667.0	15.1	14.6	13.9	10.8
B13	673.7	13.3	12.8	10.3	9.7
B14	687.9	3.4	2.9	−1.7	0.6
B15	697.3	−1.8	−2.4	−9.2	−3.8
B16	713.5	−6.4	−6.9	−14.9	−4.4
B17	727.4	−14.0	−14.7	−21.4	−9.4
B18	727.0	−7.5	−8.8	−8.6	−2.2
B19	680.3	16.5	8.8	3.8	9.1
B22	660.4	26.9	24.1	17.6	15.1
B21	710.3	−3.0	−8.0	−19.8	−3.1
B24	680.2	17.8	10.5	4.9	11.1
B25	671.9	22.2	16.2	10.0	13.5
Abendrain	679.4	8.4	7.9	5.7	7.2

and Fig. 6c). This effect is due to the constant and relatively high conduit diameter of 2.56 m for the conduits connected to the Gallusquelle spring. This allows large amounts of water to flow into the conduits in the central part of the catchment. While the low hydraulic conductivity of the matrix is limiting groundwater flow in this part of the catchment, the ability of the conduits to conduct water becomes limiting close to the Gallusquelle spring and causes water to flow out of the conduits and back into the matrix. According to the classification after Kovács et al. (2005) the flow regime in this part of the model area thus is conduit influenced.

Scenario 4 shows a significantly better fit for the hydraulic gradient distribution (Fig. 5e and Fig. 6d). The increase of conduit diameters towards the spring represents the higher degree of karstification and thus higher transmissivity close to the spring. As a consequence, the hydraulic gradient is steeper in the central part of the catchment than close to the spring (Fig. 5e). This corresponds to the matrix-influenced flow regime according to Kovács et al. (2005), where the discharge is controlled by the matrix rather than by the conduits. The effect is not strong enough to completely avoid an overestimation of hydraulic heads in the east and an underestimation in the central part and in the west (Fig. 6d). This leads to the assumption that the change in gradient is not purely derived from the higher karstification but that other, probably geologic factors contribute to the lateral differences in hydraulic conductivity. A more dendritic and farther extended conduit system could also lower the hydraulic head in the east. Due to the gradual widening of the conduits, the troughs in the hydraulic head contour lines are less pronounced in scenario 4 than in scenario 3 and occur further east.

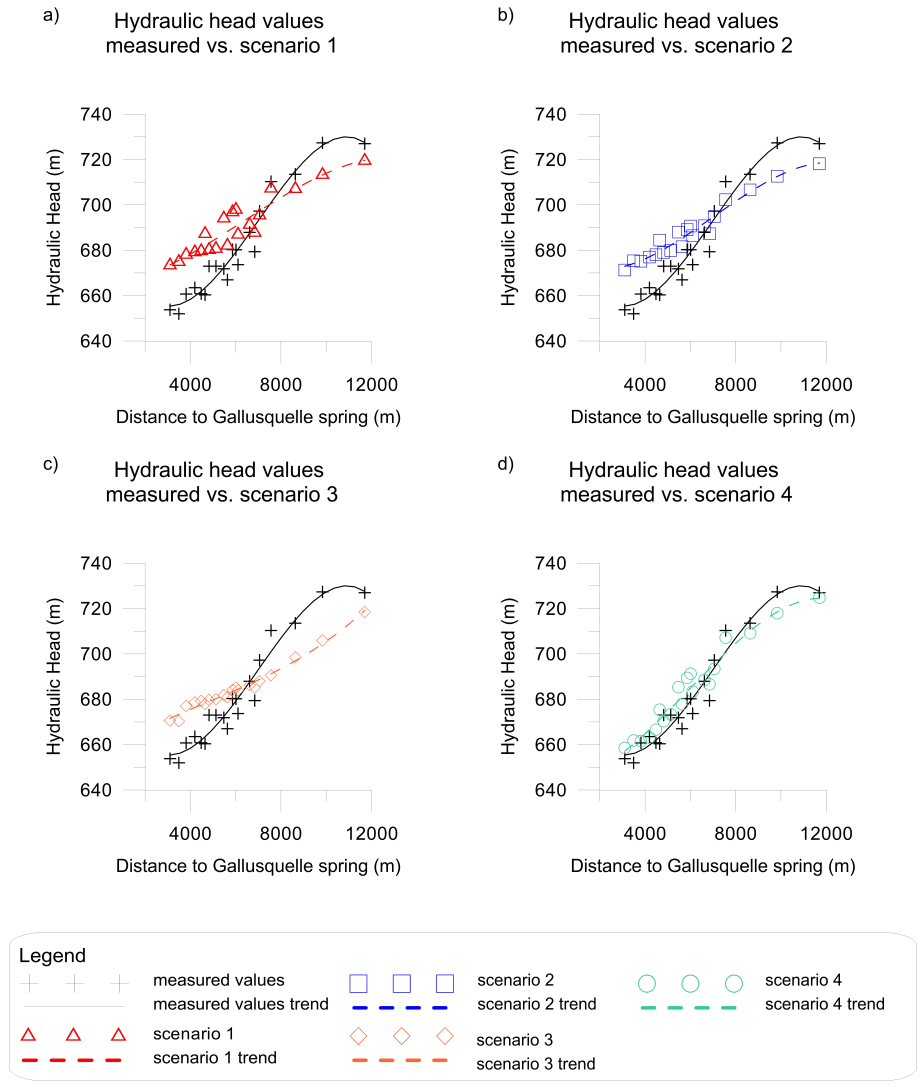

Fig. 6. Comparison of the hydraulic head values measured in the observation wells and those simulated at the well positions. **(a)** after the homogeneous simulation. **(b)** after the simulation with fracture flow along the northern fault of the Hohenzollerngraben. **(c)** after the simulation with a 1-D conduit network with constant radius. **(d)** after the simulation with a 1-D conduit network with increasing radius.

5.2 Hydraulic parameters

In heterogeneous aquifers the hydraulic conductivity strongly depends on the scale of investigation of the applied method (Geyer et al., 2013). Sauter (1992) employed several approaches to determine the hydraulic conductivity in the catchment area of the Gallusquelle spring from local to regional scale. Regional methods like the gradient (Darcy) approach or the baseflow recession method average over the whole aquifer system and yielded values between $2 \times 10^{-5}\,\mathrm{m\,s^{-1}}$ and $2 \times 10^{-4}\,\mathrm{m\,s^{-1}}$. Values obtained with local borehole methods such as pumping or slug tests ranged approximately from $1 \times 10^{-6}\,\mathrm{m\,s^{-1}}$ to $1 \times 10^{-5}\,\mathrm{m\,s^{-1}}$.

The simulated K_m values for all scenarios are well within the aforementioned ranges. The highest K_m value is obtained in scenario 1 with $5.1 \times 10^{-5}\,\mathrm{m\,s^{-1}}$. This is due to the fact that K_m for the homogeneous case averages the hydraulic conductivities of all structures in the area, since none of the discrete features is considered individually. Therefore, the calibrated K_m is within the range given by Sauter (1992) for the regional scale. The highly conductive fracture in scenario 2 allows rapid local flow and therefore lower hydraulic heads can be achieved with a lower value for the matrix conductivity of $3.1 \times 10^{-5}\,\mathrm{m\,s^{-1}}$. This trend continues for scenario 3 and 4, where K_m drops to $2.3 \times 10^{-5}\,\mathrm{m\,s^{-1}}$ and $2.6 \times 10^{-5}\,\mathrm{m\,s^{-1}}$, respectively. In these scenarios the hydraulic conductivity values approach those obtained by Sauter (1992) with borehole tests, suggesting that most of the highly conductive features in the area are explicitly taken into account.

The fracture conductivity K_f is introduced in scenario 2. Despite being in the typical range of literature of 2–10 m s^{-1} (Sauter, 1992) the obtained value of 2.7 m s^{-1} probably is too low, because all other karst features, which can drain water from the Gallusquelle spring catchment towards other springs, are neglected. If additional highly conductive features are included, higher fracture conductivities will be necessary to provide the observed average spring discharge of the Gallusquelle spring. This effect is partly responsible for the relatively high conduit conductivity K_c of 6.5 m s^{-1} in scenario 3. Even though the discharge at the Gallusquelle spring is the same as well as the integrated conduit volume, the conduit conductivity of 2 m s^{-1} obtained for scenario 4 is significantly lower than the value of 6.5 m s^{-1} obtained for scenario 3. This is because the karst conduit system with constant diameter needs a higher overall transmissivity to transport the same amount of water due to limiting flow capacity of the conduits close to the spring.

The conduit diameter in scenario 3 corresponds to a representative constant diameter for the Gallusquelle spring. Birk et al. (2005) used artificial tracer tests for calculating the representative diameter. The authors calculated a diameter of about 5 m, which is higher than the 2.56 m simulated with scenario 3. This is probably due to the fact that these tracer tests were conducted approximately 3 km northwest of the spring while in the model the conduits extend approximately 10 km to the northwest. Thus, this supports the idea that the diameters of the conduits closer to the spring are higher than those farther away (see Sect. 2.4).

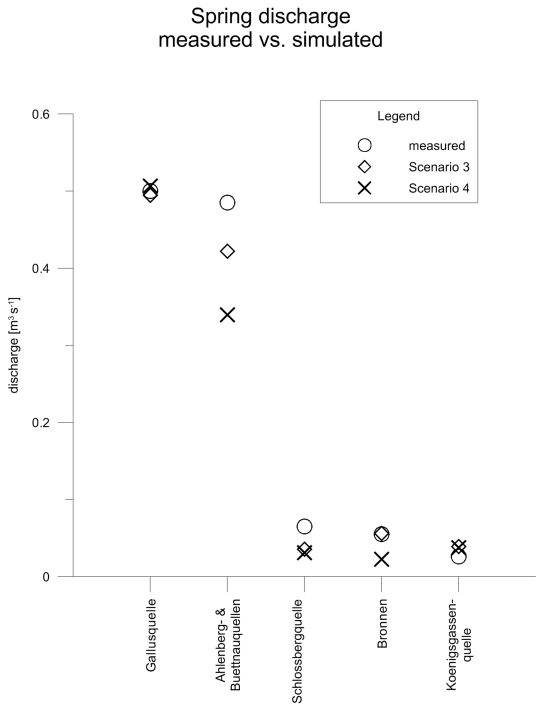

Fig. 7. Spring discharge: measured and simulated values using a conduit network with constant radius (scenario 3) and with linearly increasing radius (scenario 4).

5.3 Spring discharge

Scenario 1 fails to simulate the locally increased discharge at the karst springs (Table 2). Since there are no areas of focused flow, there is only diffuse groundwater discharge into the rivers, mainly the Lauchert. In scenario 2 fracture flow along the fault allows the simulation of increased discharge at the Gallusquelle spring (Table 2). The other springs that were not connected to highly conductive elements show no locally increased discharge (Table 2). The slightly raised discharge of the Schlossbergquelle spring compared to scenario 1 results from generally increased water flow into the river Fehla, not from locally raised discharge at the spring location. The local discharges at all springs can only be represented by scenarios 3 and 4. The simulation is satisfactory for both scenarios. The simulated discharge of the scenarios is very similar for the Gallusquelle spring, the Schlossbergquelle spring and the Königsgassenquelle spring (compare Table 2 and Fig. 7). The fit for these springs is good, even though the discharge is slightly overestimated for the Königsgassenquelle spring and underestimated for the Schlossbergquelle spring. Since the Schlossbergquelle spring is the only spring included at the river Fehla and no registration of discharge values of the river itself was conducted, it cannot be distinguished, if the underestimation at the Schlossbergquelle spring is due to an inexact karst conduit network or to an underestimated discharge into the river. For the Bronnen spring, different results can be observed for the two scenarios. While scenario 3 has a very good fit, scenario 4 underestimates the discharge. This suggests that the conduits leading to the spring are assumed too short in the simulation leading to underestimated conduit diameters in scenario 4.

The most pronounced difference between the two simulations occurs at the Büttnauquellen springs and Ahlenbergquelle spring. Both simulations underestimate their discharge with a significantly stronger underestimation in scenario 4 (Fig. 7). This is probably due to the simplified approach of treating them like a single spring and attaching them to the same conduit. While the Ahlenbergquelle spring is perennial, the Büttnauquellen springs are intermittent. This suggests that there are karst conduits in at least two different depths and thus that the representation with a conduit network in a single depth is not adequate. A too short conduit system with too little side branches has a stronger impact on scenario 4 because of the dependence of diameters on the total length and amount of intersections leading to a stronger underestimation of conduit volumes than in scenario 3.

5.4 Catchment area delineation

The spring catchment areas were delineated according to the hydraulic heads within the matrix. For the delineation

a bending of contour lines towards the springs is required, meaning they can only be generated with localized discharge at the spring positions. Therefore no catchment areas can be delineated in scenario 1. In scenario 2 a catchment area for the Gallusquelle spring can be delineated. It has approximately the size that can be expected from water balance calculations, but does not include all injection locations of tracer tests with recovery at the Gallusquelle spring. Since the hydraulic conductivity of the fault is assumed to be constant, it receives most of the inflow in the west and cannot receive more water close to the spring. Thus, the catchment area mainly includes the western part of the model area (Fig. 5c).

In scenario 3 catchment areas can be simulated for the Gallusquelle spring and for the Büttnauquellen springs and Ahlenbergquelle spring (Fig. 5d). The unusual looking shape of the areas is caused by the filling of the conduits with water in the west of the model domain which prevents drainage of the fissured matrix by the conduit system in the east of the area. Therefore the Gallusquelle spring mainly receives water from the western part of the area, where its conduits drain enormous water volumes due to their relatively large diameter. Due to outflow of water into the matrix in the east, only part of the water from the shown catchment area is transported to the springs. In the west it can be observed that the catchment areas of the Gallusquelle spring and the Büttnauquellen springs and Ahlenbergquelle spring reach across karst conduits leading to other springs (Fig. 5d). In this case the catchment areas of the springs overlap. The catchment areas were constructed in 2-D according to surface values, so that they envision the flow above the smaller conduits in the west. In the east it can be observed that the catchment areas do not include all parts of the respective karst conduit network. In these areas the conduits cannot accommodate more water and outflow occurs. The catchment area for the Gallusquelle spring that was delineated in scenario 3 includes all but one tracer test conducted. The Gallusquelle spring drains nearly all water from the springs at the river Fehla. The hydraulic heads in the west are lowered leading to influent flow conditions along parts of the western Fehla. This contradicts the development of several springs in this area and makes this scenario highly unlikely (compare Fig. 3).

Scenario 4 is the only simulation leading to reasonable results regarding the catchment areas (Fig. 5e). The size of the Gallusquelle spring catchment area is in accordance with water balance calculations and includes all tracer tests conducted in the catchment of the Gallusquelle spring. The size of the catchment area for the Büttnauquellen springs and Ahlenbergquelle spring is probably underestimated due to the underestimation of spring discharge (Table 2). Since the underestimation is more pronounced for scenario 4 than for scenario 3, the catchment area is significantly smaller (compare Fig. 5d and Fig. 5e). A small overlap of catchment areas can still be observed in the west but in scenario 4 the Gallusquelle spring only drains small amounts of water from the western part, so that the western Fehla is completely effluent. Since the simulation was performed stationary, the delineated catchment areas are only valid for the average hydraulic head distribution. As known from literature (Sect. 3) they should be representative for the usually observed variations in the Gallusquelle spring area. For reliably simulating possible shifts in the catchment areas during extreme flow conditions, more detailed information on recession behavior of the aquifer and lateral and temporal recharge distribution should be included. This is beyond the scope of this paper.

For the smaller springs, no catchment areas could be generated in either of the scenarios. They produce a very small ratio of the total discharge of the model area ($< 5\,\%$) and the resolution of the simulation was not fine enough to reliably draw their catchment boundaries.

6 Conclusions

The results show that distributive numerical simulation is a useful tool for approaching the complex subject of subsurface catchment delineation in karst aquifers as long as effects of karstification are sufficiently taken into account. Even though the Gallusquelle spring area is significantly less karstified than for example the Mammoth Cave (Kentucky, USA) (Worthington, 2009) and does not show significant troughs in the hydraulic head contour lines, it cannot be simulated with a homogeneous hydraulic parameter field. The geometry of the conduits is of major importance for the simulation. Although the Gallusquelle spring is positioned on the linear extension of the northern fault of the Hohenzollerngraben the hydraulic conditions cannot correctly be simulated without consideration of dry valleys. For catchment delineation, the approach of using conduits with constant geometric parameters is not satisfactory, either. While it is possible to fit spring discharges with a double continuum model (e.g., Kordilla et al., 2012) or a single continuum model with a highly conductive zone with constant hydraulic properties (e.g., Doummar et al., 2012) the hydraulic head distribution and hydraulic conductivities cannot be correctly approximated with these approaches.

Using numerical models for catchment delineation allows for the combination of several methods and observations under consideration of the geological and hydrogeological properties of the area. The model can be used for advanced simulations of transient groundwater flow and transport and can also account for heterogeneous distributions of recharge or aquifer properties. It therefore represents a flexible tool for risk assessment and prediction in heterogeneous flow systems.

The uncertainty of the results depends mainly on the available input data. The modeling approach allows an integrated analysis of data from different sources. Theoretically, the method requires average annual spring discharge and hydraulic head measurements in the catchment. Nonetheless, the measurement of the discharge of several springs in the

proximity of the investigated spring catchment is advisable for the simulation of catchment boundaries. In addition, deriving some knowledge about the location and properties of the karst conduit network from natural or artificial tracers, groundwater contour lines, direct investigations or the morphology of the land surface is highly recommended.

To improve simulation results, future work includes the implementation and simulation of solute transport, e.g., simulation of artificial tracer tests. Since the hydraulic head distribution and the spring discharges were found to be strongly dependent on the selected geometry of the highly conductive elements it seems unavoidable to better constrain their positions and sizes in the area. In case of the Gallusquelle spring area the smooth hydraulic gradients do not allow the localization of conduits by troughs in the hydraulic head contour lines like in some other karst areas (e.g., Joodi et al., 2010). Karst genesis simulation would provide process-based information about conduit widening towards a karst spring. Such simulations were employed for instance by Kaufmann and Braun (1999), Liedl et al. (2003), Bauer et al. (2003), and Hubinger and Birk (2011). They simulate the temporal evolution of a small fracture or fracture network due to solution with coupled transport and hydraulic models. Under the constraints of recharge conditions and initial geometries they derive the conduit size distribution. A detailed overview of the basic techniques and processes is given by Dreybrodt et al. (2005). The implementation of a karst genesis module would be possible with Comsol Multiphysics®, given sufficient input data.

Acknowledgements. The presented study was funded by the German Federal Ministry of Education and Research (promotional reference no. 02WRS1277A, AGRO, "Risikomanagement von Spurenstoffen und Krankheitserregern in ländlichen Karsteinzugsgebieten") and by the Austrian Science Fund (FWF): L576-N21. Tracer test data was provided by the Landesamt für Geologie, Rohstoffe und Bergbau (LGRB).

This Open Access Publication is funded
by the University of Göttingen.

Edited by: M. Riva

References

Bachmat, Y. and Bear, J.: Macroscopic Modelling of Transport Phenomena in Porous Media. 1: The Continuum Approach, Transport Porous Med., 1, 213–240, 1986.

Bauer, S., Liedl, R., and Sauter, M.: Modeling of karst aquifer genesis: Influence of exchange flow, Water Resour. Res., 39, 1285, doi:10.1029/2003WR002218, 2003.

Birk, S., Geyer, T., Liedl, R., and Sauter, M.: Process-Based Interpretation of Tracer Tests in Carbonate Aquifers, Ground Water, 43, 381–388, 2005.

Doummar, J., Sauter, M., and Geyer, T.: Simulation of flow processes in a large scale karst system with an integrated catchment model (Mike She) – Identification of relevant parameters influencing spring discharge, J. Hydrol., 426, 112–123, doi:10.1016/j.jhydrol.2012.01.021, 2012.

Dreybrodt, W., Gabrovšek, F., and Romanov, D.: Processes of speleogenesis: a modeling approach, Carsologica, 4, Založba ZRC, Postojna–Ljubljana, 357 pp., 2005.

Geyer, T., Birk, S., Licha, T., Liedl, R., and Sauter, M.: Multi-tracer test approach to characterize reactive transport in karst aquifers, Ground Water, 45, 36–45, 2007.

Geyer, T., Birk, S., Liedl, R., and Sauter, M.: Quantification of temporal distribution of recharge in karst systems from spring hydrographs, J. Hydrol., 348, 452–463, 2008.

Geyer, T., Selg, M., Gudera, T., and Sauter, M.: Langzeitabflussverhalten der Gallusquelle spring und des Blautopfs – relative Bedeutung der Matrix und des Karströhrensystems, Laichinger Höhlenfreund, 46, 63–74, 2011.

Geyer, T., Birk, S., Reimann, T., Dörfliger, N., and Sauter, M.: Differentiated characterization of karst aquifers: some contributions, Carbonate Evaporite, 28, 41–46, doi:10.1007/s13146-013-0150-9, 2013.

Goldscheider, N. and Drew, D.: Combined use of methods, in: Methods in Karst Hydrogeology, International contributions to hydrogeology, Taylor & Francis, London, 26, 223–228, 2007.

Golwer, A., Koerner, U., Villinger, E., and Werner, J.: Erläuterungen zu Blatt 7821 Veringenstadt, Geologische Karte 1 : 25 000 von Baden-Württemberg, 151 pp., Geologisches Landesamt Baden-Württemberg, Stuttgart, 1978.

Gwinner, M. P., Villinger, E., and Schreiner, A.: Erläuterungen zu Blatt 7721 Gammertingen, Geologische Karte 1 : 25 000 von Baden-Württemberg, 78 pp., Geologogisches Landesamt Baden-Württemberg, Freiburg/Stuttgart, 1993.

Hillebrand, O., Nödler, K., Licha, T., Sauter, M., and Geyer, T.: Identification of the attenuation potential of a karst aquifer by an artificial dualtracer experiment with caffeine, Water Res., 46, 5381–5388, 2012.

Hubinger, B. and Birk, S.: Influence of initial heterogeneities and recharge limitations on the evolution of aperture distributions in carbonate aquifers, Hydrol. Earth Syst. Sci., 15, 3715–3729, doi:10.5194/hess-15-3715-2011, 2011.

Joodi, A. S., Sizaret, S., Binet, S., Bruand, A., Alberic, P., and Lepiller, M.: Development of a Darcy-Brinkman model to simulate water flow and tracer transport in a heterogenous karstic aquifer (Val d'Orléans, France), Hydrogeol. J., 18, 295–309, doi:10.1007/s10040-009-0536-x, 2010.

Kaufmann, G. and Braun, J.: Karst aquifer evolution in fractured rocks, Water Resour. Res., 35, 3223–3238, 1999.

Kordilla, J., Sauter, M., Reimann, T., and Geyer, T.: Simulation of saturated and unsaturated flow in karst systems at catchment scale using a double continuum approach, Hydrol. Earth Syst. Sci., 16, 3909–3929, doi:10.5194/hess-16-3909-2012, 2012.

Kovács, A., Perrocket, P., Király, L., and Jeannin, P. Y.: A quantitative method for the characterisation of karst aquifers based on spring hydrograph analysis, J. Hydrol., 303, 152–164, 2005.

Liedl, R., Sauter, M., Hückinghaus, D., Clemens, T., and Teutsch, G.: Simulation of the development of karst aquifers using a coupled continuum pipe flow model, Water Resour. Res., 39, 1057, doi:10.1029/2001WR001206, 2003.

Mohrlok, U. and Sauter, M.: Modelling groundwater flow in a karst terraine using discrete and double-continuum approaches: impor-

tance of spatial and temporal distribution of recharge, in: Proceedings of the 12th International Congress of Speology, 2/6th Conference on Limestone Hydrology and Fissured Media, La Chaux-de-Fonds, Switzerland, 10–17 August 1997, 167–170, 1997.

Reimann, T., Rehrl, C., Shoemaker, W. B., Geyer, T., and Birk, S.: The significance of turbulent flow representation in single-continuum models, Water Resour. Res., 47, W09503, doi:10.1029/2010WR010133, 2011a.

Reimann, T., Geyer, T., Shoemaker, W. B., Liedl, R., and Sauter, M.: Effects of dynamically variable saturation and matrix-conduit coupling of flow in karst aquifers, Water Resour. Res., 47, W11503, doi:10.1029/2011WR010446, 2011b.

Sauter, M.: Quantification and Forecasting of Regional Groundwater Flow and Transport in a Karst Aquifer (Gallusquelle spring, Malm, SW Germany), Tübinger Geowissenschaftliche Arbeiten, C13, Tübingen, 1992.

Teutsch, G.: Groundwater Models in Karstified Terrains: Two practical Examples from the Swabian Alb (S. Germany), in: Proceedings of the 4th Conference – Solving Groundwater Problems with Models, Indianapolis, USA, 7–9 February 1989, 11 pp., 1989.

Teutsch, G. and Sauter, M.: Groundwater modeling in karst terranes: scale effects, data aquisition and field validation, in: Proceedings of the 3rd Conference on Hydrogeology, Ecology, Monitoring and Management of Ground Water in Karst Terranes, 4–6 December 1991, Nashville, USA, 17–34, 1991.

Villinger, E.: Über die Potentialverteilung und Strömungssysteme im Karstwasser der Schwäbischen Alb (Oberer Jura, SW-Deutschland), Geologisches Jahrbuch, C18, Hanover, 1977.

Worthington, S. R. H.: Diagnostic hydrogeologic characteristics of a karst aquifer (Kentucky, USA), Hydrogeol. J., 17, 1665–1678, doi:10.1007/s10040-009-0489-0, 2009.

Hydrol. Earth Syst. Sci., 19, 893–912, 2015
www.hydrol-earth-syst-sci.net/19/893/2015/
doi:10.5194/hess-19-893-2015

Hydrology and Earth System Sciences
Open Access

Reducing the ambiguity of karst aquifer models by pattern matching of flow and transport on catchment scale

S. Oehlmann[1], T. Geyer[1,2], T. Licha[1], and M. Sauter[1]

[1]Geoscience Center, University of Göttingen, Göttingen, Germany
[2]Landesamt für Geologie, Rohstoffe und Bergbau, Regierungspräsidium Freiburg, Freiburg, Germany

Correspondence to: S. Oehlmann (sandra.oehlmann@geo.uni-goettingen.de)

Received: 7 July 2014 – Published in Hydrol. Earth Syst. Sci. Discuss.: 4 August 2014
Revised: 17 December 2014 – Accepted: 17 January 2015 – Published: 12 February 2015

Abstract. Assessing the hydraulic parameters of karst aquifers is a challenge due to their high degree of heterogeneity. The unknown parameter field generally leads to a high ambiguity for flow and transport calibration in numerical models of karst aquifers. In this study, a distributed numerical model was built for the simulation of groundwater flow and solute transport in a highly heterogeneous karst aquifer in south-western Germany. Therefore, an interface for the simulation of solute transport in one-dimensional pipes was implemented into the software COMSOL Multiphysics® and coupled to the three-dimensional solute transport interface for continuum domains. For reducing model ambiguity, the simulation was matched for steady-state conditions to the hydraulic head distribution in the model area, the spring discharge of several springs and the transport velocities of two tracer tests. Furthermore, other measured parameters such as the hydraulic conductivity of the fissured matrix and the maximal karst conduit volume were available for model calibration. Parameter studies were performed for several karst conduit geometries to analyse the influence of the respective geometric and hydraulic parameters and develop a calibration approach in a large-scale heterogeneous karst system.

Results show that it is possible not only to derive a consistent flow and transport model for a 150 km^2 karst area but also to combine the use of groundwater flow and transport parameters thereby greatly reducing model ambiguity. The approach provides basic information about the conduit network not accessible for direct geometric measurements. The conduit network volume for the main karst spring in the study area could be narrowed down to approximately 100 000 m^3.

1 Introduction

Karst systems play an important role in water supply worldwide (Ford and Williams, 2007). They are characterized as dual-flow systems where flow occurs in the relatively lowly conductive fissured matrix and in highly conductive karst conduits (Reimann et al., 2011). There are a number of process-based modelling approaches available for simulating karst aquifer behaviour. Overviews on the various types of distributed process and lumped-parameter models are provided by several authors (Teutsch and Sauter, 1991; Jeannin and Sauter, 1998; Kovács and Sauter, 2007; Hartmann et al., 2014). In most cases, lumped-parameter models are applied, since they are less demanding on input data (Geyer et al., 2008; Perrin et al., 2008; Hartmann et al., 2013; Schmidt et al., 2013). These models consider neither the actual flow process nor the heterogeneous spatial distribution of aquifer parameters, but are able to simulate the integral aquifer behaviour, e.g. karst spring responses. The spatial distribution of model parameters and state variables, e.g. the hydraulic head distribution, need to be addressed with distributed numerical models should the necessary field data be available (e.g. Oehlmann et al., 2013; Saller et al., 2013). A distributed modelling approach suited for the simulation of strongly heterogeneous and anisotropic aquifers with limited data availability is the hybrid modelling approach. The approach simulates the fast flow component in the highly conductive karst conduit system in discrete one-dimensional elements and couples it to a two- or three-dimensional continuum representing the fissured matrix of the aquifer (Oehlmann et al., 2013). Hybrid models are rarely applied to real karst systems because they have a high demand of input data (Reimann

et al., 2011). They are, however, regularly applied in long-term karst genetic simulation scenarios (e.g. Clemens et al., 1996; Bauer et al., 2003; Hubinger and Birk, 2011). In these models not only groundwater flow but also solute transport is coupled in the fissured matrix and in the karst conduits. Aside from karst evolution such coupling enables models to simulate tracer or contaminant transport in the karst conduit system (e.g. Birk et al., 2005). In addition to serving for predictive purposes, such models can be used for deriving information about the groundwater catchment itself (Rehrl and Birk, 2010).

A major problem for characterizing the groundwater system with numerical models is generally model ambiguity. The large number of calibration parameters is usually in conflict with a relatively low number of field observations, e.g. different hydraulic parameter fields and process variables may give a similar fit to the observed data but sometimes very different results for prognostic simulations (Li et al., 2009). Especially the geometric and hydraulic properties of the karst conduit system are usually unknown and difficult to characterize with field experiments for a whole spring catchment (Worthington, 2009). With artificial tracer test data the maximum conduit volume can be estimated but an unknown contribution of fissured matrix water prevents further conclusions on conduit geometry (Birk et al., 2005; Geyer et al., 2008). It is well known that the use of several objective functions, i.e. several independent field observations, can significantly reduce the number of plausible parameter combinations (Ophori, 1999). Especially in hydrology (e.g. Khu et al., 2008; Hunter et al., 2005) and also for groundwater systems (e.g. Ophori, 1999; Hu, 2011; Hartmann et al., 2013), this approach has been successfully applied with a wide range of observation types, e.g. groundwater recharge, hydraulic heads, remote sensing and solute transport. Particularly, the simulation of flow and transport is known to reduce model ambiguity and yield information on karst conduit geometry (e.g. Birk et al., 2005; Covington et al., 2012; Luhmann et al., 2012; Hartmann et al., 2013). Usually, automatic calibration schemes performing a multi-objective calibration for several parameters are used for this purpose (Khu et al., 2008). However, for complex modelling studies calculation times might be large due to the high number of model runs needed (Khu et al., 2008) and a precise conceptual model is essential as basis for the automatic calibration (Madsen, 2003). In general, numerical models of karst aquifers are difficult to build because of their highly developed heterogeneity (Rehrl and Birk, 2010). Thus, automatic calibration procedures are better suited for conceptual and lumped-parameter models, where calibration parameters include effective geometric properties and no spatial representation of the hydraulic parameter field and conduit geometry is necessary. Complex distributed numerical approaches generally require longer simulation times due to the necessary spatial resolution. Long simulation times limit the number of model runs that can reasonably be performed and manual calibration based on hydrogeological knowledge is necessary (e.g. Saller et al., 2013). Therefore, applied distributed numerical models in karst systems usually focus on a smaller number of objective functions. They generally cannot simulate the hydraulic head distribution in the area, spring discharge and tracer breakthrough curves simultaneously on catchment scale. Some studies combine groundwater flow with particle tracking for tracer directions (e.g. Worthington, 2009; Saller et al., 2013) without simulating tracer transport. On the other hand there are studies simulating breakthrough curves without calibrating for measured hydraulic heads (e.g. Birk et al., 2005). For developing process-based models which can be used as prognostic tools, e.g. for the delineation of protection zones, the simulation should be able to reproduce groundwater flow and transport within a groundwater catchment. Especially in complex hydrogeological systems, this approach would reduce model ambiguity, which is a prerequisite in predicting groundwater resources and pollution risks.

This study shows how the combination of groundwater flow and transport simulation can be used not only to develop a basis for further prognostic simulations in a heterogeneous karst aquifer with a distributed modelling approach on catchment scale, but also to reduce model ambiguity and draw conclusions on the spatially distributed karst network geometries and the actual karst conduit volume. The approach shows the kind and minimum number of field observations needed for this aim. Furthermore, a systematic calibration strategy is presented to reduce the number of necessary model runs and the simulation time compared to standard multi-objective calibrations. For this purpose a hybrid model was built and a pattern matching procedure was applied for a well-studied karst aquifer system in south-western Germany. The model was calibrated for three major observed parameters: the hydraulic head distribution derived from measurements in 20 boreholes, the spring discharge of six springs and the tracer breakthrough curves of two tracer tests.

2 Modelling approach

The simulation is based on the mathematical flow model discussed in detail by Oehlmann et al. (2013). The authors set up a three-dimensional hybrid model for groundwater flow with the software COMSOL Multiphysics®. As described by Oehlmann et al. (2013) the simulation was conducted simultaneously in the three-dimensional fissured matrix, in an individual two-dimensional fault zone and in one-dimensional karst conduit elements to account for the heterogeneity of the system. Results showed that the karst conduits widen towards the springs and therefore, a linear relationship between the conduit radius and the conduit length s [L] was established. Values for s start with zero at the point farthest away from the spring and increase towards the respective karst spring.

In agreement with these results and karst genesis simulations by Liedl et al. (2003), the conduit radius is calculated as

$$r_c = ms + b, \tag{1}$$

where r_c [L] is the radius of a conduit branch and m and b are the two parameters defining the conduit size. b [L] is the initial radius of the conduit at the point farthest away from the spring and m [–] is the slope with which the conduit radius increases along the length of the conduit s.

In the following the equations used for groundwater flow and transport are described. The subscript "m" denotes the fissured matrix, "f" the fault zone and "c" the conduits hereby allowing a clear distinction between the respective parameters. Parameters without a subscript are the same for all karst features in the model.

2.1 Groundwater flow

Groundwater flow was simulated for steady-state conditions. This approach seems appropriate since this work focuses on the simulation of tracer transport in the conduit system during tracer tests, which are ideally conducted under quasi-steady-state flow conditions. Therefore, the simulations refer to periods with a small change of spring discharge, e.g. base flow recession, and are not designed to predict conditions during intensive recharge/discharge events. The groundwater flow in the three-dimensional fissured matrix was simulated with the continuity equation and the Darcy equation (Eq. 2a und b).

$$Q_m = \nabla(\rho \boldsymbol{u}_m), \tag{2a}$$

$$\boldsymbol{u}_m = -K_m \nabla H_m, \tag{2b}$$

where Q_m is the mass source term [M L^{-3} T^{-1}], ρ the density of water [M L^{-3}] and $\boldsymbol{u}_m$ the Darcy velocity [L T^{-1}]. In Eq. (2b) K_m is the hydraulic conductivity of the fissured matrix [L T^{-1}] and H_m the hydraulic head [L].

Two-dimensional fracture flow in the fault zone was simulated with the COMSOL® fracture flow interface. The interface only allows for the application of the Darcy equation inside of fractures, so laminar flow in the fault zone was assumed. In order to obtain a process-based conceptualization of flow, the hydraulic fault conductivity K_f was calculated by the cubic law (Eq. 3):

$$K_f = \frac{d_f^2 \rho g}{12\mu}, \tag{3}$$

where d_f is the fault aperture [L], ρ the density of water [M L^{-3}], g the gravity acceleration [L T^{-2}] and μ the dynamic viscosity of water [M T^{-1} L^{-1}].

For groundwater flow in the karst conduits, the Manning equation was used (Eq. 4).

$$\boldsymbol{u}_c = \frac{1}{n}\left(\frac{r_c}{2}\right)^{\frac{2}{3}} \sqrt{\frac{dH_c}{dx}}, \tag{4}$$

where $\boldsymbol{u}_c$ is the specific discharge in this case equalling the conduit flow velocity [L T^{-1}], n the Manning coefficient [T L$^{-1/3}$], $r_c/2$ the hydraulic radius [L] and dH_c/dx the hydraulic gradient [–]. The Manning coefficient is an empirical value for the roughness of a pipe with no physical nor measurable meaning. The hydraulic radius is calculated by dividing the cross section by the wetted perimeter, which in this case corresponds to the total perimeter of the pipe (Reimann et al., 2011).

The whole conduit network was simulated for turbulent flow conditions. Due to the large conduit diameters (0.01–6 m, Sect. 5) this assumption is a good enough approximation. Hereby, strong changes in flow velocities due to the change from laminar to turbulent flow can be avoided. At the same time, the model does not require an estimation of the critical Reynolds number, which is difficult to assess accurately.

The three-dimensional flow in the fissured matrix and the one-dimensional conduit flow were coupled through a linear exchange term that was defined according to Barenblatt et al. (1960) as

$$q_{ex} = \frac{\alpha}{L}(H_c - H_m), \tag{5}$$

where q_{ex} is the water exchange between conduit and fissured matrix [L^2 T^{-1}] per unit conduit length L [L], H_m the hydraulic head in the fissured matrix [L], H_c the hydraulic head in the conduit [L] and α the leakage coefficient [L^2 T^{-1}]. The leakage coefficient was defined as

$$\alpha = 2\pi r_c K_m, \tag{6}$$

where $2\,\pi\,r_c$ is the conduit perimeter [L]. Other possible influences, e.g. the lower hydraulic conductivity at the solid–liquid interface of the pipe and the fact that water is not exchanged along the whole perimeter but only through the fissures are not considered. The exact value of these influences is unknown and the exchange parameter mainly controls the reaction of the karst conduits and the fissured matrix to hydraulic impulses. Since the flow simulation is performed for steady-state conditions this simplification is not expected to exhibit significant influence on the flow field.

2.2 Solute transport

Transient solute transport was simulated based on the steady-state groundwater flow field. COMSOL Multiphysics® offers a general transport equation with its solute transport interface. This interface was applied for the three-dimensional

fissured matrix. In this work saturated, conservative transport was simulated, with an advection–dispersion equation (Eq. 7)

$$\frac{\partial}{\partial t}(\theta_{\mathrm{m}} c_{\mathrm{m}}) + \nabla(\boldsymbol{u}_{\mathrm{m}} c_{\mathrm{m}}) = \nabla[(\mathbf{D}_{\mathrm{Dm}} + \mathbf{D}_{\mathrm{e}})\nabla c_{\mathrm{m}}] + S_{\mathrm{m}}, \quad (7)$$

where θ_{m} is the matrix porosity [–], c_{m} the solute concentration [$\mathrm{M\,L^{-3}}$], $\mathbf{D}_{\mathrm{Dm}}$ the mechanical dispersion [$\mathrm{L^2\,T^{-1}}$] and $\mathbf{D}_{\mathrm{e}}$ the molecular diffusion [$\mathrm{L^2\,T^{-1}}$]. S_{m} is the source term [$\mathrm{L^3\,T^{-1}}$].

The solute transport interface cannot be applied to one-dimensional elements within a three-dimensional model. COMSOL® offers a so-called coefficient form edge PDE interface to define one-dimensional mathematical equations. There, a partial differential equation is provided (COMSOL AB, 2012) which can be adapted as needed and leads to Eq. (8) in its application for solute transport in karst conduits:

$$\theta_{\mathrm{c}} \frac{\partial c_{\mathrm{c}}}{\partial t} + \nabla(-\mathbf{D}_{\mathrm{c}} \nabla c_{\mathrm{c}} + \boldsymbol{u}_{\mathrm{c}} c_{\mathrm{c}}) = f, \quad (8)$$

where θ_{c} is the conduit porosity which is set equal to 1, $\mathbf{D}_{\mathrm{c}}$ [$\mathrm{L^2\,T^{-1}}$] the diffusive/dispersive term $\mathbf{D}_{\mathrm{c}} = (\mathbf{D}_{\mathrm{Dc}} + \mathbf{D}_{\mathrm{e}})$, f the source term and $\boldsymbol{u}_{\mathrm{c}}$ [$\mathrm{L\,T^{-1}}$] the flow velocity inside the conduits, which corresponds to the advective transport component. Flow divergence cannot be neglected, as is often the case in other studies (e.g. Hauns et al., 2001; Birk et al., 2006; Coronado et al., 2007). Different conduit sizes and in- and outflow along the conduits lead to significant velocity divergence in the conduit system. This needs to be considered for mass conservation during the simulation. The mechanical conduit dispersion $\mathbf{D}_{\mathrm{Dc}}$ was calculated with Eq. (9) (Hauns et al., 2001).

$$\mathbf{D}_{\mathrm{Dc}} = \varepsilon \boldsymbol{u}_{\mathrm{c}}, \quad (9)$$

where ε is the dispersivity in the karst conduits [L].

The source term f [$\mathrm{M\,T^{-1}\,L^{-1}}$] in Eq. (8) equals in this case the mass flux of solute per unit length L [L] due to matrix–conduit exchange of solute c_{ex}:

$$f = c_{\mathrm{ex}} = -\mathbf{D}_{\mathrm{e}} \frac{2\pi r_{\mathrm{c}}}{L}(c_{\mathrm{m}} - c_{\mathrm{c}}) - q_{\mathrm{ex}} c_i. \quad (10)$$

The first term of the right-hand side of Eq. (10) defines the diffusive exchange due to the concentration difference between conduit and fissured matrix. The second term is a conditional term adding the advective exchange of solute due to water exchange. The concentration of the advective exchange c_i is defined as

$$c_i = \begin{cases} c_{\mathrm{c}} & \text{if } q_{\mathrm{ex}} > 0 \\ c_{\mathrm{m}} & \text{if } q_{\mathrm{ex}} \leq 0 \end{cases}. \quad (11)$$

When q_{ex} is negative, the hydraulic head in the fissured matrix is higher than in the conduit (Eq. 5) and water with the solute concentration of the fissured matrix c_{m} enters the conduit. When it is positive, water with the solute concentration c_{c} of the conduit leaves the conduit and enters the fissured matrix. Since one-dimensional transport is simulated in a three-dimensional environment, the left-hand side of Eq. (8) is multiplied with the conduit cross section πr_{c}^2 [$\mathrm{L^2}$]. These considerations lead to the following transport equation for the karst conduits:

$$\pi r_{\mathrm{c}}^2 \frac{\partial c_{\mathrm{c}}}{\partial t} + \pi r_{\mathrm{c}}^2 \nabla(-\mathbf{D}_{\mathrm{c}} \nabla c_{\mathrm{c}} + \boldsymbol{u}_{\mathrm{c}} c_{\mathrm{c}}) = -\mathbf{D}_{\mathrm{e}} \frac{2\pi r_{\mathrm{c}}}{L}(c_{\mathrm{m}} - c_{\mathrm{c}}) - q_{\mathrm{ex}} c_i. \quad (12)$$

3 Field site and model design

The field site is the Gallusquelle spring area on the Swabian Alb in south-western Germany. The size of the model area is approximately 150 $\mathrm{km^2}$, including the catchment area of the Gallusquelle spring and surrounding smaller spring catchments (Oehlmann et al., 2013). The Gallusquelle spring is the main point outlet with a long-term average annual discharge of 0.5 $\mathrm{m^3\,s^{-1}}$. The model area is constrained by three rivers and no-flow boundaries derived from tracer test information and the dip of the aquifer base (Oehlmann et al., 2013) (Fig. 1).

The aquifer consists of massive and bedded limestone of the stratigraphic units Kimmeridgian 2 and 3 (ki 2/3) (Golwer, 1978; Gwinner, 1993). The marly limestones of the underlying Kimmeridgian 1 (ki 1) mainly act as an aquitard. In the west of the area where they get close to the surface, they are partly karstified and contribute to the aquifer (Sauter, 1992; Villinger, 1993). The Oxfordian 2 (ox 2) that lies beneath the ki 1 consists of layered limestones. It is more soluble than the ki 1 but only slightly karstified because of the protective effect of the overlying geological units. In the catchment areas of the Fehla-Ursprung and the Balinger springs close to the western border (Fig. 1a) the ox 2 partly contributes to the aquifer. For simplicity, only two vertical layers were differentiated in the model: the aquifer and the underlying aquitard.

The geometry of the conduit system was transferred from the COMSOL® model calibrated for flow by Oehlmann et al. (2013). It is based on the occurrence of dry valleys in the investigation area and artificial tracer test information (Gwinner, 1993). The conduit geometry for the Gallusquelle spring was also employed for distributed flow simulations by Doummar et al. (2012) and Mohrlok and Sauter (1997) (Fig. 1). In this work, all highly conductive connections identified by tracer tests in the field were simulated as discrete one-dimensional karst conduit elements. The only exception is a connection in the west of the area that runs perpendicular to the dominant fault direction and reaches the Fehla-Ursprung spring at the northern boundary (Fig. 1). While the element was regarded as a karst conduit by Oehlmann et

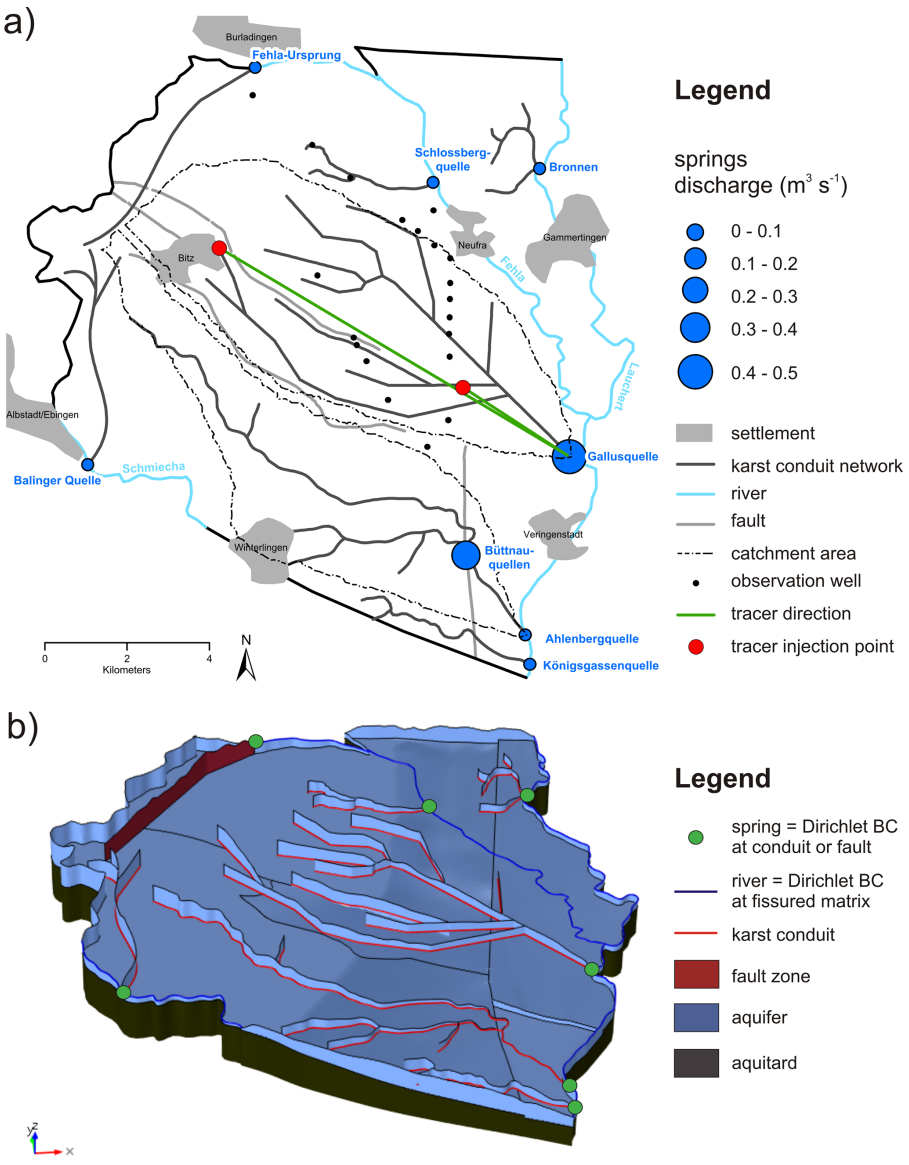

Figure 1. (a) Plan view of the model area. Settlements, fault zones and rivers in the area are plotted, as well as the 20 observation wells used for hydraulic head calibration, the six springs used for spring discharge calibration and the two tracer tests employed for flow velocity calibration. Catchment areas for the Gallusquelle spring and the Ahlenberg and Büttnauquellen springs were simulated according to Oehlmann et al. (2013). **(b)** Three-dimensional view of the model. The upper boundary is hidden to allow a view of the karst conduit system and the aquifer base. The abbreviation BC stands for boundary condition. At the hidden upper boundary, a constant recharge Neumann BC is applied.

al. (2013) it is more likely that the water crosses the graben structure by a transversal cross-fault (Strayle, 1970). Therefore, the one-dimensional conduit element was replaced by a two-dimensional fault element (Fig. 1b). This leads to a small adjustment in the catchment areas compared to the results of Oehlmann et al. (2013) (Fig. 1a). While the discharge data for the Fehla-Ursprung spring are not as extensive as for the other simulated springs, it is approximated to $0.1\,m^3\,s^{-1}$, the annual average ranging from 0.068 to $0.135\,m^3\,s^{-1}$. The fault zone aperture was calibrated accordingly (Sect. 5).

Due to a large number of studies conducted in the area during the last decades (e.g. Villinger, 1977; Sauter, 1992; Geyer et al., 2008; Kordilla et al., 2012; Mohrlok, 2014) many data for pattern matching are available even though the karst conduit network itself is not accessible. Since the groundwater flow simulation was performed for steady-state conditions, direct recharge, which is believed to play an important role during event discharge (Geyer et al., 2008), was neglected. It is not expected that recharge dynamics exhibit significant influence on the flow field during recession periods. From Sauter (1992) the long-term average annual recharge, ranges

Table 1. Calibrated and simulated parameters for the best-fit simulations. Literature values are given if available. TT 1 and TT 2 refer to the two tracer tests.

Parameter	Simulated values scenario 2	Simulated values scenario 5	Literature values
K_m ($m\,s^{-1}$)	8×10^{-6}	1.5×10^{-5}	1×10^{-6}–2×10^{-5} (local scale)[e] 2×10^{-5}–1×10^{-4} (regional scale)[e]
m_h ($m^{-2/3}\,s^{-1}$)	0.3	0.3	–
b_h ($m^{1/3}\,s^{-1}$)	0.22	0.18	–
n ($s\,m^{-1/3}$)	1.04–4.55	1.05–5.56	0.03–1.07[a]
b (m)	0.01	0.01	–
m (–)	2.04×10^{-4}	1.42×10^{-4}	–
ε_1 (m) for TT 1	7.15	7.5	4.4–6.9[f], 10[e]
ε_2 (m) for TT 2	30	23	20[g]
A^h (m^2)	11.9	13.4	13.9[f]
V (m^3)	109 351	89 286	$\leq$ 200 000[b]
RMSE H (m)	5.61	5.91	–
Peak offset TT 1 (h)	−0.28[c]	−0.28[c]	–
Peak offset TT 2 (h)	2.5[d]	−1.39[d]	–

[a] Jeannin (2001); [b] Geyer et al. (2008); [c] measurement interval 1 min, simulation interval 2.7 h; [d] measurement interval 6 h, simulation interval 2.7 h; [e] Sauter (1992); [f] Birk et al. (2005); [g] Merkel (1991); [h] average for the interval between tracer test 1 and the spring.

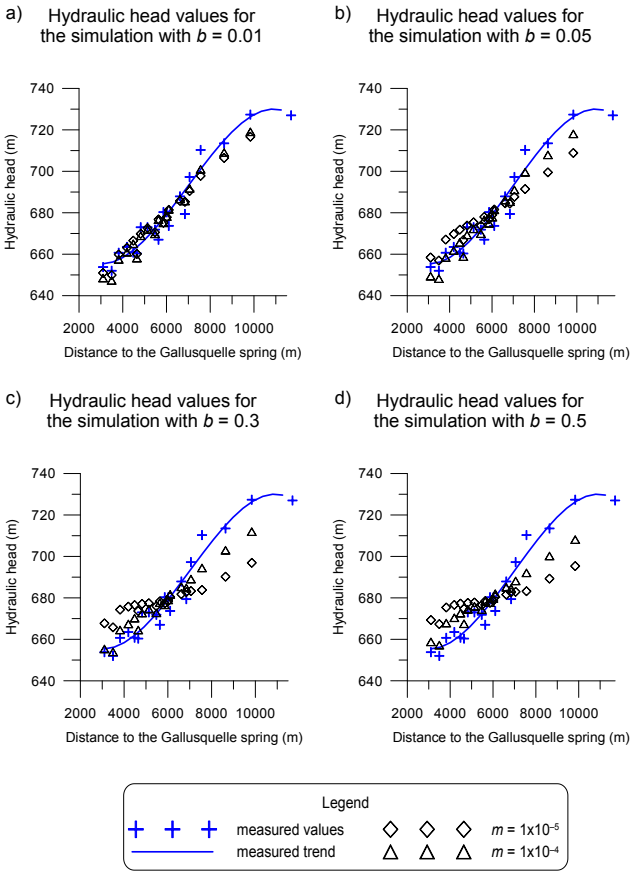

Figure 2. Hydraulic head distributions for different combinations of geometric conduit parameters for scenario 1. b is the lowest conduit radius and m the radius increase along the conduit. For comparison, a trend line is fitted to the measured hydraulic head values showing the distribution of hydraulic gradients from the Gallusquelle spring to the western border of its catchment area.

of hydraulic parameters and the average annual hydraulic head distribution derived from 20 observation wells (Fig. 1a) are available. Villinger (1993) and Sauter (1992) provided data on the geometry of the aquifer base. Available literature values for the model parameters are given in Table 1.

The observed hydraulic gradients in the Gallusquelle area are not uniform along the catchment. Figure 2 shows a S-shaped distribution with distance to the Gallusquelle spring. The gradient at each point of the area depends on the combination of the respective transmissivity and total flow. The amount of water flowing through a cross sectional area increases towards the springs due to flow convergence. In the Gallusquelle area, the transmissivity rises in the vicinity of the springs leading to a low hydraulic gradient. In the central part of the area discharge is relatively high while the transmissivities are lower leading to the observed steepening of the gradient starting in a distance of 4000 to 5000 m from the Gallusquelle spring. Towards the boundary of the catchment area in the west the water divide reduces discharge in the direction of the Gallusquelle spring leading to a smoothing of hydraulic gradients.

Geyer et al. (2008) calculated the maximum conduit volume for the Gallusquelle spring V_c [L^3] with information from the tracer test that will be referred to as tracer test 2 in the following. Since the injection point of the tracer test is close to the catchment boundary, it is assumed that it covers the whole length of the conduit system. The authors calculated the maximum volume at 218 000 m^3. Their approach assumes the volume of the conduit corresponds to the total volume of water discharged during the time between tracer input and tracer arrival neglecting the contribution of the fissured matrix.

The six springs that were monitored and therefore simulated are shown in Fig. 1. Except for the Balinger spring, their discharges were fitted to long-term average annual discharge data. For the Balinger spring discharge calibration was not possible due to lack of data. It was included as a boundary condition because several tracer tests provided a valuable basis for the conduit structure leading to the spring.

Tracer directions were available for 32 tracer tests conducted at 20 different tracer injection locations (Oehlmann et al., 2013). In all, 16 of the tracer tests were registered at the Gallusquelle spring. For this work two of them were chosen for pattern matching of transport parameters. Both of them were assumed to have a good and direct connection to the conduit network. Tracer test 1 (Geyer et al., 2007) has a tracer injection point at a distance of 3 km to the Gallusquelle spring. Tracer test 2 (MV746 in Merkel, 1991; Reiber et al., 2010) was conducted at 10 km distance to the Gallusquelle

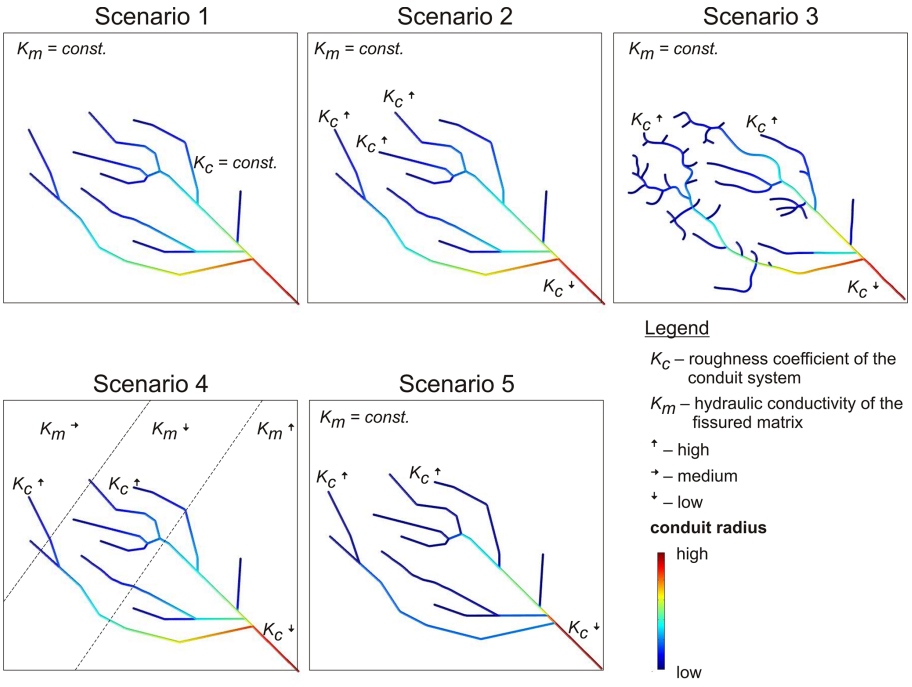

Figure 3. Conceptual overview of the simulated scenarios. The conduit geometry and the varying parameters are shown.

spring (Fig. 1a). Due to the flow conditions (Fig. 1a) it can be assumed that tracer test 2 covers the total length of the conduit network feeding the Gallusquelle spring. The recovered tracer mass was chosen as input for the tracer test simulation. The basic information about the tracer tests is given in Table 2.

Since the tracer tests were not performed at average flow conditions, the model parameters were calibrated first for the long-term average annual recharge of 1 mm d^{-1} and the long-term average annual discharge of 0.5 $m^3 s^{-1}$. For the transport simulations, the recharge was then adapted to produce the respective discharge observed during the tracer experiment (Table 2).

Table 2. Field data of the simulated tracer tests.

	Tracer test 1	Tracer test 2
Input mass (kg)	0.75	10
Recovery (%)	72	50
Distance to spring (km)	3	10
Spring discharge ($m^3 s^{-1}$)	0.375	0.76
Sampling interval	1 min	6 h
Peak time (h)	47	79.5

4 Parameter analysis

An extensive parameter analysis was performed in order to identify parameters determining the hydraulic parameter field in the model area, as well as their relative contributions to the discharge and conduit flow velocities. The fitting parameters include the parameters controlling the respective transmissivities of the fissured matrix and the karst conduit system, i.e. the geometry and roughness of the conduit system, the hydraulic conductivity of the fissured matrix and the fracture aperture for the Fehla-Ursprung spring. Furthermore, the apparent dispersivities for the two artificial tracer tests were calibrated (Table 1). Since all model runs were performed for steady-state conditions parameters controlling the temporal distribution of recharge were not considered. The parameter analysis was performed with COMSOL Multiphysics® parametric sweep tool, which sweeps over a given parameter range. Parameter ranges were chosen according to literature values (Table 1). For the conduit geometry parameters, lowest conduit radius b and slope of radius increase m, no literature values are available. Therefore, the ranges were chosen so that conduit volumes ranged below the maximum volume given by Geyer et al. (2008). In addition to the variation of the fitting parameters, five basic scenarios were compared. They correspond to different conceptual representations of the area and are summarized in Fig. 3 and Table 3.

Three objective functions were employed for pattern matching: spring discharge, hydraulic head distribution and flow velocities of the two tracer tests (Sect. 3). The average spring discharge of the Gallusquelle spring was set by the difference between simulated and the measured discharge. A difference of 10 L s^{-1} was considered as acceptable. Param-

Table 3. Specifics of the different scenarios. The bold writing indicates the parameter that is analysed in the respective scenario. The results are indicated by comparative markers. "+" means good, "o" means average and "–" means bad compared to the other scenarios. Details to the scenarios and results evaluation can be found in Sect. 4.

Parameter	Scenario 1	Scenario 2	Scenario 3	Scenario 4	Scenario 5
K_c	constant	**linear increase**	linear increase	linear increase	linear increase
Lateral network	minimal	minimal	**extended**	minimal	minimal
K_m	constant	constant	constant	**variable**	constant
Intersection radius r_{c2}	r_{c0}	r_{c0}	r_{c0}	r_{c0}	$\sqrt{r_{c0}^2 + r_{c1}^2}$
Main results					
Hydraulic head fit	+	+	+	+	+
Fit of breakthrough	–	+	+	+	+
Model applicability	+	o	–	–	o

eter sets, which could not fulfil this criterion, were not considered for parameter analysis. The other low-discharge and less-investigated springs (Sect. 3) were used to inspect the flow field and water balance in the modelling area, i.e. they were only considered after parameter fitting to check the plausibility of the deduced parameter set.

The fit of the tracer tests was determined by comparing the arrival times of the highest peak concentration of the simulation with the measured value (peak offset). Since tracer experiments conducted in karst conduits usually display very narrow breakthrough curves, this procedure appears to be justified. The quality of the fit was judged as satisfactory if the peak offset was lower than either the simulation interval or the measurement interval.

The fit of the hydraulic head distribution was determined by calculating the root mean square error (RMSE) between the simulated and the observed values at the respective locations of the observation wells. Since the fit at local points with a large-scale modelling approach generally shows large uncertainties due to low-scale heterogeneities, an overall fit of < 10 m RMSE was accepted. Furthermore, a qualitative comparison with the hydraulic gradients in the area was performed (e.g. Fig. 2) to ensure that the general characteristics of the area were represented instead of only the statistical value.

4.1 Scenario 1 – standard scenario

In scenario 1 all features were implemented as described in Sects. 2 and 3. The parameter analysis shows that for each conduit geometry, defined by their smallest conduit radii b and their slopes of radius increase along the conduit length m (Eq. 1), only one value of the Manning coefficient n allows a simulated discharge for the Gallusquelle spring of $0.5\,m^3\,s^{-1}$. The n value correlates well with that for the total conduit volume due to the fact that the spring discharge is predominantly determined by the transmissivity of the karst conduit system. The transmissivity of the conduit system at each point in space is the product of its hydraulic conductivity, which is proportional to $1/n$, and the cross sectional area of the conduit A. Thus, to keep the spring discharge at $0.5\,m^3\,s^{-1}$ a higher conduit volume requires a higher calibrated n value (Eq. 4).

With scenario 1 it is possible to achieve a hydraulic head fit resulting in a RMSE of 6 m that can be judged as adequate on catchment scale. Regarding the conduit geometry, a good hydraulic head fit can be achieved with small b values independently of the chosen m value (Fig. 2a). The higher the b value, the higher the m value to reproduce the hydraulic gradients of the area (Fig. 2). This implies that the hydraulic head fit is independent of the conduit volume during steady-state conditions but depends on the b/m ratio. The influence of the b/m ratio on the hydraulic head fit depends on the hydraulic conductivity of the fissured matrix K_m. For low K_m values of ca. $1 \times 10^{-6}\,m\,s^{-1}$ the hydraulic head fit is completely independent of the conduit geometry and the RMSE is very high (Fig. 4a). For high K_m values of ca. $5 \times 10^{-4}\,m\,s^{-2}$ (Fig. 4a) the dependence is also of minor importance and the RMSE is relatively stable at ca. 11 m. Due to the high hydraulic conductivity of the fissured matrix the hydraulic gradients do not steepen in the vicinity of the spring even for high b/m ratios. For K_m values between the above values the RMSE significantly rises for b/m ratios above 1000 m. For the range of acceptable errors, i.e. lower than 10 m, it is apparent in Fig. 4a that the best-fit K_m value is approximately $1 \times 10^{-5}\,m\,s^{-1}$ independent of the conduit geometry. However, no distinct best-fit conduit geometry can be derived. There are several parameter combinations providing a good fit for the Gallusquelle spring discharge and the hydraulic head distribution.

The goodness of the fit of the simulation of the tracer breakthrough is mainly determined by the conduit geometry. The influence of the hydraulic conductivity of the fissured matrix K_m on flow velocities inside the karst conduits is comparatively low and decreases even further in the vicinity of the springs (Fig. 4b and c) leading to minor influences on tracer travel times. Instead, the quality of the fit

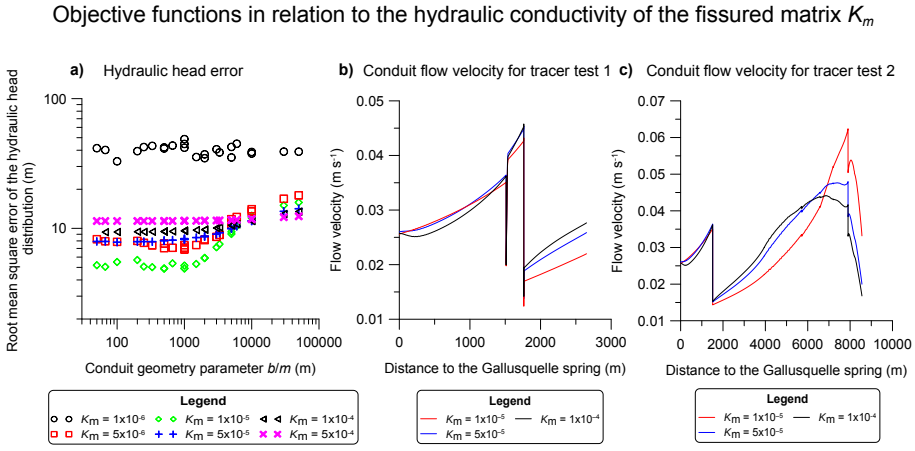

Figure 4. Influence of the hydraulic conductivity of the fissured matrix on the objective functions. **(a)** Influence on the root mean square error of the hydraulic head distribution in relation to the conduit geometry. The conduit geometry is represented by the parameter b/m (Eq. 1), which is the ratio of the smallest radius to the slope of radius increase along the conduit length. **(b)** Influence on the conduit flow velocity for tracer test 1. **(c)** Influence on the conduit flow velocity for tracer test 2.

mainly depends on the conduit volume and accordingly on the Manning coefficient n (Fig. 5). It is possible to simulate only one of the two tracer experiments with this scenario (Fig. 5). Given the broad range of geometries for which an adequate hydraulic head fit can be achieved (Figs. 2 and 4) it is possible to simulate one of the two tracer peak velocities and the hydraulic head distribution with the same set of parameters. While the simulation of the breakthrough of tracer test 1 requires relatively high n values, of ca. $2.5\,\mathrm{s\,m^{-1/3}}$, that of tracer test 2 can only be calibrated with lower values of ca. $1.7\,\mathrm{s\,m^{-1/3}}$ (cf. Fig. 5a and b). For every parameter set, where the travel time of the simulated tracer test 2 is not too long, that of tracer test 1 is too short. For the simulation of tracer test 2, the velocities at the beginning of the conduits must be relatively high. To avoid the flow velocities from getting too high in downgradient direction, the conduit size would have to increase drastically due to the constant additional influx of water from the fissured matrix. In the given geometric range, the conduit system has a dominant influence on spring discharge. Physically, this situation corresponds to the conduit-influenced flow conditions (Kovács et al., 2005). Thus, conduit transmissivity is a limiting factor for conduit–matrix exchange and a positive feedback mechanism is triggered, if the conduit size is increased. A higher conduit size leads to higher groundwater influx from the fissured matrix and spring discharge is overestimated. Therefore, parameter analysis shows that scenario 1 is too strongly simplified to correctly reproduce the complex nature of the aquifer.

4.2 Scenario 2 – conduit roughness coefficient K_c

In scenario 2 the Manning coefficient n was changed from constant to laterally variable. In the literature, n is generally

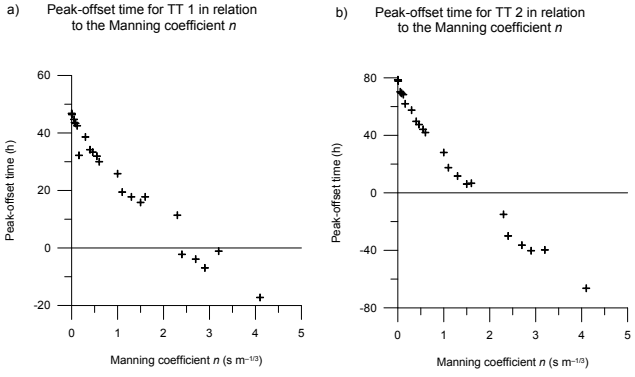

Figure 5. Difference between peak concentration times vs. the Manning n value for scenario 1. High n values correspond to high conduit volumes and high cross sectional areas at the spring **(a)** for tracer test 1 and **(b)** for tracer test 2.

kept constant throughout the conduit network (e.g. Jeannin, 2001; Reimann et al., 2011) for lack of information on conduit geometry. However, it is assumed that the Gallusquelle spring is not fed by a single large pipe. Rather there is some evidence in the spring area that a bundle of several small-interconnected pipes feed the spring. Since the number of individual conduits per bundle is unknown and the regional modelling approach limits the resolution of local details, the small diameter conduits, which the bundle consists of, cannot be simulated individually. Therefore, each single pipe in the model represents a bundle of conduits in the field.

It can be assumed that the increase in conduit cross section is at least partly provided by additional conduits added to the bundle rather than a single individual widening conduit. Therefore, while the cross section of the simulated conduit, i.e. the total effective cross section of the conduit bundle, in-

creases towards the springs, it is not specified how much of this increase is due to the individual conduits widening and how much is due to additional conduits, not distinguishable in the simulation. If the simulated effective cross sectional area increase is mainly due to additional conduits being included in the bundle, the surface / volume ratio increases with the cross section, contrary to what would be observed, if a single conduit in the model would represent a single conduit in the field. The variation in surface area / volume ratio implicitly leads to a larger roughness in the simulation, even further enhanced by exchange processes between the individual conduits. This effect again leads to an increase in the Manning coefficient n in the downgradient direction towards the spring for a simulated single conduit. Since the number and size of the individual conduits is unknown, it is impossible to calculate the change of n directly from the geometry. Thus, a simple scenario was assumed where the roughness coefficient K_c, which is the reciprocal of n, was linearly and negatively coupled to the rising conduit radius (Eq. 13).

$$K_c = \frac{1}{n} = -m_h r_c + m_h r_{c,max} + b_h, \quad (13)$$

where r_c [L] is the conduit radius and $r_{c,max}$ [L] the maximum conduit radius simulated for the respective spring, which COMSOL® calculates from Eq. (1). m_h [$L^{-2/3}\,T^{-1}$] and b_h [$L^{1/3}\,T^{-1}$] are calibration parameters determining the slope and the lowest value of the roughness coefficient respectively.

For every conduit geometry several combinations of m_h and b_h lead to the same spring discharge. However, hydraulic head fit and tracer velocities are different for each m_h–b_h combination even if spring discharge is the same. With the new parameters a higher variation of velocity profiles is possible. This allows for the calibration of the tracer velocities of both tracer tests. The dependence of tracer test 2 on m_h is much higher than that of tracer test 1 since it is injected further upgradient towards the beginning of the conduit (Fig. 6). Therefore, tracer test 2 is influenced more strongly by the higher velocities far away from the spring introduced by high m_h values and always shows a significant positive correlation with m_h (Fig. 6).

Since the slope of K_c is negative with respect to the conduit length, the variable K_c leads to a slowing down of water towards the springs. As discussed in detail by Oehlmann et al. (2013) a rise of transmissivity towards the springs is observed in the Gallusquelle area. Therefore, adequate hydraulic head fits can only be obtained, if the decrease of K_c towards the spring is not too large and compensates the effect of the increase in conduit transmissivity due to the increasing conduit radius. This effect reduces the number of possible and plausible parameter combinations. From these considerations a best-fit model can be deduced capable of reproducing all objective functions within the given error ranges (Fig. 7a). According to the model simulations, karst groundwater discharge and flow velocities significantly depend on

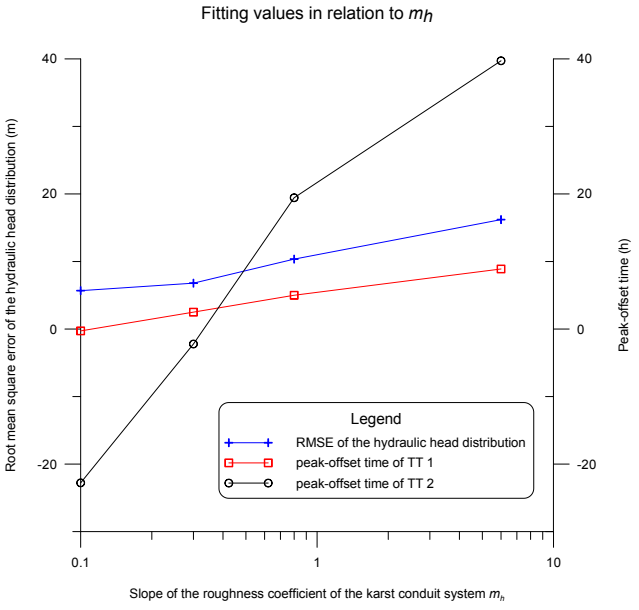

Figure 6. Hydraulic head errors and differences between peak concentration times for both tracer tests for scenario 1. The example is shown for a conduit geometry with a starting value $b = 0.01$ m and a radius increase of $m = 2 \times 10^{-4}$. Each m_h ($m^{-2/3}\,s^{-1}$) value corresponds to a respective value of the highest conduit roughness b_h ($m^{1/3}\,s^{-1}$) and each combination results in the same spring discharge.

the total conduit volume as is to be expected. It can be deduced from the parameter analysis that the conduit volume can be estimated at ca. 100 000 m^3 for the different parameters to match equally well (Fig. 7a).

4.3 Scenario 3 – extent of conduit network

In scenario 3, a laterally further extended conduit system was employed, assuming the same maximum conduit volume as in scenarios 1 and 2 but with different spatial distribution along the different total conduit lengths. The original conduit length for the Gallusquelle spring in scenarios 1 and 2 is 39 410 m, for scenario 3 it is 63 490 m; therefore, the total length was assumed to be larger by ca. 50 % (Fig. 8). The geometry of the original network was mainly constructed along dry valleys where point-to-point connections are observed based on qualitative evaluation from artificial tracer tests. Of the dry valleys without tracer tests, only the larger ones were included, where the assumption of a high karstification is backed up by the occurrence of sinkholes (Mohrlok and Sauter, 1997). Therefore, it represents the minimal extent of the conduit network. For scenario 3 the network was extended along all dry valleys within the catchment, where no tracer tests were conducted.

The results of the parameter variations are comparable to those of scenario 2 (cf. Fig. 7a and b). While the hydraulic head contour lines are smoother than for the original conduit

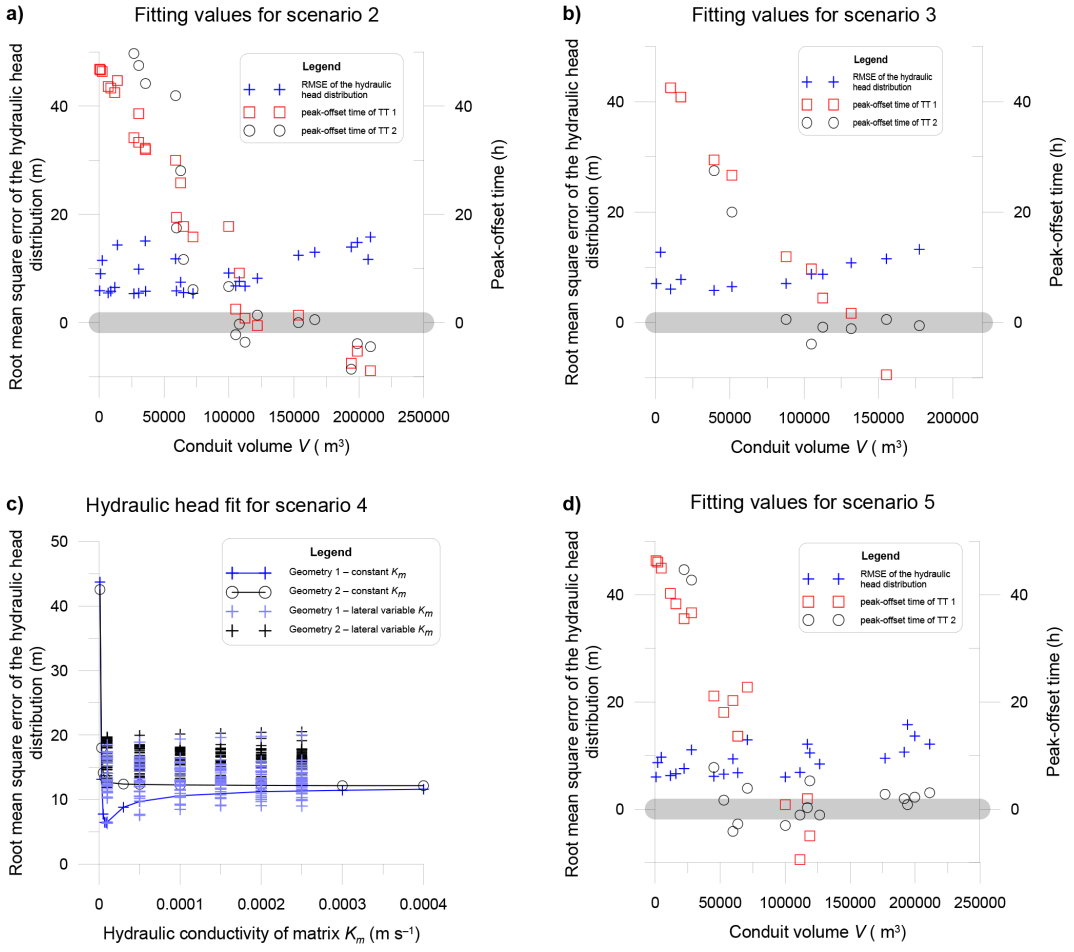

Figure 7. Calibrated values for the simulated scenarios. For scenarios 2, 3 and 5 **(a, b, d)** hydraulic head fit and the peak-offset times of both tracer tests (referred to as TT 1 and TT 2) are shown in relation to conduit volume. The thick grey bar marks the target value of zero. For scenario 4 **(c)** the root mean square error of the hydraulic heads is given for two different conduit geometries in relation to the hydraulic conductivity of the fissured matrix K_m. For the version with laterally variable matrix conductivity the axis shows as an example the hydraulic conductivity of the north-western part. The parameters for the two geometries are given in Table 3.

length the general hydraulic head fit is the same (Fig. 7b). It seems possible to obtain a good fit for all model parameters but the scenario is more difficult to handle numerically. Calculation times are up to 10 times larger compared to the other scenarios and goodness of convergence is generally lower. Since the calibrated parameters are not significantly different from those deduced in scenario 2 it is concluded that the ambiguity introduced by the uncertainty in total conduit length is small if hydraulic conduit parameters and total conduit volumes are the aim of investigation.

4.4 Scenario 4 – matrix hydraulic conductivity K_m

In scenario 4, the homogeneously chosen hydraulic conductivity of the fissured matrix K_m was changed into a laterally variable conductivity based on different types of lithology and the spatial distribution of the groundwater potential. Sauter (1992) found from field measurements that the area can be divided into three parts with different hydraulic conductivities. Oehlmann et al. (2013) discussed that the major influence is the conduit geometry leading to higher hydraulic transmissivities close to the springs in the east of the area. It is also possible that not only the conduit diameters change towards the spring but the hydraulic conductivity of the fissured matrix as well, since the aquifer cuts through three stratigraphic units (Sect. 3). These geologic changes are likely to affect the lateral distribution of hydraulic conductivities (Sauter, 1992). Figure 9 shows the division into three different areas. K_m values were varied in the range of the values measured by Sauter (1992).

It was expected that a laterally variable K_m value has a major influence on the hydraulic head distribution. All variations of scenario 2 that produce good results for both tracer tests and have a high total conduit volume above 100 000 m^3 yield poor results for hydraulic head errors and spatial dis-

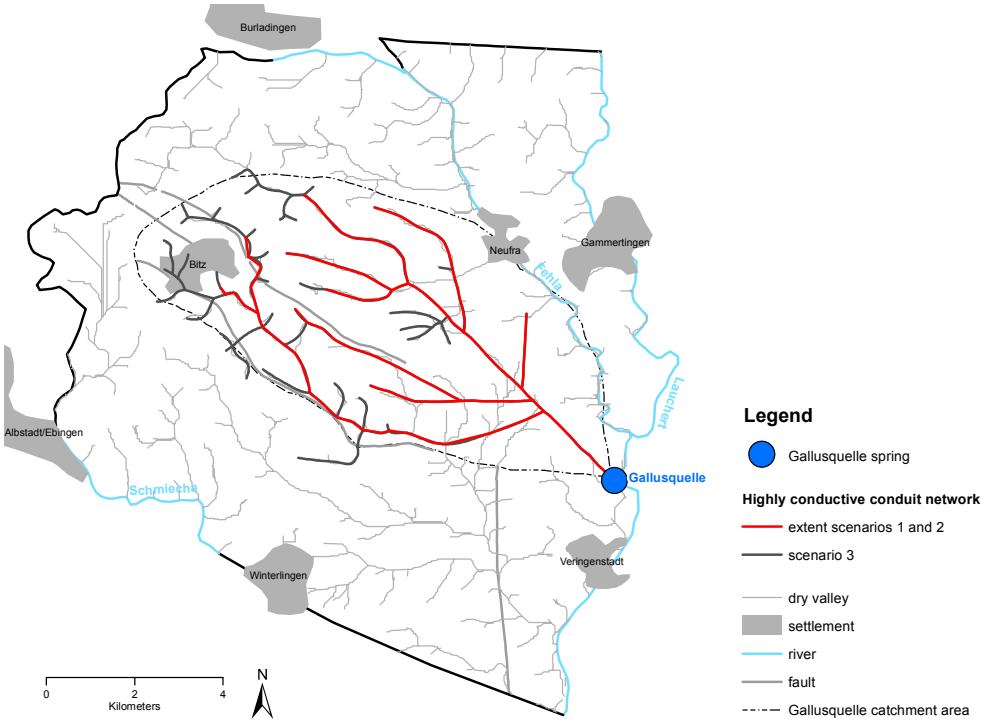

Figure 8. Extended conduit system for scenario 3. The conduit configuration (extent) that is used for the other scenarios is marked in red.

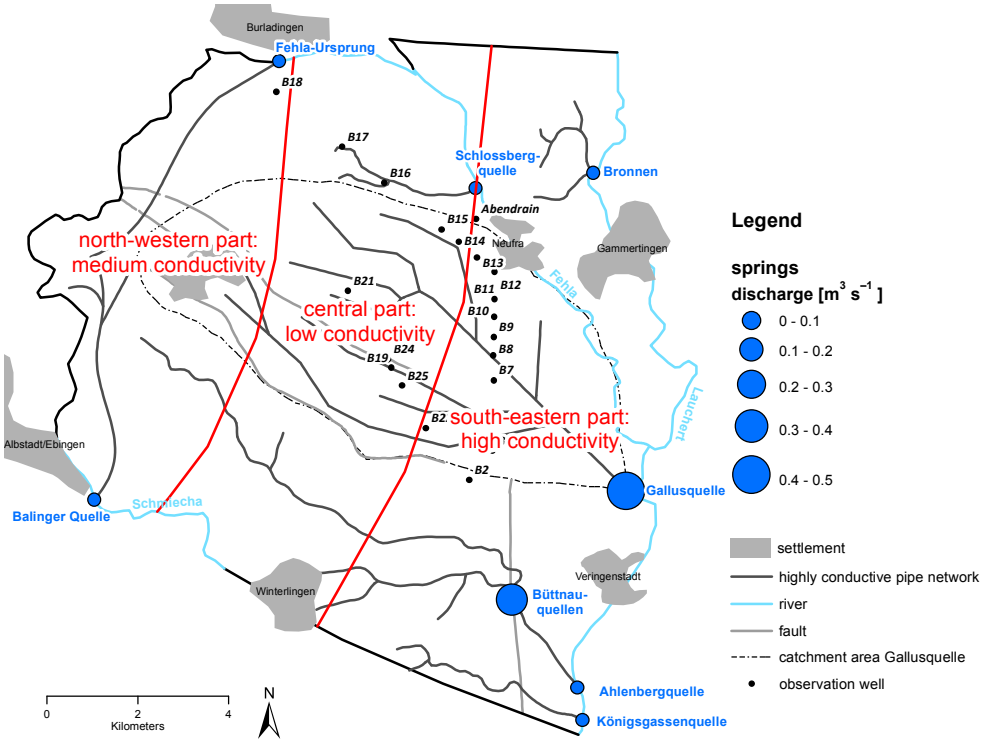

Figure 9. Model catchment with spatially distributed hydraulic conductivities. The model area is divided into three parts after geologic aspects. For each segment different values of the hydraulic conductivity were examined during parameter analysis in scenario 4.

tributions of the hydraulic heads (Fig. 7a). For scenario 4, two different conduit configurations (geometries) were chosen that achieve good results with respect to conduit flow velocities. Geometry G1 has a conduit volume of 112 000 m^3. G2 has a higher b value which leads to the maximum conduit volume of ca. 150 000 m^3. All parameters for the two simulations are given in Table 4.

It was found that while the maximum root mean square error of the hydraulic head fit is similar for both geometries, the minimum RMSE for the hydraulic head is determined by the conduit system. It is not possible to compensate an unsuitable conduit geometry with suitable K_m values (Fig. 7c), which assists in the independent conduit network and fissured matrix calibration. This observation increases the confidence in the representation of the conduits and improves the possibility to deduce the conduit geometry from field measurements. For an adequate conduit geometry, laterally variable matrix conductivities do not yield any improvement. The approach introduces additional parameters and uncertainties because the division of the area into three parts is not necessarily obvious without detailed investigation. From the distribution of the exploration and observation wells (Fig. 1a) it is apparent that especially in the south and west the boundaries are not well defined.

4.5 Scenario 5 – conduit intersections

In scenario 5, the effect of the conduit diameter change at intersections was investigated. In the first four scenarios the possible increase in cross sectional area at intersecting conduits was neglected. In nature, however, the influx of water from another conduit is likely to influence conduit evolution and therefore its diameter. In general, higher flow rates lead to increased dissolution rates because dissolution products are quickly removed from the reactive interface. If conditions are turbulent the solution is limited by a diffusion dominated layer that gets thinner with increasing flow velocities (Clemens, 1998). Clemens (1998) simulated karst evolution in simple Y-shaped conduit networks and found higher diameters for the downstream conduit even after short simulation times. Preferential conduit widening at intersections could further be enhanced by the process of mixing corrosion (Dreybrodt, 1981). However, Hückinghaus (1998) found during his karst network evolution simulations that the water from other karst conduits has a very high saturation with respect to Ca^{2+} compared to water entering the system through direct recharge. Thus, if direct recharge is present, the mixing with nearly saturated water from an intersecting conduit could hamper the preferential evolution of the conduit downstream slowing down the aforementioned processes. In scenario 5 the influence of an increase in diameter at conduit intersections was investigated. Since the amount of preferential widening at intersections is unknown, the cross sections of two intersecting conduits were added and used as starting cross section for the downstream conduit. The new conduit radius was then calculated according to Eq. (14) at each intersection.

Table 4. Parameters for the two different conduit configurations compared in scenario 4. b is the minimum conduit radius, m the slope of radius increase towards the springs, b_h the highest conduit roughness, m_h the slope of roughness decrease away from the spring and V the conduit volume.

	Geometry 1	Geometry 2
b (m)	0.01	0.5
m (–)	2.07×10^{-4}	1.5×10^{-4}
b_h ($m^{1/3}\,s^{-1}$)	0.17	0.15
m_h ($m^{-2/3}\,s^{-1}$)	0.4	0.6
V (m^3)	112 564	153 435

$$r_{c2} = \sqrt{r_{c0}^2 + r_{c1}^2}, \tag{14}$$

where r_{c2} is the conduit radius downstream of the intersection and r_{c0} and r_{c1} the conduit radii of the two respective conduits before their intersection.

Results are very similar to those of scenario 2 (cf. Fig. 7a and d). Both simulations result in nearly the same set of parameters (Table 1). The estimated conduit volume is even a little smaller for scenario 5 since larger cross sections in the last conduit segment near the spring are reached for a lower total conduit volume. The drastic increase of conduit cross sections at the network intersections leads to higher variability in the cross sections along the conduit segments. The differences between the peak offsets of both tracer tests are higher compared to those of scenario 2. While the peak time of tracer test 2 can be calibrated for large conduit volumes, i.e. conduit volumes above 120 000 m^3 (Fig. 7d), the peak time of tracer test 1 is too late for large conduit volumes. This is due to the fact that the injection point for tracer test 1 is much closer to the spring than that for tracer test 2. In scenario 5 the conduit volume is spatially differently distributed from that of scenario 2 for the identical total conduit volume. The drastic increase in conduit diameters downgradient of conduit intersections leads to rather high conduit diameters in the vicinity of the spring. Therefore, while tracer transport in tracer test 2 occurs in relatively small conduits with high flow velocities and larger conduits with lower velocities, the tracer in tracer test 1 is only transported through the larger conduits whose flow velocities are restricted by the spring discharge. In Fig. 7d the parameter values for the best fit would lie well below the lower boundary of the diagram at negative values below −10 h. However, since the fit for conduit volumes around 100 000 m^3 is similar to that of scenario 2, the two scenarios can in this case not be distinguished based on field observations.

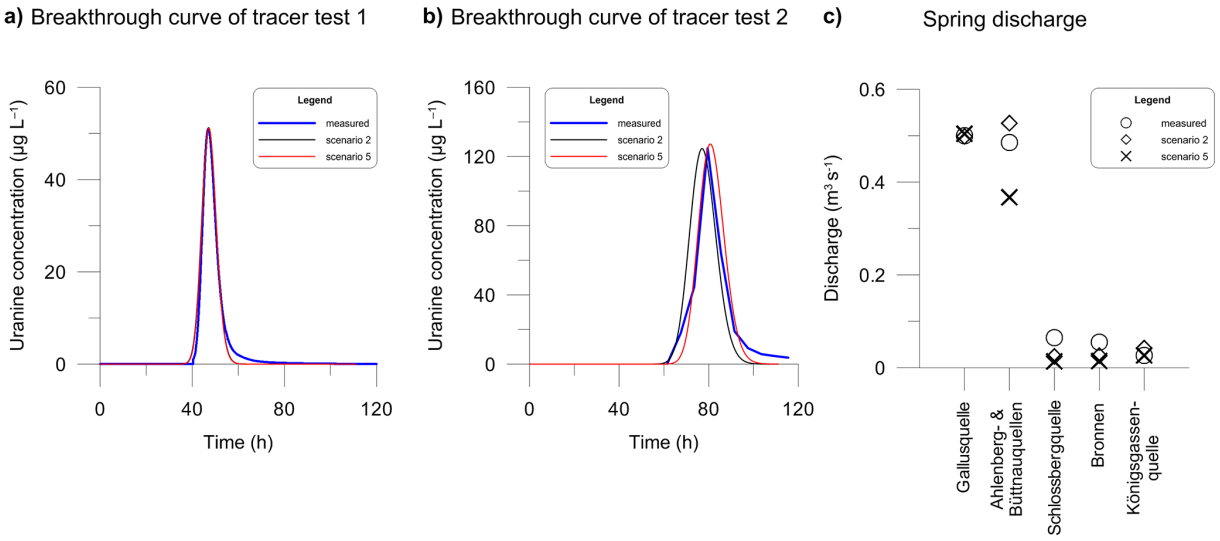

Figure 10. Comparison of the best-fit simulations with field data for scenarios 2 and 5. **(a)** Breakthrough curve of tracer test 1, **(b)** breakthrough curve of tracer test 2 and **(c)** spring discharge.

5 Conclusions of the parameter analysis

Table 3 provides a comparison, i.e. the characteristics for all scenarios. The parameter analysis shows that there is only a limited choice of parameters with which the spring discharges (water balance), the hydraulic head distribution and the tracer velocities can be simulated. Scenario 1 is the only scenario that cannot reproduce the peak travel times observed in both tracer tests simultaneously (Sect. 4.1). It underestimates the complexity of the geometry and internal surface characteristics (e.g. roughness) of the conduit system.

Scenario 4 introduces two additional model parameters. The best fit for this scenario is, however, still achieved with all three K_m values being equal, which basically results in the parameter set of scenario 2. This implies that the major influence leading to the differences in hydraulic gradients observed throughout the area is the conduit system and not the variability of the fissured matrix hydraulic conductivity. It was also shown that for the Madison aquifer (USA), by Saller et al. (2013), a better representation of the hydraulic head distribution can be achieved by including a discrete conduit system even for reduced variability in the hydraulic conductivity of the fissured matrix. Their conclusion complies very well with the findings for scenario 4.

Scenario 3 simulates the presence of a couple of additional smaller dendritic branches. The deduced parameter values and the fit of the objective functions are similar to those of scenarios 2 and 5. Because of long calculation times without additional advantage for the presented study, scenario 3 is not considered for further analysis.

Scenarios 2 and 5 are both judged as suitable. Their parameters and the quality of the fit are similar. Therefore, it is not possible to decide which one is the better representation of reality. Regarding the different processes interacting during karst evolution (Sect. 4.5) it is most likely that the actual geometry ranges somewhat in between these two scenarios. Table 1 summarizes all parameters of both simulations and Fig. 10 shows the simulated tracer breakthrough curves and spring discharges.

6 Discussion

6.1 Plausibility of the best-fit simulations

The main objective of the model simulation is not only to reproduce the target values but also to provide insight into dominating flow and transport processes, sensitive parameters and to check the plausibility of the model set-up. Possible ambiguities in parameterizations can also be checked, i.e. different combinations of parameters producing identical model output.

For these aims model parameters and aquifer properties simulated with scenarios 2 and 5 are compared to those observed in the field. As seen in Table 1 most of the calibrated parameters range well within values provided in the literature. The calibrated Manning coefficients are relatively high compared to other karst systems. Jeannin (2001) lists effective conductivities for several different karst networks that translate into n values of between 0.03 and 1.07 s m$^{-1/3}$, showing that the natural range of n values easily extends across 2 orders of magnitude and the minimum n values of the simulation lie within the natural range. The maximum n values are significantly higher than those given by Jeannin (2001). This is not surprising since the calibrated n value reflects the total roughness of the conduit bundles and therefore includes geometric conduit properties in addition to the

wall roughness that it was originally defined for. This effect is specific for the Gallusquelle area but it might be important to consider for other moderately karstified areas as well where identification of conduit geometries is especially difficult.

The total conduit volume of the Gallusquelle spring derived from scenarios 2 and 5 is only 50 % of that estimated with traditional methods (Geyer et al., 2008). Since the conduit transmissivity increases towards the spring water enters the conduits preferably in the vicinity of the spring in the Gallusquelle area. Therefore, the matrix contribution is high. In addition, the travel time at peak concentration of tracer test 2, which was used for the volume estimation by Geyer et al. (2008), is longer than 3 days, during which time matrix–conduit water exchange can readily take place. Based on the results of a tracer test conducted in a distance of 3 km to the Gallusquelle spring Birk et al. (2005) estimated the error incurred by deducing the conduit volume without taking conduit–matrix exchange fluxes into account with a very simple numerical model. The authors found a difference in conduit volumes of approximately 50 %. This fits well with the results of the present simulation. Birk et al. (2005) also the simulated equivalent conduit cross sectional area between their tracer injection point and the spring to be 13.9 m^2. For scenario 2 the simulated average cross sectional area is 11.9 m^2 and for scenario 5 13.4 m^2, which compares very well with the results of Birk et al. (2005).

It was not possible to match the shape of both breakthrough curves with the same dispersivity. The apparent dispersion in the tracer test 2 breakthrough is much higher compared to that of tracer test 1, while the breakthrough of tracer test 1 shows a more expressed tailing (Fig. 10a and b). This corresponds to the effect observed by Hauns et al. (2001). The authors found scaling effects in karst conduits: the larger the distance between input and observation point, the more mixing occurred. The tailing is generally induced by matrix diffusion or discrete geometric changes such as pools, where the tracer can be held back and released more slowly. Theoretically, every water drop employs medium and slow flow paths if the distance is large enough, leading to a more or less symmetrical, but broader, distribution and therefore a higher apparent dispersion (Hauns et al., 2001). To quantify this effect, exact knowledge of the geometric conduit shape such as the positions and shapes of pools would be necessary. Furthermore, an additional unknown possibly influencing the observed retardation and dispersion effects is the input mechanism. The simulation assumes that all introduced tracers immediately and completely enter the conduit system, which neglects effects of the unsaturated zone on tracer breakthrough curves. In addition, the shape of the breakthrough curve of tracer test 2 is difficult to deduce since the 6 h sampling interval can be considered as rather low leading to a breakthrough peak which is described by only seven measurement points. Therefore, the apparent dispersivity was calibrated for both breakthrough curves separately. Calibrated dispersivity ranges well within those quoted in literature (Table 1). The mass recovery during the simulation was determined to range between 98.4 and 99.9 % in all simulations. The slight mass difference results from a combination of diffusion of the tracer into the fissured matrix and numerical inaccuracies.

The spring discharge of the minor springs in the area (Sect. 3) was slightly underestimated in most cases (Fig. 10c). For most springs the models of scenarios 2 and 5 provide similar results. The underestimation of discharge is in the order of $< 0.05\,m^3\,s^{-1}$and is not expected to significantly influence the general flow conditions. It probably results from the unknown conduit geometry in the catchments of the different minor springs. The only case in which the two scenarios give significantly different results is the spring discharge of the spring group consisting of the Ahlenberg and Büttnauquellen springs (Fig. 10c). Scenario 2 overestimates and scenario 5 underestimates the discharge. This is due to the fact that the longest conduit of the Ahlenberg and Büttnauquellen springs is longer than the longest one of the Gallusquelle spring but the conduit network has less intersections (Fig. 1). Therefore, the conduit volume of the Ahlenberg and Büttnauquellen springs is 134 568 m^3 in scenario 2 and only 75 085 m^3 in scenario 5 leading to the different discharge values. It is reasonable to assume that a better fit for the spring group can be achieved, if more variations of conduit intersections are tested. An adequate fit for the Fehla-Ursprung spring of $0.1\,m^3\,s^{-1}$ was achieved for both scenarios with a fault aperture of 0.005 m.

6.2 Uncertainties and limitations

The most important uncertainties regarding the reliability of the simulation include the assumptions that were made prior to modelling. First, flow dynamics were neglected. This approach was chosen because tracer tests are supposed to be conducted during quasi-steady-state flow conditions. However, this is only the ideal case. During both tracer tests spring discharge declined slightly. The influence of transient flow on transport velocities inside the conduits was estimated by a very simple transient flow simulation for the best-fit models in which recharge and storage coefficients were calibrated to reproduce the observed decline in spring discharges. The transient flow only slightly affected peak velocities but lead to a larger spreading of the breakthrough curves and therefore lower calibrated dispersion coefficients. This effect occurred because the decline in flow velocities is not completely uniform inside the conduits and depending on where the tracer is at which time it experiences different flow velocities in the different parts of the conduits, which leads to a broader distribution at the spring. The same breakthrough curves can be simulated under steady-state flow conditions with slightly higher dispersivity coefficients. So, the calibrated dispersivities do not only represent geometrical heterogeneities but also temporal effects as is the case for all standard evaluations of dispersion from tracer breakthrough curves.

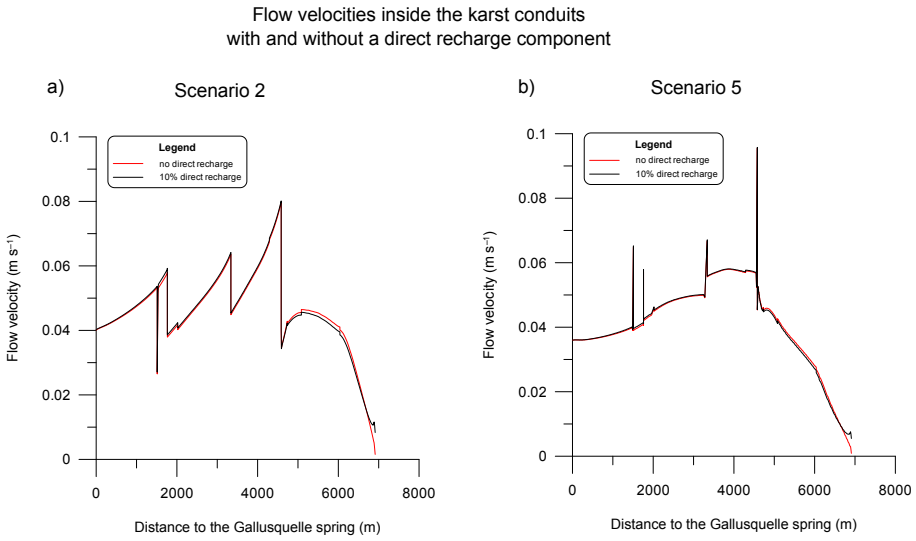

Figure 11. Flow velocities inside the main conduit branch of the Gallusquelle spring during the simulation of tracer test 2. The best-fit simulations for scenarios 2 and 5 are compared to simulations where a direct recharge of 10 % is introduced.

The influence of rapid recharge is not to considered in the simulation of baseflow conditions. However, there might be an influence on flow velocities during the actual recharge events, i.e. if rapid recharge is intensive and strong enough to lead to a reversal of the flow gradients between conduit and fissured matrix. Therefore, an alternative simulation was performed for tracer test 2, which was conducted during high flow conditions (Table 2) after a recharge event. The maximum percentage of direct recharge of 10 % estimated by Sauter (1992) and Geyer et al. (2008) was used for this simulation. Neither for scenario 2 nor for scenario 5 a gradient reversal between conduit and matrix occurred and the influence on flow velocities was negligible (Fig. 11).

Furthermore, flow in all karst conduits was simulated for turbulent conditions. Turbulent conditions can be generally assumed in karst conduits (Reimann et al., 2011) and also apply to all calibrated model conduit cross sections. Since the conduit cross section presents the total cross section of the conduit bundle, the cross sections of the individual tubes are uncertain, though. The high n values suggest that the surface / volume ratio is relatively high, which implies that the individual conduit cross sections are rather small. Therefore, laminar flow in some conduits is likely. While laminar flow conditions in the conduits influence hydraulic gradients considerably, this fact is believed not to influence the overall results and conclusions of this study, i.e. the relative significance of the parameters deduced from parameter analysis and the deduced conduit volume, especially since flow is simulated for steady-state conditions.

For all distributed numerical karst simulations, uncertainties regarding the exact positions and interconnectivities of the conduit branches still remain. Due to the extensive investigations already performed in previous work (Sect. 3) these uncertainties are reduced in the Gallusquelle area and the above scenarios include the most probable ones. However, the flexibility of the modelling approach allows for the integration of any future information that might enhance the numerical model further.

6.3 Calibration strategy

For a successful calibration of a distributed groundwater flow and transport model for a karst area on catchment scale certain constraints have to be set a priori. The geometry of the model area, i.e. locations/types of boundary conditions and aquifer base, fixed during calibration, has to be known with sufficient certainty. Furthermore, the objective functions for calibration have to be defined, i.e. the hydraulic response of the system and transport velocities. In a karst groundwater model, these consist of measurable variables, i.e. spring discharges, hydraulic heads in the fissured matrix and two tracer breakthrough curves. The hydraulic head measurements should be distributed across the entire catchment and preferably close to the conduit system, should geometric conduit parameters be calibrated for as well. It is expected that the influence of the conduits on the hydraulic head decreases and the influence of matrix hydraulic conductivities increases with distance to the conduit system. In the design of the tracer experiment, the following criteria should be observed: for a representative calibration, the dye should be injected at as large a distance to each other as possible with one of them including the length of the whole conduit system. Each tracer test gives integrated information about its complete flow path. If the injection points lie close together, no information about the development of conduit geometries from water divide to spring can be obtained. Further, the dye should be injected as directly as possible into the conduit

system, e.g. via a flushed sinkhole, to obtain information on the conduit flow regime and to minimize matrix interference. To ease interpretation a constant spring discharge during the tests is desirable.

In this study, the flow field was simulated not only for the catchment area of the Gallusquelle spring, but also for a larger area including the catchment areas of several smaller springs (Fig. 1). This is in general not essential for deducing conduit volumes and setting up a flow and transport model. Simulating several catchments, however, helps to increase the reliability of the simulation. The positions of water divides are majorly determined by the hydraulic conductivity of the fissured matrix K_m, so that the simulated catchment areas of the different springs can be used to estimate how realistic the simulated flow field is and decrease the range of likely K_m values. In this study, high K_m values above ca. $3 \times 10^{-5}\,m\,s^{-1}$ made the simulation of the spring discharge of the Fehla-Ursprung spring (Fig. 1) impossible because the water divide in the west could not be simulated and most of the water in the area discharged to the east towards the river Lauchert resulting in a very narrow and long catchment area for the Gallusquelle spring.

There are eight parameters available for model calibration in this study. Two of these parameters define the conduit geometry: b is the lowest conduit radius and m the slope with which the conduit radius increases. One parameter, d_f, defines the aperture of the fault zone. The hydraulic conductivity of the fissured matrix is represented by the parameter K_m and the roughness of the conduit system by two parameters: b_h represents the highest roughness and m_h the slope of roughness decrease in upgradient direction from the spring. The last two parameters ε_1 and ε_2 are the respective conduit dispersivities obtained from the two artificial tracer experiments (Table 1).

For efficiency reasons it is important to know which of these parameters can be calibrated independently. The apparent transport dispersivities ε_1 and ε_2 are pure transport parameters, which influence only the shape of the breakthrough curves and not the flow field. The hydraulic model parameters influence the shape of the tracer breakthrough curves as well. Therefore, dispersivities ε_1 and ε_2 should be calibrated separately after calibrating the hydraulic model parameters.

Only for hydraulically dominant fault zones knowledge of the fault zone aperture d_f is required. For the model area this parameter was required for one fault zone lying in the west of the area feeding the Fehla-Ursprung spring (Fig. 1). Since the Fehla-Ursprung spring has its own catchment area the fault zone has only minor influence on the flow regime in the Gallusquelle catchment. Its hydraulic parameters were calibrated at the beginning of the simulation procedure to reproduce the catchment and the discharge of the Fehla-Ursprung spring adequately and kept constant throughout all the simulations. In the final calibrated models it was rechecked, but the calibrated value was still acceptable.

The hydraulic conductivity of the fissured matrix K_m can be calibrated independently in principle as well. The influence on spring discharge is relatively small. The best-fit K_m value depends on the conduit parameters, i.e. geometry and roughness, since the hydraulic conductivities of the conduit system and of the fissured matrix define the total transmissivity of the catchment area together. Nonetheless, the best-fit value lies in the same range for different conduit geometries (Figs. 4a and 7c). The greater the difference between the simulated conduit geometries, the more likely is a slight shift of the best-fit K_m value. Therefore, it is advisable to calibrate it anew for significant model changes, e.g. different scenarios, but to keep it constant during the rest of the calibrations. For the best-fit configuration, potentially used as a prognostic tool, the K_m value needs to be checked and adapted if necessary. This observation is, however, only valid for steady-state flow conditions. The dynamics of the hydraulic head and spring discharge might be highly sensitive to the matrix hydraulic conductivity, the conduit–matrix exchange coefficient and the lateral conduit extent. This work focuses on the conduits as highly conductive pathways for e.g. contaminant transport, but the calibration of matrix velocities, e.g. by use of environmental tracers, would likely be sensitive to the K_m values as well. Therefore, the choice of the flow regime and the objective functions determines the strength of the interdependencies between fissured matrix and conduit system parameters and therefore whether K_m can be calibrated independently.

The conduit parameters for geometry and roughness, here four parameters (lowest conduit radius b, slope of radius increase m, highest roughness b_h and slope of roughness decrease m_h), have to be varied simultaneously. All of them have a major influence on spring discharge and cannot be varied separately without introducing discharge errors. For each conduit geometry, there are a number of possible b_h–m_h combinations that result in the observed spring discharge. In general, the slowest transport velocities are achieved with a m_h value of zero. So, to deduce the range of geometric parameters that reproduce the objective functions, it is advisable to check the minimum conduit volume for which the tracer tests are not too fast for a value of m_h equal to zero. For the Gallusquelle area, transmissivities significantly increase towards the springs, which is characteristic for most karst catchments. Therefore, low b_h values oppose the general hydraulic head trend: they increase the conduit roughness at the spring leading to slower flow and higher gradients. The higher the conduit volume, the higher b_h is required to reproduce the observed transport velocities. Therefore, the best-fit model likely has the smallest conduit volume for which both tracer tests can be reproduced. In Fig. 7 this condition can be seen to clearly range in the order of $100\,000\,m^3$ for the Gallusquelle area. While the four conduit parameters allow for a good model fit, they are pure calibration parameters. They show that the karst conduit system has a high complexity, which cannot be neglected for distributed velocity and hy-

draulic head representation. A systematic simulation of the heterogeneities, e.g. with a karst genesis approach, would be a process-based improvement to the current method and give more physical meaning to the parameters.

7 Conclusions

The study presents a large-scale catchment-based distributed hybrid karst groundwater flow model capable of simulating groundwater flow and solute transport. For flow recession conditions this model can be used as a predictive tool for the Gallusquelle area with relative confidence. The approach of simultaneous pattern matching of flow and transport parameters provides new insight into the hydraulics of the Gallusquelle conduit system. The model ambiguity was significantly reduced to the point where an estimation of the actual karst conduit volume for the Gallusquelle spring could be made. This would not have been possible simulating only one or two of the three objective functions, i.e. the spring discharge, the hydraulic head distribution and two tracer tests.

The model allows for the identification of the relevant parameters affecting karst groundwater discharge and transport in karst conduits and the examination of the respective overall importance in a well-investigated karst groundwater basin for steady-state flow conditions. While a differentiated representation of the roughness values in the karst conduits is substantial for buffering the lack of knowledge of the exact conduit geometry, e.g. local variations in cross section and the number of interacting conduits, variable matrix hydraulic conductivities cannot improve the simulation. It was shown that the effect of the unknown exact lateral extent of the conduit system and the change in conduit cross section at conduit intersections is of minor importance for the overall karst groundwater discharge. This is important since these parameters are usually unknown and difficult to measure in the field.

For calibration purposes, this study demonstrates that for a steady-state flow field and the observed objective functions the hydraulic conductivities of the fissured matrix can practically be calibrated independently of the conduit parameters. Furthermore, a strategy for the simultaneous calibration of conduit volumes and conduit roughness in a complex karst catchment was developed.

As discussed in Sect. 5 the major limitation of the simulation is the neglect of flow dynamics, which limits the applicability to certain flow conditions. Therefore, transient flow simulation is the focus of on-going work. This will enhance the applicability of the model as a prognostic tool to all essential field conditions and lead to further conclusions regarding the important karst system parameters, their influences on karst hydraulics and their interdependencies. It can be expected that some parameters, which are of minor importance in a steady-state flow field, e.g. the lateral conduit extent and the percentage of recharge entering the conduits directly, will exhibit significant influence for transient flow conditions.

Acknowledgements. The presented study was funded by the German Federal Ministry of Education and Research (promotional reference no. 02WRS1277A, AGRO, Risikomanagement von Spurenstoffen und Krankheitserregern in ländlichen Karsteinzugsgebieten).

This open-access publication is funded by the University of Göttingen.

Edited by: M. Giudici

References

Barenblatt, G. I., Zheltov, I. P., and Kochina, I. N.: Basic concepts in the theory of seepage in fissured rocks (strata), J. Appl. Math. Mech.-USS, 24, 1286–1303, 1960.

Bauer, S., Liedl, R., and Sauter, M.: Modeling of karst aquifer genesis: Influence of exchange flow, Water Resour. Res., 39, 1285, doi:10.1029/2003WR002218, 2003.

Birk, S., Geyer, T., Liedl, R., and Sauter, M.: Process-Based Interpretation of Tracer Tests in Carbonate Aquifers, Ground Water, 43, 381–388, 2005.

Birk, S., Liedl, R., and Sauter, M.: Karst Spring responses examined by process-based modeling, Ground Water, 44, 832–836, 2006.

Clemens, T.: Simulation der Entwicklung von Karstaquiferen, PhD thesis, Eberhard-Karls-Universität zu Tübingen, Tübingen, 1998.

Clemens, T., Hückinghaus, D., Sauter, M., Liedl, R., and Teutsch, G.: A combined continuum and discrete network reactive transport model for the simulation of karst development, in: Proceedings of the ModelCARE 96 Conference, 24–26 September 1996, Golden, Colorado, USA, 309–318, 1996.

COMSOL AB: COMSOL Multiphysics® User's Guide v4.3, 1292 pp., 2012.

Coronado, M., Ramírez-Sabag, J., and Valdiviezo-Mijangos, O.: On the boundary conditions in tracer transport models for fractured porous underground formations, Rev. Mex. Fís., 53, 260–269, 2007.

Covington, M. D., Luhmann, A. J., Wicks, C. M., and Saar, M. O.: Process length scales and logitudinal damping in karst conduits, J. Geophys. Res., 117, F01025, doi:10.1029/2011JF002212, 2012.

Doummar, J., Sauter, M., and Geyer, T.: Simulation of flow processes in a large scale karst system with an integrated catchment model (Mike She) – Identification of relevant parameters influencing spring discharge, J. Hydrol., 426, 112–123, doi:10.1016/j.jhydrol.2012.01.021, 2012.

Dreybrodt, W.: Mixing in $CaCO_3$–CO_2–H_2O systems and its role in the karstification of limestone areas, Chem. Geol., 32, 221–236, 1981.

Ford, D. C. and Williams, P. W.: Karst geomorphology and hydrology, Wiley, West Sussex, 562 pp., 2007.

Geyer, T., Birk, S., Licha, T., Liedl, R., and Sauter, M.: Multi-tracer test approach to characterize reactive transport in karst aquifers, Ground Water, 45, 36–45, 2007.

Geyer, T., Birk, S., Liedl, R., and Sauter, M.: Quantification of temporal distribution of recharge in karst systems from spring hydrographs, J. Hydrol., 348, 452–463, 2008.

Golwer, A.: Erläuterungen zu Blatt 7821 Veringenstadt, Geologische Karte 1 : 25 000 von Baden-Württemberg, Geologisches Landesamt Baden-Württemberg, Stuttgart, 151 pp., 1978.

Gwinner, M. P.: Erläuterungen zu Blatt 7721 Gammertingen, Geologische Karte 1 : 25 000 von Baden-Württemberg, Geologisches Landesamt Baden-Württemberg, Freiburg, Stuttgart, 78 pp., 1993.

Hartmann, A., Weiler, M., Wagener, T., Lange, J., Kralik, M., Humer, F., Mizyed, N., Rimmer, A., Barberá, J. A., Andreo, B., Butscher, C., and Huggenberger, P.: Process-based karst modelling to relate hydrodynamic and hydrochemical characteristics to system properties, Hydrol. Earth Syst. Sci., 17, 3305–3321, doi:10.5194/hess-17-3305-2013, 2013.

Hartmann, A., Goldscheider, N., Wagener, T., Lange, J., and Weiler, M.: Karst water resources in a changing world: Review of hydrological modeling approaches, Rev. Geophys., 52, 1–25, doi:10.1002/2013RG000443, 2014.

Hauns, M., Jeannin, P.-Y., and Atteia, O.: Dispersion, retardation and scale effect in tracer breakthrough curves in karst conduits, J. Hydrol., 241, 177–193, 2001.

Hu, R.: Hydraulic tomography: A new approach coupling hydraulic travel time, attenuation and steady shape inversions for high-spatial resolution aquifer characterization, PhD thesis, University of Göttingen, Göttingen, 116 pp., 2011.

Hubinger, B. and Birk, S.: Influence of initial heterogeneities and recharge limitations on the evolution of aperture distributions in carbonate aquifers, Hydrol. Earth Syst. Sci., 15, 3715–3729, doi:10.5194/hess-15-3715-2011, 2011.

Hückinghaus, D.: Simulation der Aquifergenese und des Wärmetransports in Karstaquiferen, C42, Tübinger Geowissenschaftliche Arbeiten, Tübingen, 1998.

Hunter, N. M., Bates, P. D., Horritt, M. S., De Roo, A. P. J., and Werner, M. G. F.: Utility of different data types for calibrating flood inundation models within a GLUE framework, Hydrol. Earth Syst. Sci., 9, 412–430, doi:10.5194/hess-9-412-2005, 2005.

Jeannin, P.-Y.: Modeling flow in phreatic and epiphreatic karst conduits in the Hölloch cave (Muotatal, Switzerland), Water Resour. Res., 37, 191–200, 2001.

Jeannin, P.-Y. and Sauter, M.: Modelling in karst systems, Bulletin d'Hydrogéologie, 16, Université de Neuchâtel, Neuchâtel, 1998.

Khu, S.-T., Madsen, H., and di Pierro, F.: Incorporating multiple observations for distributed hydrologic model calibration: An approach using a multi-objective evolutionary algorithm and clustering, Adv. Water Resour., 31, 1387–1398, 2008.

Kordilla, J., Sauter, M., Reimann, T., and Geyer, T.: Simulation of saturated and unsaturated flow in karst systems at catchment scale using a double continuum approach, Hydrol. Earth Syst. Sci., 16, 3909–3923, doi:10.5194/hess-16-3909-2012, 2012.

Kovács, A. and Sauter, M.: Modelling karst hydrodynamics, in: Methods in karst hydrogeology, edited by: Goldscheider, N. and Drew, D., Taylor and Fracis, London, 201–222, 2007.

Kovács, A., Perrochet, P., Király, L., and Jeannin, P.-Y.: A quantitative method for the characterisation of karst aquifers based on spring hydrograph analysis, J. Hydrol., 303, 152–164, 2005.

Li, H. T., Brunner, P., Kinzelbach, W., Li, W. P., and Dong, X. G.: Calibration of a groundwater model using pattern information from remote sensing data, J. Hydrol., 377, 120–130, doi:10.1016/j.jhydrol.2009.08.012, 2009.

Liedl, R., Sauter, M., Hückinghaus, D., Clemens, T., and Teutsch, G.: Simulation of the development of karst aquifers using a coupled continuum pipe flow model, Water Resour. Res., 39, 1057, doi:10.1029/2001WR001206, 2003.

Luhmann, A. J., Covington, M. D., Alexander, S. C., Chai, S. Y., Schwartz, B. F., Groten, J. T., and Alexander, E. C.: Comparing conservative and nonconservative tracers in karst and using them to estimate flow path geometry, J. Hydrol., 448–449, 201–211, doi:10.1016/j.jhydrol.2012.04.044, 2012.

Madsen, H.: Parameter estimation in distributed hydrological catchment modelling using automatic calibration with multiple objectives, Adv. Water Resour., 26, 205–216, 2003.

Merkel, P.: Karsthydrologische Untersuchungen im Lauchertgebiet (westl. Schwäbische Alb), Diplom thesis, University of Tübingen, Tübingen, 108 pp., 1991.

Mohrlok, U.: Numerische Modellierung der Grundwasserströmung im Einzugsgebiet der Gallusquelle unter Festlegung eines Drainagesystems, Grundwasser, 19, 73–85, doi:10.1007/s00767-013-0249-x, 2014.

Mohrlok, U. and Sauter, M.: Modelling groundwater flow in a karst terraine using discrete and double-continuum approaches: importance of spatial and temporal distribution of recharge, in: Proceedings of the 12th International Congress of Speology, 2/6th Conference on Limestone Hydrology and Fissured Media, 10–17 August 1997, La Chaux-de-Fonds, Switzerland, 167–170, 1997.

Oehlmann, S., Geyer, T., Licha, T., and Birk, S.: Influence of aquifer heterogeneity on karst hydraulics and catchment delineation employing distributive modeling approaches, Hydrol. Earth Syst. Sci., 17, 4729–4742, doi:10.5194/hess-17-4729-2013, 2013.

Ophori, D. U.: Constraining permeabilities in a large-scale groundwater system through model calibration, J. Hydrol., 224, 1–20, 1999.

Perrin, C., Andréassian, V., Serna, C. R., Mathevet, T., and Le Moine, N.: Discrete parameterization of hydrological models: Evaluating the use of parameter sets libraries over 900 catchments, Water Resour. Res., 44, W08447, doi:10.1029/2007WR006579, 2008.

Rehrl, C. and Birk, S.: Hydrogeological characterisation and modelling of spring catchments in a changing environment, Aust. J. Earth Sci., 103/2, 106–117, 2010.

Reiber, H., Klein, F., Selg, M., and Heidland, S.: Hydrogeologische Erkundung Baden-Württemberg – Mittlere Alb 4 – Markierungsversuche, Abwassereinleitungen, Landesamt für Umwelt, Messungen und Naturschutz Baden-Württemberg, Tübingen, 71 pp., 2010.

Reimann, T., Rehrl, C., Shoemaker, W. B., Geyer, T., and Birk, S.: The significance of turbulent flow representation in single-continuum models, Water Resour. Res., 47, W09503, doi:10.1029/2010WR010133, 2011.

Saller, S. P., Ronayne, M. J., and Long, A. J.: Comparison of a karst groundwater model with and without discrete conduit flow, Hydrogeol. J., 21, 1555–1566, doi:10.1007/s10040-013-1036-6, 2013.

Sauter, M.: Quantification and Forecasting of Regional Groundwater Flow and Transport in a Karst Aquifer (Gallusquelle, Malm, SW Germany), C13, Tübinger Geowissenschaftliche Arbeiten, Tübingen, 1992.

Schmidt, S., Geyer, T., Marei, A., Guttman, J., and Sauter, M.: Quantification of long-term wastewater impacts on karst groundwater resources in a semi-arid environment by chloride mass balance methods, J. Hydrol., 502, 177–190, 2013.

Strayle, G.: Karsthydrologische Untersuchungen auf der Ebinger Alb (Schwäbischer Jura), in: Jahreshefte des Geologischen Landesamtes Baden-Württemberg, Freiburg im Breisgau, 109–206, 1970.

Teutsch, G. and Sauter, M.: Groundwater Modeling in karst terranes: scale effects, data aquisition and field validation, in: Proceedings of the 3rd Conference on Hydrogeology, Ecology, Monitoring and Management of Ground Water in Karst Terranes, 4–6 December 1991, Nashville, USA, 17–34, 1991.

Villinger, E.: Über Potentialverteilung und Strömungssysteme im Karstwasser der Schwäbischen Alb (Oberer Jura, SW-Deutschland), Geologisches Jahrbuch, C18, Bundesanstalt für Geowissenschaften und Rohstoffe und Geologische Landesämter der Bundesrepublik Deutschland, Hannover, 1977.

Villinger, E.: Hydrogeologie, in: Erläuterungen zu Blatt 7721 Gammertingen, Geologische Karte 1 : 25 000 von Baden-Württemberg, edited by: Gwinner, M. P., Geologisches Landesamt Baden-Württemberg, Freiburg, Stuttgart, 30–57, 1993.

Worthington, S. R. H.: Diagnostic hydrogeologic characteristics of a karst aquifer (Kentucky, USA), Hydrogeol. J., 17, 1665–1678, doi:10.1007/s10040-009-0489-0, 2009.